

ADVERTIMENT. L'accés als continguts d'aquesta tesi queda condicionat a l'acceptació de les condicions d'ús establertes per la següent llicència Creative Commons:  http://cat.creativecommons.org/?page_id=184

ADVERTENCIA. El acceso a los contenidos de esta tesis queda condicionado a la aceptación de las condiciones de uso establecidas por la siguiente licencia Creative Commons:  <http://es.creativecommons.org/blog/licencias/>

WARNING. The access to the contents of this doctoral thesis it is limited to the acceptance of the use conditions set by the following Creative Commons license:  <https://creativecommons.org/licenses/?lang=en>



Universitat Autònoma de Barcelona

Advances in NMR spectroscopic methodology and
applications: time-efficient methods, ultra long-
range heteronuclear correlation experiments and
enantiospecific analysis of complex mixtures

Kumar Motiram Corral

Doctoral thesis

Ph.D. in Chemistry

Chemistry Department

Faculty of Science

2021

Supervisors:

Teodor Parella Coll

Míriam Pérez Trujillo

Pau Nolis Fañanas

Tutor:

Carlos Jaime Cardiel



Universitat Autònoma de Barcelona

Chemistry Department

Faculty of Science

Memòria presentada per aspirar al Grau de Doctor per Kumar Motiram Corral

Vist i plau,

Dr. T. Parella Coll

Dr. M. Pérez Trujillo

Dr. P. Nolis Fañanas

K. Motiram Corral

Bellaterra, 12 de Julio de 2021

Agradecimientos

Me gustaría agradecer en primer lugar a todos aquéllos que hacen posible que cada mañana, tarde y noche, podamos venir a trabajar a la UAB y nos tratan como princesas, en especial a María de los Ángeles, Elisa, Ana, Paula, Teresa, Mari José, Manel...

A todas las personas que he conocido en el SAF tanto usuarios como monitores que han aguantado mi histerismo en muchas ocasiones pero que tantos momentos de diversión hemos compartido.

A mi grupo, el SeRMN que han acogido desde un primer momento, se han ofrecido a todo lo que podían y más. Silvia siempre dispuesta a escuchar, Eva siempre disponible para ayudar, y Miquel, la persona que todo lo soluciona y está ahí cuando se le necesita. Muchas gracias por estos 4 años (+ 5 meses). A mis directores, Pau por hacerme tantas aclaraciones sin saber que sería finalmente director, a Míriam por su paciencia, su disponibilidad y todas las horas de formación que me ha brindado, y al Teo no solo por abrirme las puertas del Servei, sino por dedicar muchísimo tiempo en darme una visión lo suficientemente amplia en el campo de la RMN y compartir tantas impresiones sobre política, gastronomía y turismo catalán. ¡¡¡A todos muchas gracias!!!

A todas las personas que he conocido en Cataluña y hemos pasado muchos momentos, haciendo turismo, remo, barbacoas. Pedro, Jaume, Raúl, Jana, Pierre, Artur..., gracias por hacer que el tiempo que he estado en BCN fuera muy positiva. Pero sobre todo a mis compis de piso en Cerdanyola, Alberto, Saioa, Dani y Jaime por ser tan importantes para mí. Y por supuesto al Adrià y Floriane, sin los que mi estancia en Tromsø no hubiese sido igual.

Mención especial a mi gran amigo Eudald Jordá, compañero de viajes y de confidencias, gracias por darme lo mejor de ti, probablemente muchas cosas no las hubiese podido hacer sin contar con tu apoyo, muchas gracias.

Por último, a mis amigos de siempre, a mi hermano, a mi madre y a mis abuelos, que sois los que me habéis impulsado siempre a seguir adelante sin mirar atrás. Les quiero.

ACKNOWLEDGMENTS

I would like to thank the financial support for this research by Spanish MINECO projects “DISEÑO Y APLICACION DE NUEVAS METODOLOGIAS EN RESONANCIA MAGNETICA NUCLEAR” (CTQ2015-64436-P) and “METODOLOGIAS MODERNAS EN RESONANCIA MAGNETICA NUCLEAR DE MOLECULAS PEQUEÑAS” (PGC2018-095808-B-I00) and for the grant BES-2016-078903. I must also thank the Servei de Ressonància Magnètica Nuclear (UAB) for providing me with a workspace and for being able to use all its instrumentation.

Table of Contents

1. Acronyms.....	1
2. Introduction.....	5
2.1. 2D NMR experiments	8
2.2. 2D HSQC experiment	11
2.2.1. ^1H - ^{13}C HSQC-PEP experiment	16
2.3. Pure-Shift NMR	18
2.3.1. Pure-Shift HSQC	23
2.4. Long-Range ^1H-^{13}C Correlation NMR Experiments	25
2.4.1. ^1H - ^{13}C -HMBC experiment.....	25
2.4.2. ^1H - ^{13}C HSQMBC experiment	27
2.4.2.1. LR-HSQMBC	28
2.4.2.2. Frequency-Selective HSQMBC experiments	30
2.5. Time-Efficient NMR techniques	34
2.5.1. Time-Sharing	34
2.5.2. Multiple-FID detection.....	36
2.5.3. NOAH supersequences	39
2.6. Spectral resolution enhancement	41
2.7. NMR-aided enantiodifferentiation using chiral solvating agents.....	43
3. Objectives	49
4. Results and discussion	51
4.1. Publication 1: Implementing one-shot multiple-FID acquisition into homonuclear and heteronuclear NMR experiments.	54
4.1.1. Introduction.....	54

4.1.2. Original paper	55
4.1.3. Supporting information	59
4.2. Publication 2: Simultaneous acquisition of two 2D HSQC spectra with different ^{13}C spectral widths.	81
4.2.1. Introduction.....	81
4.2.2. Original paper	82
4.2.3. Supporting information	89
4.3. Publication 3: Interleaved Dual NMR Acquisition of Equivalent Transfer Pathways in TOCSY and HSQC Experiments.	99
4.3.1. Introduction.....	99
4.3.2. Original paper	100
4.3.3. Supporting information	105
4.4. Publication 4: Broadband homodecoupled time-shared ^1H-^{13}C and ^1H-^{15}N HSQC experiments.	138
4.4.1. Introduction.....	138
4.4.2. Original paper	139
4.4.3. Supporting information	147
4.5. Publication 5: LR-selHSQMBC: Simultaneous Detection and Quantification of Very Weak Long-Range Heteronuclear NMR Correlations.	167
4.5.1. Introduction.....	167
4.5.2. Original paper	168
4.5.3. Supporting information	172
4.6. Publication 6: LR-HSQMBC versus LR-selHSQMBC: Enhancing the Observation of Tiny Long-Range Heteronuclear NMR Correlations.	183
4.6.1. Introduction.....	183
4.6.2. Original paper	184

4.6.3. Supporting information	192
4.7. Publication 7: Simultaneous Enantiospecific Detection of Multiple Compounds in Mixtures using NMR Spectroscopy.	202
4.7.1. Introduction.....	202
4.7.2. Original paper	203
4.7.3. Supporting information	208
5. Conclusions.....	221

1. Acronyms

1D	O ne-dimensional
2D	T wo-dimensional
ADEQUATE	Adequate sensitivity D ouble E - Q U A n T um sp E ctroscopy
AP	A nti- P hase
AQ	A c Q uisition time
ASAP	A cceleration by S haring A djacent P olarization
BB	B road B and
BIRD	B ilinear R otation D ecoupling
CASE	C omputer- A ssisted S tructure E lucidation
CLAP	C lean A nti- P hase
CLIP	C lean I n- P hase
COCONOSY	C ombined C orrelation and N uclear O verhauser enhanced S pectroscop Y
COSY	C orrelation S pectroscop Y
CPMG	C arr- P urcell- M eiboom- G ill
CSA	C hiral S olvating A gent
CT	C onstant- T ime
CTP	C oherence T ransfer P athway
DENA	D ifferential E volution for N on-ambiguous A liasing

DEPT	D istortionless E nhancement by P olarization T ransfer
DIPSI	D ecoupling I n the P resence of S calar I nteractions
DQ	D ouble- Q uantum
DQC	D ouble- Q uantum C oherence
DQF	D ouble- Q uantum F ilter
E/A	E cho/ A nti-echo
ESI	E lectronic S upplementary I nformation
F1	Indirect Dimension
F2	Direct Dimension
FID	F ree I nduction D ecay
FT	F ourier T ransform
HMBC	H eteronuclear M ultiple B ond C orrelation
HMQC	H eteronuclear M ultiple- Q uantum C orrelation
HSQC	H eteronuclear S ingle Q uantum C orrelation
HSQMBC	H eteronuclear S ingle- Q uantum M ultiple- B ond C orrelation
Hz	H ertz
INADEQUATE	I ncredible N atural A bundance D ouble- Q uantum T ransfer s p E ctroscopy
INEPT	I nsensitive N uclei E nhanced by P olarization T ransfer
IP	I n- P hase
K	K elvin

LR	L ong- R ange
LR-HSQMBC	L ong- R ange H eteronuclear S ingle- Q uantum M ultiple- B ond C orrelation
MBOB	M ultiple B roadband O ne- B ond
MFA	M ultiple F id A cquisition
MQC	M ultiple- Q uantum C oherence
NMR	N uclear M agnetic R esonance
NOAH	N MR by O rdered A cquisition using ^1H detection
NOE	N uclear O verhauser E ffect
NOESY	N uclear O verhauser E nhancement S pectroscop Y
NUS	N on- U niform S ampling
PE	P erfect- E cho
PEP	P reservation of E quivalent P athways
PFG	P ulsed- F ield G radient
PS	P ure S hift
PSYCHE	P ure S hift Y ielded by C hirp E xcitation
RDC	R esidual D ipolar C oupling
SA	S pectral A liasing
SADA	S pectral A liasing in D ually A cquired
SAPS	S pectral A liasing P ure S hift
SE	S ensitivity E nhanced

SNR	Signal-to-Noise R atio
SQC	Single- Q uantum Coherence
SW	Spectral W idth
T_1	Longitudinal Relaxation Time
T_2	Transversal Relaxation Time
TD	T ime D omain
TOCSY	T Otal Correlation Spectroscop Y
TPPI	T ime- P roportional P hase I ncrementation
TROSY	Transverse R elaxation O ptimized Spectroscop Y .
TS	T ime- S hared
ZQ	Z ero- Q uantum
ZQC	Z ero- Q uantum Coherence
ZQF	Z ero- Q uantum F ilter

2. Introduction

In 1936, Nuclear Magnetic Resonance (NMR) spectroscopy was the object of study by Groter¹ who published three papers with unsuccessful results due to non-optimal material used (with unsuitable T_1 values and low Signal-to-Noise Ratio (SNR)). In the early 50s, NMR fundamentals were successfully developed by the physicists Bloch and Purcell who were granted the Nobel Prize for Physics (1952) “for their development of new methods for nuclear magnetic precision measurements and discoveries in connection therewith”². Important advances were made to study the influence of molecular motion, the magnetic dipolar splitting in solids, the influence of electric quadrupoles moments, chemical shift, indirect spin-spin coupling and general aspects of theory about NMR³. During the 60’s decade, the power of computers technology and mathematic algorithms was incorporated in NMR, highlighting the importance of the Fourier Transform (FT) concept to speed up data acquisition and to improve SNR. Thus, the NMR technique was rapidly assumed by chemists for unprecedented chemical structure elucidation studies. The incorporation of high-field superconducting magnets was the next step in NMR in the early '70s and the important role of Pulsed Field Gradients (PFGs) for spatial encoding and its power in imaging MRI were revealed and applied for the first time to a wide range of substrates. During the '80s, many homonuclear and carbon-detected heteronuclear 2D experiments were developed and the first 3D experiments were published. The introduction of PFG in high-resolution NMR spectroscopy facilitated the development of many proton-detected 2D⁴, 3D and 4D NMR experiments during the 90’s decade when Ernst won the Nobel Prize (1991) due to his

¹ C.J. Groter, “Negative results of an attempt to detect nuclear magnetic spins”. *Physica* 9, 995–998. 1936.

² “Nobel Lectures Physics 1942-1962”. *Elsevier Publishing Company*, Amsterdam, 1964.

³ H. Pfeifer, “A short history of nuclear magnetic resonance spectroscopy and of its early years in Germany”, *Magn. Reson. Chem.* 37(13):154-159. 1999.

⁴ P. Stilbs, “Fourier transform pulsed-gradient spin-echo studies of molecular diffusion”. *Progress in Nuclear Magnetic Resonance Spectroscopy*, 19(1), 1–45. 1987.

pioneering work on FT and 2D NMR experiments⁵. Since then, technological advances in the design of NMR spectrometers (magnets, probes, receivers, etc.) and in methodology (e.g. pulse sequence design) have made NMR an essential tool for structural and conformational studies of small to medium-sized molecules and biomolecules. In addition, not only isolated compounds in dissolution can be analysed in depth by NMR, but also complex mixtures (e.g. biofluids like urine, plasma, etc.), inhomogeneous samples (e.g. biological tissues, polymers, etc.) and solids (e.g. pharmaceuticals polymorphs). The availability of modern NMR equipment and powerful accessories, such as stronger magnetic fields, and volume-reduced and helium-cooled probes, have greatly improved sensitivity limitations.

NMR is a physical phenomenon based on the interaction of RF (Radio-Frequency) pulses with atomic nuclei. The main parameter to consider is the angular momentum caused by the spin of the magnetically active atomic nuclei (gyromagnetic ratio $\gamma \neq 0$). In a classical view, the magnetization axis spins over the direction of B_0 (static magnetic field) with a characteristic Larmor Frequency (ω_0) which is defined as $\omega_0 = \gamma B_0$. The power of the NMR as an analytical tool/technique lies in the variety of experiments (based on pulse sequences design) that can be performed, which provides a lot of different structural (and conformational) information of molecules at an atomic level. The pulse sequences are built by sequentially applying radiofrequency pulses, typically 90° or 180° , which move the active magnetization components between the z-, x- and y-axis, depending on the phase of such pulses. A suitable combination of consecutive pulses and delays applied together with optimum phase cycling and PFGs for adequate Coherence Transfer Pathway (CTP) selection ends in a final Free Induction Decay (FID) period for data acquisition, allowing the design of a great multitude of useful and robust NMR

⁵ Ernst, R. R., Bodenhausen, G. and Wokaun, A., "Principles of NMR in one and two dimensions", *Clarendon Press, Oxford*. 1987.

experiments. When recording an NMR experiment, the pulse sequence is repeated a specific number of times to enhance the overall SNR after applying an adequate relaxation recovery time.

Relaxation is a magnetic field dependent effect, and it is an essential process with numerous implications in the overall NMR process⁶. The spin-lattice T_1 and spin-spin T_2 relaxation times are time-dependent processes involved in the recovery of the equilibrium states of the original longitudinal and transverse magnetization, respectively. Therefore, both T_1 and T_2 play an important role regarding quantification, spectral resolution, sensitivity, and experimental time. Both T_1 and T_2 relaxation times are intrinsic parameters for each proton signal, and they depend globally on several factors such as the magnetic field, the molecular size and molecular motion, the temperature of the sample during the experiment or the solvent viscosity, among others. The initial recycle delay of any NMR experiment depends on the existing T_1 times and is important in terms of quantification and saturation, and T_2 influences the linewidths of the NMR signals. Small molecules have usually longer T_2 values than large molecules, and this permits the use of longer sequences.

Sensitivity and digital resolution are key points related to the quality of NMR spectra and they are directly related to the overall acquisition time. Sensitivity is related to the amount of detected signal (Eq. 1) that depends on sample concentration, magnetic field strength, the gyromagnetic ratio of the nucleus observed, coil temperature or the number of average transitions.

$$SNR \propto \frac{N \cdot A}{T_s} * B_0^{3/2} \gamma^{5/2} T_2^* (NS)^{1/2} \quad (\text{Eq. 1})^7$$

⁶ S. Meiboom and D. Gill, "Modified Spin-Echo Method for Measuring Nuclear Relaxation Times", *Rev. Sci. Instrum.*, 29:688-691. 1958.

⁷ Where SNR refers to Signal-to-Noise Ratio, N is the number of molecules, A is the abundance of nuclide, T_s is the temperature of the sample, B_0 is the static magnetic field, γ is the gyromagnetic constant, T_2 is the transversal relaxation time, and NS is the number of scans.

The digital resolution in an NMR experiment is related to the separation between two data points and is defined by the number of points in the time-domain dimension (Hz/pt). Digital resolution can be enhanced by some NMR tools such as Spectral Aliasing (SA)⁸ or Non-Uniform Sampling (NUS)⁹. On the other hand, the spectral resolution in an NMR spectrum obtained after Fourier transform of the time-dependent NMR data can also be enhanced by other complementary methods including data processing tools such as zero filling or linear prediction, or new NMR concepts such as Pure-shift NMR¹⁰.

2.1. 2D NMR experiments

2D NMR experiments are related to NMR spectra with two orthogonal frequency axes and they can be classified as homonuclear or heteronuclear NMR experiments. 2D homonuclear NMR experiments display the same nuclei (typically ^1H - ^1H or ^{13}C - ^{13}C) on the two different frequency axes of the 2D spectrum. Table 1 lists the most important homonuclear NMR experiments used for structural elucidation of small molecules.

⁸ G. B. Ba Njock *et al.*, “Spectral aliasing: A super zoom for 2DNMR spectra. Principles and applications”, *Chimia (Aarau)*, 64:235-240. 2010.

⁹ J. C. Hoch, “Modern spectrum analysis in nuclear magnetic resonance: Alternatives to the fourier transform”, *Methods Enzymol.*, 176:216–241. 1989.

¹⁰ L. Castañar and T. Parella, “Broadband ^1H homodecoupled NMR experiments: recent developments, methods and applications”, *Magn. Reson. Chem.*, 53, 399–426. 2015.

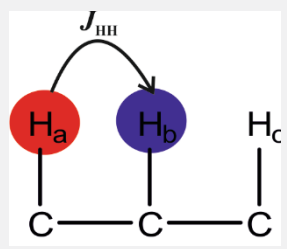
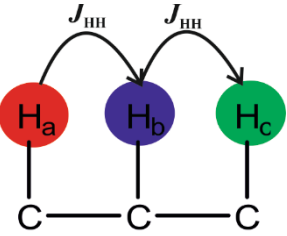
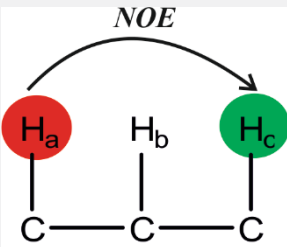
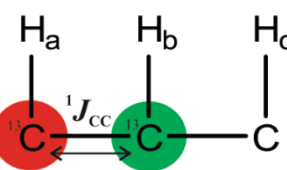
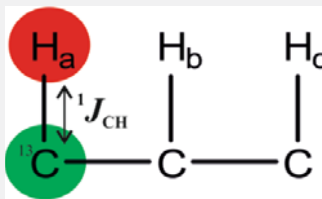
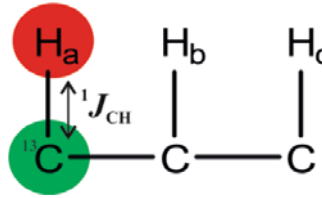
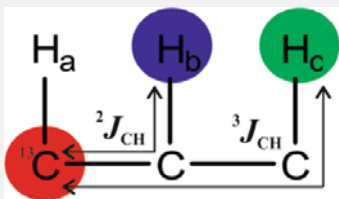
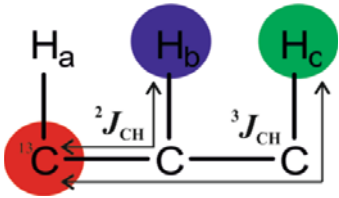
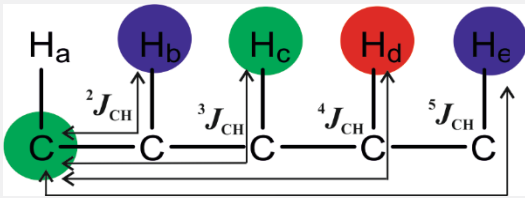
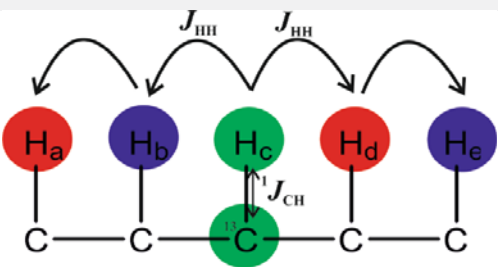
Experiment	Applications	Graphical Representation
COSY	The C ORrelation Spectroscop Y experiment correlates J -coupled homonuclear spins.	 <p>The diagram shows a horizontal chain of three carbon atoms (C-C-C). Above the first carbon is a red circle labeled H_a, above the second is a blue circle labeled H_b, and above the third is a green circle labeled H_c. A curved arrow labeled J_{HH} connects H_a and H_b, indicating scalar coupling between them.</p>
TOCSY	The T OTAL Correlation Spectroscop Y experiment allows the correlation between J -coupled homonuclear spins from the same spin-system network.	 <p>The diagram shows a horizontal chain of three carbon atoms (C-C-C). Above the first carbon is a red circle labeled H_a, above the second is a blue circle labeled H_b, and above the third is a green circle labeled H_c. Two curved arrows labeled J_{HH} are shown: one connecting H_a and H_b, and another connecting H_b and H_c.</p>
NOESY/ROESY	The Nuclear Overhauser Effect Spectroscop Y experiment affords through-space correlations between protons via dipolar interaction.	 <p>The diagram shows a horizontal chain of three carbon atoms (C-C-C). Above the first carbon is a red circle labeled H_a, above the second is a blue circle labeled H_b, and above the third is a green circle labeled H_c. A long curved arrow labeled NOE connects H_a and H_c, indicating through-space interaction.</p>
INADEQUATE	Incredible Natural Abundance Double-QUAntum Transfer spectroscopy experiments provide the information from correlating $J(CC)$ -coupled homonuclear ^{13}C spins at low natural abundance	 <p>The diagram shows a horizontal chain of three carbon atoms. The first and second carbons are labeled ^{13}C and are colored red and green respectively. The third carbon is labeled C and is white. Above the first ^{13}C is a red circle labeled H_a, above the second ^{13}C is a blue circle labeled H_b, and above the third C is a green circle labeled H_c. A double-headed arrow labeled J_{CC} connects the two ^{13}C atoms.</p>

Table 1: General schemes for the most popular 2D homonuclear NMR experiments.

2D heteronuclear NMR experiments display information about two different nuclei on the two orthogonal axes of a 2D spectrum. For instance, in proton-detected experiments such as the classical HSQC or HMQC experiments, the 1H nucleus frequency information is usually displayed on the F2 dimension (horizontal axis) and ^{13}C (or ^{15}N ...) nuclei are shown onto the indirect F1 dimension (vertical axis). Table 2 illustrates the most relevant heteronuclear NMR experiments used for the study of small chemical molecules.

Experiment	Applications	Graphical Representation
HSQC	The H eteronuclear S ingle Q uantum C orrelation experiment shows the correlation between directly bonded $^1J_{CH}$ -coupled heteronuclear spins.	
HMQC	The H eteronuclear M ultiple- Q uantum C orrelation experiment shows the correlation between directly bonded $^1J_{CH}$ -coupled heteronuclear spins.	
HMBC	The H eteronuclear M ultiple B ond C orrelation experiment shows the connectivities between J -coupled heteronuclear spins separated for multiple bonds via $^nJ_{CH}$ ($n=2,3$).	
HSQMBC	The H eteronuclear S ingle- Q uantum M ultiple- B ond C orrelation experiment shows the connectivities between J -coupled heteronuclear spins separated for multiple bonds via $^nJ_{CH}$ ($n=2,3$).	
LR-HSQMBC	The L ong- R ange H eteronuclear S ingle- Q uantum M ultiple- B ond C orrelation experiment can provide information about weak long-range heteronuclear connectivities involving more than three bonds, $^nJ_{CH}$ ($n>3$).	
HSQC-TOCSY	The H eteronuclear S ingle Q uantum C orrelation - T otal C orrelation S pectroscopy experiment provides information about heteronuclear long-range connectivities via a two-step $^1J_{CH}$ + $^nJ_{HH}$ process.	

ADEQUATE

The Adequate sensitivity Double-QUAnTum spEctroscopy experiment provides two-bond heteronuclear connectivities through the ^1H -(^{13}C)- ^{13}C coupling pathway via sequential $^1J_{\text{CH}}$ and $^1J_{\text{CC}}$ transfer.

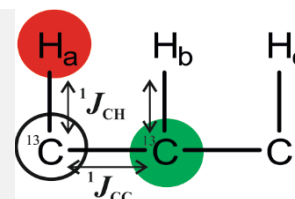


Table 2: General schemes for the most popular 2D heteronuclear NMR experiments.

2.2. 2D HSQC experiment

HSQC is one of the most important 2D NMR experiments for small molecules and biomolecules, yielding direct correlations between two different nuclei directly bonded via the heteronuclear one-bond coupling, typically proton-carbon coupling constant ($^1J_{\text{CH}}$) or one-bond proton-nitrogen coupling constant ($^1J_{\text{NH}}$). A conventional 2D ^1H - ^{13}C HSQC spectrum affords cross-peaks between carbons and directly bonded proton resonances (Figure 1), therefore non-protonated carbons are not observed.

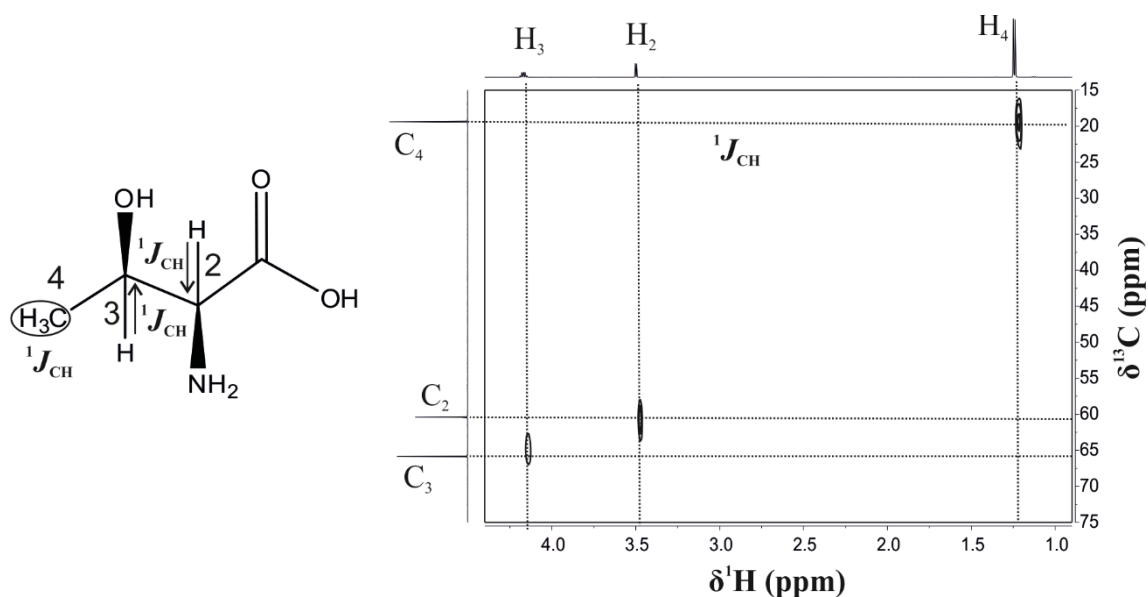


Figure 1: 2D ^1H - ^{13}C HSQC spectrum of threonine in D_2O where chemical shifts of H_4 , H_2 and H_3 along the horizontal F2 axis are directly correlated with chemical shift of C_4 , C_2 and C_3 in the vertical F1 axis, respectively.

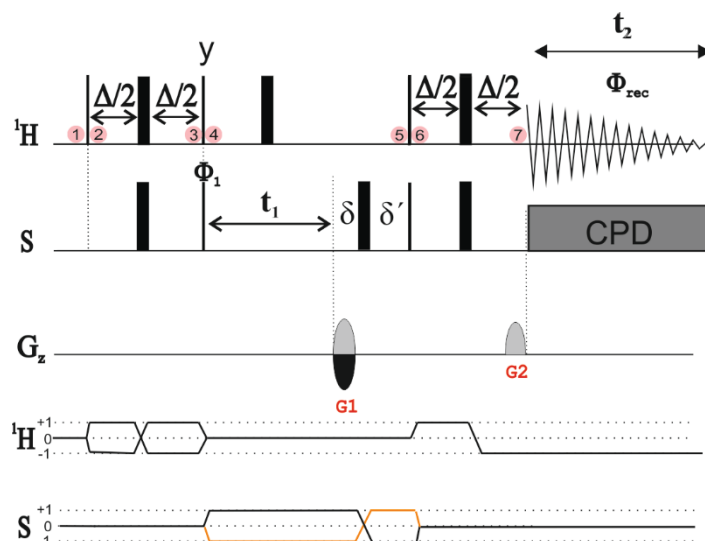


Figure 2: Schematic pulse sequence of the HSQC experiment. Black narrow and black wide rectangles represent ^1H and S, 90° and 180° hard pulses, respectively. S could be ^{13}C , ^{15}N , ^{19}F ... The t_1 period represents the variable delay, whereas t_2 represents the acquisition time where NMR data is acquired. The delay Δ corresponds to $0.5/{}^1J_{\text{XH}}$ (For $\text{X} = {}^{13}\text{C}$, ${}^1J_{\text{CH}}$ is usually set to 145 Hz and therefore $\Delta \approx 3.5$ ms) and δ represents the duration of a PFG. A basic two-step phase-cycle is applied: $\Phi_1 = (x, -x)$ and $\Phi_{\text{rec}} = (x, -x)$. The grey box (CPD) during the ^1H acquisition indicates the possibility to apply broadband heteronuclear X decoupling. Proper coherence selection is achieved by applying the gradients G1 and G2 using the E/A protocol. For $\text{S} = {}^{13}\text{C}$, G1 is set to 80% and G2 to 20.1%. In the CTP diagram, the orange line represents echo data (N-type magnetization) and the black line represents anti-echo data (P-type magnetization). Steps 1-7 are the points where product operators are commented on in the main text.

A basic analysis of the magnetization behaviour during the HSQC pulse sequence for an isolated heteronuclear two-spin ^1H -S spin system with a $^1J_{\text{HS}}$ coupling constant can be performed using the product operator formalism (see steps 1-7 in Figure 2). The starting point of any NMR experiment is at the Boltzmann equilibrium condition, \hat{H}_z (point 1). After the first 90° ^1H pulse, transverse ^1H magnetization is created (point 2):

$$\hat{H}_z \xrightarrow{\frac{\pi}{2}(\hat{H}_x)} -\hat{H}_y \quad (\text{Eq. 2})$$

Then, the magnetization evolution during the INEPT (Intensive Nuclei Enhanced by Polarization Transfer) block (point 2 to 3) under the unique effect of $^1J_{\text{HS}}$ must be considered because ^1H chemical shift effects are refocused at the end of the heteronuclear echo (the effects of passive J_{HH} are here also neglected).

$$\hat{H}_y \cos(\pi J_{\text{HS}}\Delta) - 2\hat{H}_x\hat{S}_z \sin(\pi J_{\text{HS}}\Delta) \quad (\text{Eq. 3})$$

At the beginning of the t_1 period (point 4), we have the following terms.

$$\text{Eq. 3} \xrightarrow{\frac{\pi}{2}\hat{H}_y} \hat{H}_y \cos(\pi J_{\text{HS}}\Delta) + 2\hat{H}_z\hat{S}_z \sin(\pi J_{\text{HS}}\Delta) \xrightarrow{\frac{\pi}{2}\hat{S}_x} \hat{H}_y \cos(\pi J_{\text{HS}}\Delta) - 2\hat{H}_z\hat{S}_y \sin(\pi J_{\text{HS}}\Delta) \quad (\text{Eq. 4})$$

Note that the first 90° H_y pulse produces zz -magnetization ($2\text{H}_z\text{S}_z$) and the subsequent 90° S_x pulse generates AP (Anti-Phase) magnetization for the S nucleus. During the t_1 period, a central decoupling 180° ^1H pulse is applied to avoid $^1J_{\text{SH}}$ evolution. Thus, during the t_1 evolution period only S chemical shift evolution must be considered (point 5) as well as of the dephasing effect caused by gradient G_1 . At the end of t_1 , the remaining active AP heteronuclear SQC (Single Quantum Coherence) components are:

$$\text{Eq. 4} \xrightarrow{t_1} 2\hat{H}_z\hat{S}_y \cos(\Omega_s t_1) \sin(\pi J_{\text{HS}}\Delta) - 2\hat{H}_z\hat{S}_x \sin(\Omega_s t_1) \sin(\pi J_{\text{HS}}\Delta) \quad (\text{Eq. 5})$$

For a better understanding of the PFG role, eq. 5 must be written using shift operators^{11, 12}:

$$\frac{1}{i} \hat{H}_z(S^+ + S^-) \cos(\Omega_s t_1) \sin(\pi J_{HS} \Delta) - \hat{H}_z(S^+ + S^-) \sin(\Omega_s t_1) \sin(\pi J_{HS} \Delta) \text{ (Eq. 6)}$$

The coherence selection using PFGs in HSQC improves the distinction between the unwanted ^1H - ^{12}C (about 99% at natural abundance) and the chosen ^1H - ^{13}C (only about 1%) magnetization, strongly enhancing the spectral quality by reducing artefacts and also, very importantly, reducing the number of phase cycles steps and therefore minimizing the required experimental time for data recording. In the HSQC scheme, G_1 is strategically placed during the t_1 period for selecting a specific SQC for ^{13}C whereas G_2 selects ^1H coherence before the t_2 acquisition time. When PFG's are applied during a variable t_1 period, signals are phase modulated (S^+ , echo or S^- , anti-echo). That means during P-type data selection (anti-echo) the frequency modulation has the same sense in both periods (t_1 and t_2), and in the N-type data (echo) the frequency modulation has an opposite sense for each period¹³. However, amplitude-modulated data is required to obtain pure absorption spectra and therefore the E/A (Echo/Antiecho) protocol for data acquisition and data processing is usually applied¹⁴. During each scan only one CTP can be selected according to the predefined gradient ratios and the refocusing condition: $\frac{G_1}{G_2} = \frac{\gamma_1}{\gamma_2}$. Thus, for HSQC, $\frac{G_1}{G_2} = \frac{\gamma_H}{\gamma_C} = 4$

¹¹ O. W. Sørensen, G. W. Eich, M. H. Levitt, G. Bodenhausen, and R. R. Ernst, "Product operator formalism for the description of NMR pulse experiments", *Progress in Nuclear Magnetic Resonance Spectroscopy*. 16:163–192. 1984.

¹² To describe the effect of PFG, cartesian operators H_x and H_y should be converted to terms of raising and lowering operators for an easier understanding:

$$\begin{aligned} H^+ &= H_x + iH_y & H^- &= H_x - iH_y \\ H_x &= \frac{1}{2}(H^+ + H^-) & H_y &= \frac{1}{2i}(H^+ - H^-) \end{aligned}$$

¹³ Expressions for the sense of magnetization due to echo or anti-echo approach:

$$\begin{aligned} S(t_1, t_2)_{anti-echo} &= \gamma e^{i\Omega_s t_1} e^{i\Omega_s t_2} \\ S(t_1, t_2)_{echo} &= \gamma e^{-i\Omega_s t_1} e^{i\Omega_s t_2} \end{aligned}$$

¹⁴ J. Keeler and D. Neuhaus, "Comparison and evaluation of methods for two-dimensional NMR spectra with absorption-mode lineshapes". *J. Magn. Reson.*, 63(3):454–472. 1985.

for P-type coherence and $\frac{G_1}{G_2} = \frac{\gamma_H}{\gamma_C} = -4$ for N-type coherence. Typical values for G_1 and G_2 (in percentage) in gradient-selected ^1H - ^{13}C HSQC are $\pm 80:20.1$.

At point 6, after the application of simultaneous 90° pulses on H and S from the x-axis, the following magnetization components are recovered:

$$\text{Eq 5} \xrightarrow{\begin{matrix} \frac{\pi}{2} \hat{H}_x \\ \frac{\pi}{2} \hat{S}_x \end{matrix}} \begin{matrix} -2\hat{H}_y\hat{S}_z \cos(\Omega_s t_1) \sin(\pi J_{HS}\Delta) \\ +2\hat{H}_y\hat{S}_x \sin(\Omega_s t_1) \sin(\pi J_{HS}\Delta) \end{matrix} \quad (\text{Eq. 7})$$

The second term represents Multiple Quantum Coherences (MQCs) and can be omitted for simplicity, although that is highly relevant to understand the sensitivity enhancement related to the HSQC-PEP (Preservation of Equivalent Pathways) experiment¹⁵. The first term evolves during the final retro-INEPT period under the effect of $^1J_{\text{SH}}$ (point 7):

$$\begin{aligned} & -2\hat{H}_y\hat{S}_z \cos(\Omega_s t_1) \cos(\pi J_{HS}\Delta) \sin(\pi J_{HS}\Delta) \\ & + \hat{H}_x \cos(\Omega_s t_1) \sin^2(\pi J_{HS}\Delta) \end{aligned} \quad (\text{Eq. 8})$$

In principle, the detected signal is a mixture of the two IP (In-Phase) and AP components. In the case to apply CPD (Composite Programmed Decoupling) during acquisition, the AP term is cancelled out.

The basic HSQC pulse scheme has been vastly modified throughout the years which have improved its general application and performance under different experimental conditions. Very useful versions of modified HSQC experiments are: i) multiplicity-edited HSQC to distinguish between CH/CH₃ (up) from CH₂ (down) signals¹⁶; ii) sensitivity-enhanced HSQC (HSQC-PEP)

¹⁵ L. Kay, P. Keifer, and T. Saarinen, "Pure absorption gradient enhanced heteronuclear single quantum correlation spectroscopy with improved sensitivity", *J. Am. Chem. Soc.*, 114(26):10663–10665. 1992.

¹⁶ D. G. Davis, "Improved multiplet editing of proton-detected, heteronuclear shift-correlation spectra", *J. Magn. Reson.*, 91(3):665–672. 1991.

to increase the sensitivity for CH cross-peaks¹⁵; iii) use of adiabatic 180° ¹³C pulses to improve the inversion and refocusing effects of the hard 180° ¹³C pulses¹⁷; iv) use of purging gradients during the INEPT/retroINEPT periods to improve the echo performance¹⁸; v) use of purging gradients during the zz-filter¹⁹; vi) use of water-selective pulses to remove the strong solvent signal when working with aqueous solutions²⁰, vii) removing the central 180° ¹H pulse during the t₁ period or CPD during acquisition for the measurement of ¹J_{CH} coupling values²¹. In addition, the basic HSQC pulse scheme is used in more complex experiments such as HSQC-TOCSY, HSQMBC (both will be explained in next chapters), ADEQUATE and most of the 3D/4D experiments designed for proteins and nucleic acids ^{22, 23}.

2.2.1. ¹H-¹³C HSQC-PEP experiment

Since the introduction of PFG, the HSQC pulse scheme has been improved with several modifications such as the incorporation of a second refocused INEPT block. This HSQC-PEP pulse scheme, illustrated in Figure 3, achieves an improvement of sensitivity given by a factor of $\sqrt{2}$ only for HS spin systems¹⁵.

¹⁷ Bendall MR, Garwood M, Uğurbil K, and Pegg DT. "Adiabatic refocusing pulse which compensates for variable rf power and off-resonance effects". *Magn Reson Med*, 4(5):493-9. 1987.

¹⁸ A. G. Palmer, J. Cavanagh, P. E. Wright, and M. Rance, "Sensitivity improvement in proton-detected two-dimensional heteronuclear correlation NMR spectroscopy", *J. Magn. Reson.*, 93(1):151–170. 1991.

¹⁹ A. L. Davis, G. Estcourt, J. Keeler, and J. J. Titman, "Improvement of z Filters and Purging Pulses by the Use of Zero-Quantum Dephasing in Inhomogeneous B1 or B0 Fields", *J. Magn. Reson. Ser. A*, 105(2):167–183. 1993.

²⁰ R. J. Ogg, P. B. Kingsley, and J. S. Taylor, "WET, a T1- and B1-Insensitive Water-Suppression Method for in Vivo Localized ¹H NMR Spectroscopy", *J. Magn. Reson. Ser. B*, 104(1):1–10. 1994.

²¹ W. P. Aue, J. Karhan, and R. R. Ernst, "Homonuclear broad band decoupling and two-dimensional J-resolved NMR spectroscopy", *J. Chem. Phys.* 64:4226. 1976.

²² B. Reif, M. Köck, R. Kerssebaum, H. Kang, W. Fenical, and C. Griesinger, "ADEQUATE, a New Set of Experiments to Determine the Constitution of Small Molecules at Natural Abundance", *J. Magn. Reson. Ser. A*, 118:282-285. 1996.

²³ J. P. Marino, H. Schwalbe, C. Anklin, W. Bermel, D. M. Crothers, and C. Griesinger, "Sequential correlation of anomeric ribose protons and intervening phosphorus in RNA oligonucleotides by a ¹H, ¹³C, ³¹P triple resonance experiment: HCP-CCH-TOCSY", *J. Biomol NMR*. 5(1):87-92. 1995.

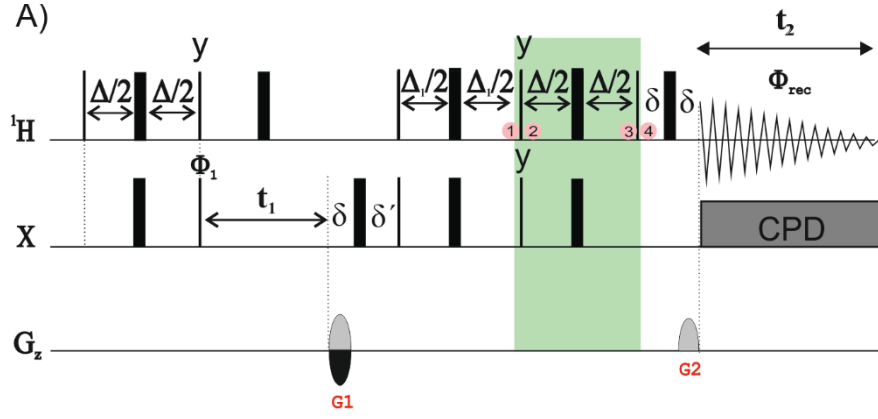


Figure 3: Pulse scheme of the HSQC-PEP experiment derived from the scheme of Figure 2. The highlighted green box represents the addition of a PEP building block.

The magnetization follows the same evolution as described for the regular HSQC scheme, where two terms as resulting of Eq. 7 contribute to the final detected signal. The addition of the second retroINEPT is designed to convert the MQC term into AP magnetization ($2\hat{H}_{1y}\hat{S}_z$), while \hat{H}_x (IP) term flips along the z -axis (\hat{H}_z) (point 2). After the second INEPT evolution, the $2\hat{H}_{1y}\hat{S}_z$ the term is converted to transverse magnetization (\hat{H}_x), whereas \hat{H}_z remains unaltered (point 3). A final 90° ^1H , which only affects Term II, flips the z -magnetization into the transverse plane (\hat{H}_y). The mixture of \hat{H}_x and \hat{H}_y IP terms at the end of the sequence achieve a signal sensitivity enhancement by 41% for HS spin systems.

The HSQC-TOCSY experiment is a hybrid experiment in where a homonuclear ^1H - ^1H TOCSY transfer is added before acquisition of the HSQC sequence (Figure 3), providing direct and relayed heteronuclear correlations. The HSQC-TOCSY experiment can also be improved by the incorporation of a PEP building block (HSQC-PEP-TOCSY scheme is illustrated in Figure 4) which also reaches enhanced sensitivity by a factor of $\sqrt{2}$ for CH spin systems. Coupled versions

of the HSQC-TOCSY experiment are very useful to extract the magnitude and the sign of small heteronuclear coupling constants for protonated heteronuclei²⁴.

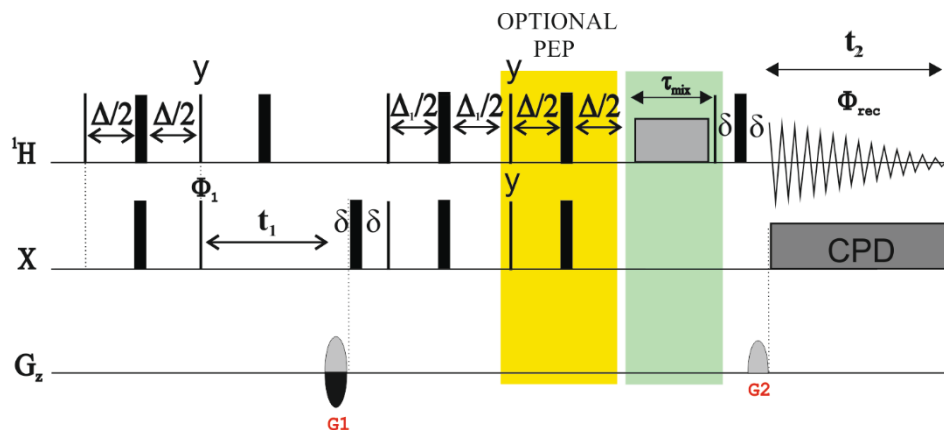


Figure 4: Schematic pulse sequence of the HSQC-TOCSY experiment (with optional PEP module highlighted in yellow) derived from the scheme of Figure 2. The highlighted green box represents the addition of a TOCSY building block as a homonuclear mixing time.

2.3. Pure-Shift NMR

The lack of enough ^1H spectral resolution, typically found in complex NMR spectra, is usually produced because of the small chemical shift dispersion. The possibility to remove the scalar coupling multiplicities by homodecoupling opens new opportunities for the analysis and interpretation of complex proton NMR spectra, making possible the elucidation of challenging chemical structures and the analysis of complex mixtures. In the early beginning, Bloch suggested

²⁴ S. Subramanian and A. Bax, "Generation of pure phase NMR subspectra for measurement of homonuclear coupling constants" *J. Magn. Reson.*, 71(2):325–330. 1987.

that the use of a double-irradiation experiment could simplify multiplet analysis^{25, 26}. This method was improved using multiple selective irradiations on more than one signal or selecting regions with multiple signals which were irradiated at the same time^{27, 28, 29}. These selective approaches are effective for simple cases but in general, broadband homodecoupling methods have been persecuted insistently to provide full ^1H NMR spectra with complete suppression of all J -splitting, the so-called pure-shift (PS) NMR spectra (Figure 5)³⁰.

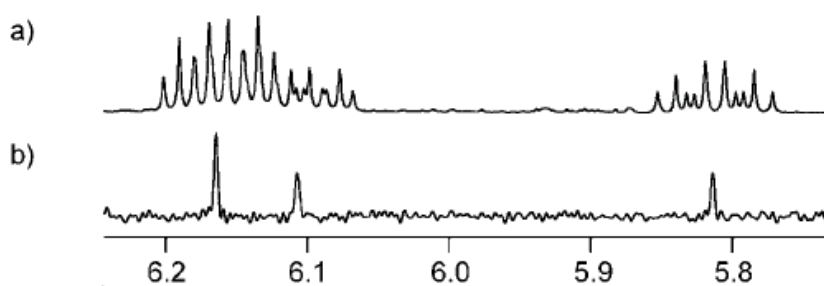


Figure 5: Comparison between a) conventional and b) pure-shift ^1H NMR spectra of a sample of calix[4]arenes acquired with the ZS pulse sequence shown in Figure 8. The Figure is taken from reference [30].

Modern broadband homodecoupling methods involve different selective refocusing elements (Figure 6): (A) $^{12}\text{C}/^{13}\text{C}$ BIRD-based clusters, (B-D) homonuclear frequency-selective elements (HOBS), (E-G) slice-selective elements consisting of simultaneous selective elements and gradients, or (G) the PSYCHE block consisting of simultaneous application of adiabatic pulses and weak phase encoding gradients. The homodecoupling effects are achieved by combining the

²⁵ F. Bloch and A. Siegert, "Magnetic Resonance for Nonrotating Fields" *Phys. Rev.* 57:522. 1940.

²⁶ W. A. Anderson and R. Freeman, "Influence of a Second Radiofrequency Field on High-Resolution Nuclear Magnetic Resonance Spectra", *J. Chem. Phys.* 37:85. 1962.

²⁷ R. Freeman and W. A. Anderson, "Use of weak perturbing radio-frequency fields in nuclear magnetic double resonance," *J. Chem. Phys.*, 37(9):2053-2073. 1962.

²⁸ A. P. D. M. Espindola, R. Crouch, J. R. DeBergh, J. M. Ready, and J. B. MacMillan, "Deconvolution of complex NMR spectra in small molecules by multi frequency homonuclear decoupling (MDEC)" *J. Am. Chem. Soc.*, 131(44):15994-15995. 2009.

²⁹ E. Kupce and R. Freeman, "Band-Selective Decoupling", *J. Magn. Reson. Ser. A*, 102(3):364-369. 1993.

³⁰ J. A. Aguilar, S. Faulkner, M. Nilsson, and G. A. Morris, "Pure Shift ^1H NMR: A resolution of the resolution problem?" *Angew. Chemie - Int. Ed.*, 49, 3901-3903. 2010.

broadband inversion by a non-selective 180° ^1H pulse and a selective refocusing element described before^{31, 32}.

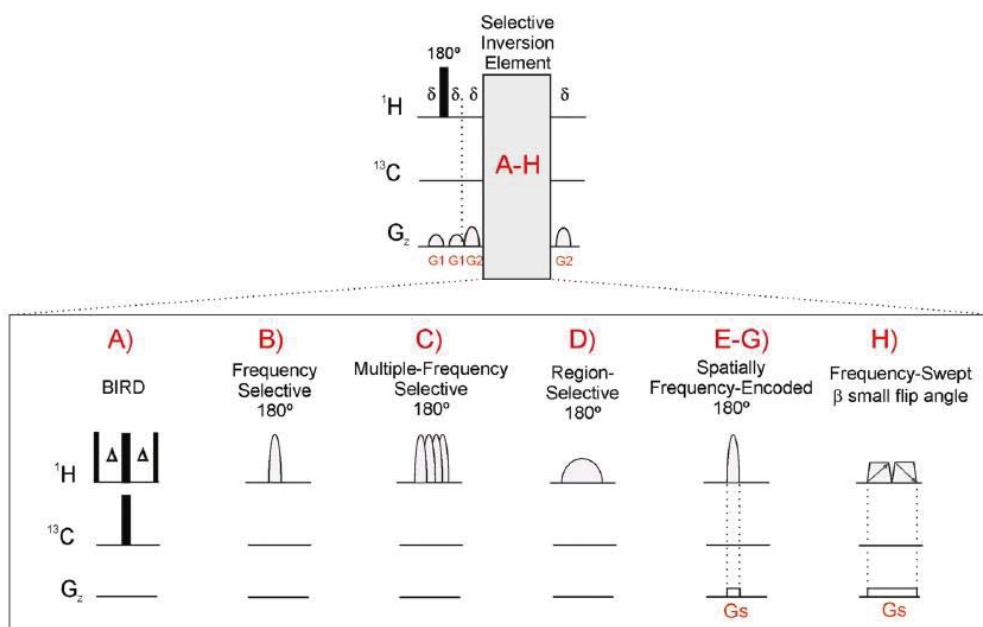


Figure 6: General scheme of the PS refocusing element using a selective inversion element. (Figure extracted from Reference [10]).

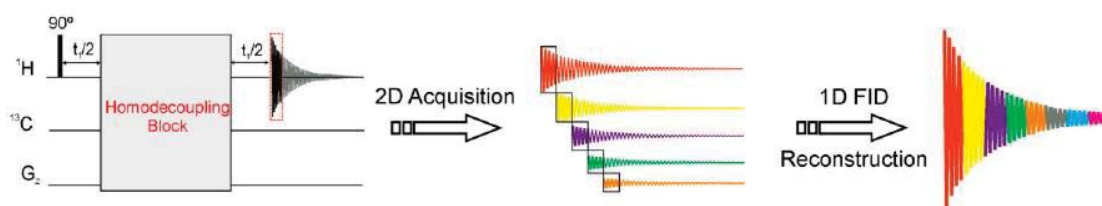
Two main acquisition schemes have been developed to obtain broadband homodecoupled ^1H spectra (Figure 7). The interferogram-based acquisition mode is a pseudo-2D method based on the obtention of a re-constructed FID from data chunks extracted from 2D serials (Figure 7A). On the other hand, real-time homodecoupled data can be directly recorded by including homodecoupling elements into the FID period (Figure 7B)¹⁰. The original ZS (Figure 8) used the acquisition method of Figure 7A and the inversion element described in Figure 6G³³.

³¹ L. Castañar, "Pure shift ^1H NMR: what is next?" *Magn. Reson. Chem.*, 55: 47– 53. 2017.

³² R. W. Adams, "Pure Shift NMR Spectroscopy". *eMagRes*, 3:1-15. 2014.

³³ K. Zangger and H. Sterk, "Homonuclear Broadband-Decoupled NMR Spectra", *J. Magn. Reson. Ser. A*, 124(2), 486–489. 1997.

A) Pseudo-2D ZS Experiment



B) Real-time ZS Experiment

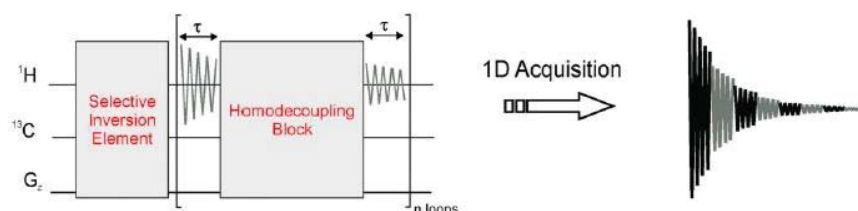


Figure 7: A) Interferogram-based and B) real-time acquisition modes pure-shift NMR experiments (Figure extracted from Reference [10]).

In most cases, pure-shift NMR techniques are related to time-consuming, longer acquisition times and a severe loss of SNR. To enhance sensitivity and improve automation, the PSYCHE experiment has now become the best choice to obtain a PS ^1H NMR spectrum³⁴. The key point of the PSYCHE element is the simultaneous application of a weak rectangular gradient and low-flip angle (β) swept-frequency pulses as a selective refocusing element in the original ZS experiment. As a rule of thumb, the PSYCHE element (Figure 8) can be incorporated in most of the conventional 2D homonuclear and heteronuclear experiments to afford pure-shift 2D NMR spectra^{35, 36, 34}.

³⁴ M. Foroozandeh, R. W. Adams, N. J. Meharry, D. Jeannerat, M. Nilsson, and G. A. Morris, "Ultrahigh-resolution NMR spectroscopy", *Angew. Chemie - Int. Ed.*, (53)27:6990-6992. 2014.

³⁵ M. Foroozandeh, R. W. Adams, P. Kiraly, M. Nilsson, and G. A. Morris, "Measuring couplings in crowded NMR spectra: Pure shift NMR with multiplet analysis," *Chem. Commun.*, 51(84):15410–15413. 2015.

³⁶ M. Foroozandeh, G. A. Morris, and M. Nilsson, "PSYCHE Pure Shift NMR Spectroscopy", *Chem. Eur. J.*, 24:13988-14000. 2018.

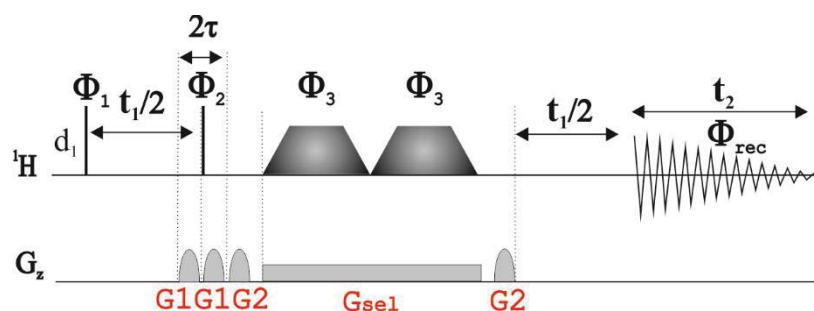


Figure 8: Pulse scheme of the PSYCHE 1D ^1H -NMR pulse sequence where trapezoids shapes represent low-power saltire pulses of nominal flip angle $<90^\circ$. d_1 is the relaxation delay (1s), the delay t_1 is the incremented evolution time in the 2D acquisition mode, and $t_2=1/\text{SW1}$ (where SW1 is the width of F1). G1 corresponds to 77% and, G2 to 42%, whereas G_{sel} is the spatial encoding PSYCHE gradient.

The real-time Homodecoupled Band-Selective (HOBS) approach does not suffer from a sensitivity penalty, but it is limited to a specific number of resonances³⁷. HOBS has been incorporated into many 1D and 2D NMR experiments, as into the HSQMBC experiment to detect and quantify long-range heteronuclear correlations³⁸ or to increase the spectral resolution in spectral-aliased HSQC spectra³⁹. On the other hand, the incorporation of HOBS into the CPMG experiment has been crucial to reaching T_1/T_2 relaxation times measurements from crowded areas⁴⁰.

³⁷ L. Castañar, P. Nolis, A. Virgili, T. Parella, "Full sensitivity, and enhanced resolution in homodecoupled band-selective NMR experiments". *Chemistry*, 16;19(51):17283-6. 2013.

³⁸ L. Castañar, J. Sauri, P. Nolis, A. Virgili, T. Parella, "Implementing homo- and heterodecoupling in region-selective HSQMBC experiments". *J. Magn. Reson*, 238:63-69. 2014.

³⁹ L. Castañar, r. Roldán, P. Clapés, A. Virgili, T. and Parella, "Disentangling Complex Mixtures of Compounds with Near-Identical ^1H and ^{13}C NMR Spectra using Pure Shift NMR Spectroscopy". *Chem. Eur. J.*, 21:7682-7685. 2015.

⁴⁰ L. Castañar, P. Nolis, A. Virgili, T. Parella, "Measurement of T_1/T_2 relaxation times in overlapped regions from homodecoupled ^1H singlet signals". *J. Magn. Reson*, 244:30-35. 2014.

2.3.1. Pure-Shift HSQC

Inversion and refocusing BIRD elements were developed to invert selectively ^1H - ^{12}C from ^1H - ^{13}C magnetization, or vice versa⁴¹. BIRD clusters have been extensively implemented in a multitude of heteronuclear NMR pulse sequences. As an example, the pure-shift HSQC experiment incorporates real-time BIRD-based homodecoupling⁴² that combines a BIRD element and a hard 180° pulse for selecting ^1H - ^{13}C magnetization and remove all homonuclear ^1H - ^{13}C - ^{12}C - ^1H couplings (Figure 9 (bottom)). The benefits of this approach can be observed by comparing the conventional and the PS-HSQC spectra (Figure 9 (top)). This experiment provides excellent results in terms of sensitivity and better signal resolution⁴³. Due to the HSQC scheme acts as an efficient isotope filter, the real-time BIRD decoupling does not affect the overall sensitivity of the experiment. Linewidths can be slightly broader, but signal collapse usually compensates for such drawbacks. As a limitation, the experiment does not eliminate the geminal $^2J_{\text{HH}}$ splitting in methylene CH_2 cross-peaks.

⁴¹ J. R. Garbow, D. P. Weitekamp, and A. Pines, "Bilinear rotation decoupling of homonuclear scalar interactions", *Chem. Phys. Lett.*, 93(5):504-509. 1982.

⁴² A. Bax, "Broadband homonuclear decoupling in heteronuclear shift correlation NMR spectroscopy", *J. Magn. Reson.* 53: 517–520. 1983.

⁴³ L. Paudel, R.W. Adams, P. Király, J.A. Aguilar, M. Foroozandeh, M.J. Cliff, M. Nilsson, P. Sándor, J. P. Waltho, G.A. Morris, "Simultaneously enhancing spectral resolution and sensitivity in heteronuclear correlation NMR spectroscopy", *Angew Chem Int Ed Engl.* 25;52(44):11616-9. 2013.

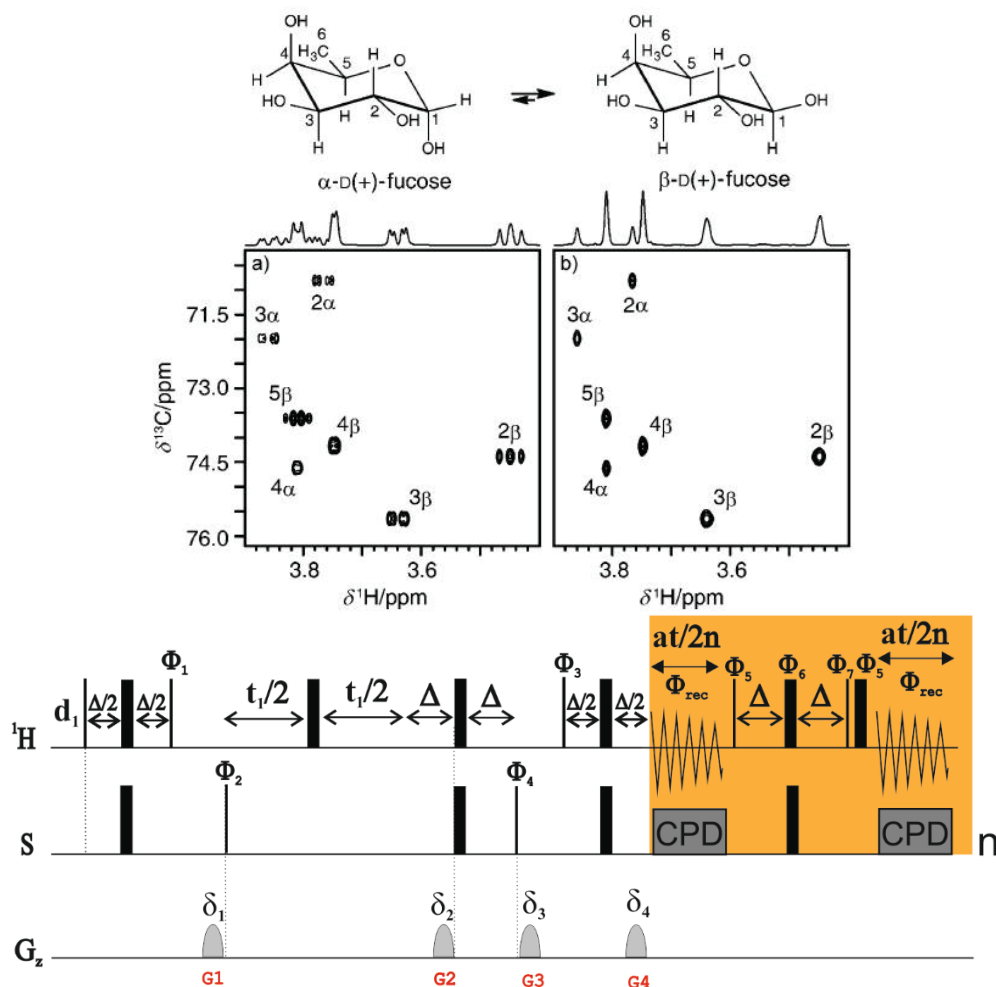


Figure 9: (Bottom) Pulse scheme of the pure-shift HSQC experiment, where the orange box is the final BIRD-based homodecoupled FID period. (Top) Comparison between the conventional HSQC (left) and the pure-shift HSQC (right) spectra of (+)-fucose in D_2O . Figure extracted from reference [43].

The homodecoupled real-time BIRD-based element included during the FID period has been also integrated into a wide family of HSQC-based experiments, such as the CLIP/CLAP HSQC⁴⁴ or the J -resolved HSQC⁴⁵ experiments for measuring $^1J_{\text{CH}}$ and/or residual dipolar couplings (RDCs), providing important information about molecules dissolved in anisotropic media. BIRD

⁴⁴ I. Timári *et al.*, “Real-time broadband proton-homodecoupled CLIP/CLAP-HSQC for automated measurement of heteronuclear one-bond coupling constants”. *RSC Adv.*, 6:87848-87855. 2016.

⁴⁵ K. Zangger, “Pure shift NMR”. *Progress in Nuclear Magnetic Resonance Spectroscopy*, 86–87:1–20. 2015.

homodecoupling has also been implemented into ADEQUATE which provides essential carbon-carbon structural information. 1,n-HD-ADEQUATE is a robust experiment to assign non-protonated centres where other NMR experiments such as LR-HSQMBC could fail⁴⁶. The complementary addition of NUS enhancement has been also applied to pure-shift *J*-modulated ADEQUATE experiments to measure J_{CC} coupling constants^{47, 48}.

2.4. Long-Range ^1H - ^{13}C Correlation NMR Experiments

2.4.1. ^1H - ^{13}C -HMBC experiment

The ^1H - ^{13}C HMBC experiment has become one of the most important routine NMR experiments for chemists due to its feasibility and versatility. Highly important is that both protonated and non-protonated carbon centres can be determined and assigned. The HMBC pulse scheme can be understood as a non-refocused HMQC pulse sequence, without ^{13}C decoupling during proton acquisition, where the interpulse delay is optimized to small $^nJ_{CH}$ values (Figure 10A). 2D HMBC spectra usually show the correlation between heteronuclei separated by two- and three-bonds. Signal intensities depend on the relationship between the active $^nJ_{CH}$ value and the interpulse delay optimization. Thus, an HMBC spectrum informs us on which carbons are two-bonds or three-bonds away from the protons, and vice-versa (Figure 10B).

⁴⁶ J. Saurí, W. Bermel, A. V. Buevich, E. C. Sherer, L. A. Joyce, M. H. M. Sharaf, P. L. Schiff, T. Parella, R.T. Williamson, and G.E. Martin, “Homodecoupled 1,1- and 1,n-ADEQUATE: Pivotal NMR Experiments for the Structure Revision of Cryptospirolepine”. *Angew. Chem. Int. Ed.*, 54:10160-10164. 2015.

⁴⁷ J. Saurí, T. Parella, R. T. Williamson, and G. E. Martin, “Improving the performance of *J*-modulated ADEQUATE experiments through homonuclear decoupling and non-uniform sampling”, *Magn. Reson. Chem.*, 55:191– 197. 2017.

⁴⁸ J. Saurí, W. Bermel, T. Parella, R. T. Williamson, G. E. Martin, “Incorporating BIRD-based homodecoupling in the dual-optimized, inverted $^1J_{CC}$ 1,n-ADEQUATE experiment”. *Magn Reson Chem.* 56:1029– 1036. 2018.

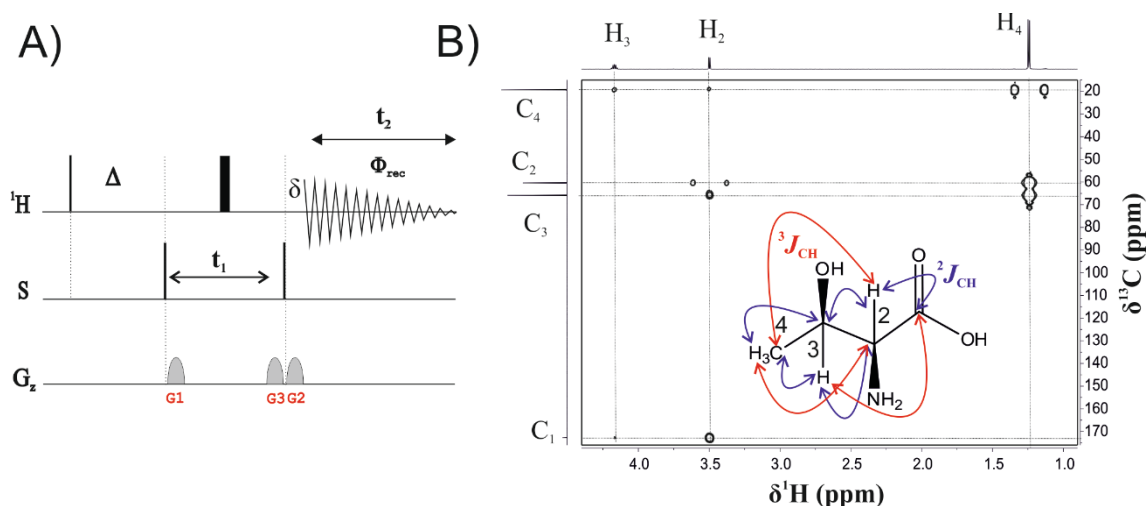


Figure 10: A) Schematic pulse sequence of the HMBC experiment, where G1:G2:G3 correspond to 50:30:20, and the delay Δ is adjusted to $0.5/{}^nJ_{\text{XH}}$ (For $\text{X} = {}^{13}\text{C}$, ${}^nJ_{\text{CH}}$ is usually set to 8 Hz and therefore $\Delta \approx 65$ ms), and B) 8-Hz optimized 2D HMBC spectrum of threonine in D_2O , where several peaks show correlations of each carbon with its neighbouring protons. The spectrum shows how H_2 is correlated with C_4 , C_3 and C_1 , H_3 with C_4 and C_1 , and H_4 with C_2 and C_3 .

The correct analysis and interpretation of the HMBC spectrum must be carefully made. Some expected signals can present minimum intensity or are not detected because signal intensities in HMBC experiments depend on $\sin^2(\pi J_{\text{HS}}\Delta) \exp\left(-\Delta/T_2\right)$, which means that null points can be achieved for coupling adjusted to $\kappa * J^{\text{opt}}$, where κ is an even number, J^{opt} is the mentioned long-range coupling constant value (${}^nJ_{\text{XH}}$) and Δ is set to $0.5/{}^nJ_{\text{XH}}$. In these simple relationships, the important effect of J_{HH} is omitted. However, the effect of J_{HH} is very important in the HMBC experiment, since the signals detected present an AP character concerning the ${}^nJ_{\text{CH}}$ and mixed-phase to the passive J_{HH} that can produce accidental signal cancellation.

A priori, no distinction between two from three bonds connectivities can be made from the analysis of an HMBC spectrum. For protonated carbons, this distinction can be accomplished from an alternative HMQC-COSY or H2BC experiment. For non-protonated carbons, two-bond connectivities can be established from a more insensitive 1,1-ADEQUATE experiment.

2.4.2. ^1H - ^{13}C HSQMBC experiment

The HSQMBC pulse scheme is equivalent to the HMBC discussed previously, and it can be understood as a non-refocused HSQC pulse sequence, without decoupling during proton acquisition and where the interpulse Δ delay is optimized to smaller $^nJ_{\text{CH}}$ values (Figure 11A). In general, HMBC tends to have more sensitivity than HSQMBC, but HSQMBC allows better control of the flux of magnetization (SQC are always involved) and cross-peaks present a better J -coupling pattern. The analysis by product operator formalism of the HSQMBC scheme is very similar to the HSQC experiment. The main differences rely on the delay Δ of the INEPT building block that is optimised to long-range correlations ($^nJ_{\text{CH}}$), and the omission of the refocused INEPT period. Both J_{HH} and $^nJ_{\text{CH}}$ evolve simultaneously during the initial INEPT block which generates mixtures of AP and IP magnetization components⁴⁹. The impact on the effects of J_{HH} in HSQMBC has been extensively studied and discussed in the manuscripts (section 4.5. and 4.6.) of this thesis, Figure 11B illustrates an example of HSQMBC spectrum of tryptophan in D_2O .

According to a heteronuclear three spin system $\text{H}_1\text{H}_2\text{S}$ with $^nJ_{\text{H}_1\text{S}}$, and $J_{\text{H}_1\text{H}_2}$, and $^nJ_{\text{H}_2\text{S}} = 0$, the observable magnetization term just before the acquisition is defined by:

$$-2\hat{H}_{1y}\hat{S}_z \cos(\pi J_{\text{H}_1\text{H}_2}\Delta) \sin(\pi ^nJ_{\text{H}_1\text{S}}\Delta) \quad (\text{Eq. 9})$$

⁴⁹ R.T. Williamson, B. L. Márquez, W. H. Gerwick, and K.E. Kövér, "One- and two-dimensional gradient-selected HSQMBC NMR experiments for the efficient analysis of long-range heteronuclear coupling constants". *Magn. Reson. Chem.*, 38: 265-273. 2000.

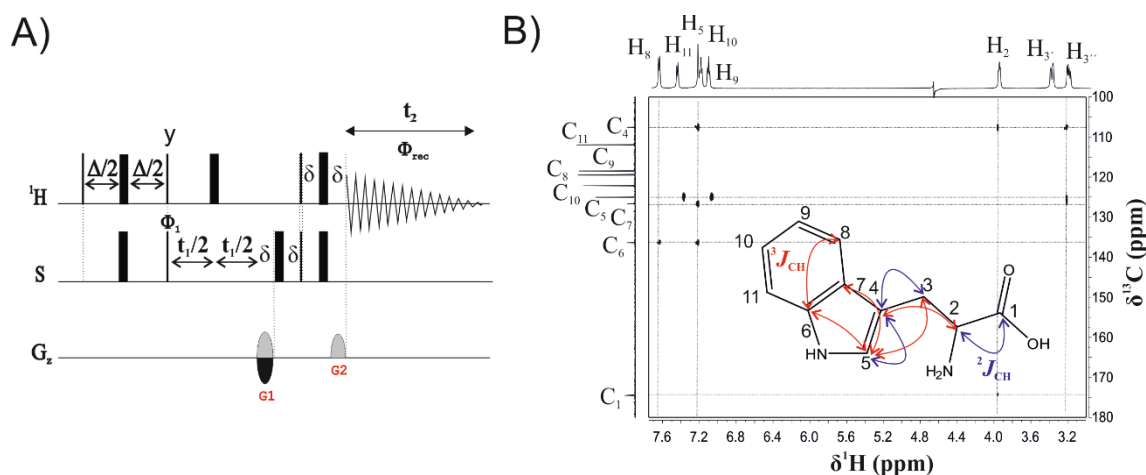


Figure 11: A) Schematic pulse sequence of HSQMBC experiment. B) HSQMBC spectrum of L-tryptophan in D_2O , where several peaks show correlations of each carbon with the neighbouring protons. To show the long-range correlations, arrows on the spectrum indicates how H₅ is correlated with C₄ ($^2J_{\text{CH}}$), C₆ ($^3J_{\text{CH}}$), and with C₇ ($^3J_{\text{CH}}$); H₂ with C₄ ($^3J_{\text{CH}}$), and with C₁ ($^2J_{\text{CH}}$); H₃ with C₄ ($^2J_{\text{CH}}$), and with C₅ ($^2J_{\text{CH}}$); and H₈ with C₆ ($^3J_{\text{CH}}$).

2.4.2.1. LR-HSQMBC

The long-range version of the HSQMBC experiment (the 2D ^1H - ^{13}C LR-HSQMBC experiment)⁵⁰ can solve some limitations of the HSQMBC and HMBC-type experiments, which is the detection of connectivities corresponding to small heteronuclear long-range coupling constants with values below 2-3 Hz, most of them corresponding to heteronuclear correlations to four-, five- or even six-bonds away.

⁵⁰ R. Thomas Williamson, A. V. Buevich, G. E. Martin, and T. Parella, "LR-HSQMBC: A Sensitive NMR Technique To Probe Very Long-Range Heteronuclear Coupling Pathways". *J. Org. Chem.*, 79(9):3887–3894. 2014.

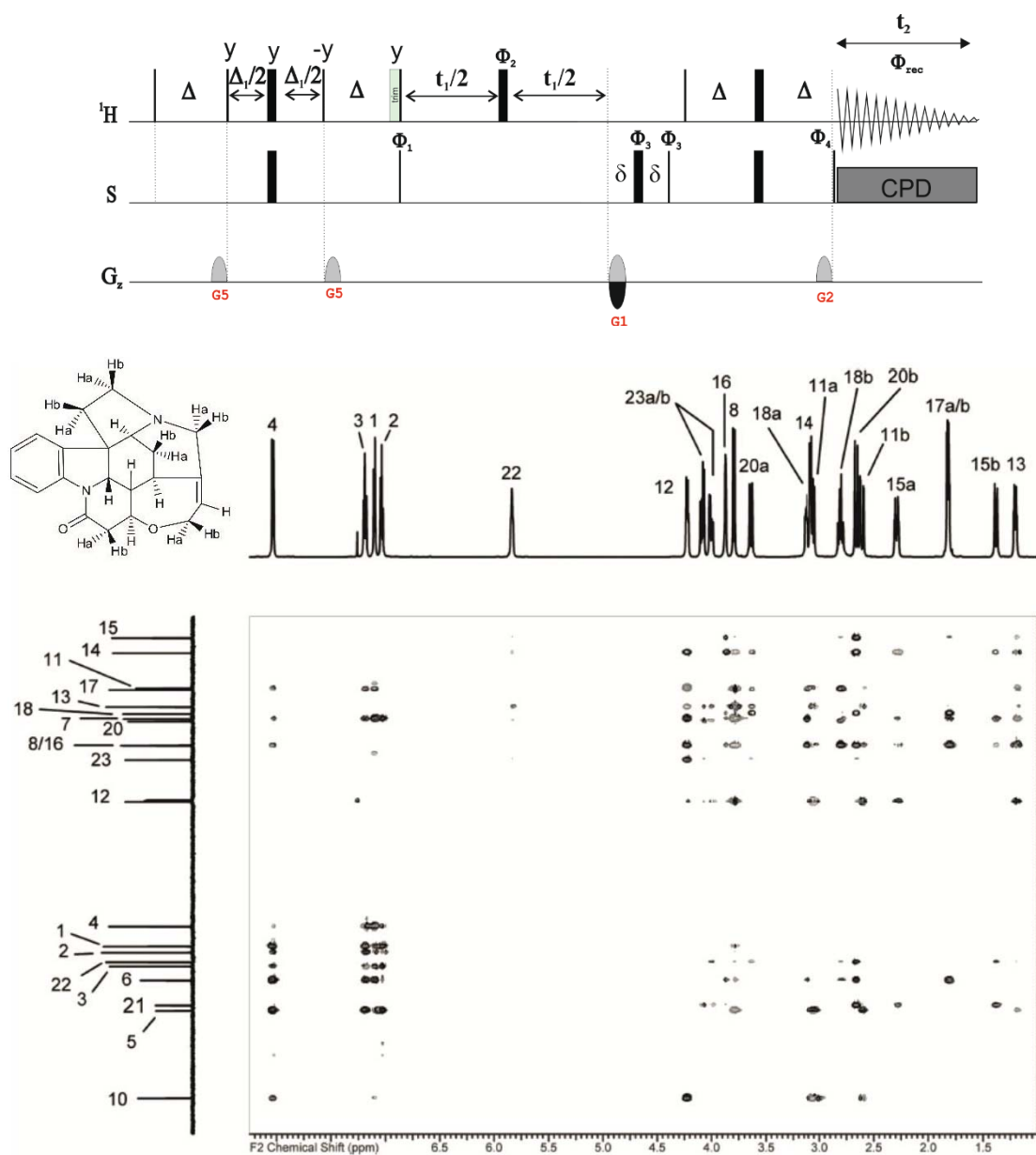


Figure 12: Pulse sequence of 2D LR-HSQMBC experiment (top). LR-HSQMBC spectrum (bottom) of strychnine optimized to $^nJ_{\text{CH}} = 2$ Hz (extracted from reference [50]).

The pulse sequence of the LR-HSQMBC experiment (Figure 12 (top)), is based on a G-BIRD_{R,X}-HSQMBC scheme optimized to analyse long-range correlations, but uses a refocusing period to avoid AP contributions due to $^nJ_{\text{CH}}$. Such contributions are particularly negative for small $^nJ_{\text{CH}}$ of the same order as the linewidth because can produce signal cancellation and therefore preventing cross-peak observation. The LR-HSQMBC spectrum of strychnine

optimized to ${}^nJ_{\text{CH}}$ 2 Hz (Figure 12 (bottom)) reveals a greater number of correlations than traditional HMBC and HSQMBC optimized to ${}^nJ_{\text{CH}}$ 8 Hz. An alternative experiment to detect ultra-long-range correlations should be the HSQMBC-COSY and HSQMBC-TOCSY experiments⁵¹ that can be understood as the long-range versions of the HSQC-COSY and HSQC-TOCSY experiments, respectively.

2.4.2.2. Frequency-Selective HSQMBC experiments

The ${}^1\text{H}$ frequency-selective version of the refocused HSQMBC experiment (selHSQMBC) is a straightforward method to measure small long-range proton-carbon coupling constants with high accuracy. The main difference concerning HSQMBC is the replacement of 180° hard ${}^1\text{H}$ pulses by 180° frequency-selective pulses during the INEPT block which produces a selective heteronuclear propagation between a proton with all their coupled heteronuclei. The method avoids any unwanted phase and amplitude signal modulation due to passive J_{HH} coupling constants and therefore can afford pure in-phase multiplets where the extraction of ${}^nJ_{\text{CH}}$ values can be performed by direct multiplet analysis (see Figure 13 (right)).^{52, 53, 54}

In complex multiplet patterns, accurate analysis of ${}^nJ_{\text{CH}}$ values can be made by comparing α/β cross-peaks as a result of the addition and subtraction of IP/AP data which are acquired following the same pulse scheme but changing a pulse phase and omitting the last ${}^{13}\text{C}$ 180° hard pulse (highlighted in red, Figure 13 (left)).

⁵¹ J. Saurí, T. and Parella, “Efficient measurement of the sign and the magnitude of long-range proton-carbon coupling constants from a spin-state-selective HSQMBC-COSY experiment”. *Magn. Reson. Chem.*, 50:717-721. 2012.

⁵² S. Gil, J. F. Espinosa, and T. Parella, “Accurate measurement of small heteronuclear coupling constants from pure-phase α/β HSQMBC cross-peaks” *J. Magn. Reson.* 213(1):145–150. 2011.

⁵³ J. F. Espinosa, P. Vidal, T. Parella, S. Gil. “Measurement of long-range proton–carbon coupling constants from pure in-phase 1D multiplets” *Magn. Reson. Chem.* 49(8): 502–507. 2011.

⁵⁴ J. Saurí, T. Parella, And, J. F. Espinosa, “CLIP-HSQMBC: easy measurement of small proton– carbon coupling constants in organic molecules”, *Org. Biomol. Chem.* 11:4473-4478. 2013.

The IP/AP protocol consists of a separate acquisition of two complementary IP and AP selHSQMBC spectra. Analysing the displacement between α/β components as a result of the addition or subtraction of both datasets (IP+AP and IP-AP), clean α and β HSQMBC subspectra are obtained (Figure 14). The IP-selHSQMBC shows a sensitivity dependence of $\sin^2(\pi^n J_{CH}\Delta)$, while the AP-selHSQMBC presents a $\sin(\pi^n J_{CH}\Delta)$ because the last 180° ^{13}C pulse is excluded. The IPAP-selHSQMBC method is highly effective for $^nJ_{\text{CH}}$ measurements and this approach can be also implemented in non-selective IPAP-HMBC and IPAP-HSQMBC experiments⁵⁵.

31

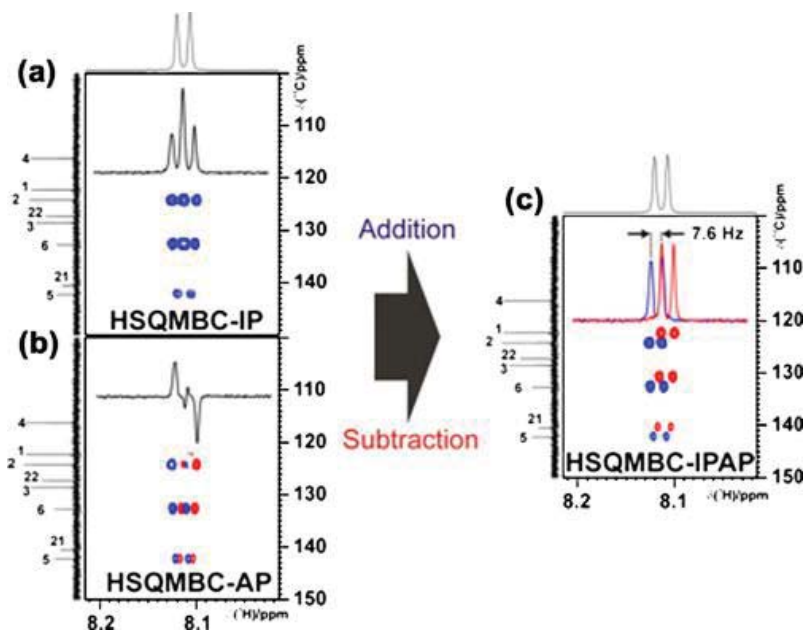


Figure 14. IPAP methodology applied in selHSQMBC experiments: a) IP-HSQMBC, b) AP-HSQMBC, c) overlaid spin-state-selective α/β -HSQMBC spectra corresponding to IP+AP and IP-AP data combination. (Figure has been extracted from reference [52]).

The selHSQMBC experiment can be extended to a complementary selHSQMBC-TOCSY experiment (Figure 15) by appending a homonuclear TOCSY transfer before ^1H acquisition, in an analogous way made for the HSQC-TOCSY experiment⁵⁶. The selHSQMBC-TOCSY experiment combined with the IPAP methodology is a powerful tool to measure the sign and the magnitude of $^nJ_{\text{CH}}$. This experiment presents some interesting advantages: i) all carbons can be observable, ii) a large number of t_1 is not essential because the measurements are made in the direct dimension, iii) tiny coupling constants values can be resolved even when they are smaller

⁵⁶ J. Saurí, J. F. Espinosa, and, T. Parella, "A Definitive NMR Solution for a Simple and Accurate Measurement of the Magnitude and the Sign of Small Heteronuclear Coupling Constants on Protonated and Non-Protonated Carbon Atoms". *Angew. Chem. Int. Ed.*, 51:3919-3922. 2012.

than the line width, iv) the inclusion of TOCSY building block allows analysing crowded areas, v) additional positive/negative sign information is obtained, allowing distinction between two- and three-bond connectivities.

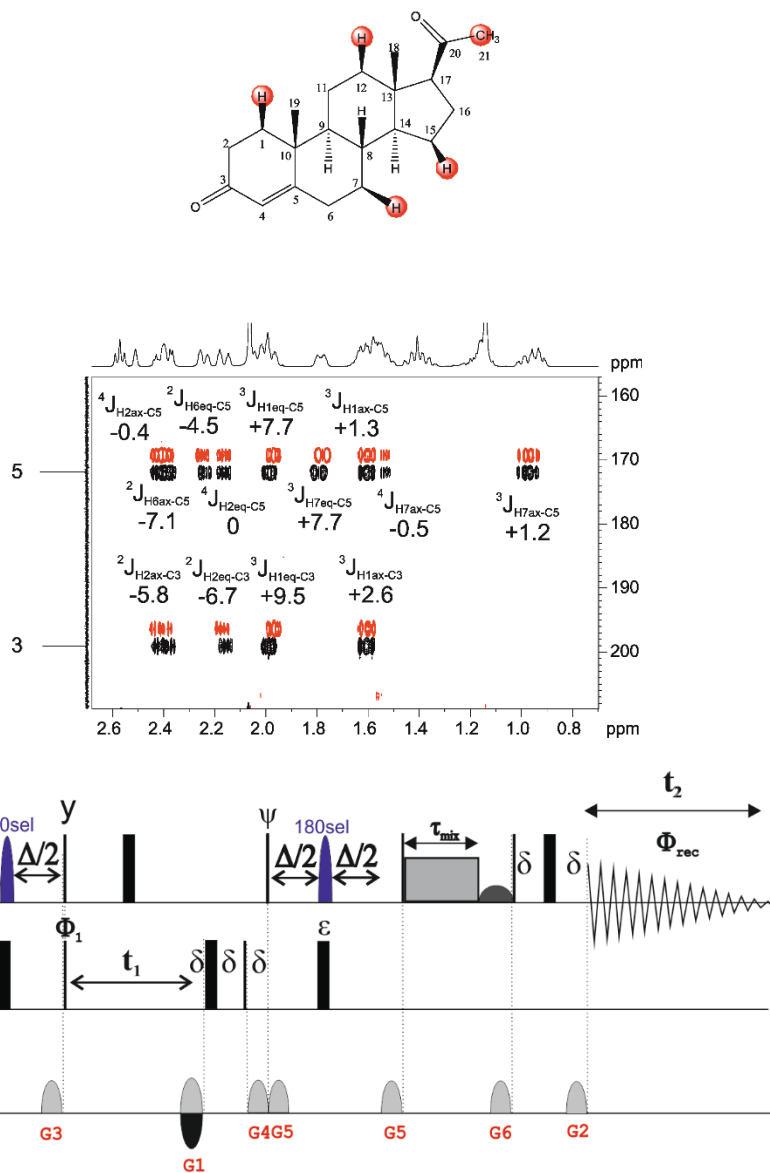


Figure 15: Schematic pulse sequence of 2D ¹H-selective HSQMBC-TOCSY experiment (bottom). Example of a selHSQMBC-TOCSY spectrum (right) using a sample of progesterone (molecule on top). Spectrum extracted from reference [56].

2.5. Time-Efficient NMR techniques

2.5.1. Time-Sharing

The Time-Shared approach is an interesting strategy that provides ^{13}C and ^{15}N information from a single NMR experiment and it can be useful for both nitrogen-containing small molecules and biomolecules at natural abundance. The TS concept is based on the fact that ^1H attached to ^{13}C are not attached to ^{15}N , and therefore their CTPs can be considered and treated independently. Figure 16 shows the basic pulse scheme of a sensitivity-enhanced TS-HSQC-PEP experiment that requires a triple-channel probe configuration. In the first and last steps, both coupling constants ($^1J_{\text{CH}}$ and $^1J_{\text{NH}}$) evolve simultaneously during a concatenated INEPT and retro-INEPT blocks. On the other hand, to monitor different chemical shift evolutions, two partially overlapped chemical shift evolution periods are implemented (variable t_1 and t_1' periods, purple box in Figure 16)⁵⁷. During ^1H acquisition, CPD is applied to both ^{13}C and ^{15}N channels.

TS has been successfully implemented into proton-detected HSQC, HSQC-TOCSY, HMBC and HSQMBC experiments⁵⁸. Figure 17 shows the TS-HSQC spectrum of cyclosporine where CH and NH cross-peaks can be easily distinguished because show an opposite positive/negative phase.

⁵⁷ M. Sattler, M. Maurer, J. Schleucher, and C. Griesinger, "A simultaneous (^{15}N) , (^1H) - and (^{13}C) , (^1H) -HSQC with sensitivity enhancement and a heteronuclear gradient echo". *J Biomol NMR*. Jan;5(1):97-102. 1995.

⁵⁸ P. Nolis, M. Pérez, and T. Parella, "Time-sharing evolution and sensitivity enhancements in 2D HSQC-TOCSY and HSQMBC experiments" *Magn. Reson. Chem.*46(11):1031-6. 2006.

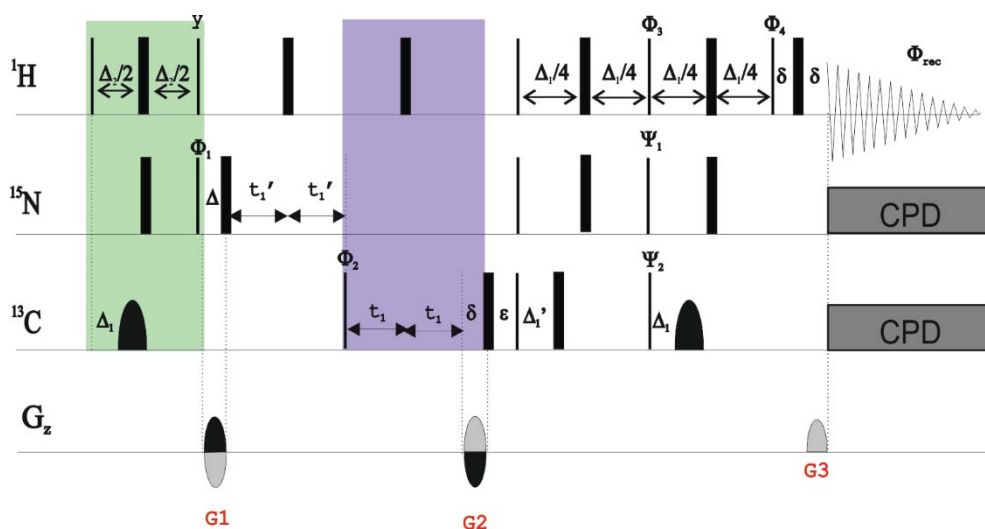


Figure 16. Schematic pulse sequence of time-shared ^{13}C - ^{15}N HSQC experiment⁵⁹.

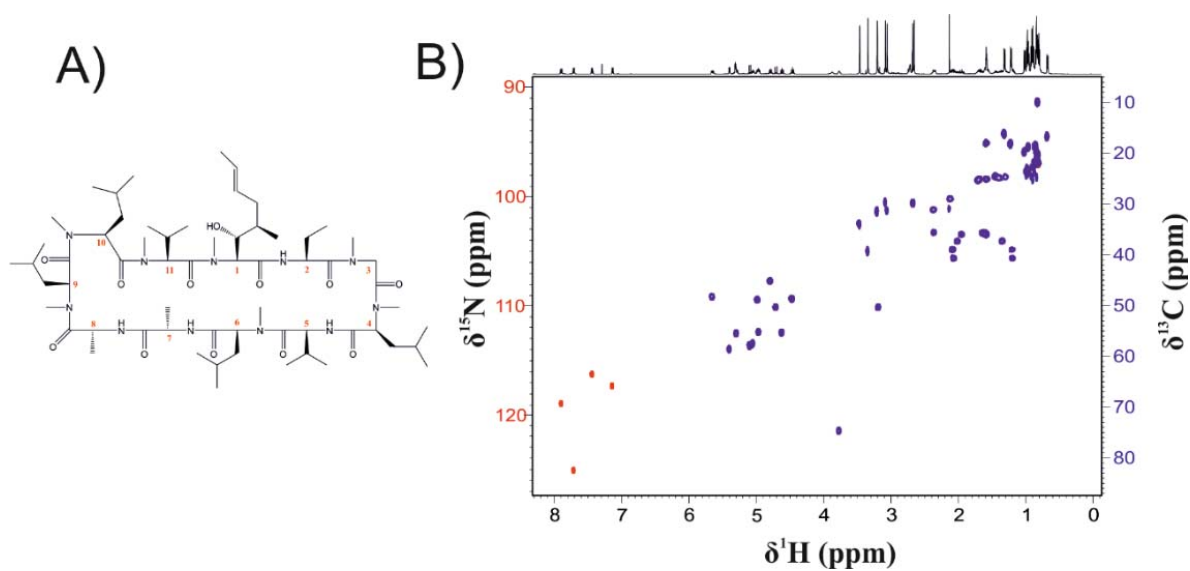


Figure 17: A) Chemical structure of cyclosporine and B) the time-shared HSQC spectrum of cyclosporine in CDCl_3 , where blue signals show ^{13}C - ^1H correlations and red signals show ^{15}N - ^1H correlations. Illustration extracted from reference [59].

⁵⁹ T. Parella and P. Nolis, "Time-shared NMR experiments", *Concepts Magn. Reson. Part A Bridg. Educ. Res.* 36(1):1-23. 2010.

The main benefit of time-shared NMR experiments is that both nucleus ^{13}C and ^{15}N can be collected simultaneously in the same spectrum with a substantial decrease of spectrometer time and relevant sensitivity enhancement per time unit. Time-shared version of HMBC has shown its effectiveness in terms of decreasing acquisition time ($\approx 50\%$) and a considerable sensitivity enhanced (up to 41%) without losing spectral resolution⁶⁰. IPAP method has been also incorporated into TS pulse sequences: TS-HSQC-F2-IPAP and TS-HSQC-F1-IPAP have been successfully developed for the simultaneous measurement of $^1J_{\text{CH}}$ and $^1J_{\text{NH}}$ coupling constants.^{61, 62}.

2.5.2. Multiple-FID detection

MFA approach was proposed for the first time in 1984 for the COCONOSY experiment. The main characteristic is the co-acquisition of two different FIDs into the same scan. This method allows the possibility to record different experiments simultaneously which provides an important goal in terms of spectrometer time efficiency. Figure 18 illustrates how COCONOSY is a simultaneous combination between COSY (Figure 18A) and NOESY (Figure 18B) experiment with an extra FID. After the second pulse, a first FID is found (Figure 18C) where a COSY experiment is recorded and stored. During t_{mix} the components of longitudinal magnetization as a result of the second 90° pulse are mixed by the influence of the cross-relaxation process⁶³. The second FID records and stores the NOESY experiment. At the end of the experiment, two different

⁶⁰ M. Pérez, P. Nolis, and T. Parella, "CN-HMBC: A Powerful NMR Technique for the Simultaneous Detection of Long-Range ^1H , ^{13}C and ^1H , ^{15}N Connectivities", *Organic Letters*, 9(1):29-32. 2007.

⁶¹ P. Nolis, T. Parella, "Simultaneous α/β spin-state selection for ^{13}C and ^{15}N from a time-shared HSQC-IPAP experiment". *J Biomol NMR* 37:65–77. 2007.

⁶² M. Pérez-Trujillo, P. Nolis, W. Bermel, and, T. Parella, "Optimizing sensitivity and resolution in time-shared NMR experiments". *Magn. Reson. Chem.*, 45:325-329. 2007.

⁶³ C. A. G. Haasnoot, F. J. M. van de Ven, and C. W. Hilbers, "COCONOSY. Combination of 2D correlated and 2D nuclear overhauser enhancement spectroscopy in a single experiment", *J. Magn. Reson.*, 56:343-349. 1984.

spectra can be simultaneously acquired, avoiding spending the whole time for both experiments. As a consequence, two complementary COSY and NOESY spectra can be obtained during the time needed to get a conventional NOESY experiment.

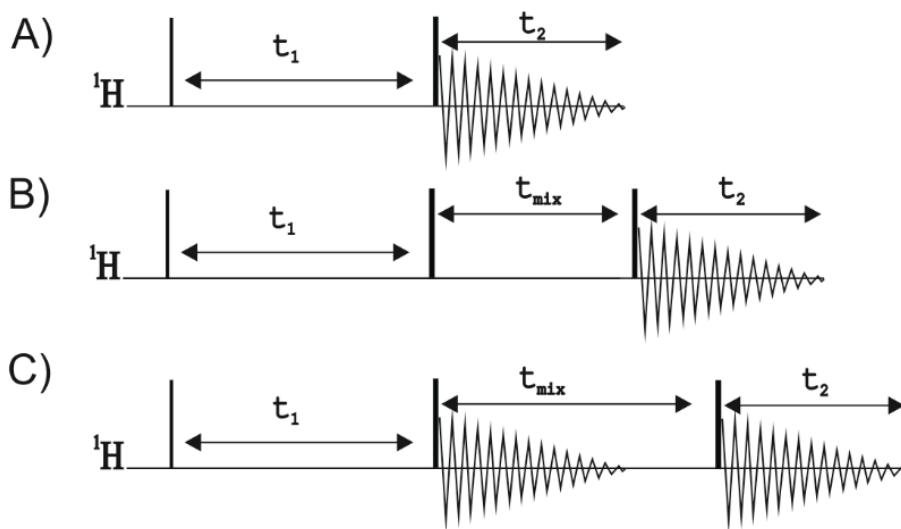


Figure 18: Comparison between A) pulse scheme of COSY experiment, B) pulse scheme of NOESY experiment and C) pulse scheme of COCONOSY experiment.

MFA can be applied to homonuclear and heteronuclear experiments as COSY, TOCSY and HMBC experiments. MFA is based on taking advantage of the remaining transversal magnetization (afterglow magnetization) which normally recovers to the original z-magnetization. This residual magnetization is manipulated properly with an additional mixing process and recorded into a second and/or a third FID which is stored in different memory blocks. MFA is fully compatible with other time-efficient techniques, such as NUS or TS, as shown for the MATS-HMBC experiment (Figure 19) which is built from a conventional TS-HMBC and followed by a TOCSY mixing time and a second FID to record TS-HMBC-TOCSY data. In this MATS_HMBC experiment up to four different complementary HMBC spectra (see Figure 20) are simultaneously acquired in a single shot which is an interesting goal in terms of time efficiency. The major limitation of the MFA strategy is the intensity of the remaining afterglow

magnetization. The larger the number of acquired experiments, the worst sensitivity in the successive experiments due to the lack of signal (T_2 losses).

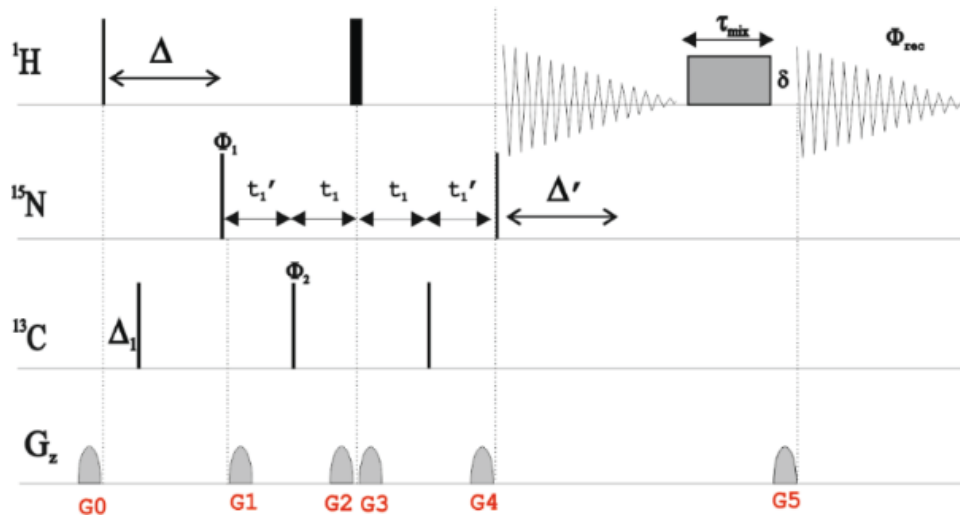


Figure 19. Schematic pulse sequence of MATS- HMBC experiment⁶⁴.

⁶⁴ P. Nolis, M. Pérez-Trujillo, and T. Parella, "Multiple FID Acquisition of Complementary HMBC Data", *Angew. Chem. Int. Ed.*, 46:7495-7497. 2007.

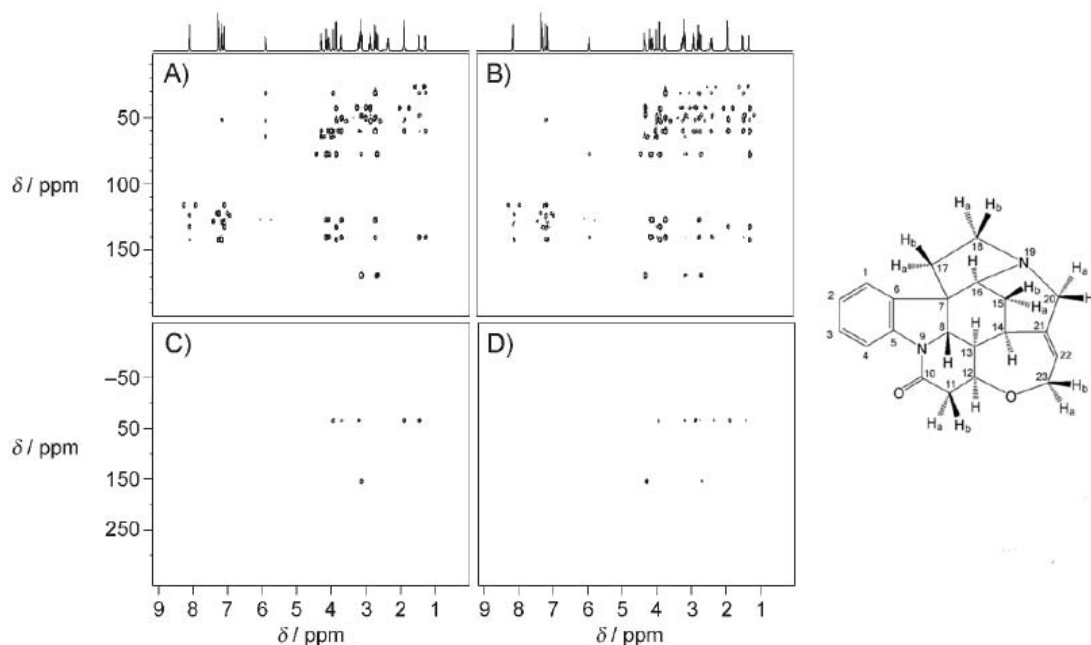


Figure 20: Simultaneous ^1H - ^{13}C -HMBC (A), ^1H - ^{13}C -HMBC-COSY (B), ^1H - ^{15}N -HMBC (C), and ^1H - ^{15}N -HMBC-COSY (D) spectra of a sample of strychnine acquired with the MATS- HMBC pulse scheme. Figure extracted from reference [64].

2.5.3. NOAH supersequences

NOAH experiments are supersequences based on the concatenation of multiple NMR pulse sequences to avoid the application of the long recycled delay in the second, third... experiment⁶⁵,^{66, 67, 68}. A key point for the success of NOAH proposals is to avoid signal saturation. For this reason, experiments are selected as a function of the involved magnetization. The strategy is based on the retention of unused magnetization in the z-axis while the active magnetization is

⁶⁵ E. Kupče and R. Freeman, “Fast multidimensional NMR by polarization sharing”, *Magn. Reson. Chem.*, 45(1):2-4, 2007

⁶⁶ E. Kupče and T. D. W. Claridge, “NOAH: NMR Supersequences for Small Molecule Analysis and Structure Elucidation”, *Angew. Chemie - Int. Ed.*, 56(39):11779-11783, 2017.

⁶⁷ E. Kupče and T. D. W. Claridge, “Molecular structure from a single NMR supersequence”. *Chem Comm.* 26;54(52):7139-7142

⁶⁸ E. Kupče and T. D. W. Claridge, “New NOAH modules for structure elucidation at natural isotopic abundance”. *J Magn Reson.* 307:106568, 2019.

manipulated under the effect of the current pulse sequence. NOAH affords the possibility to acquire up to five different spectra with a single-shot acquisition. Figure 21 shows the most basic NOAH-2 sequence which is a combination of zz-HMBC and multiplicity-edited HSQC schemes. The non-needed recycle delay in NOAH-2 can offer a substantial gain in terms of spectrometer time. A recent NORD (NO Relaxation Delay) experiment has been reported which avoid the application of any recycle delays in all involved experiments⁶⁹.

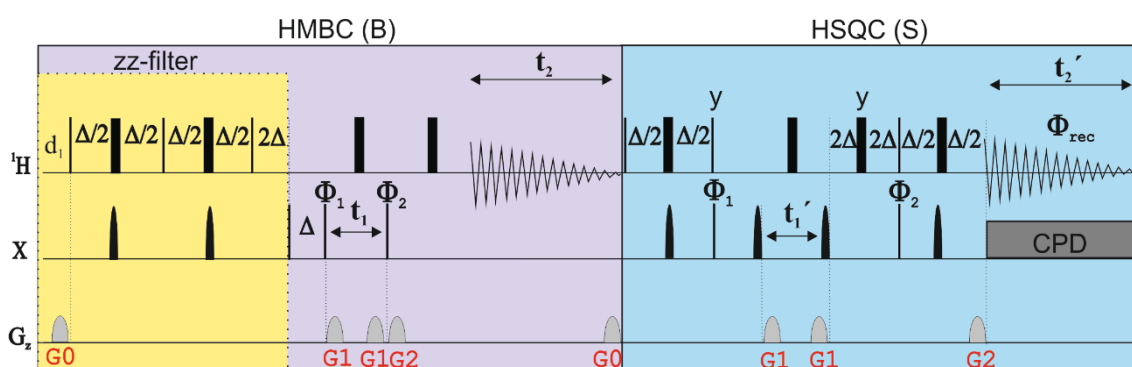


Figure 21: Pulse sequence of NOAH-2 (BS) experiment consisting of consecutive zz-HMBC and -multiplicity edited HSQC pulse schemes.

For instance, a NOAH-4 experiment consisting of concatenated ^1H - ^{15}N HMQC, ^1H - ^{13}C HSQC, ^1H - ^1H NOESY and ^1H - ^1H COSY schemes could be very efficient in spectrometer time savings because each sequence manipulates individual ^1H - ^{15}N , ^1H - ^{13}C and ^1H - ^{12}C magnetization, respectively (Figure 22).

⁶⁹ T.M. Nagy, K. E. Kövér, and O. W. Sørensen, "NORD: NO Relaxation Delay NMR Spectroscopy". *Angew. Chem. Int. Ed.* 60. 2021.

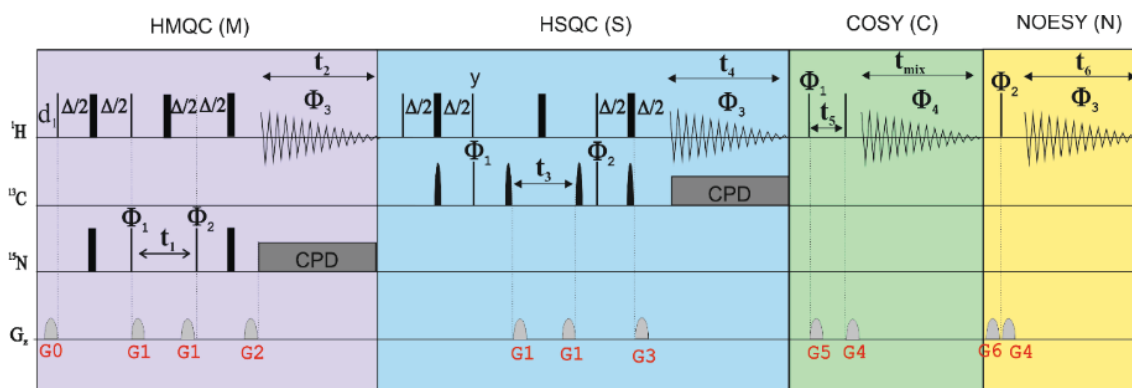


Figure 22: Basic concatenation strategy corresponding to the NOAH-4 (MSCN) pulse scheme.

2.6. Spectral resolution enhancement

Optimal spectral resolution along the indirect dimension in multidimensional NMR experiments is a real challenge for optimizing spectral quality and spectrometer time which are directly proportional to the number of incremented t_1 points. In the case to have large spectral widths or severe signal overlapping, a minimum number of t_1 are always required. A very simple solution to increase the spectral resolution along with F1 for a given experimental time is the reduction of the $SW(F1)$, which means increase sample rating Δt_1 ⁷⁰. Figures 23A and 23B exemplify the enhanced effect to implement this so-called spectral-aliased method (SA) in HSQC experiments. Both spectra are obtained from the same pulse program and similar experimental time. Figure 23D shows another complementary method to increase spectral resolution per time unit in multidimensional NMR: the use of NUS. NUS⁷¹ is available in commercial software and

⁷⁰ Where δ_0 is the real chemical shift and δ_a is the apparent chemical shift limited by the length of $SW1$.

⁷¹ J. C. J. Barna and E. D. Laue, "Conventional and exponential sampling for 2D NMR experiments with application to a 2D NMR spectrum of a protein". *J. Magn. Reson.*, 75(2):384–389. 1987.

can be implemented in any 2D experiment very easily. NUS allows acquiring a percentage of the required t_1 points, reducing the overall experimental time. Thus, 50% of NUS represents saving 50% of spectrometer time. However, imperfect data reconstruction must be avoided because unwanted artefacts can be generated and relative sensitivity losses can arise. The efficiency of NUS has been demonstrated in many 2D heteronuclear and homonuclear experiments for small molecules and biomolecular multidimensional NMR spectroscopy⁷². In addition, NUS can be combined with other resolution and time-efficient NMR approaches.

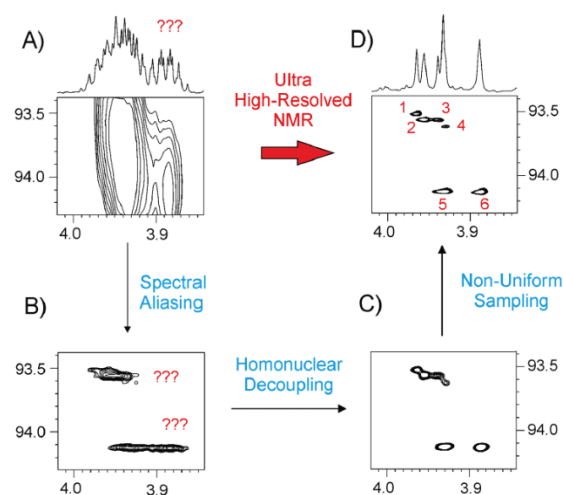


Figure 23. Enhanced spectral resolution in HSQC. The graphical representation displays an area of A) conventional HSQC, B) HSQC with spectral aliasing, C) homonuclear decoupled HSQC after applying real-time BIRD-based homodecoupling and, D) spectrum acquired using 50% NUS. The illustration is taken from reference [10].

⁷² A. Le Guennec, J. N. Dumez, P. Giraudeau, and S. Caldarelli, “Resolution-enhanced 2D NMR of complex mixtures by non-uniform sampling”, *Magn. Reson. Chem.*, 2015.

2.7. NMR-aided enantiodifferentiation using chiral solvating agents

The chiral analysis and the differentiation of enantiomeric molecules by enantiospecific analytical methods still face important limitations. Enantiomers are mirror-image molecules that are not superimposable (Figure 24). Though enantiomers have similar chemical structures and identical physical properties (except their ability to rotate plane-polarized light), they are different entities; distinct molecules with different biological activities, toxicities, and origins (in the case of naturally occurred enantiomeric pairs). The identification of chiral molecules requires enantiospecific analytical methods, which discriminate enantiomers and allow their identification.

Chirality plays a key role in nature; it is fundamental to biological processes at a molecular level. Most biological molecules are chiral; for example, many metabolites such as sugars, amino acids (Figure 24), some hydroxy acids and nucleotides. Thus, enantiospecific analyses are of paramount importance to biological applications.

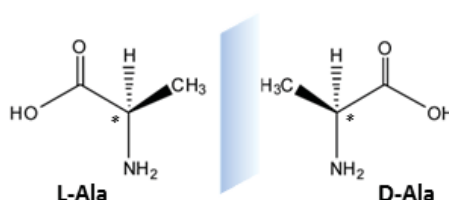


Figure 24: Example of an enantiomeric pair. Mirror image isomers of amino acid alanine.

Chirality is crucial, as well, in synthetic chemistry; the differentiation and identification of stereoisomers and, in particular of enantiomers, are essential in areas like asymmetric synthesis or catalysis. The study of pharmacokinetics and drug metabolism plays an important role in drug efficacy and safety. Being most drugs chiral, enantiospecific analyses are mandatory in the pharmaceutical industry. The case of thalidomide, which was dispensed as a racemic mixture - having the R- enantiomer beneficial effects for morning sickness of pregnant women, while the

S- enantiomer was teratogenic and caused serious side effects in babies in the early '50s⁷³, exemplifies the importance of having enantiospecific methods of analysis to distinguish both enantiomers and the study of the behaviour of each enantiomer separately.

To date, the enantiospecific analysis of chiral molecules in mixtures necessarily requires the isolation of the chiral individual compound before its detection. Enantiospecific analytes are conducted mainly in two ways: i) the chiral compound of interest is initially isolated and then specifically detected using chiroptical or spectroscopic techniques (e.g., circular dichroism or NMR together with a chiral auxiliary, etc.) or ii) chiral compounds of interest are enantiospecifically separated using separation analytical platforms (e.g. HPLC equipped with a chiral column) and then they are non-enantiospecifically detected (e.g. with MS)^{74, 75, 76, 77}. This necessary isolation of enantiomeric individuals carries important potential risks (e.g., kinetic resolution of enantiomeric pairs, stereochemical instability of chiral analytes, degradation of the sample, loss of information related to the original matrix, etc.) that can introduce significant errors in the measurement.

⁷³ M. E. Franks, , G. R. Macpherson and W. D. Figg, "Thalidomide". *Lancet*. 363(9423):1802-1811. 2004.

⁷⁴ A. J. Hutt, M. R. Hadley, and S. C. Tan, "Enantiospecific analysis: applications in bioanalysis and metabolism". *Eur J Drug Metab macokinet*. 19(3):241-51. 1994.

⁷⁵ N. Berova, P. L. Polavarapu, K. Nakanishi, and R.W. Woody, "Comprehensive Chiroptical Spectroscopy", Vol. 1 and 2 (Eds.: N. Berova, P. L. Polavarapu, K. Nakanishi, R.W. Woody), *Wiley-VCH*, 1 – 853. 2012.

⁷⁶ D . Patterson, M. Schnell, J. M. Doyle, "Enantiomer-specific detection of chiral molecules via microwave spectroscopy". *Nature*:23;497(7450):475-7. 2013.

⁷⁷ V. Schurig, "Differentiation of Enantiomers II" (Ed.: V. Schurig), *Springer International Publishing*. 1 – 348. 2013.

CSAs are chiral enantiopure molecules capable to interact weakly with the chiral analyte forming diastereomeric complexes, which can be distinguished via NMR experiments (Figure 25)^{78, 79, 80, 81}.

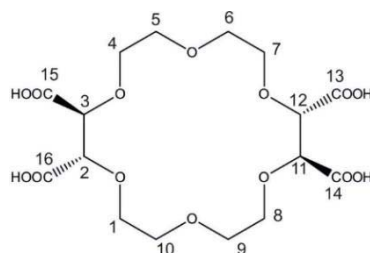


Figure 25: Example of a CSA. Chemical structure of (-)-(18-crown-6)-2,3,11,12-tetracarboxylic acid, (-)-18C6H₄, which is an effective CSA for α - and β -amino acids.

The differentiation of enantiomeric pairs using NMR spectroscopy and CSAs is simple, fast (once the method has been set up) and robust. The method consists of the addition of a specific amount of an adequate CSA into the NMR tube where the analytes (typically, a mixture of enantiomers) are dissolved. After that, the complexation of the analytes with the CSA takes place and an equilibrium between the free analytes and the CSA-analyte diastereomeric complexes is reached (Figure 26). This new situation results in the split of some resonances of the spectrum of the original sample (before adding the chiral auxiliary). For those signals split into two (enantiodifferentiated), one of them corresponds to the R- enantiomer and the other to the S-

⁷⁸ W. H. Pirkle and D. J. Hoover, "NMR chiral Solvating Agents", *Top. Stereochem.*, 13, 263. 1982.

⁷⁹ T. J. Wenzel, "Discrimination of Chiral Compounds Using NMR Spectroscopy", *Wiley-VCH Verlag GmbH & Co.* 2007.

⁸⁰ M. Pérez-Trujillo, A. Virgili "Efficient and rapid determination of the enantiomeric excess of drugs with chiral solvating agents: carvedilol, fluoxetine and a precursor of diarylether lactams", *Tetrahedron. Asymmetry*, 2006, 17, 2842-2846.

⁸¹ M. Pérez-Trujillo, J. C. Lindon, T. Parella, H.C. Keun, J. K. Nicholson, T. J. Athersuch, "Chiral metabonomics: ¹H NMR-based enantiospecific differentiation of metabolites in human urine via direct cosolvation with β -cyclodextrin", *Anal. Chem.* Mar 20;84(6):2868-74. 2012.

enantiomer. The enantiomeric analysis is made by detection of non-equivalences in terms of the difference of chemical shift between the diastereomeric analyte and the free enantiomer^{82, 83}.



Figure 26: Equilibrium between free enantiomeric analytes, R and S, and diastereomeric complexes, CSA---R and CSA---S.

Figure 27 shows an example of the application of the CSA NMR method to racemic DL-threonine. In this case, (-)-18C6H₄ was used as CSA. Spectra before (Figure 27A) and after the addition of 0.2, 0.6, 1.7, 2.1 and 2.2 equivalents of CSA (Figure 27B to 27F) are shown. Spectrum G) is like F) but after spiking the sample with L-threonine and was used for D/L identification. Proton signals corresponding to H₃ (left) and H₄ (right) were enantiodiscriminated.

⁸² D. Parker, "NMR determination of enantiomeric purity", *Chem. Rev.*, 91(7):1441–1457. 1991.

⁸³ M. Pérez-Trujillo, E. Monteagudo, and T. Parella, "13C NMR spectroscopy for the differentiation of enantiomers using chiral solvating agents", *Analytical Chemistry*. 85(22):10887-10894. 2013.

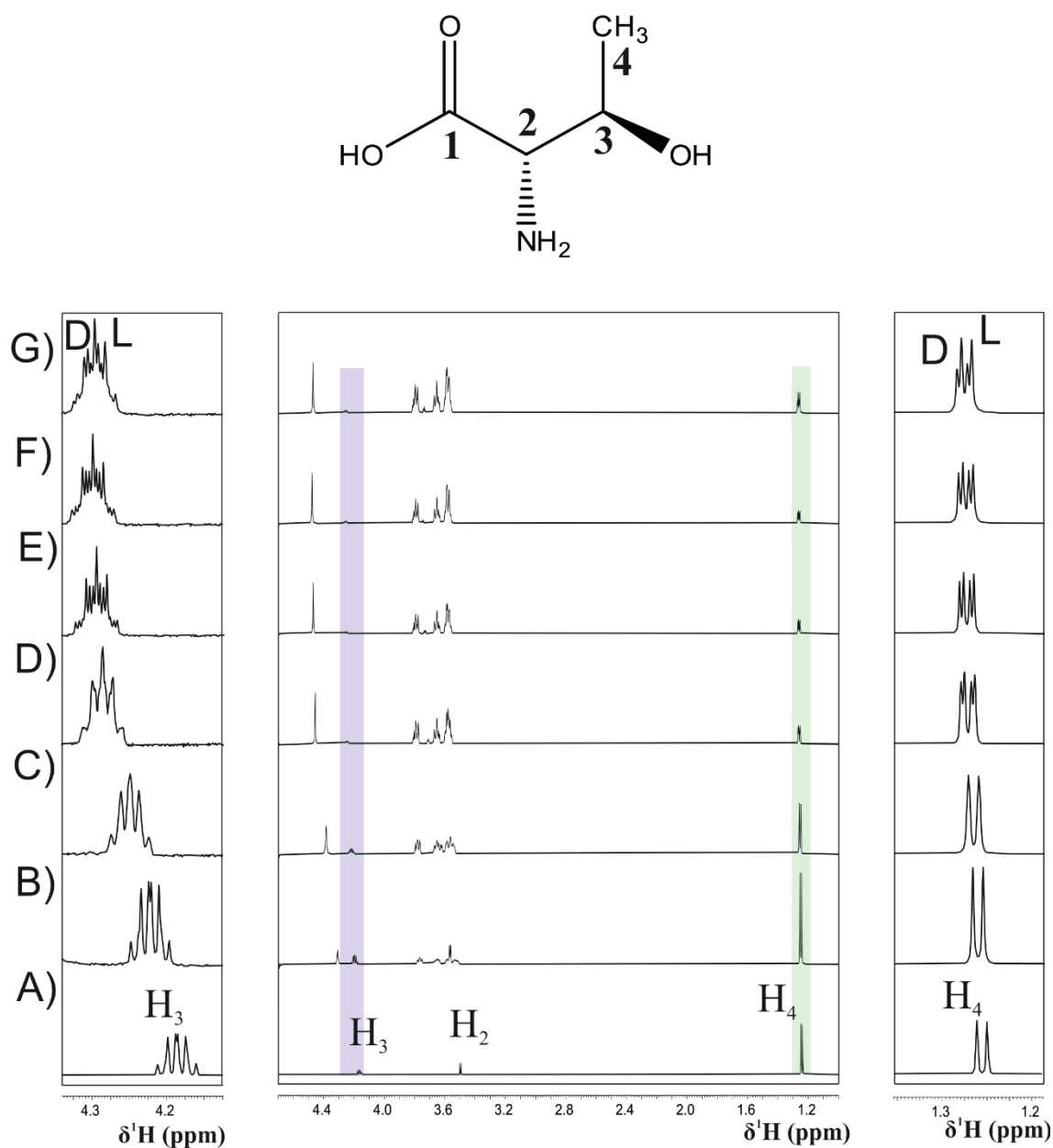


Figure 27. 1D ^1H NMR experiments (noesy1dpr) of a 4.03 mM racemic mixture of DL-threonine in D_2O A) before and B) after the addition of 0.212, C) 0.574, D) 1.662, E) 2.07 and F) 2.21 equivalents of $(-)\text{-}18\text{C}_6\text{H}_4$. G) Spectrum corresponding to sample in F) after spiking the sample with L-threonine. Notice that H_2 is overlapped with the CSA signals after its addition.

There are two main parameters to analyse results from NMR-based enantiodifferentiation experiments: the enantiodifferentiation value (or δ non-equivalence), $\Delta\Delta\delta$, and the enantioresolution quotient, E . Both parameters are measured for those signals that are

enantiodifferentiated (split into two) after adding the CSA. $\Delta\Delta\delta$ is measured directly from the NMR spectrum resulting after the addition of the chiral auxiliary and corresponds to the chemical shift difference (in ppm) between split signals (Equation 9). E is defined as the absolute value of $\Delta\Delta\delta$ divided by three times their width, W , (Equation 10)^{84, 85}.

$$\Delta\Delta\delta = \Delta\delta_R - \Delta\delta_S \quad (\text{Eq. 10})$$

$$E = \frac{|\Delta\Delta\delta|}{3W} \quad (\text{Eq. 11})$$

Thus, $\Delta\Delta\delta$ gives direct information about the value of the separation between the two signals, and E gives information about the quality of that separation, i.e. how good these signals have been resolved.

Recent NMR strategies, such as homodecoupled pure-shift experiments and the spectral aliasing in 2D ^1H , ^{13}C correlations have demonstrated their advantage and effectiveness in CSA NMR analysis^{86, 87}. PS experiments allow the analysis of resulting spectra more straightforwardly due to the presence of singlets instead of multiplets. In addition, the sky projection onto the direct dimension of suitable PS-*J*Resolved^{36, 30} experiments provides a pseudo-PS ^1H spectrum from where small $\Delta\Delta\delta$ values in crowded spectral areas can be easily analysed.

⁸⁴ M. Pérez-Trujillo, T. Parella, and L. T. Kuhn, "NMR-aided differentiation of enantiomers: Signal enantioresolution", *Analytica Chimica Acta*. 876:63-70. 2015.

⁸⁵ W is defined as the average width of the two split signals considering their multiplicity (for more details see reference 84). Notice that: $E = 0$ corresponds to no enantioresolution; $E < 1$ corresponds to a not complete enantioresolution; $E > 1$ corresponds to a complete enantioresolution.

⁸⁶ M. Pérez-Trujillo, L. Castañar, E. Monteagudo, L.T. Kuhn, P. Nolis, A. Virgili, R. T. Williamson, T. Parella, "Simultaneous (1)H and (13)C NMR enantiodifferentiation from highly-resolved pure shift HSQC spectra". *Chem Commun*. Sep 14;50(71):10214-7. 2014.

⁸⁷ L. Castañar, M. Pérez-Trujillo, P. Nolis, E. Monteagudo, A. Virgili and T. Parella, "Enantiodifferentiation through frequency-selective pure-shift ^1H nuclear magnetic resonance spectroscopy". *ChemPhysChem*. 15:854-857. 2014.

3. Objectives

General Objectives of this work:

1. Learn and understand the fundamentals of NMR pulse sequences design and its application as a powerful tool in the structural and conformational analysis of small molecules in solution.
2. Development of new high-resolution NMR pulse schemes to be applied for small molecules in liquid state conditions. To get that, a continuous time-consuming learning process and a permanent updating of bibliographic works to achieve a solid knowledge on basic concepts, existing NMR experiments and NMR building blocks available are strongly mandatory.
3. Development of novel and improved NMR pulse sequences to be applied in small molecules.
4. Development of time-efficient NMR solutions offering spectrometer time savings and faster acquisition times.
5. Implementation of modern methodologies in novel NMR experiments. Combination of multiple-purpose technologies such as pure-shift NMR, spectral-aliasing, time-sharing, non-uniform sampling, Multiple FID acquisition ... into a single pulse sequence.
6. Development of NMR experiments providing the maximum information in a single-shot NMR acquisition.
7. Design of sensitivity-enhanced and resolution-enhanced NMR methods.
8. Detection and quantification of heteronuclear coupling constants, concentrating on the accurate measurement of small values corresponding to ultra-long-range correlations.
9. Learn about the differentiation of enantiomers using NMR spectroscopy and chiral solvating agents (CSA) as chiral auxiliaries.
10. Development of CSA NMR-based methods for the *in situ* multicomponent enantiodifferentiation of mixtures.

11. Development of CSA NMR-based methods compatible with the analysis of multiple metabolites at physiological concentrations.

4. Results and discussion

This section is presented as a compendium of seven publications that have been published in recognized peer-reviewed scientific journals. The six first publications are related to the development of new NMR pulse sequences involving improvements in terms such as spectral resolution, sensitivity, spectrometer time economy and more accurate measurement of NMR parameters. On the other hand, the last publication is focused on the development of new CSA-NMR based methods for the enantiospecific analysis of complex (biological) mixtures *in situ* and multicomponent.

- Time-efficient methods applied to structure elucidation NMR experiments with noticeable enhancing spectral resolution and/or sensitivity per time unit.

Publication 1:

Motiram-Corral, K., Pérez-Trujillo, M., Nolis, P., & Parella, T.

Implementing one-shot multiple-FID acquisition into homonuclear and heteronuclear NMR experiments.

Chem Comm, 2018 Dec 14;54(96):13507-13510.

DOI: doi.org/10.1039/C8CC08065H

Publication 2:

Nolis, P., Motiram-Corral, K., Pérez-Trujillo, M., & Parella, T.

Interleaved Dual NMR Acquisition of Equivalent Transfer Pathways in TOCSY and HSQC experiments.

ChemPhysChem, 2019 Jan;298:23-30.

DOI: [dx.doi.org/10.1002/cphc.20180103](https://doi.org/10.1002/cphc.20180103)

Publication 3:

Nolis, P., Motiram-Corral, K., Pérez-Trujillo, M., & Parella, T.

Simultaneous acquisition of two 2D HSQC spectra with different ^{13}C spectral widths.

Journal Magnetic Resonance, 2019 Jan 14;300:1-7.

DOI: doi.org/10.1016/j.jmr.2019.010.04

- One-shot acquisition of ^{13}C and ^{15}N pure shift HSQC spectra and simultaneous measurements of $^1J_{\text{CH}}$ and $^1J_{\text{NH}}$ coupling constants in a single NMR spectrum.

Publication 4:

Nolis, P., Motiram-Corral, K., Pérez-Trujillo, M., & Parella, T.

Broadband homodecoupled Time-Shared ^1H - ^{13}C and ^1H - ^{15}N HSQC experiments.

Journal Magnetic Resonance, 2018 Nov 28.

DOI: doi.org/10.1016/j.jmr.2018.11.005

- Detection and quantification of tiny long-range heteronuclear connectivities using time-shared methods and selective HSQMBC pulse schemes.

Publication 5:

Motiram-Corral, K., Souza, A., Saurí, J., Nolis, P., Parella, T.

LR-selHSQMBC: Simultaneous detection and quantification of very weak long-range heteronuclear NMR correlations.

ChemPhysChem, 2020 Jan. 21,1-5: 1439-4235.

DOI: doi.org/10.1002/cphc.201901142

Publication 6:

Motiram-Corral K., Nolis P., Saurí J., Parella T.

LR-HSQMBC versus LR-seHSQMBC: Enhancing the Observation of Tiny Long-Range Heteronuclear NMR Correlations.

J Nat Prod. 2020;10.1021.

DOI: [10.1021/acs.jnatprod.0c00058](https://doi.org/10.1021/acs.jnatprod.0c00058)

- Enantiospecific multicomponent analysis of complex mixtures without prior isolation of chiral individuals using CSAs and NMR spectroscopy.

Publication 7:

Kuhn L. T., Motiram-Corral K., Athersuch T. J., Parella T., Pérez-Trujillo M.
Simultaneous Enantiospecific Detection of Multiple Compounds in Mixtures using NMR Spectroscopy.

Angew. Chem. Int. Ed. 2020, 59, 23615-23619.

DOI: [10.1002/anie.202011727](https://doi.org/10.1002/anie.202011727)

4.1. Publication 1: Implementing one-shot multiple-FID acquisition into homonuclear and heteronuclear NMR experiments.

4.1.1. Introduction

Despite the large number of techniques that are highly efficient to decrease experimental time in NMR experiments, the long spectrometer time needed for data collection is still a challenge for spectroscopists. For instance, NUS and time-shared based experiments are two useful tools to reduce NMR acquisition times. The main objective of our MFA approach is to reduce the experimental time by acquiring multiple NMR data in a single-shot acquisition step. MFA takes profit of the afterglow magnetization at the end of a pulse scheme to avoid the use of a second or a third pre-scan “d1” delay. In this work, combined NMR experiments using the MFA strategy are presented.

MFA-COSY/RELAY consists of the addition of one 90° pulse after the first FID. Successive 90° pulses can be added after the last FID to generate additional MFA-COSY/RELAY-2 or MFA-COSY/RELAY-3 spectra. On the other hand, the MFA-COSY/TOCSY experiment works like the original COCONESY. Heteronuclear MFA experiments such as the combined MFA-HMBC/HMBC-TOCSY, MFA-HMBC/HMBC-TOCSY and MFA-HMBC/HMBC-COSY experiments are also introduced in this paper. For instance, the MFA-MBOB-COSY experiment offers the possibility to simultaneously obtain HMQC and HMBC NMR datasets.






Cite this: *Chem. Commun.*, 2018, 54, 13507

Received 9th October 2018,
Accepted 7th November 2018

DOI: 10.1039/c8cc08065h

rsc.li/chemcomm

Implementing one-shot multiple-FID acquisition into homonuclear and heteronuclear NMR experiments†

Kumar Motiram-Corral,  Miriam Pérez-Trujillo,  Pau Nolis * and Teodor Parella *

Multiple-FID acquisition (MFA) within the same scan is applied to acquire simultaneously multiple 2D spectra from a single NMR experiment. A discussion on the incorporation of the MFA strategy in several homonuclear and heteronuclear 2D pulse sequences is presented. As a proof of concept, a set of novel COSY, TOCSY and HMBC experiments are reported as a time-efficient solution in small-molecule NMR spectroscopy.

The reduction in the experimental time required to collect essential NMR data is a challenging task for the efficient structure characterisation of small and medium-sized molecules. Another important aspect is how to get maximum chemical information from a single NMR experiment, thus minimising spectrometer time. Several fast NMR strategies tackling the problem have been proposed. For instance, time-shared (TS) techniques yield the same spectra for two different nuclei by selecting independent coherence transfer pathways.¹ The acquisition of multidimensional NMR spectra within a single scan is another interesting approach to record all increments of a given 2D experiment in different spatially encoded *z*-slices of the NMR tube.² Non-uniform sampling (NUS)³ algorithms actively reduce the number of variable *t*₁ increments to be recorded in multidimensional experiments, and parallel or interleaved acquisition of different nuclei using multiple-receiver coil technologies has shown its potential to reduce spectrometer time occupancy.⁴ Recently, the so-called NOAH supersequences based on the interleaved acquisition of multiple experiments have been proposed to minimize the effects of using long pre-scan delays,^{5,6} which are critical for an appropriate relaxation and an optimum repetition rate.⁷ Another alternative is the use of paramagnetic relaxation to speed up spin-lattice relaxation and NMR data collection.^{8,9} On the other hand, the multiple-FID acquisition (MFA) strategy was proposed

many years ago with the COCONOSY experiment,^{10–12} where 2D COSY and NOESY data could be simultaneously collected using a single pulse scheme, affording a theoretical gain in spectrometer time. MFA has also been implemented in magic-angle-spinning solid-state NMR experiments devoted to biomacromolecules using a standard spectrometer configuration.^{13–16} However, the general use of MFA has been limited due to the difficulties related to the use of long acquisition of free-induction decays (FIDs) to accurately digitalise the data, the need for long phase cycles for convenient pathway selection and the real compatibility between experiments that justify this parallel acquisition instead of the traditional sequential one. Nowadays, with the advances in electronics and the widely extended use of pulsed field gradients (PFGs) for efficient magnetization transfer pathway selection,¹⁷ MFA can play an exciting role in modern NMR pulse sequence design.¹⁸ Herein, we want to recover these old concepts by detailing how MFA can be incorporated into basic NMR techniques, providing some useful 2D experiments for both routine homonuclear and heteronuclear applications in small molecule NMR spectroscopy. MFA is based on a simple idea: after data acquisition using a pattern pulse sequence, the remaining transverse magnetization that usually relaxes to its original *z* magnetization can still be manipulated *via* an appropriate additional mixing process and recorded again to obtain a second and/or a third NMR spectrum provided that the *T*₂ relaxation times are long enough. In practical terms, these additional data can be considered free because the total experimental time of the extended sequence varies minimally. These experiments can be implemented in spectrometers having a standard configuration with a single receiver.

Fig. 1A shows the pulse scheme of a novel MFA-COSY/RELAY-3 method which provides sequential proton-proton *J* connectivities from a single NMR experiment. The first part is a regular gradient-enhanced two-pulse COSY scheme that affords a magnitude-mode 2D COSY spectrum after conventional data acquisition and data processing. In this case, the MFA strategy involves the incorporation of three sequential RELAY transfer steps, each one with its FID detection. This approach generates

Servei de Resonància Magnètica Nuclear, Universitat Autònoma de Barcelona, E-08193 Bellaterra, Barcelona, Catalonia, Spain. E-mail: Teodor.parella@uab.cat, Pau.nolis@uab.cat

† Electronic supplementary information (ESI) available. See DOI: 10.1039/c8cc08065h

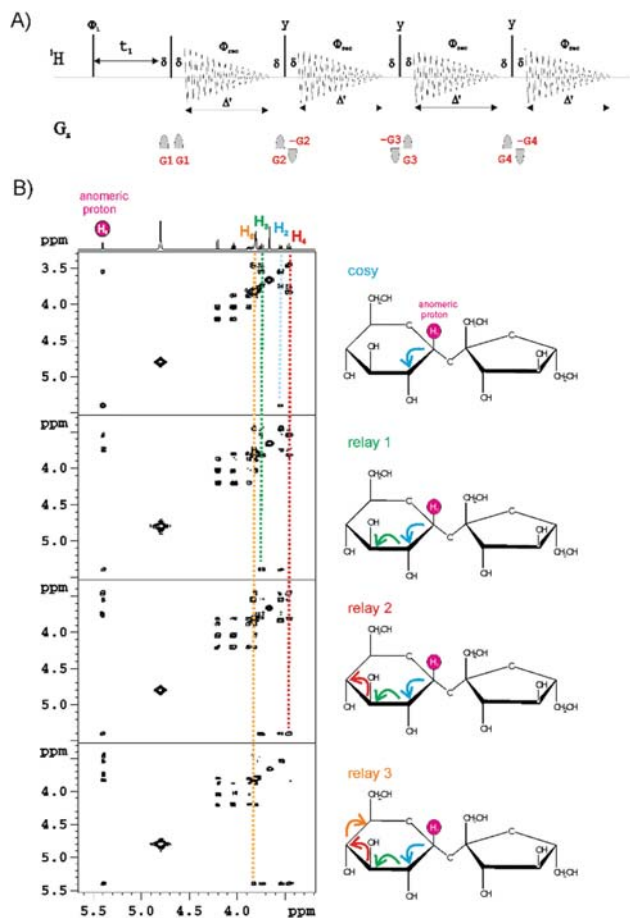


Fig. 1 (A) Pulse scheme of the MFA-COSY/RELAY-3 experiment. Each FID is stored in separate memory blocks and processed individually in the usual way. (B) 2D COSY, RELAY, RELAY-2 and RELAY-3 spectra of sucrose ($M_W = 342$) in D_2O simultaneously obtained from the one-shot MFA-COSY/RELAY-3 scheme.

four spectra obtained with the same acquisition and processing conditions, providing complementary NMR spectra which can be analyzed and interpreted in a concerted manner. PFGs are used for coherence selection in each step, and each FID can be collected individually with a simple two-scan acquisition per t_1 increment, as performed for COSY data. In this case, refocusing echo pulses typically used in RELAY experiments are not applied during the proton–proton relay transfer (Δ') because a long enough FID period (we have used ~ 90 ms) is required to get an acceptable digital resolution in the acquisition dimension. In practice, the complex nature of the cross-peaks forces the use of a magnitude-mode display to avoid the visualization of phase signal distortions.

As a proof of concept, we tested MFA-COSY-RELAY-3 on a sample of disaccharide sucrose (Fig. 1B). The sequential structural assignment of a whole spin system can be made without ambiguities from the analysis of COSY, RELAY, RELAY-2 and RELAY-3 spectra, as can be seen in the assignment of pyranose ring protons taking the anomeric H-1 proton as the starting point. All the resulting spectra provide the same sequential information as a TOCSY experiment recorded with a long

mixing time but adding the significant advantage that each transfer step is stored and analysed individually. Regarding the spectrometer time, the addition of subsequent MFA steps represents an important time saving, because MFA only lengthens the acquisition time of the single pattern experiment by 6–20%. For instance, if a 2D COSY experiment is executed in 4 min 54 s, the equivalent MFA-COSY/RELAY-3 is acquired in 5 min 57 s (see Table S1, ESI† for more details about experimental times, acquisition conditions and MFA experiments). Although the sensitivity of the added RELAY experiments is not the same as we would get in an independent acquisition, MFA offers an interesting benefit regarding the multiple and diverse NMR data achieved per spectrometer time unit. Thus, in a tiniest fraction of added time, we have additional NMR spectra that can help our analysis and interpretation. Besides, it is also worth mentioning that these new RELAY data are complementary to the original COSY data, which are not affected in sensitivity by the MFA method. All these advantages must be valued appropriately concerning efficiency and compatibility because the overall procedure of multiple data acquisition is made under common experimental conditions. Other approaches to obtain different NMR experiments (say, for instance, simultaneous collection of COSY and HMQC data) in a one-shot acquisition mode have serious drawbacks when analysing sensitivity per time unit. They often fail because they present distinct requirements in terms of number of scans per t_1 increment due to the existence of diverse ranges of relative sensitivities or different phase cycles, number of t_1 increments due to the different frequencies and spectral widths involved in the indirect dimension, or need for different data acquisition and data representation modes (for instance, basic COSY is usually represented in the magnitude mode, but NOESY requires phase-sensitive data).

Similarly, an MFA-COSY/TOCSY experiment is feasible to collect both COSY and TOCSY spectra simultaneously (Fig. 2). The TOCSY transfer is appended in a similar way as described in the original COCONOSY experiment. After the first COSY acquisition, a 90° pulse followed by a purging gradient is applied to select I_z magnetization, whereas a DIPSI-2 train is used for propagation. MFA can also be incorporated in conventional proton-detected HMQC-type (see Fig. S3, ESI†) and HMBC-type heteronuclear experiments. For instance, Fig. 3A shows the MFA-HMBC/HMBC-TOCSY pulse scheme where the TOCSY transfer has been added after the regular collection of a magnitude-mode HMBC experiment. Again, the sensitivity of the resulting HMBC-TOCSY spectrum will depend on the involved T_2 relaxation times, but excellent results are obtained for a molecule like strychnine having $T_2(^1H)$ around 100–250 ms at 500 MHz.

A similar approach can be applied in an equivalent MFA-HMBC/HMBC-COSY experiment (Fig. S4, ESI†) and extended to other reported HMBC-type experiments. For instance, we show here how the MFA version of the MBOB (MFA-MBOB-COSY) experiment^{19,20} (Fig. 4A) allows the simultaneous one-shot collection of four complementary NMR spectra: coupled 1H - ^{13}C HMQC, 1H - ^{13}C HMQC-COSY, 1H - ^{13}C HMBC and 1H - ^{13}C HMBC-COSY. The MBOB experiment was reported some years ago to optimize spectrometer time occupancy by extracting one-bond

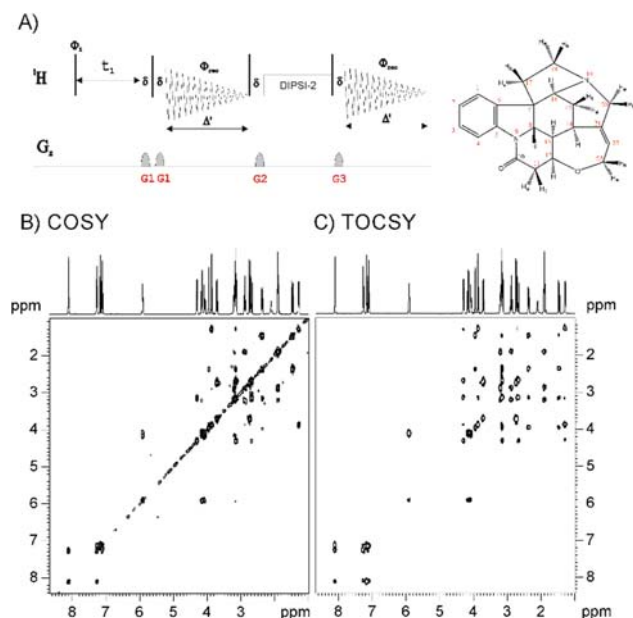


Fig. 2 (A) Pulse scheme of the MFA-COSY/TOCSY experiment. (B) 2D magnitude-mode COSY and (C) 2D magnitude-mode TOCSY (60 ms mixing time) spectra of strychnine ($M_W = 334$) in CDCl_3 obtained from the one-shot MFA-COSY/TOCSY scheme.

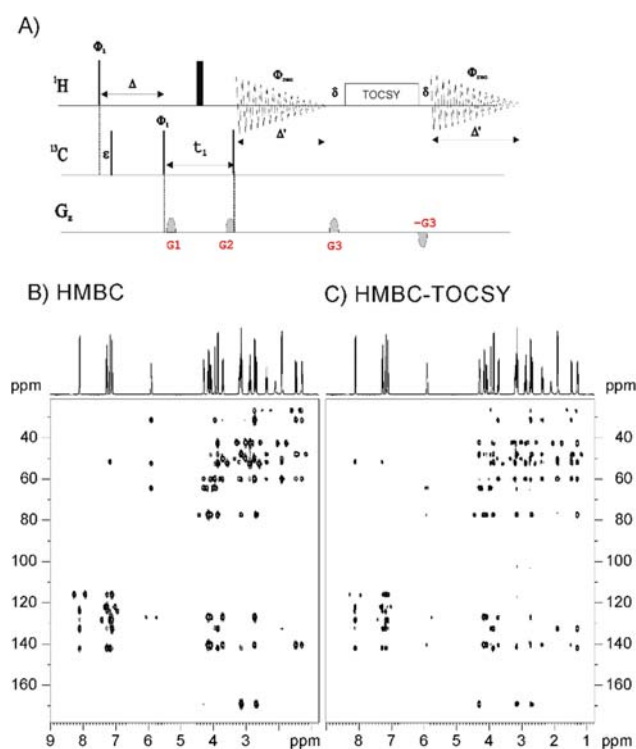


Fig. 3 (A) Pulse scheme of the MFA-HMBC/HMBC-TOCSY experiment. (B) 2D HMBC and (C) 2D HMBC-TOCSY spectra of strychnine simultaneously obtained from the pulse scheme of (A).

correlation data (HMQC) while long-range HMBC data were acquired. Not going into detail, the MBOB strategy consists of performing the HMBC experiment using a low-pass J filter in a

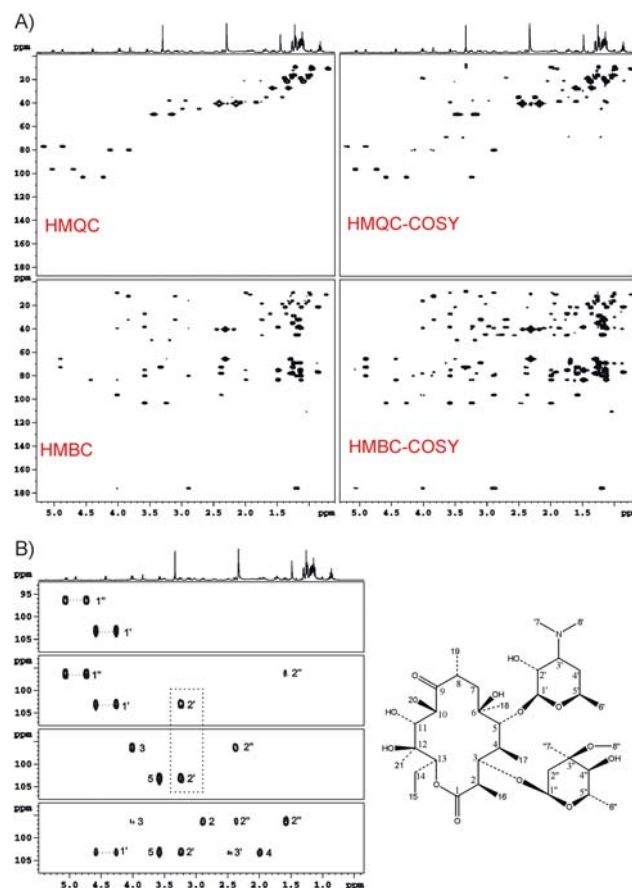


Fig. 4 (A) Separated 2D HMQC, 2D HMQC-COSY, 2D HMBC and 2D HMBC-COSY spectra of erythromycin A ($M_W = 734$) in CDCl_3 obtained simultaneously by the herein proposed MA-MBOB-COSY pulse sequence of Fig. S5 (ESI †). (B) Expanded areas showing one-bond (HMQC), two-bond (HMQC-COSY), two- and three-bond (HMBC), and two, three- and four-bond correlations (HMBC-COSY).

non-destructive way, allowing the recovery of the HMQC data while recording the HMBC experiment. It is worth mentioning that the herein presented MFA-MBOB-COSY experiment is well suited for solving one of the most relevant problems of the HMBC experiment. The distinction between two-bond and three-bond correlation peaks can be made by comparison between HMQC-COSY (two-bond correlation peaks *via* $^1J(\text{CH}) + J(\text{HH})$) and HMBC data (usually having a mixture of two- and three-bond correlation peaks). Furthermore, the HMBC-COSY data are obtained independently at the same time, which give us valuable information, mainly originating from consecutive $^nJ(\text{CH}) + J(\text{HH})$ magnetization transfers. Thus, four-bond correlation peaks can be observed, as well as two- and three-bond missing peaks in regular HMBC. A sample of erythromycin A, a macrocyclic antibiotic compound containing 14-membered lactone with ten asymmetric centers and two sugars (L-cladinose and D-desosamine), is used to exemplify the utility of the MFA-MBOB-COSY experiment (Fig. 4B). Several peaks are highlighted in Fig. 4B. The two-bond correlation peak $\text{C}1'-\text{H}2'$ is assigned in a non-dubious way so that it appears in both HMBC and HMQC-COSY spectra. Four-bond correlation peaks, $\text{C}1''-\text{H}2$ and $\text{C}1'-\text{H}4$, are obtained

in HMBC-COSY. Furthermore, it is important to notice the HMBC missing data as C1''-H2'' and C1'-H3' correlation peaks reappear in HMBC-COSY. In the case of C1''H2'', they also appear in HMQC-COSY, thus a two-bond correlation is its clear assignment. It is worth mentioning that all proposed HMBC experiments do not use heteronuclear decoupling during all ^1H acquisition periods because of the anti-phase nature of the cross-peaks. In fact, heteronuclear decoupling is not a limitation in MFA experiments and it could be applied as in conventional experiments if required. The power of the MFA method opens new horizons in pulse sequence design because it could be combined with other time-optimized NMR approaches. For instance, the incorporation of time-sharing frequency evolution in the proposed MFA-MBOB-COSY experiment could give rise to simultaneous recording of eight NMR spectra using a single NMR pulse sequence: $^1\text{H}/^{13}\text{C}$ -HMQC, $^1\text{H}/^{15}\text{N}$ -HMQC, $^1\text{H}/^{13}\text{C}$ -HMQC-COSY, $^1\text{H}/^{15}\text{N}$ -HMQC-COSY, $^1\text{H}/^{13}\text{C}$ -HMBC, $^1\text{H}/^{15}\text{N}$ -HMBC, $^1\text{H}/^{13}\text{C}$ -HMBC-COSY and $^1\text{H}/^{15}\text{N}$ -HMBC-COSY. This experiment should be of high interest for those research groups working on nitrogen-containing small molecules.

In summary, it has been shown how the proof-of-concept MFA strategy can be successfully implemented in standard 2D COSY and HMBC experiments for routine applications in small molecules. The feasibility of such an approach strongly depends on the existing T_2 values, and it can be implemented in NMR spectrometers having a standard single-receiver configuration. The application of MFA in large biomolecules is also feasible but more compromised due to the existence of shorter T_2 relaxation times. This single-shot acquisition methodology affords considerable spectrometer time savings when compared to the individual recording of separate experiments. It has been shown that additional NMR spectra can be collected within a minimum extra time and under identical conditions, offering interesting advantages in terms of spectrometer economy, simplicity, and automation. Much work is in progress to expand the performance of the MFA experiments, namely (i) the use of data processing algorithms to improve the resolution in experiments involving short FIDs, (ii) the complementarity of MFA methods with other resolution-enhanced (the success to apply the same non-uniform sampling algorithms in similar experiments) and

time-optimized (time-shared, NOAH experiments, or multiple-receiver configuration) techniques and (iii) the design of novel and more powerful MFA experiments involving phase-sensitive data.

Financial support for this research provided by Spanish MINECO (project CTQ2015-64436-P) is gratefully acknowledged. We also thank the Servei de Resonància Magnètica Nuclear, Universitat Autònoma de Barcelona, for allocating instrument time to this project.

Conflicts of interest

There are no conflicts to declare.

Notes and references

- 1 T. Parella and P. Nolis, *Concepts Magn. Reson., Part A*, 2010, **36**, 1–23.
- 2 A. Tal and L. Frydman, *Prog. Nucl. Magn. Reson. Spectrosc.*, 2010, **57**, 241–292.
- 3 K. Kazimierczuk and V. Y. Orekhov, *Angew. Chem., Int. Ed.*, 2011, **50**, 5556–5559.
- 4 E. Kupče, *Top. Curr. Chem.*, 2013, **335**, 71–96.
- 5 Ě. Kupče and T. D. W. Claridge, *Angew. Chem., Int. Ed.*, 2017, **56**, 11779–11783.
- 6 E. Kupče and T. D. W. Claridge, *Chem. Commun.*, 2018, **54**, 7139–7142.
- 7 E. Kupče and R. Freeman, *Magn. Reson. Chem.*, 2007, **45**, 2–4.
- 8 P. S. Nadaud, J. J. Helmus, I. Sengupta and C. P. Jaroniec, *J. Am. Chem. Soc.*, 2010, **132**, 9561–9563.
- 9 K. Yamamoto, J. Xu, K. E. Kawulka, J. C. Vederas and A. Ramamoorthy, *J. Am. Chem. Soc.*, 2010, **132**, 6929–6931.
- 10 A. Z. Gurevich, I. L. Barsukov, A. S. Arseniev and V. F. Bystrov, *J. Magn. Reson.*, 1984, **56**, 471–478.
- 11 C. A. G. Haasnoot, F. J. M. van de Ven and C. W. Hilbers, *J. Magn. Reson.*, 1984, **56**, 343–349.
- 12 J. Cavanagh and M. Rance, *J. Magn. Reson.*, 1990, **14**, 408–414.
- 13 T. Gopinath and G. Veglia, *Angew. Chem., Int. Ed.*, 2012, **51**, 2731–2735.
- 14 T. Gopinath and G. Veglia, *J. Magn. Reson.*, 2015, **253**, 143–153.
- 15 T. Gopinath and G. Veglia, *J. Magn. Reson.*, 2016, **267**, 1–8.
- 16 G. Abramov and N. J. Traaseth, in *Methods in Molecular Biology*, 2018, vol. 1688, pp. 55–66.
- 17 T. Parella, *Magn. Reson. Chem.*, 1998, **36**, 467–495.
- 18 P. Nolis, M. Pérez-Trujillo and T. Parella, *Angew. Chem., Int. Ed.*, 2007, **46**, 7495–7497.
- 19 T. Schulte-Herbrüggen, A. Meissner, A. Papanikos, M. Meldal and O. W. Sørensen, *J. Magn. Reson.*, 2002, **156**, 282–294.
- 20 A. Meissner and O. W. Sørensen, *Magn. Reson. Chem.*, 2000, **38**, 981–984.

Supporting Information

**Implementing one-shot multiple-FID acquisition into homonuclear and
heteronuclear NMR experiments**

Kumar Motiram, Miriam Pérez-Trujillo, Pau Nolis* and Teodor Parella*

Servei de Ressonància Magnètica Nuclear,

Universitat Autònoma de Barcelona, E-08193, Bellaterra, Barcelona, Catalonia, Spain.

Table of contents:

Experimental Section

Table S1. Comparison of experimental measurement times between different pattern and MFA experiments.

Figure S1: General scheme showing the incorporation of the MFA strategy in homonuclear and heteronuclear NMR experiments.

Figure S2: Pulse scheme of the MFA-COSY-RELAY² experiment and example.

Figure S3: Pulse scheme of the MFA-HMQC/HMQC-COSY experiment and example.

Figure S4: Pulse scheme of the MFA-HMBC/HMBC-COSY experiment and example.

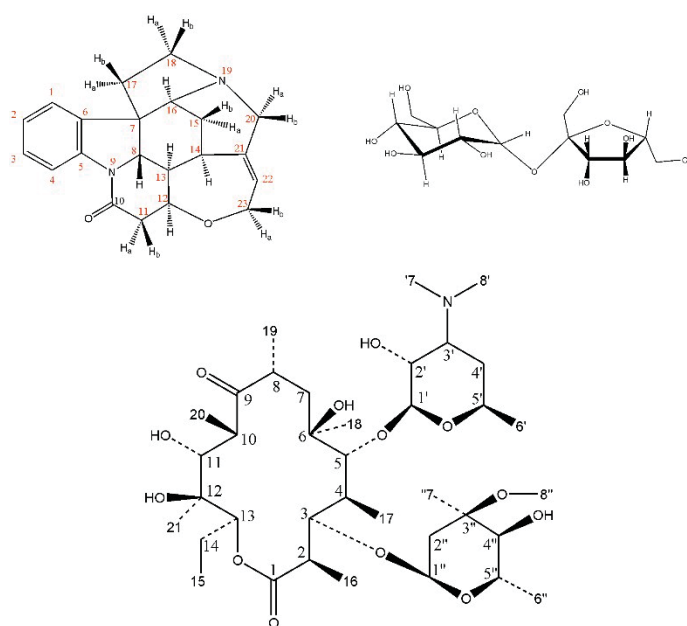
Figure S5: Pulse sequence of the

Figure S6: Example of the MA-MBOB-COSY experiment.

Pulse Programs

Experimental Section

All experimental NMR spectra were recorded on a Bruker AVANCE spectrometer equipped with a 5mm TCI $^1\text{H}/^{13}\text{C}/^{15}\text{N}$ cryoprobe operating at 500.13 MHz for ^1H at 298K. Our starting point to record the reported MFA-COSY and MFA-HMBC experiments was those of the conventional gradient-selected magnitude-mode COSY (BRUKER pulse program: cosygpqf), HMQC (BRUKER pulse program: hmqcgpqf) and HMBC (BRUKER pulse program: hmbcgpqf) experiments, respectively. The samples used in this work were: 20 mg of sucrose dissolved in 0.6 ml of D_2O , 25 mg of erythromycin A dissolved in CDCl_3 , and 20 mg of strychnine dissolved in CDCl_3 .



Basic conditions for the MFA-COSY/RELAY-3 experiment (Figure 1A): A pre-scan delay of 1s and 2 scans for each one of the 128 t_1 increment was used (1024 points of time domain in the acquisition F2 dimension). A basic two-step phase cycling was applied: $\Phi_1 = x, -x$; $\Phi_{\text{rec}} = x, -x$. The acquisition time Δ' was of 93 ms, the overall duration of the gradient (1 ms) and its recovery delay (δ) was 1.2 ms and the gradient ratio G1:G2:G3:G4 used was 50:30:40:17. The equivalent MFA-COSY/RELAY and MFA-COSY/RELAY-2 (Figure S2A) were acquired exactly under the same conditions. MFA-COSY/TOCSY experiment (Figure 2A) was also recorded under the same conditions, using a z-filtered DIPSI pulse trains of 60 ms and a gradient ratio G1:G2:G3 of 10:33:20. The heteronuclear MFA-HMBC/HMBC-TOCSY (Figure 3A) and MFA-HMBC/HMBC-COSY (Figure S4A) experiments were recorded under the same conditions described previously, using a Δ delay adjusted to 62.5 ms (8 Hz

optimization). The gradient ratio G1:G2:G3 in MFA-HMBC/HMBC-TOCSY was 30:50:17 and in MFA-HMBC/HMBC-COSY of 30:50:40. Experimental times are shown in Table S1.

Basic conditions for the MFA-MBOB-COSY experiment (Figure S5): A pre-scan delay of 1s and 8 scans for each t_1 increment was used (TD2=1K, TD1=128), with an overall experimental time of 2 h. The Δ and Δ' delay were adjusted to 62.5 ms (8 Hz) and 85ms, respectively. Gradient ratio used was 50:30:40:15. J_{\min} and J_{\max} for 1J filtering were adjusted to 120 Hz and 170 Hz respectively.

For all homonuclear and heteronuclear NMR experiments: Because each FID is allocated in different memory blocks, they were individually processed in the usual way using a zero-filling in both F1 and F2 dimensions, up 2048 and 1024 data matrix respectively, and applying a non-shifted sine-bell window function in both dimensions prior to Fourier transformation.

Pattern Experiment	Experimental time	MFA Experiment	Experimental Time	Comparative Incremental (in %)
COSY	4m 54s	MFA-COSY/RELAY	5m 11s	6%
		MFA-COSY/RELAY-2	5m 34s	14%
		MFA-COSY/RELAY-3	5m 57s	21%
		MFA-COSY/TOCSY	5m 31s	13%
HMQC	4m 50s	MFA-HMQC/HMQC-COSY	5m 14s	8%
		MFA-HMQC/HMQC- RELAY-3	6m 3s	25%
		MFA-HMQC/HMQC-TOCSY	5m 31s	14%
HMBC	5m 11s	MFA-HMBC/HMBC-COSY	5m 37s	8%
		MFA-HMBC/HMBC-TOCSY	5m 53s	14%

Table S1. Comparison of experimental measurement times between different pattern and MFA experiments. Experimental parameters: pre-scan delay of 1 s; 2 scans per t_1 increment; 128 t_1 increments of 1024 points each one; $sw(^1H)$ = 10 ppm, $sw(^{13}C)$ =160 ppm; FID acquisition time of 90 ms; TOCSY mixing time of 60 ms.

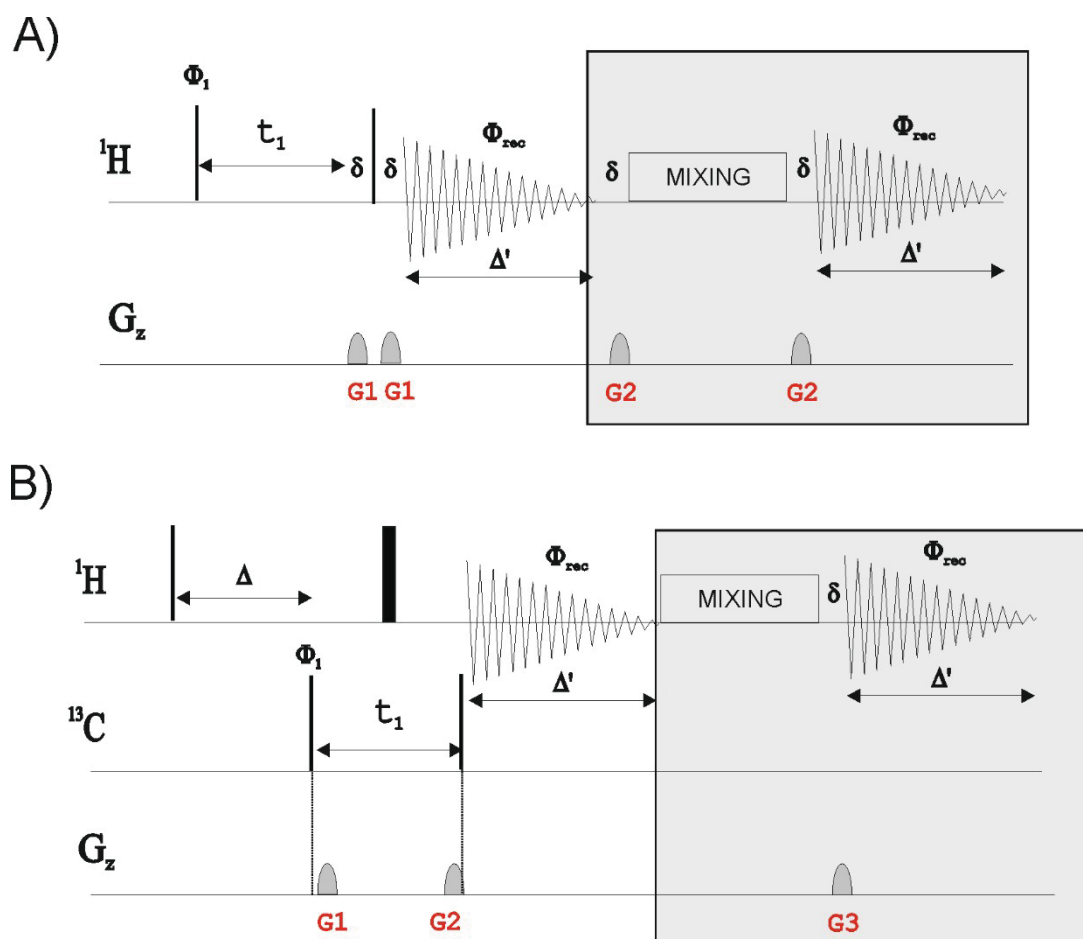


Figure S1: General scheme showing the incorporation of the MFA strategy in A) homonuclear (the example shows the gradient-enhanced COSY as a pattern experiment) and B) heteronuclear (the example shows the gradient-enhanced HMBC as a pattern experiment) NMR experiments. Grey boxes stand for additional COSY-based or TOCSY-based transfers appended after the conventional FID acquisition with the aim of collecting multiple NMR data into the same scan.

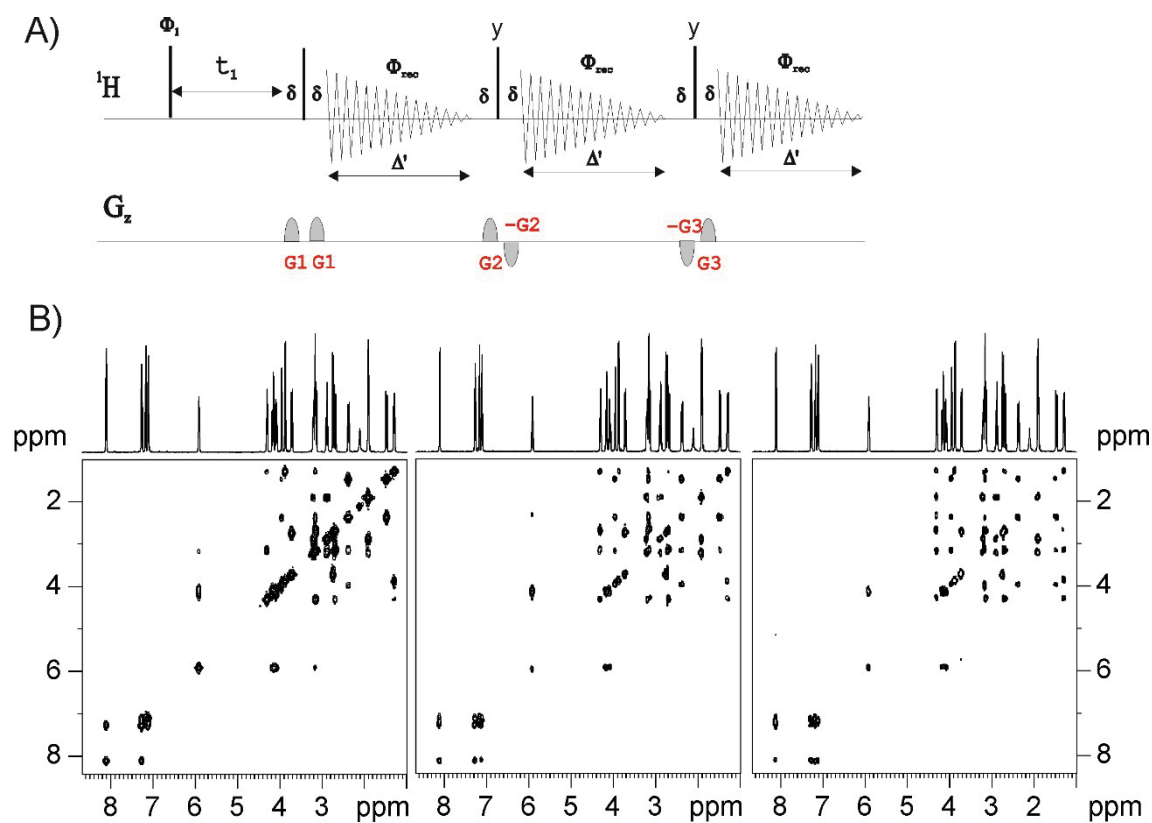


Figure S2: A) Pulse scheme of the MFA-COSY-RELAY-2 experiment. B) Separated 2D COSY, RELAY, and RELAY-2 NMR spectra of strychnine simultaneously obtained from the pulse scheme of Fig. A. See experimental section for details.

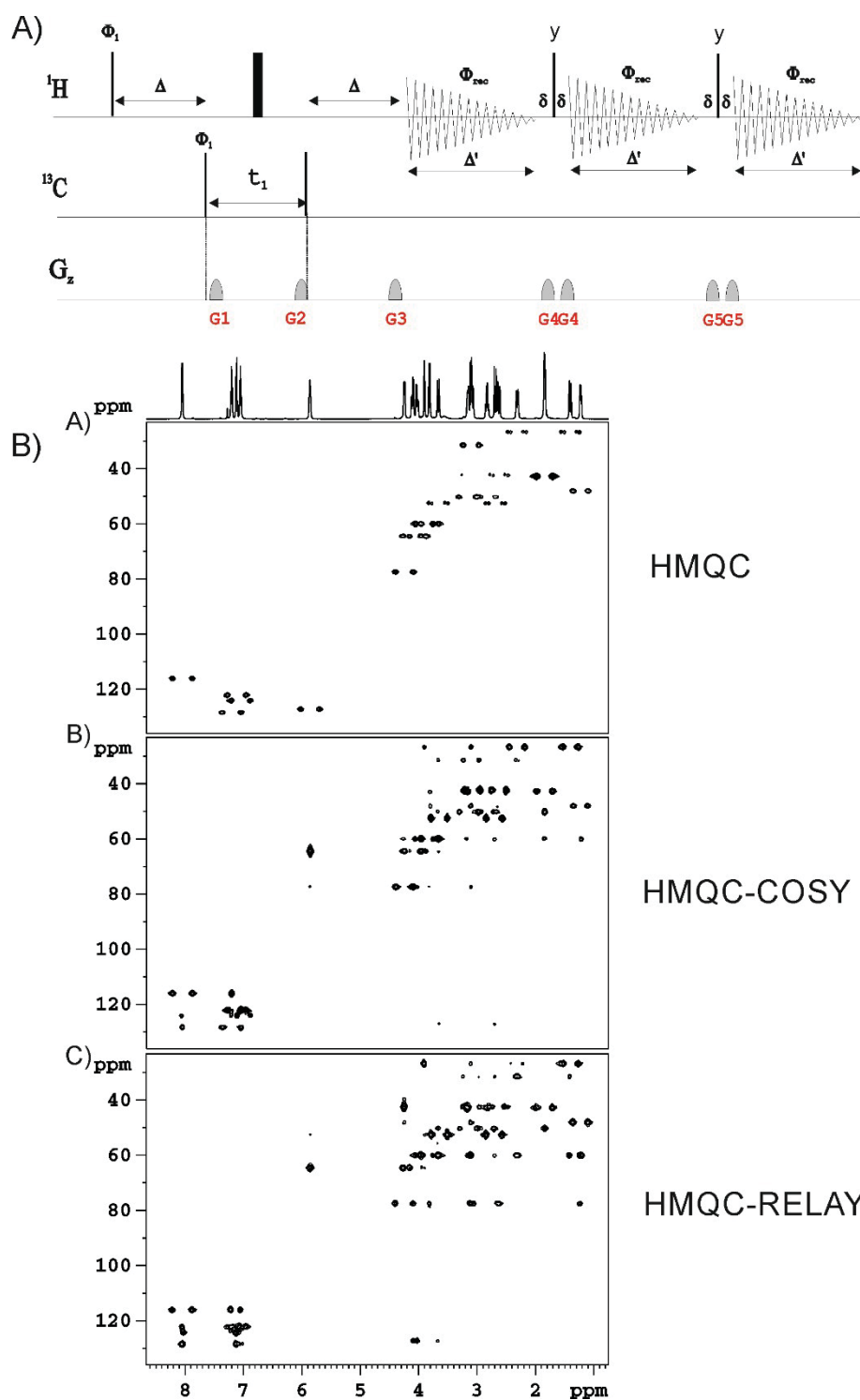


Figure S3: A) Pulse scheme of the MFA-HMQC/HMQC-COSY experiment. B) Separated 2D HMQC, 2D HMQC-COSY and 2D HMQC-RELAY NMR spectra of strychnine simultaneously obtained from the pulse scheme of Fig. S3A.

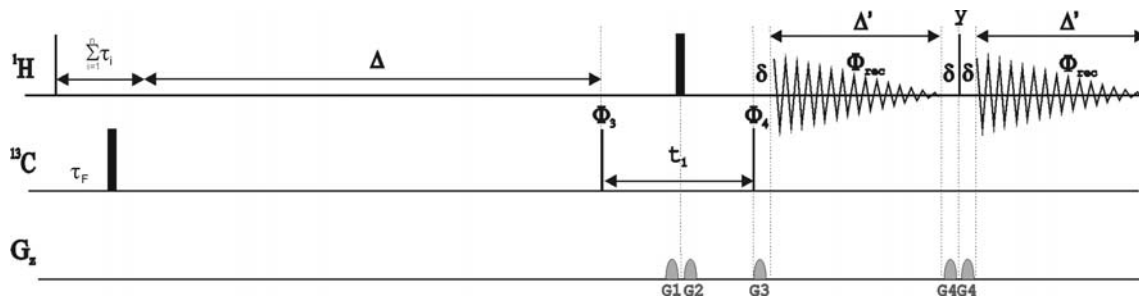


Figure S5: Pulse sequence of the MA-MBOB-COSY experiment. τ_i is the overall duration of low-pass J filter. The durations into the second-order low-pass J filter element were $\tau_F = (0, \tau_1, \tau_2, \tau_1 + \tau_2)$, $\tau_1 = (2 * ({}^1J_{\min} + 0.146({}^1J_{\max} - {}^1J_{\min})))^{-1} \propto \nu \delta$, $\tau_2 = (2 * ({}^1J_{\min} - 0.146({}^1J_{\max} - {}^1J_{\min})))^{-1}$. The interpulse Δ delay in the MBOB experiment was optimized at 8 Hz ($=1/(2 * {}^nJ_{CH})$) and Δ' stands for the acquisition time. The duration of each gradient is specified as δ and the gradient ratio was set to G1:G2:G3:G4 is 50:30:40:15. Phase cycling is $\Phi_1=x, -x, x, -x$; $\Phi_2=x, x, -x, -x$. $\Phi_{\text{rec}}=x, -x, -x, x$.

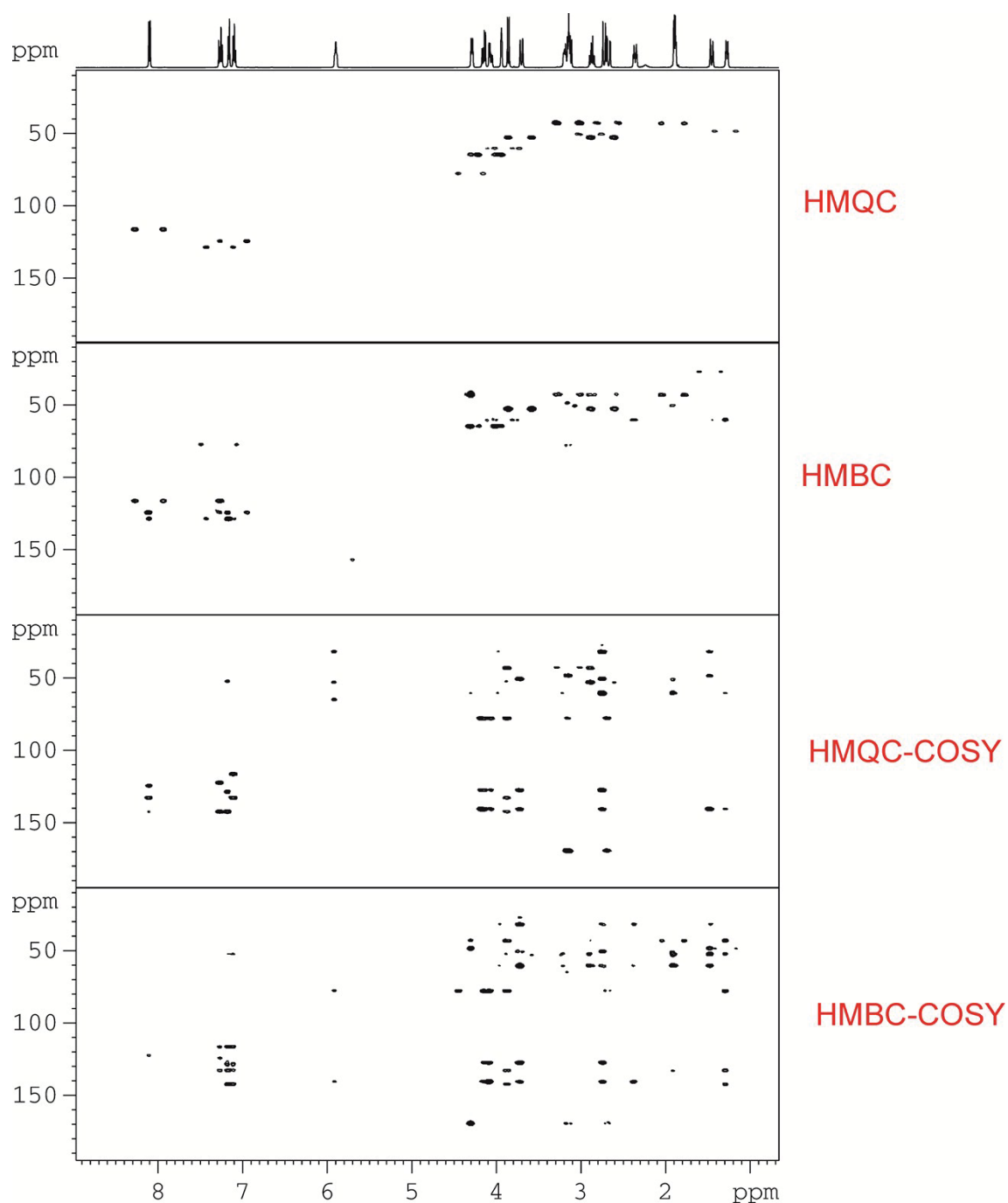


Figure S6: A) Separated 2D HMQC, 2D HMQC-COSY, 2D HMBC and 2D HMBC-COSY spectra of strychnine obtained simultaneously by the herein proposed MA-MBOB-COSY pulse sequence of Fig. S5. B) Expanded areas showing one-bond (HMQC), two-bond (HMQC-COSY), two- and three-bond (HMBC), and two, three- and four-bond correlations (HMBC-COSY).

Pulse Programs (for Topspin v1.3)

```
; mfa-cosyrelay
;topspin v1.3
#include <Avance.incl>
#include <Grad.incl>
"d0=3u"
"d13=4u"
1 ze
2 d1
3 50u
  p1 ph1
  d0
  d13 UNBLKGRAD
  p16:gp1
  d16
  p1 ph2
  d13
  p16:gp1
  d16
  goscnp ph31
  d13 wr #1
  p16:gp2
  d16
  p1 ph11
  d13
  p16:gp2*-1
  d16
  goscnp ph31
  d13 wr #2
  p16:gp3*-1
  d16
  p1 ph11
  d13
  p16:gp3
  d16
  goscnp ph31
  d13 wr #3
  p16:gp4
  d16
  p1 ph11
  d13
  p16:gp4*-1
  d16 BLKGRAD
  gosc ph31
  d1 wr #4
  lo to 3 times 2
  30u if #1
  30u if #2
  30u if #3
  30u if #4
  30u id0
  lo to 3 times tdl
```

```

exit

ph1=0 2
ph2=0
ph11=1
ph31=0 2

;p11 : f1 channel - power level for pulse (default)
;p0 : f1 channel - 20 to 90 degree high power pulse
;p1 : f1 channel - 90 degree high power pulse
;p16: homospoil/gradient pulse
;d0 : incremented delay (2D) [3 usec]
;d1 : relaxation delay; 1-5 * T1
;d13: short delay [4 usec]
;d16: delay for homospoil/gradient recovery
;in0:  $1/(1 * SW) = 2 * DW$ 
;nd0: 1
;NS: 1 * n
;DS: 16
;td1: number of experiments
;FnMODE: QF
;for z-only gradients:
;gpz1: 50%
;gpz2: 30%
;gpz3: 40%
;gpz4: 17%
;use gradient files:
;gpnam1: SINE.100
;gpnam2: SINE.100
;gpnam3: SINE.100
;gpnam4: SINE.100

```

```

;mf_cosy-tocsy
;topspin vl.3
#include <Avance.incl>
#include <Grad.incl>
#include <Delay.incl>
"p7=p6*2"
"d13=4u"
"d0=in0/2-p1*2/3.1416-4u"
"FACTOR1=(d9/(p6*115.112))/2+0.5"
"l1=FACTOR1*2"
1 ze
2 d1
3 50u
  p1 ph1
  d0
  50u UNBLKGRAD
  p16:gp1
  d16
  p1 ph2
  50u
  p16:gp1
  d16 BLKGRAD
  goscnp ph31
  50u wr #1
  50u UNBLKGRAD
  p1 ph2
  50u
  p16:gp3
  d16
  4u p110:f1
4 p6*3.556 ph23
  p6*4.556 ph25
  p6*3.222 ph23
  p6*3.167 ph25
  p6*0.333 ph23
  p6*2.722 ph25
  p6*4.167 ph23
  p6*2.944 ph25
  p6*4.111 ph23
  p6*3.556 ph25
  p6*4.556 ph23
  p6*3.222 ph25
  p6*3.167 ph23
  p6*0.333 ph25
  p6*2.722 ph23
  p6*4.167 ph25
  p6*2.944 ph23
  p6*4.111 ph25
  p6*3.556 ph25
  p6*4.556 ph23
  p6*3.222 ph25
  p6*3.167 ph23
  p6*0.333 ph25
  p6*2.722 ph23
  p6*4.167 ph25
  p6*2.944 ph23

```

```

p6*4.111 ph25
p6*3.556 ph23
p6*4.556 ph25
p6*3.222 ph23
p6*3.167 ph25
p6*0.333 ph23
p6*2.722 ph25
p6*4.167 ph23
p6*2.944 ph25
p6*4.111 ph23
lo to 4 times l1
d12 pl1:f1
p1 ph2
50u
p16:gp2
d16 BLKGRAD
goscnp ph31
d1 wr #2
lo to 3 times 2
30u if #1
30u if #2
30u id0
lo to 3 times tdl
exit

ph1=0 2
ph2=0
ph23=3
ph25=1
ph31=0 2

;p11 : f1 channel - power level for pulse (default)
;p110: f1 channel - power level for TOCSY-spinlock
;p1 : f1 channel - 90 degree high power pulse
;p5 : f1 channel - 60 degree low power pulse
;p6 : f1 channel - 90 degree low power pulse
;p7 : f1 channel - 180 degree low power pulse
;p17: f1 channel - trim pulse [2.5 msec]
;d0 : incremented delay (2D)
;d1 : relaxation delay; 1-5 * T1
;d9 : TOCSY mixing time
;d12: delay for power switching [20 usec]
;in0: 1/(1 * SW) = 2 * DW
;nd0: 1
;NS: 2 * n
;DS: 8
;td1: number of experiments
;FnMODE: QF
;for z-only gradients:
;gpz1: 10%
;gpz2: 20%
;gpz3: 33%
;use gradient files:
;gpnam1: SINE.100
;gpnam2: SINE.100
;gpnam3: SINE.100

```

```

;mf_hmbctocsy
;topspin vl.3
#include <Avance.incl>
#include <Grad.incl>
#include <Delay.incl>
"p5=p6*.667"
"p7=p6*2"
"p2=p1*2"
"d0=3u"
"d13=3u"
"d6=1s/(cnst13*2)"
"DELTA1=50u+p16+d16+4u"
"SCALEF=p7*2/p5+0.5"
"FACTOR1=((d9-p17*2)/(p6*64+p5))/SCALEF+0.5"
"l1=FACTOR1*SCALEF"

1 ze
2 d1
3 d12 p11:f1
  p1 ph1
  d6
  p3:f2 ph4
  d0
  50u UNBLKGRAD
  p16:gp1
  d16
  p2 ph2
  50u
  p16:gp2
  d16
  d0
  p3:f2 ph5
  goscnp ph31
  50u wr #1
  p16:gp3
  d16
  4u p110:f1
  (p17 ph26)

;begin MLEV17
4 (p6 ph22 p7 ph23 p6 ph22)
  (p6 ph24 p7 ph25 p6 ph24)
  (p6 ph24 p7 ph25 p6 ph24)
  (p6 ph22 p7 ph23 p6 ph22)
  (p6 ph24 p7 ph25 p6 ph24)
  (p6 ph24 p7 ph25 p6 ph24)
  (p6 ph22 p7 ph23 p6 ph22)
  (p6 ph22 p7 ph23 p6 ph22)
  (p6 ph24 p7 ph25 p6 ph24)
  (p6 ph22 p7 ph23 p6 ph22)
  (p6 ph22 p7 ph23 p6 ph22)
  (p6 ph24 p7 ph25 p6 ph24)
  (p6 ph22 p7 ph23 p6 ph22)
  (p6 ph22 p7 ph23 p6 ph22)
  (p6 ph24 p7 ph25 p6 ph24)
  (p6 ph24 p7 ph25 p6 ph24)
  (p5 ph23)

```

```

lo to 4 times l1

;end MLEV17

(p17 ph26)
50u
p16:gp3*-1
d16 BLKGRAD
gosc ph31
d1 wr #2
lo to 3 times 2
10m if #1
10m if #2
10m id0
lo to 3 times tdl
exit

ph1=0
ph11=1
ph2=0
ph3=0
ph4=0 2
ph5=0 0 2 2
ph22=3
ph23=0
ph24=1
ph25=2
ph26=0
ph31=0 2 2 0

;p11 : f1 channel - power level for pulse (default)
;p12 : f2 channel - power level for pulse (default)
;p1 : f1 channel - 90 degree high power pulse
;p2 : f1 channel - 180 degree high power pulse
;p3 : f2 channel - 90 degree high power pulse
;p16: homospoil/gradient pulse
;id0 : incremented delay (2D) [3 usec]
;d1 : relaxation delay; 1-5 * T1
;d2 : 1/(2J)XH
;d6 : delay for evolution of long range couplings
;d16: delay for homospoil/gradient recovery
;cnst2: = J(XH)
;cnst13: = J(XH) long range
;in0: 1/(2 * SW(X)) = DW(X)
;nd0: 2
;NS: 2 * n
;DS: 16
;td1: number of experiments
;FnMODE: QF
;for z-only gradients:
;gpz1: 30%
;gpz2: 50%
;gpz3: 17% for C-13
;use gradient files:
;gpnam1: SINE.100
;gpnam2: SINE.100
;gpnam3: SINE.100

```



```

;teo_mf_hmbccosy

#include <Avance.incl>
#include <Grad.incl>
#include <Delay.incl>

"p2=p1*2"
"d0=3u"
"d13=3u"
"d6=1s/(cnst13*2)"
"DELTA1=50u+p16+d16+4u"

1 ze
2 d1
3 p1 ph1
  d6
  p3:f2 ph4
  d0
  50u UNBLKGRAD
  p16:gp1
  d16
  p2 ph2
  50u
  p16:gp2
  d16
  d0
  p3:f2 ph5
  goscnp ph31
  50u wr #1
  p16:gp3
  d16
  p1 ph11
  50u
  p16:gp3*-1
  d16 BLKGRAD
  gosc ph31
  d1 wr #2
  lo to 3 times 2
  10m if #1
  10m if #2
  10m id0
  lo to 3 times td1
exit

ph1=0
ph11=1
ph2=0
ph3=0
ph4=0 2
ph5=0 0 2 2
ph31=0 2 2 0

;p11 : f1 channel - power level for pulse (default)

```

```

;pl2 : f2 channel - power level for pulse (default)
;p1 : f1 channel - 90 degree high power pulse
;p2 : f1 channel - 180 degree high power pulse
;p3 : f2 channel - 90 degree high power pulse
;p16: homospoil/gradient pulse
;d0 : incremented delay (2D) [3 usec]
;d1 : relaxation delay; 1-5 * T1
;d2 : 1/(2J)XH
;d6 : delay for evolution of long range couplings
;d16: delay for homospoil/gradient recovery
;cnst2: = J(XH)
;cnst13: = J(XH) long range
;in0: 1/(2 * SW(X)) = DW(X)
;nd0: 2
;NS: 2 * n
;DS: 16
;td1: number of experiments
;FnMODE: QF

```

```

;mf-mbob-cosy

#include <Avance.incl>
#include <Grad.incl>
#include <Delay.incl>

"p4=p3*2"
"p2=p1*2"
"d0=3u"
"d13=3u"
"d2=0s"
"d3=0.5s*(1/(cnst8+0.146*(cnst9-cnst8)))" ;cnst9: jmax
"d4=0.5s*(1/(cnst9-0.146*(cnst9-cnst8)))" ;cnst8: jmin
"d5=d3+d4"

"d6=1s/(cnst13*2)"
"d7=d2+d3+d4+d5"

"DELTA2=d7-d2-p4"
"DELTA3=d7-d3-p4"
"DELTA4=d7-d4-p4"
"DELTA5=d7-d5-p4"

1 ze
2 d1 p11:f1 p12:f2
3 p1 ph1

    if "cnst26 == 0"
        {
            d2
        }
    if "cnst26 == 1"
        {
            d3
        }
    if "cnst26 == 2"
        {
            d4
        }
    if "cnst26 == 3"
        {
            d5
        }

p4:f2 ph1

    if "cnst26 == 0"
        {
            DELTA2
        }
    if "cnst26 == 1"
        {
            DELTA3

```

```

    }
    if "cnst26 == 2"
    {
        DELTA4
    }
    if "cnst26 == 3"
    {
        DELTA5
    }

d6
p3:f2 ph3
d0
50u UNBLKGRAD
p16:gp1
d16
p2 ph2
50u
p16:gp2
d16
d0
p3:f2 ph4
4u
p16:gp3
d16
goscnp ph31
10u wr #1
p16:gp4
d16
p1 ph11
10u
p16:gp4
d16 BLKGRAD
gosc ph31
d1 wr #2
lo to 3 times ns
10u if #1
10u if #2
10u id0
lo to 2 times td1
exit

ph1=0
ph11=1
ph2=0
ph3=0 2
ph4=0 0 2 2
ph31=0 2 2 0

;p11 : f1 channel - power level for pulse (default)
;p12 : f2 channel - power level for pulse (default)
;p1 : f1 channel - 90 degree high power pulse
;p2 : f1 channel - 180 degree high power pulse
;p3 : f2 channel - 90 degree high power pulse
;p16: homospoil/gradient pulse
;d0 : incremented delay (2D) [3 usec]

```

```

;dl : relaxation delay; 1-5 * T1
;d2 : 1/(2J)XH
;d6 : delay for evolution of long range couplings
;dl6: delay for homospoil/gradient recovery
;cnst2: = J(XH)
;cnst13: = J(XH) long range
;in0: 1/(2 * SW(X)) = DW(X)
;nd0: 2
;NS: 2 * n
;DS: 16
;td1: number of experiments
;FnMODE: QF

```

4.2. Publication 2: Simultaneous acquisition of two 2D HSQC spectra with different ^{13}C spectral widths.

4.2.1. Introduction

Enhancing resolution into NMR spectra has become an essential objective for spectroscopists. Many approaches have been developed to improve spectral and/or digital resolution along the indirect dimension in multidimensional NMR experiments. Spectral aliasing (SA) is one of the most simple tools for this purpose. For instance, the incorporation of SAPS in the HSQC experiment has been verified as a powerful strategy for enantioresolution studies because achieving enhanced digital and spectral resolution applying SA in F1 and improved spectral resolution by broadband homodecoupling in F2 at the same time. In this work, a suitable combination between SA and MFA provides the opportunity to get complementary HSQC spectra with excellent F1 spectral resolution and without the temporary loss of chemical shift information due to SA. Herein is proposed a time efficiency approach that provides two HSQC FIDs at the same time needed to acquire the original spectrum. Thus, an SA-HSQC spectrum is acquired on FID1 with enhanced F1 resolution whereas a conventional HSQC is collected on FID2. The concerted analysis of both spectra affords accurate assignments of ^{13}C chemical shifts.



Simultaneous acquisition of two 2D HSQC spectra with different ^{13}C spectral widths

Pau Nolis, Kumar Motiram-Corral, Míriam Pérez-Trujillo, Teodor Parella *

Servei de Resonància Magnètica Nuclear, Universitat Autònoma de Barcelona, E-08193, Bellaterra, Barcelona, Catalonia, Spain

ARTICLE INFO

Article history:

Received 15 November 2018

Revised 10 January 2019

Accepted 11 January 2019

Available online 14 January 2019

Keywords:

NMR

PEP

HSQC

MFA

Multiple FID acquisition

Spectral aliasing

ABSTRACT

A time-efficient NMR strategy that involves the interleaved acquisition of two 2D HSQC spectra having different spectral widths in the indirect ^{13}C dimension is presented. We show how the two equivalent coherence transfer pathways involved in sensitivity-enhanced HSQC experiments are managed selectively and detected separately in different FID periods within the same scan. The feasibility of this new SADA-HSQC (Spectral Aliasing in Dually Acquired HSQC) technique is demonstrated by recording simultaneously two complementary datasets, conventional and highly-resolved spectral-aliased 2D HSQC spectra, in a single NMR experiment. Combining the information from both datasets, accurate chemical shift determination and excellent signal dispersion is achieved in a unique measurement using only few t_1 increments.

© 2019 Elsevier Inc. All rights reserved.

1. Introduction

The digital resolution that is achieved along the indirect ^{13}C dimension (DR1) in 2D HSQC spectra is directly proportional to the number of collected t_1 increments (TD1) and indirectly proportional to the ^{13}C spectral width (SW1) to be monitored. Several techniques are available to improve such DR1, for instance, incorporating ^{13}C band-selective excitation into the pulse scheme and reducing SW1 to the region of interest [1,2], using non-uniform sampling (NUS) to reduce the effective TD1 [3–5], or applying resolution-enhanced data processing tools such as zero-filling or linear prediction [6]. Another simple but powerful approach to increase DR1 without changing the original pulse program or the acquisition mode is the re-acquisition of a second HSQC dataset with a reduced SW1. Thus, the DR1 before processing is 377.3 Hz/pt for a 2D HSQC experiment acquired with 128 t_1 increments and SW1 = 160 ppm at 600 MHz. On the other hand, by merely setting SW1 to a small value of 5 ppm, DR1 is improved by a factor of 32 until 11.8 Hz/pt without practically changing the duration of the experiment. The inconvenience of such an approach is that cross-peaks appear folded or aliased depending on the quadrature detection method applied in the indirect dimension. Sometimes, the concepts of spectral aliasing (SA) and spectral folding have been used indistinctly, introducing some confusion.

To clarify, Echo-anti/echo, States or States-TPPI quadrature detection in F1 affords aliased (superimposed) signals whereas TPPI generates folded (mirrored) signals [9]. For instance, a ^{13}C signal resonating at 110 ppm appeared at 10 ppm in an aliased HSQC experiment using an SW1 of 100 ppm and centered to 50 ppm. On the other hand, this same signal would appear at 90 ppm in the equivalent folded HSQC spectrum. Specifically, the regular sensitivity-enhanced HSQC (SE-HSQC) scheme uses the echo-anti/echo protocol to obtain pure absorption lineshapes [7,8], and signals are aliased in the resulting spectral-aliased HSQC (SA-HSQC) spectrum. The superimposed character of aliased signal allows a simple and accurate determination of true chemical shifts ($\delta(^{13}\text{C})^{\text{true}}$) by applying Eq. (1):

$$\delta(^{13}\text{C})^{\text{true}} = \delta(^{13}\text{C})^{\text{aliased}} \pm \kappa * \text{SW1}^{\text{aliased}} \quad (1)$$

where κ is the aliasing factor which depends on the ^{13}C frequency carrier and $\text{SW1}^{\text{aliased}}$ is the spectral width utilized in the aliased experiment [9–12]. SA has been reported for several 2D experiments and some computer-aided spectral reconstruction procedures have been proposed to recover the classical spectral representation with their full spectral width [13–16]. In contrast to other experiments, SA is particularly recommended in HSQC because each ^1H signal only correlates with its directly attached ^{13}C nucleus, minimizing misassignments and allowing direct analysis and an accurate determination of $\delta(^{13}\text{C})$ values without the need of specialized reconstruction programs. [17] Several options have been proposed to determine the signal-dependent κ factor: from

* Corresponding author.

E-mail address: teodor.parella@uab.cat (T. Parella).

a regular 1D $^{13}\text{C}\{^1\text{H}\}$ or DEPT spectrum, [18] using a reference 2D HSQC spectrum with its full SW1, or acquiring two aliased datasets with slightly different SW1 [10,14,15,19]. All these options are time-consuming because two different datasets need to be recorded separately. We have also demonstrated that superb resolution conditions are achieved when SA in the F1 dimension and real-time broadband homodecoupling in the F2 dimension are simultaneously incorporated in the SAPS-HSQC (Spectral Aliased Pure Shift HSQC) experiment. The power of the SAPS-HSQC method to afford ultra-high-resolution 2D NMR maps has been demonstrated in enantiodifferentiation NMR studies [20], to discern between diastereoisomers with near-identical ^1H and ^{13}C NMR spectra [21] and to measure the sign and the magnitude of small coupling constants with high accuracy. [22] Definitively, the SA method is a clear competitor, and also compatible, to other F1 resolution-enhanced methods such as pure shift NMR, NUS or linear prediction.

We present here a novel time-efficient strategy for the simultaneous acquisition of both the reference and the aliased HSQC spectra using a single pulse scheme. Our proposal is based on the implementation of multiple-FID acquisition within the same scan (MFA) [23]. For instance, MFA offers the possibility to acquire simultaneously 2D COSY and 2D TOCSY experiments or 2D HMBC and 2D HMBC-TOCSY experiments using a single acquisition in spectrometers having a basic single-receiver configuration. This approach recovers the afterglow magnetization that remains active in the transverse plane after conventional FID acquisition. MFA has also been combined with other time-efficient NMR strategies such as time-sharing NMR. As an example, the recording of multiple FIDs in time-shared ^1H - ^{13}C , ^1H - ^{15}N HMBC affords four different HMBC spectra in a single collection step [24]. The proposal outlined here uses a different MFA approach based on the management of the two active coherence transfer pathways (CTP) involved in SE-HSQC and their separate detection in two different FID periods [25]. In contrast to the afterglow MFA method, the success of this approach relies on the fact that one of the components resides in the z-axis whereas the other one is detected. After this first detection period (FID1), a purge gradient is applied to remove any residual transverse magnetization and the second component

becomes observable in a second acquisition (FID2) by a final 90° pulse.

2. Results and discussion

The proposed SADA-HSQC (Spectral Aliasing in Dually Acquired HSQC) experiment is displayed in Fig. 1. The SADA-HSQC pulse scheme handles the two components detected jointly in the SE-HSQC experiment in a separate way, allowing them a different behaviour during a double-stage variable evolution period and detecting them separately in different FID periods into the same pulse sequence. The method is related to the DENA (Differential Evolution for Non-ambiguous Aliasing) [14,19] and AMNA (Additional Modulation for Non-ambiguous Aliasing) [19] HSQC experiments where two different aliased signals were simultaneously detected taking advantage of a differential evolution of carbon chemical shift that encodes the aliasing factor. The analysis of these experiments needs a separate HSQC spectrum as a reference, and the aliased spectrum contains two different components than double the number of cross-peaks and therefore increases the probability of signal overlap.

To analyse how SADA-HSQC works, we start with the two operators available at the end of the first t_1 period, I_zS_x (term I) and I_zS_y (term II). After this period, a 90° (^{13}C) pulse retains the first term unaltered in the transverse plane while the term II is converted to zz magnetization. A second λ -scaled t_1 evolution time is applied to allow further ^{13}C chemical shift evolution exclusively for term I. Thus, term I evolves during $\lambda * t_1$ with a dephasing gradient effect proportional to $G2 + G2$ whereas term II evolves exclusively during t_1 with a dephasing proportional to $G2$. After this second variable period, a 90° (^1H) pulse converts term I to multiple-quantum coherences (I_yS_x) whereas the term II is converted to anti-phase (AP) ^1H magnetization (I_xS_z) which evolve to in-phase (IP) magnetization (I_y) in the subsequent echo period. The following 90° pulses applied to both ^1H and ^{13}C from the y-axis, convert term I in AP ^1H magnetization (I_yS_z) whereas term II is stored as I_z magnetization. The subsequent echo period refocuses term I to IP magnetization which is detected during the FID1 period whereas term II remains unused along the z-axis. After that, a purging gradient is

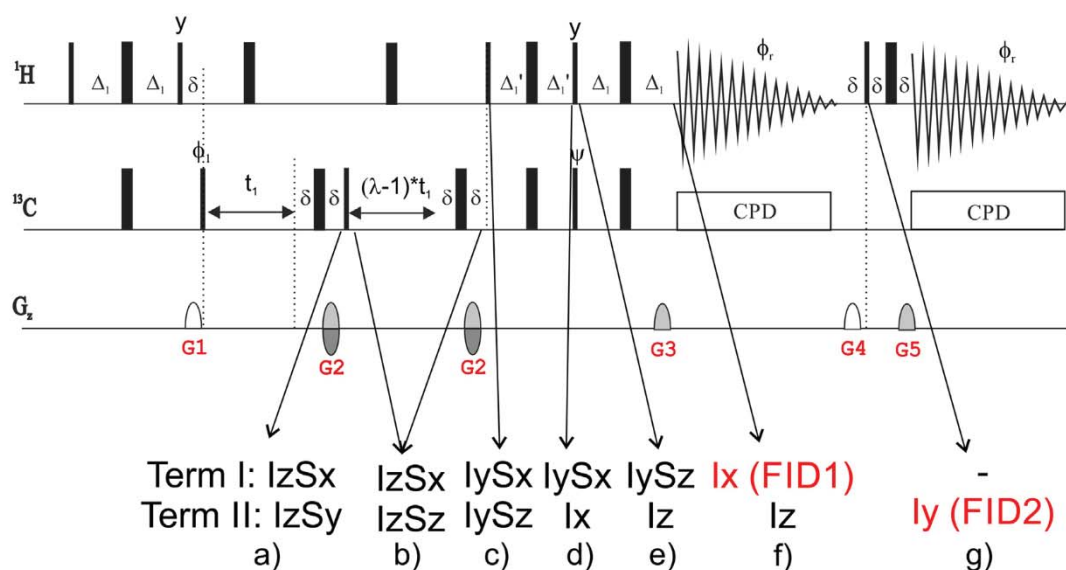


Fig. 1. Pulse sequence scheme of the SADA-HSQC experiment designed to record two HSQC datasets with different ^{13}C spectral windows in an interleaved mode. The two active terms in each key point into the sequence are shown. Narrow and wide filled bars correspond to 90° and 180° pulses, respectively, with phase x unless indicated otherwise. The inter-pulse delays were optimized to $\Delta_1 = 1/(4 * J_{\text{CH}})$ and $\Delta_2 = 1/(8 * J_{\text{CH}})$ and δ stand for the duration of a pulsed field gradient and its recovery delay. A λ -scaled evolution period is incorporated for the selective monitoring of terms I and II which are detected in separate FID1 and FID2 periods, respectively. The spectral width in the indirect dimension (SW1) is set to $1/(2 * \lambda * \Delta t_1)$ and $1/(2 * \Delta t_1)$ for FID1 and FID2 datasets, respectively. A minimum phase cycle is used: $\phi_1 = x, -x$ and $\phi_2 = x, -x$. More details can be found in the experimental section.

applied to remove any residual magnetization coming from term I and a last 90° (^1H) pulse flips term II to the transverse plane, which is detected during the FID2 period. For a proper selection of both CTPs, gradients G_2 , G_3 and G_5 are set to 40%, 20.1% and 10.05% according to Eqs. (2) and (3):

$$\text{Term I(FID1)} : p1 * G_2 * \gamma_C + p1 * G_2 * \gamma_C - G_3 * \gamma_H = 0 \quad (2)$$

$$\text{Term 2(FID2)} : p1 * G_2 * \gamma_C - G_5 * \gamma_H = 0 \quad (3)$$

Data acquisition in FID1 and FID2 are made in identical conditions, and therefore the detected F2 dimension in both spectra is the same. The SADA-HSQC experiment yields a 2D HSQC spectrum with its full spectral width ($\text{SW1}^{\text{normal}}$) in FID 2 whereas an aliased HSQC spectrum showing a reduced $\text{SW1}^{\text{aliased}}$ according to the λ factor is obtained in FID1:

$$\text{SW1}^{\text{aliased}} = \text{SW1}^{\text{normal}} / \lambda \quad (4)$$

The practical aspects of the new SADA-HSQC technique are here assessed regarding the importance of the inter-pulse delay optimization, the relationship between the λ scaling factor and the digital resolution in F1, the duration of FID periods and their effects on sensitivity in both FID1 and FID2 data. Also, the influence of the number of increments to be collected and the overall experimental times that can recommend the use of the MFA approach instead of the conventional sequential step-by-step acquisition is discussed. The performance of the SADA-HSQC experiment has been verified using a test sample of the cyclic peptide cyclosporine dissolved in CDCl_3 that was also used to evaluate the performance of previous spectral aliased HSQC methods [13–15,19]. The collection of a set of different experiments varying the λ factor, the number of increments and the duration of the FIDs was performed. Initially, the acquisition conditions included 128 increments and $\text{SW1} = 100$ ppm. Fig. 2 shows the 2D HSQC spectra obtained from FID1 and FID2 in the SADA-HSQC scheme after conventional Four-

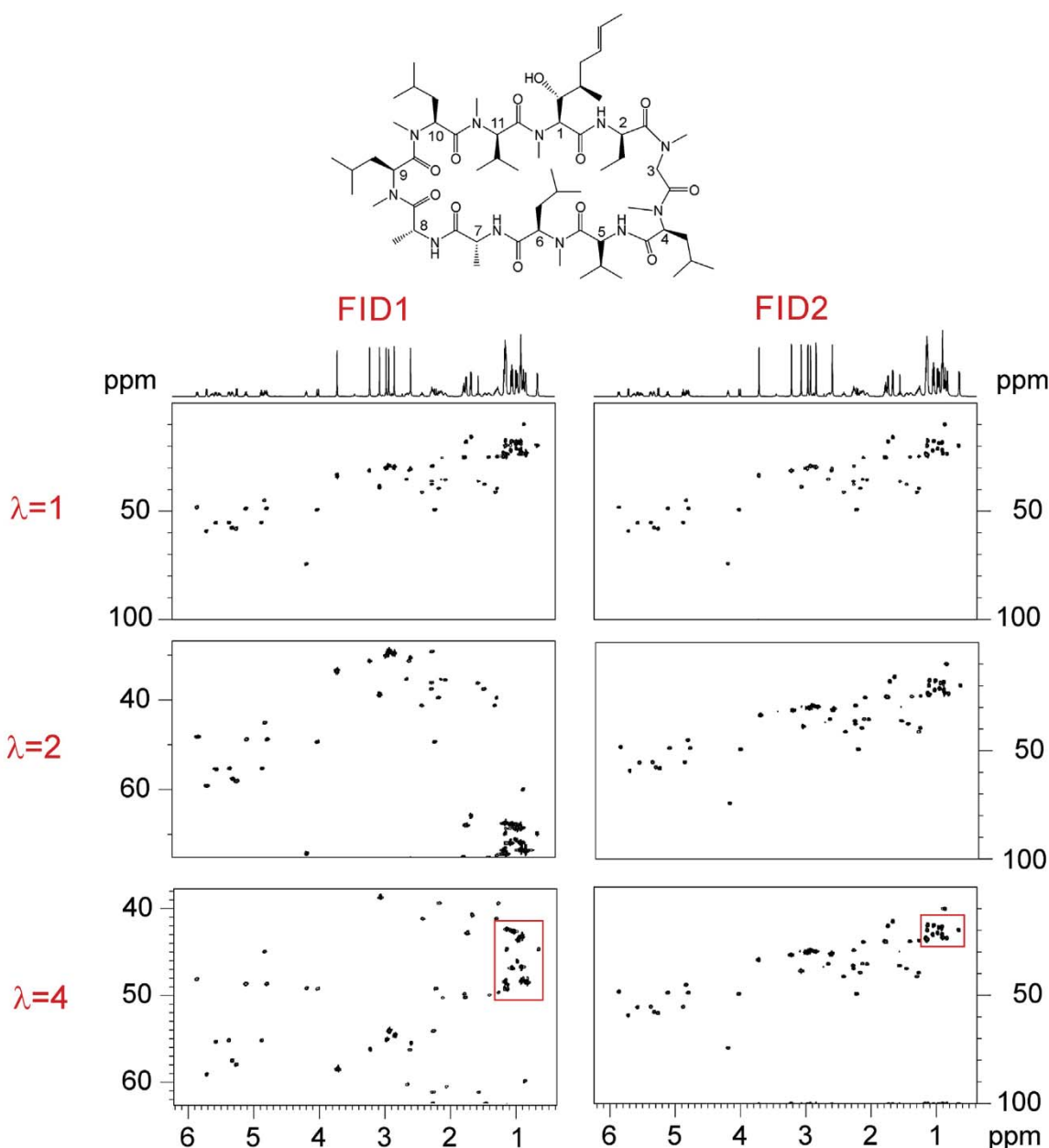


Fig. 2. (Left) Spectral-aliased (FID1) and (Right) conventional (FID2) 2D HSQC spectra of the peptide cyclosporine in CDCl_3 acquired simultaneously with the SADA-HSQC pulse scheme, with λ -scaling factors of 1, 2 and 4. SW1 in FID1 are 100, 50 and 25 ppm, respectively. Note that the aliphatic methyl signals are better dispersed in the FID1 spectrum, as shown in the highlighted boxes.

ier transformation, using λ factors of 1, 2 and 4. As shown, FID2 always affords the regular HSQC spectrum with its full $SW1^{\text{normal}}$ (100 ppm) whereas FID1 yields the corresponding aliased HSQC spectrum according to the applied λ factor, with $SW1^{\text{aliased}}$ of 100, 50 and 25 ppm, respectively. At first glance, the complementarity and different DR1 between the two spectra is displayed in the region of the aliphatic methyl signals highlighted in boxes.

Fig. 3 compares the relative sensitivities achieved for each FID1 and FID2 datasets in experiments recorded with scaling factors of $\lambda = 1, 8$ and 16. In the basic experiment acquired with $\lambda = 1$, FID2 affords the same spectrum (same $SW1$) than FID1 but differing of the signal intensities due to different factors. Most of the signal attenuation observed in FID1 is due to the additional gradient CTP selection applied in the second t_1 period. In addition, signal

intensity for the different CH_n multiplicities strongly depends on Δ_1 , and Δ_1 delays optimization (see Fig. S3 for simulations). When λ is increased, the overall sensitivity in both FID1 and FID2 is attenuated by $\sim 10\%$ and $\sim 20\%$ for $\lambda = 8$ and $\lambda = 16$, respectively, due to T_2 relaxation effects as similarly observed when comparing conventional HSQC and SA-HSQC spectra. In these cases, t_1^{max} is 8.48, 67.85 and 135.7 ms for $\lambda = 1, 8$ and 16, respectively. The practical limits on important parameters such as the optimum λ factors, the $SW1$ to be monitored and the FID1/FID2 durations depend on each sample, as a function of the existing signal overlapping and the T_2 relaxation times. Despite the mentioned sensitivity drawbacks, SADA-HSQC experiments with high λ factors corresponding to $SW1$ of 1–2 ppm can be executed for a medium-sized molecule like cyclosporine (MW = 1202) with an obvious progressive signal

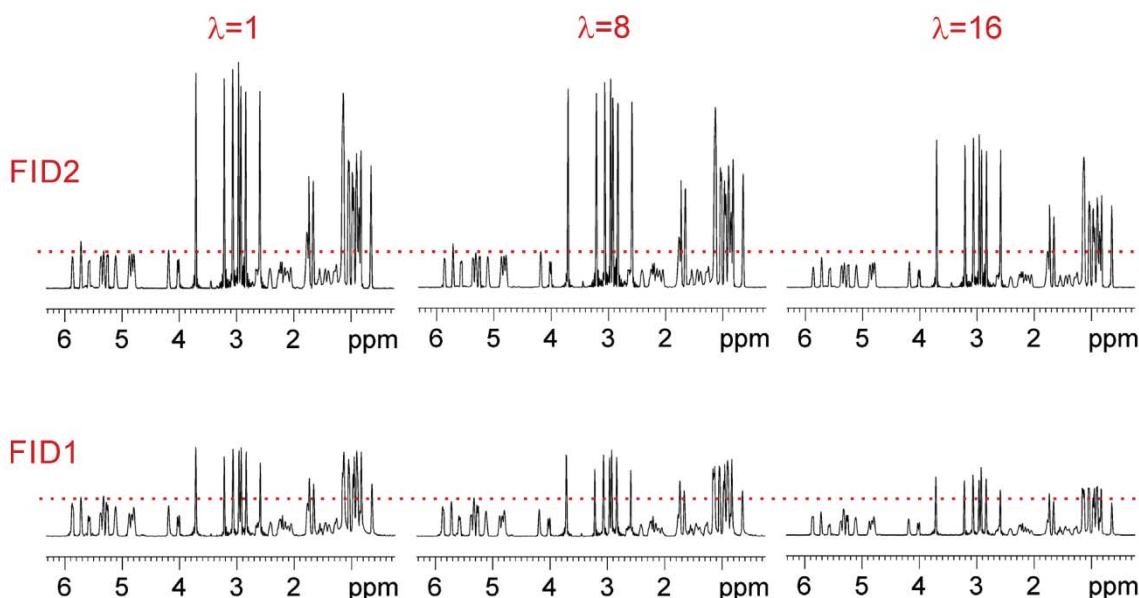


Fig. 3. 1D internal F2 projections to correlate relative sensitivities for the (bottom) SA-HSQC (FID1) and (top) HSQC (FID2) spectra simultaneously collected with the SADA-HSQC pulse scheme, with λ scaling factors of 1, 8 and 16.

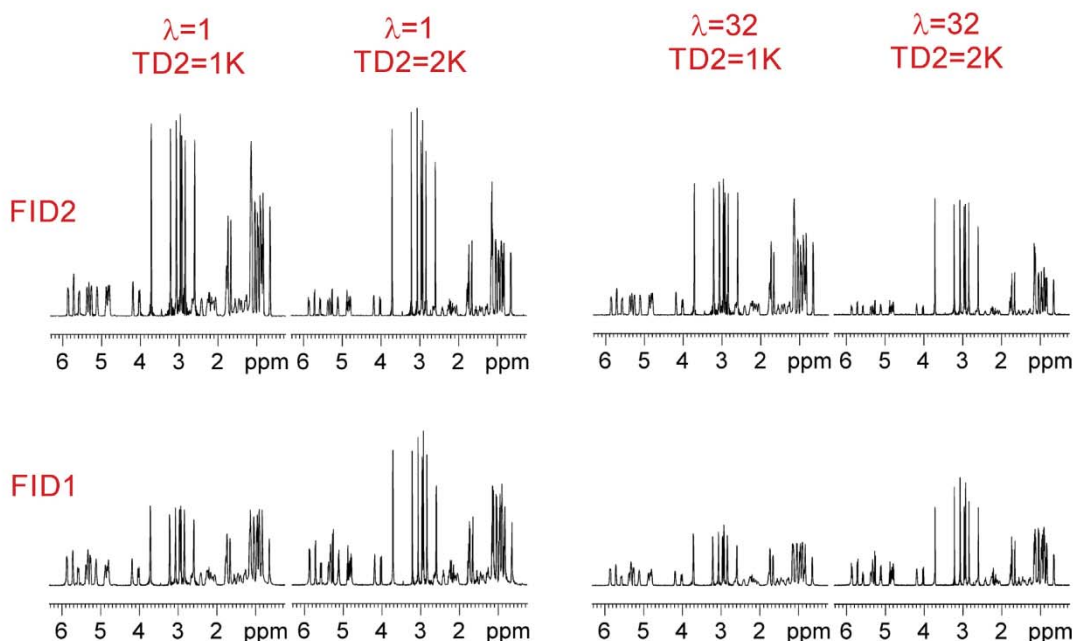


Fig. 4. 1D internal projections extracted from the F2 dimensions in (bottom) spectral-aliased (FID1) and (top) conventional (FID2) 2D HSQC spectra obtained simultaneously from the SADA-HSQC pulse scheme using λ values of 1 and 32, and $TD2$ of 1 K and 2 K.

decrease but with very high levels of DR1 that can reach 2–4 Hz/pt before data transformation, of the same order as what is obtained in conventional 1D ^{13}C spectra. Experimental times of HSQC, SA-HSQC, SADA-HSQC (with different λ factors) experiments are shown in Tables S1–S2. The implementation of SA in conventional HSQC experiments only lengthens the duration of the SA-HSQC experiment by 5% due to t_1^{max} . Regarding spectrometer times, SADA-HSQC is collected in about the 55% of the time needed for the separate acquisition of HSQC and SA-HSQC experiments.

Another key parameter to evaluate the feasibility of MFA experiments is the duration of the FID1 and FID2 periods (AQ) which defines the resolution in the acquisition dimension. Using routine conditions such as TD2 of 1024 points and SW2 = 10 ppm, the duration of each FID is 85 ms. Doubling TD2 to 2048 points, AQ is extended to 170 ms. Fig. 4 compares the experimental sensitivities achieved when $\lambda = 1$ and $\lambda = 32$ and using TD2 values of 1 K and 2 K. As it can be observed, the extension of AQ is beneficial for FID1 because the better resolution offers sharper lines and therefore improved sensitivity ($\sim 20\%$), more than compensating for the relaxation effects due to the increased t_1^{max} . Otherwise, the sensitivity of FID2 is decreased by $\sim 25\%$ due to the potential losses by diffusion and/or relaxation effects. However, this loss is irrelevant because the sensitivity in FID1 is the limiting factor in the SADA-HSQC experiment. As a conclusion, the duration of AQ

and therefore the resolution in F2 is not a limitation in the performance of SADA-HSQC experiments.

When sensitivity is not the limiting factor, SADA-HSQC experiments can be recorded with only two scans per increment. To maximize spectrometer time efficiency and to achieve maximum F1 resolution per time unit, the acquisition of the SADA-HSQC experiment using a low number of increments may be advisable. Fig. 5 shows the results obtained for a different number of increments (from 16 to 128). For instance, collecting only 64 increments with SW1 = 100 ppm, the increment Δt_1 value is set to 66.26 μs and a DR1 of 235.8 Hz/pt. On the other hand, the aliased spectrum (with $\lambda = 32$) acquired simultaneously yields an SW1 = 5 ppm and Δt_1 of 2.12 ms, affording an increase of resolution by a factor of 32 up to 7.37 Hz/pt. Under these conditions, the DR1 provided by the SA spectrum would equal to a conventional spectrum recorded with 2048 increments. The SADA-HSQC experiment acquired with $\lambda = 32$ and TD1 = 64 is quickly executed in about 3 min. It is shown how the lack of resolution of FID2 is compensated with the superb resolution and signal dispersion achieved in FID1, even collecting only 16 increments, allowing clear signal identification and assignment as well as of the accurate determination of chemical shift values in very reduced spectrometer times.

Fig. 6 shows the expansion of the aliphatic methyl region of both HSQC and SA-HSQC spectra acquired simultaneously with the SADA-HSQC experiment using $\lambda = 32$ and 64 increments. SW1

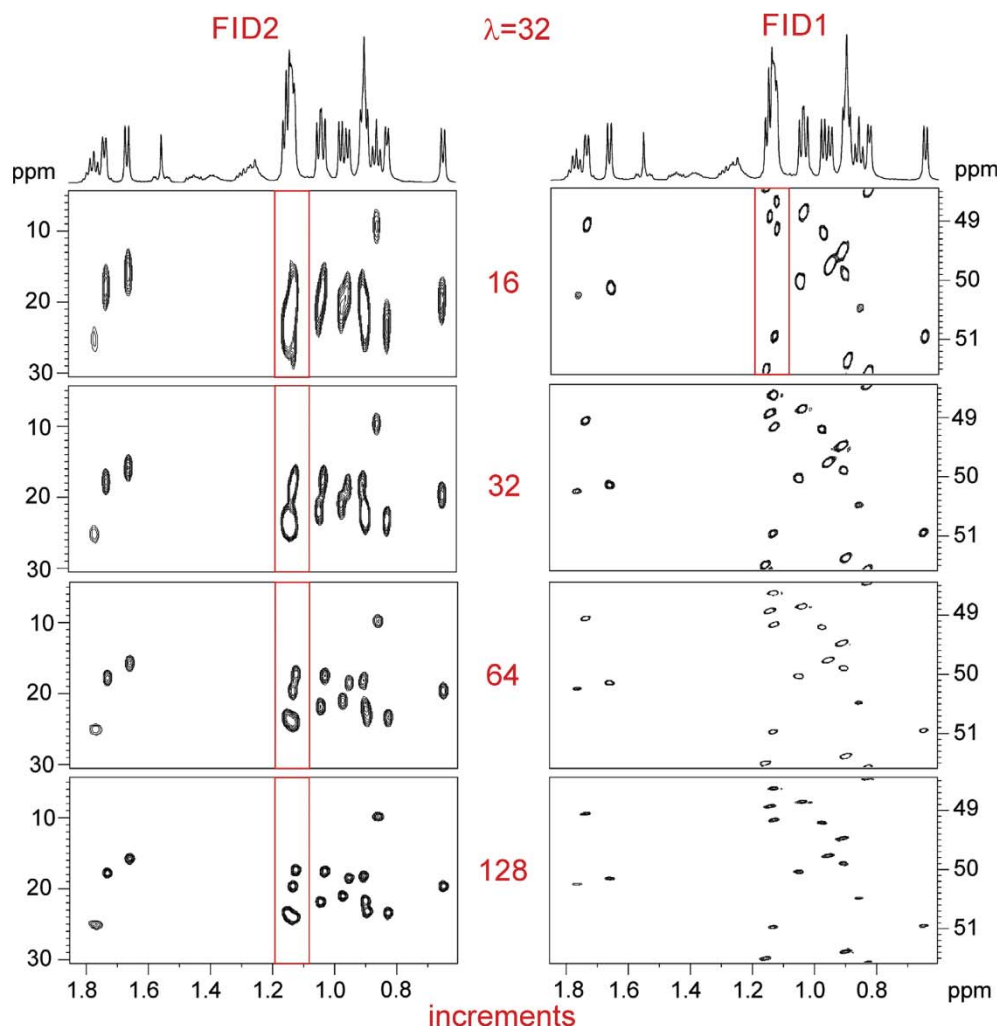


Fig. 5. Expansions of the aliphatic methyl region corresponding to the HSQC (SW1 = 100 ppm) and SA-HSQC (SW1 = 3.125 ppm) spectra acquired simultaneously with the SADA-HSQC experiment with $\lambda = 32$ and TD1 values from (top) 128 to (bottom) 16 increments. The ^{13}C offset of the original experiment was set to 50 ppm.

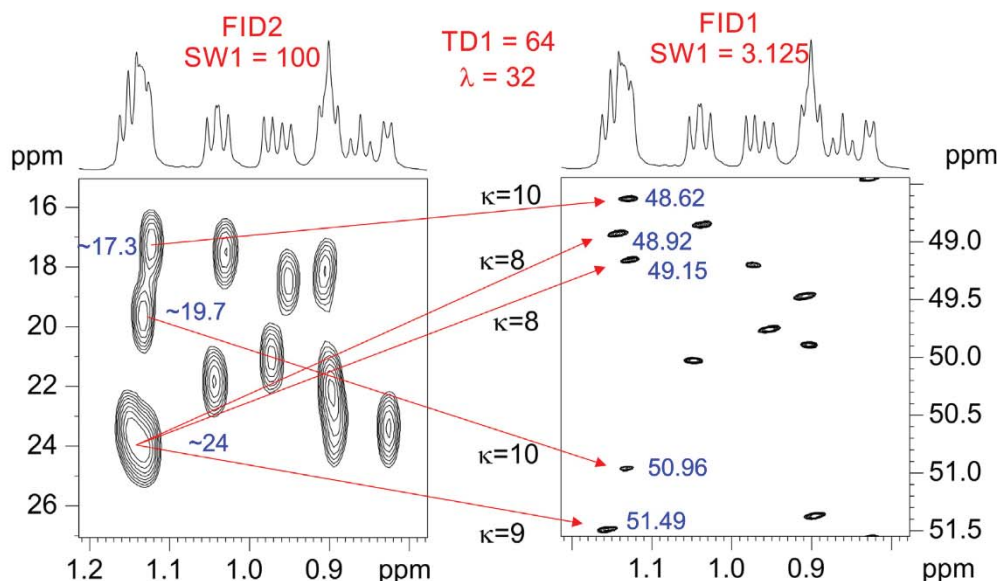


Fig. 6. Expansions of the HSQC (SW1 = 100 ppm) and SA-HSQC (SW1^{aliased} = 3.125 ppm) spectra acquired simultaneously with the SADA-HSQC experiment with $\lambda = 32$ and TD1 = 64 increments. The ^{13}C offset of the original experiment was set to 50 ppm. The experimental time to record both datasets was 3 min. All methyl signals in FID1 are distinguished, and their chemical shifts accurately determined using the relationship $\delta(^{13}\text{C})^{\text{aliased}} = \delta(^{13}\text{C})^{\text{true}} \pm \kappa \cdot 3.125$.

are set to 100 ppm and 3.125 ppm for FID2 and FID1, respectively. Note how the non-resolved cross-peaks in the regular low-resolved HSQC spectrum are dispersed in the highly-resolved SA spectrum. The reference spectrum is needed to obtain a rough estimation of $\delta(^{13}\text{C})^{\text{true}}$, and it is fundamental to deduce the κ factor observed for each cross-peak in the aliased spectrum. All methyl signals in FID1 can be distinguished, and their chemical shifts accurately determined to apply meticulously the relationship described in Eq. (1). For instance, note the excellent dispersion achieved for the fully overlapped five Me signals resonating in the narrow ^1H range between 1.13 and 1.17 ppm.

3. Conclusions

In summary, we have proposed an interesting NMR strategy to obtain high levels of digital resolution and spectral dispersion per time unit in the HSQC experiment. It has been shown that conventional and aliased 2D HSQC spectra can be simultaneously collected using a single pulse sequence, in minutes and a full automation mode. The method does not require many t_1 increments because accurate chemical shift determinations can be performed from the highly-resolved aliased spectrum. The signal-dependent κ aliasing factors are determined by comparing chemical shift values from the regular and the aliased HSQC spectra. The method described here is also suitable to record two aliased 2D HSQC spectra by scaling the two different t_1 periods differently [10,14,19], it is extensible to other HSQC-like experiments and also compatible with computer-assisted spectral reconstruction methods developed to obtain high-resolution NMR spectra with their full spectral width representation.

4. Experimental part

NMR spectra were recorded on a Bruker AVANCE spectrometer equipped with a 5 mm TBI probehead operating at 600.13 MHz for ^1H at 298 K. The sample used in this work was 25 mM of cyclosporine dissolved in 0.6 ml of C_6D_6 . The pre-scan delay was set to 1 s, and two scans for each one of the 128 t_1 increments were acquired (1024 points of time domain in the acquisition dimension). Spectral widths in the detected (SW2) and indirect (SW1) dimensions

were 10 ppm (6009 Hz) and 100 ppm (15,091 Hz), respectively. The acquisition time (AQ) for each FID1 and FID2 period was of 85 ms. The inter-pulse delays were optimized to 140 Hz ($\Delta_1 = 1.78$ ms and $\Delta_1' = 0.89$ ms) and the gradient ratio G1:G2:G3:G4:G5 was set to 11:40:20.1:–17:10.05 (gradient shape SINE.100). The overall duration involving the gradient (1 ms) and its recovery delay was 1.02 ms (δ). A basic two-step phase cycling was applied: $\Phi_1 = x, -x$; $\Phi_{\text{rec}} = x, -x$. Comparison of experimental times and FID resolution before processing along the F1 dimension between the standard HSQC, spectral aliased HSQC and several λ -scaled SADA-HSQC experiments are summarized in Tables S1–S2.

SADA-HSQC experiments were acquired using the echo/anti-echo protocol where the gradient G2 was inverted for every second FID. All data is individually processed in the usual way using a zero-filling in both F1 and F2 dimensions, up 2048 and 1024 data matrix respectively, and applying a non-shifted sine-bell window function in both dimensions before Fourier transformation. For processing, the automation AU program splitx rewrites the original FID1 and FID2 data allocated in different memory blocks to independent files. FID1 is transformed with the AU program fix_ali to recalculate SW1, according to the λ scaling factor. The SADA-HSQC pulse program is available in the SI.

Acknowledgments

Financial support for this research provided by Spanish MINECO (project CTQ2015-64436-P) is gratefully acknowledged. We also thank the Servei de Resonància Magnètica Nuclear, Universitat Autònoma de Barcelona, for allocating instrument time to this project.

Appendix A. Supplementary material

Supplementary data associated with this article can be found, in the online version, at <https://doi.org/10.1016/j.jmr.2019.01.004>.

References

- [1] C. Dalvit, Semi-selective two-dimensional homonuclear and heteronuclear NMR experiments recorded with pulsed field gradients, *Magn. Reson. Chem.* 33 (1995) 570–576, <https://doi.org/10.1002/mrc.1260330713>.

- [2] C. Gaillet, C. Lequart, P. Debeire, J.M. Nuzillard, Band-selective HSQC and HMBC experiments using excitation sculpting and PFGSE, *J. Magn. Reson.* 139 (1999) 454–459, <https://doi.org/10.1006/jmre.1999.1808>.
- [3] J.C. Hoch, M.W. Maciejewski, M. Mobli, A.D. Schuyler, A.S. Stern, Nonuniform sampling and maximum entropy reconstruction in multidimensional NMR, *Acc. Chem. Res.* 47 (2014) 708–717, <https://doi.org/10.1021/ar400244v>.
- [4] K. Kazimierczuk, J. Stanek, A. Zawadzka-Kazimierczuk, W. Koźmiński, Random sampling in multidimensional NMR spectroscopy, *Prog. Nucl. Magn. Reson. Spectrosc.* 57 (2010) 420–434, <https://doi.org/10.1016/j.pnmrs.2010.07.002>.
- [5] M. Mobli, J.C. Hoch, Nonuniform sampling and non-Fourier signal processing methods in multidimensional NMR, *Prog. Nucl. Magn. Reson. Spectrosc.* 83 (2014) 21–41, <https://doi.org/10.1016/j.pnmrs.2014.09.002>.
- [6] W.F. Reynolds, R.G. Enriquez, The advantages of forward linear prediction over multiple aliasing for obtaining high-resolution HSQC spectra in systems with extreme spectral crowding, *Magn. Reson. Chem.* 41 (2003) 927–932, <https://doi.org/10.1002/mrc.1271>.
- [7] L.E. Kay, P. Keifer, T. Saarinen, Pure absorption gradient enhanced heteronuclear single quantum correlation spectroscopy with improved sensitivity, *J. Am. Chem. Soc.* 114 (1992) 10663–10665, <https://doi.org/10.1021/ja00052a088>.
- [8] J. Schleucher, M. Schwendinger, M. Sattler, P. Schmidt, O. Schedletsky, S.J. Glaser, O.W. Sørensen, C. Griesinger, A general enhancement scheme in heteronuclear multidimensional NMR employing pulsed field gradients, *J. Biomol. NMR* 4 (1994) 301–306, <https://doi.org/10.1007/BF00175254>.
- [9] D. Jeannerat, Rapid multidimensional NMR: high resolution by spectral aliasing, *Encycl. Magn. Reson.* (2011), <https://doi.org/10.1002/9780470034590.emrstm1187>.
- [10] I. Baskyr, T. Brand, M. Findeisen, S. Berger, Acquisition regime for high-resolution heteronuclear 2D NMR spectra, *Angew. Chem. Int. Ed.* 45 (2006) 7821–7824, <https://doi.org/10.1002/anie.200603036>.
- [11] A. Cotte, M. Foroozandeh, D. Jeannerat, Combination of homonuclear decoupling and spectral aliasing to increase the resolution in the 1H dimension of 2D NMR experiments, *Chim. Int. J. Chem.* 66 (2012) 764–769, <https://doi.org/10.2533/chimia.2012.764>.
- [12] A. Cotte, D. Jeannerat, 1D NMR homodecoupled (1)H spectra with scalar coupling constants from 2D NemoZS-DIAG experiments, *Angew. Chem. Int. Ed.* 54 (2015) 6016–6018, <https://doi.org/10.1002/anie.201500831>.
- [13] D. Jeannerat, Computer optimized spectral aliasing in the indirect dimension of 1H–13C heteronuclear 2D NMR experiments. A new algorithm and examples of applications to small molecules, *J. Magn. Reson.* 186 (2007) 112–122, <https://doi.org/10.1016/j.jmr.2007.02.003>.
- [14] M. Foroozandeh, D. Jeannerat, Reconstruction of full high-resolution HSQC using signal split in aliased spectra, *Magn. Reson. Chem.* 53 (2015) 894–900, <https://doi.org/10.1002/mrc.4283>.
- [15] K. Ramírez-Gualito, D. Jeannerat, Exploiting the phase of NMR signals to carry useful information. Application to the measurement of chemical shifts in aliased 2D spectra, *Magn. Reson. Chem.* 53 (2015) 901–907, <https://doi.org/10.1002/mrc.4301>.
- [16] G.B.B. Njock, T.A. Bartholomeusz, M. Foroozandeh, D.E. Pegnyemb, P. Christen, D. Jeannerat, NASCA-HMBC, a new NMR methodology for the resolution of severely overlapping signals: application to the study of agathisflavone, *Phytochem. Anal.* 23 (2012) 126–130, <https://doi.org/10.1002/pca.1333>.
- [17] B. Vitorge, S. Bieri, M. Humam, P. Christen, K. Hostettmann, O. Muñoz, S. Loss, D. Jeannerat, High-precision heteronuclear 2D NMR experiments using 10-ppm spectral window to resolve carbon overlap, *Chem. Commun.* (2009) 950–952, <https://doi.org/10.1039/b820478k>.
- [18] D. Jeannerat, High resolution in heteronuclear 1H–13C NMR experiments by optimizing spectral aliasing with one-dimensional carbon data, *Magn. Reson. Chem.* 41 (2003) 3–17, <https://doi.org/10.1002/mrc.1118>.
- [19] M. Foroozandeh, D. Jeannerat, Deciphered chemical shifts in aliased spectra recorded with two slightly different narrow windows or differential chemical shift evolution, *ChemPhysChem* 11 (2010) 2503–2505, <https://doi.org/10.1002/cphc.201000421>.
- [20] M. Pérez-Trujillo, L. Castañar, E. Monteagudo, L. Kuhn, P. Nolis, A. Virgili, R.T. Williamson, T. Parella, Simultaneous 1H and 13C NMR enantiodifferentiation from highly-resolved pure shift HSQC spectra, *Chem. Commun.* 50 (2014) 10214–10217, <https://doi.org/10.1039/C4CC04077E>.
- [21] L. Castañar, R. Roldán, P. Clapés, A. Virgili, T. Parella, Disentangling complex mixtures of compounds with near-identical 1H and 13C NMR spectra using pure shift NMR spectroscopy, *Chem. – A Eur. J.* 21 (2015) 7682–7685, <https://doi.org/10.1002/chem.201500521>.
- [22] N. Marcó, A. Fredi, T. Parella, Ultra high-resolution HSQC: Application to the efficient and accurate measurement of heteronuclear coupling constants, *Chem. Commun.* 51 (2015) 3262–3265, <https://doi.org/10.1039/c4cc10279g>.
- [23] K. Motiram Corral, M. Pérez-Trujillo, P. Nolis, T. Parella, Implementing one-shot multiple-FID acquisition into homonuclear and heteronuclear NMR experiments, *Chem. Commun.* 54 (2018) 13507–13510, <https://doi.org/10.1039/C8CC08065H>.
- [24] P. Nolis, M. Pérez-Trujillo, T. Parella, Multiple FID acquisition of complementary HMBC data, *Angew. Chem. Int. Ed.* 46 (2007) 7495–7497, <https://doi.org/10.1002/anie.200702258>.
- [25] P. Nolis, K. Motiram-Corral, M. Pérez-Trujillo, T. Parella, Interleaved Dual NMR acquisition of equivalent transfer pathways in TOCSY and HSQC experiments, *ChemPhysChem* (2018), <https://doi.org/10.1002/cphc.201801034>.

Supporting Information

Simultaneous acquisition of two HSQC spectra with different ^{13}C spectral widths

Pau Nolis, Kumar Motiram-Corral, Míriam Pérez-Trujillo and Teodor Parella*

Servei de Ressonància Magnètica Nuclear,
Universitat Autònoma de Barcelona, E-08193, Bellaterra, Barcelona, Catalonia, Spain.

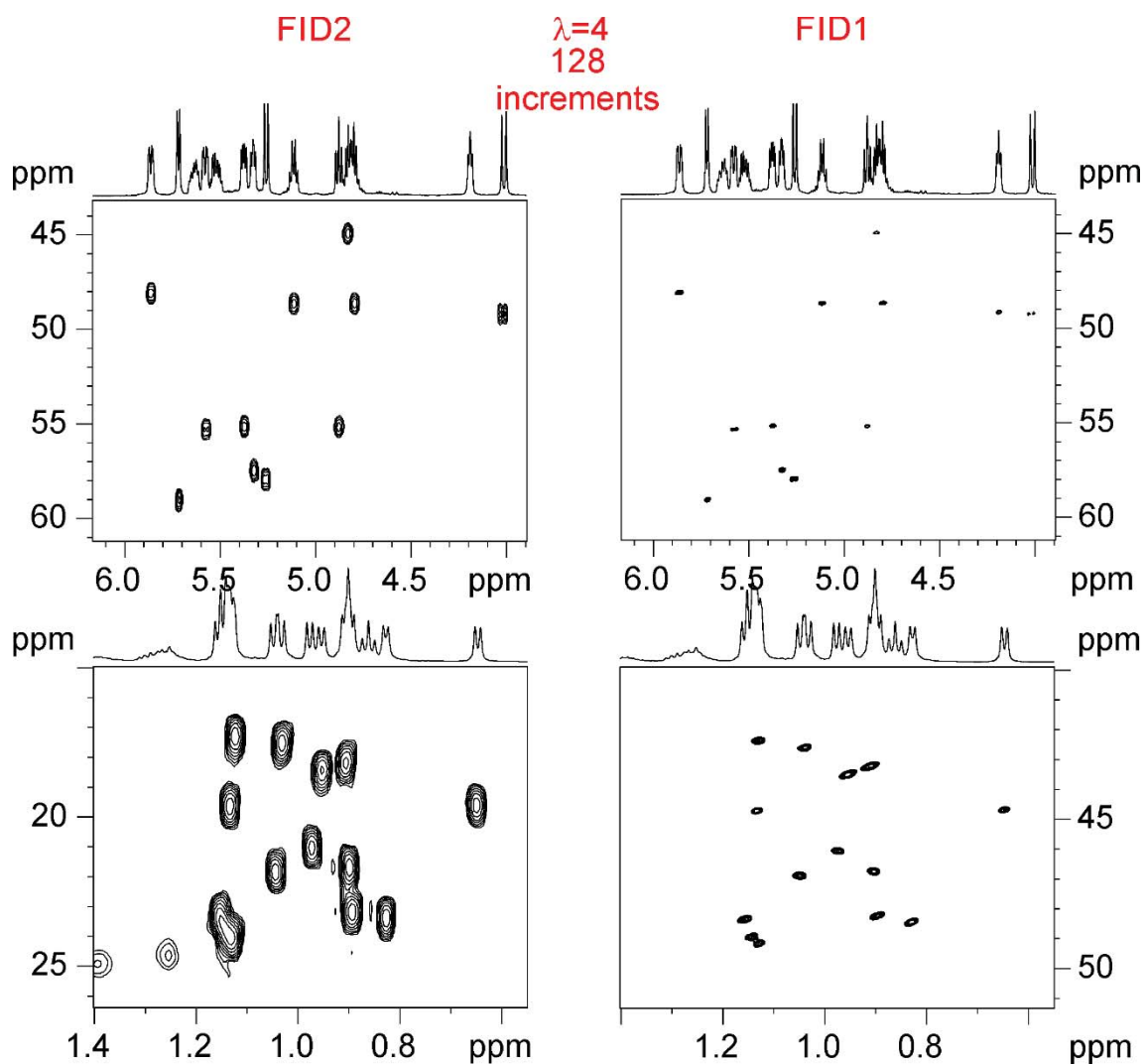


Figure S1: Comparison of the HSQC data of cyclosporine obtained from the SADA-HSQC pulse scheme acquired with $TD1=128$ and $\lambda=4$. Note the better resolution achieved in FID1 ($SW1 = 25$ ppm) that allows a clear distinction of all cross-peaks and accurate chemical shift determination. The ^{13}C offset was 50 ppm and the scaling κ factor for all the $\text{CH}\alpha$ cross-peaks is 1. The SA-HSQC spectrum in the left has the same digital resolution than a full spectral-width 2D HSQC with 1028 increments.

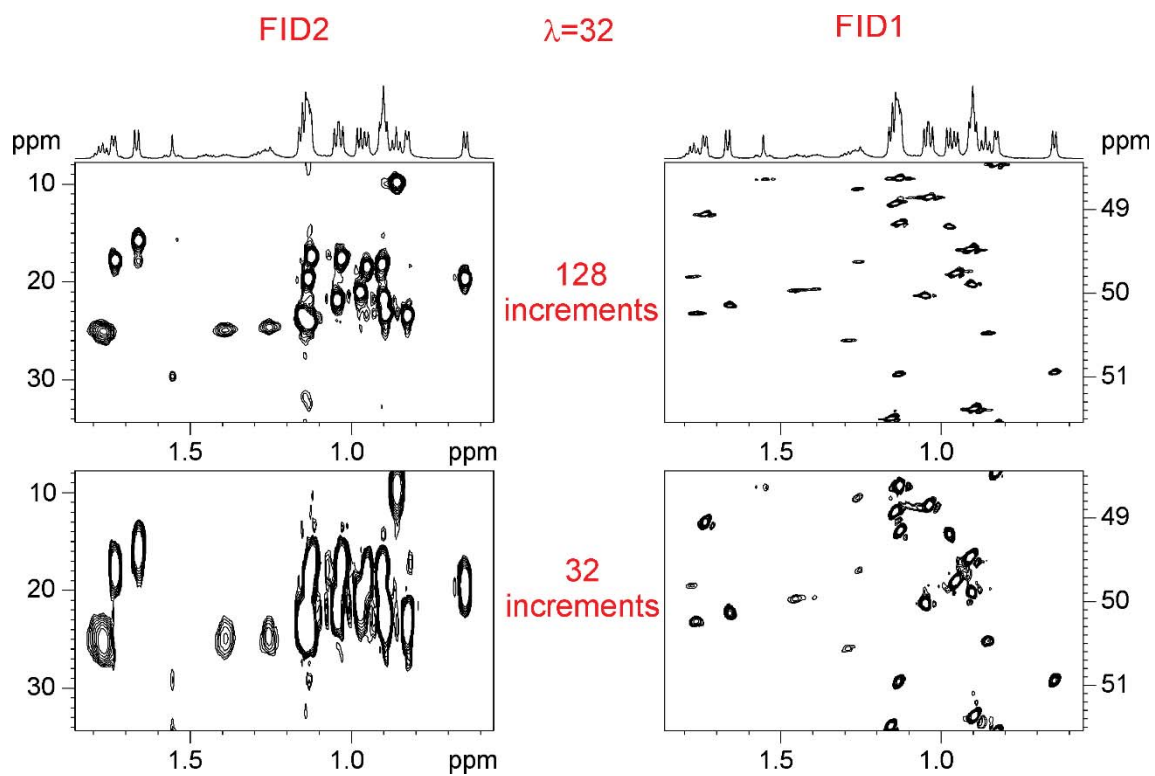


Figure S2: Effects of the number of increments (TD1) on the F1 digital resolution in the HSQC and SA-HSQC spectra acquired with SADA-HSQC pulse scheme.

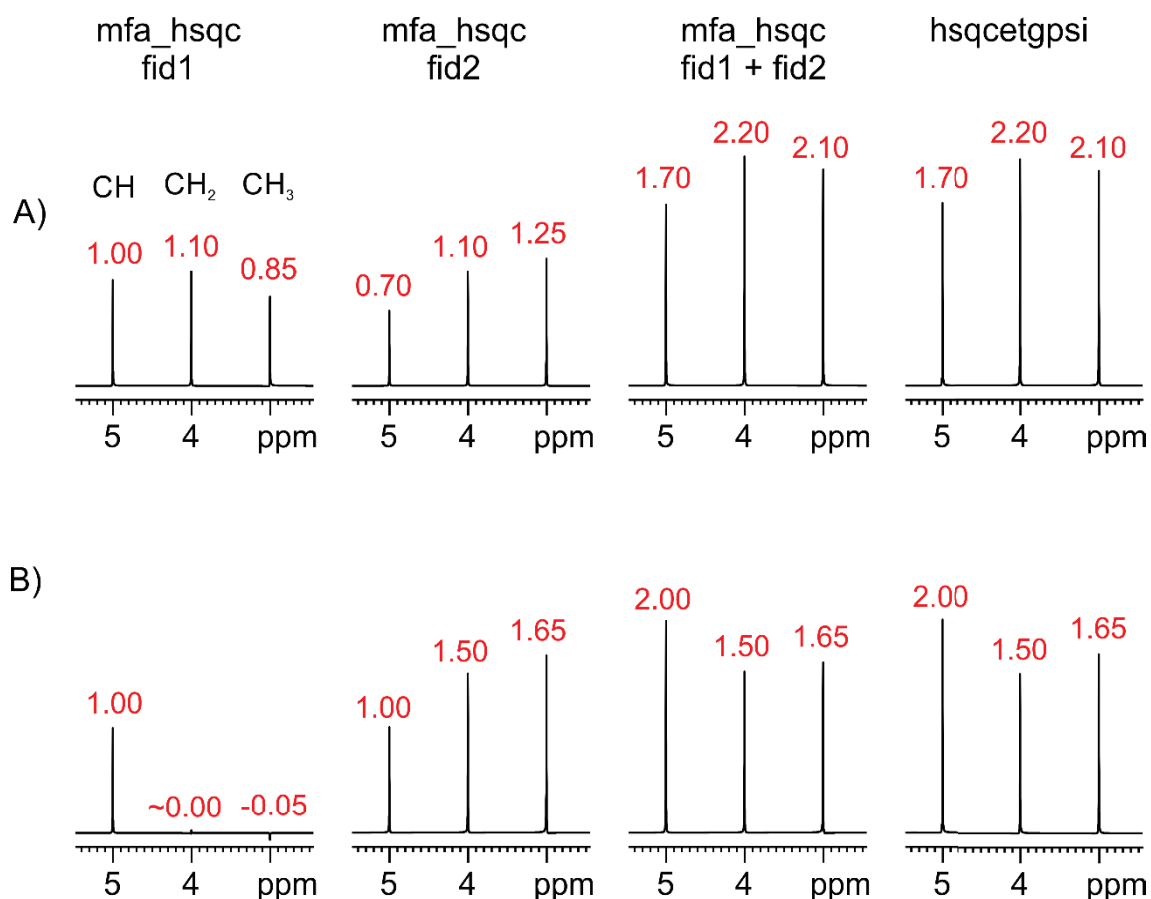


Figure S3: 1D simulations showing signal intensity dependences for all multiplicities using the MFA strategy versus standard acquisition in SE-HSQC experiment. (A) Delay optimization: $\Delta_1=1/8J$ and $\Delta_1=1/4J$. B) Delay optimization: $\Delta_1=1/4J$ and $\Delta_1=1/4J$. The spin systems used in the simulation are a CH at 5 ppm, a CH₂ group at 4 ppm, and a CH₃ system at 3 ppm with $^1J_{CH}$ set to 145 Hz in all cases. As expected, FID1+FID2 obtained in the MFA acquisition give rise to the same result as SE-HSQC. With this results in hand, it is highly advisable to avoid (B) delay optimization in MFA strategy due to the complete loss of signal for CH₂ and CH₃ groups in FID1. The experimental signal lost observed at FID2 due to diffusion phenomena is not considered along simulations.

Table S1: Experimental Conditions for the SE-HSQC, SA-HSQC and SADA-HSQC Experiments. Acquisition Parameters: TD(F2/F1) = 1024/128, SW1 = 160ppm, SW2 = 10ppm, NS = 2, D1 = 1s, AQ2 = 85.2ms

Experiment	Expt	Δt_1 (μ s)	$(\lambda-1)*\Delta t_1$ (μ s)	λ factor	t_1^{\max} (ms)	SW1 (ppm)	FIDRES (Hz/pt)
SE-HSQC	4min 44s	41,42	---	1	5,30	160	377.28
SA-HSQC	4min 44s	82,84	---	2	10,60	80	188.64
	4min 45s	165,68	---	4	21,21	40	94.32
	4min 46s	331,36	---	8	42,41	20	47.16
	4min 49s	662,72	---	16	84,83	10	23.58
	4min 54s	1325,44	---	32	169,66	5	11.79
	5min 5s	2650,88	---	64	339,31	2,5	5.89
	5min 26s	5301,76	---	128	678,62	1,25	2.95
SADA-HSQC	5min 8s	41,42	0	1	5,30	160	377.28
	5min 8s	41,42	41,42	2	10,60	80	188.64
	5min 9s	41,42	124,26	4	21,21	40	94.32
	5min 10s	41,42	289,94	8	42,41	20	47.16
	5min 13s	41,42	621,3	16	84,83	10	23.58
	5min 18s	41,42	1284,02	32	169,66	5	11.79
	5min 29s	41,42	2609,46	64	339,31	2,5	5.89
	5min 50s	41,42	5260,34	128	678,62	1,25	2.95

Table S2: Experimental Conditions for the SE-HSQC, SA-HSQC and SADA-HSQC Experiments. Acquisition Parameters: TD(F2/F1) = 1024/128, SW1 = 100ppm, SW2 = 10ppm, NS = 2, D1 = 1s, AQ2 = 85.2ms.

Experiment	Expt	Δt_1 (μ s)	$(\lambda-1)*\Delta t_1$ (μ s)	λ factor	t_1^{\max} (ms)	SW1 (ppm)	FIDRES (Hz/pt)
SE-HSQC	4min 44s	66,26	- - -	1	8,48	100	235.80
SA-HSQC	4min 44s	132,52	- - -	2	16,96	50	117.90
	4min 45s	265,04	- - -	4	33,92	25	58.95
	4min 46s	530,08	- - -	8	67,85	12,5	29.47
	4min 49s	1060,16	- - -	16	135,70	6,25	14.74
	4min 54s	2120,32	- - -	32	271,40	3,125	7.37
	5min 5s	4240,64	- - -	64	542,80	1,5625	3.68
	5min 26s	8481,28	- - -	128	1085,60	0,78125	1.84
SADA-HSQC	5min 8s	66,26	0	1	8,48	100	235.80
	5min 9s	66,26	66,26	2	16,96	50	117.90
	5min 10s	66,26	198,78	4	33,92	25	58.95
	5min 12s	66,26	463,82	8	67,85	12,5	29.47
	5min 16s	66,26	993,9	16	135,70	6,25	14.74
	5min 25s	66,26	2054,06	32	271,40	3,125	7.37
	5min 42s	66,26	4174,38	64	542,80	1,5625	3.68
	6min 16s	66,26	8415,02	128	1085,60	0,78125	1.84

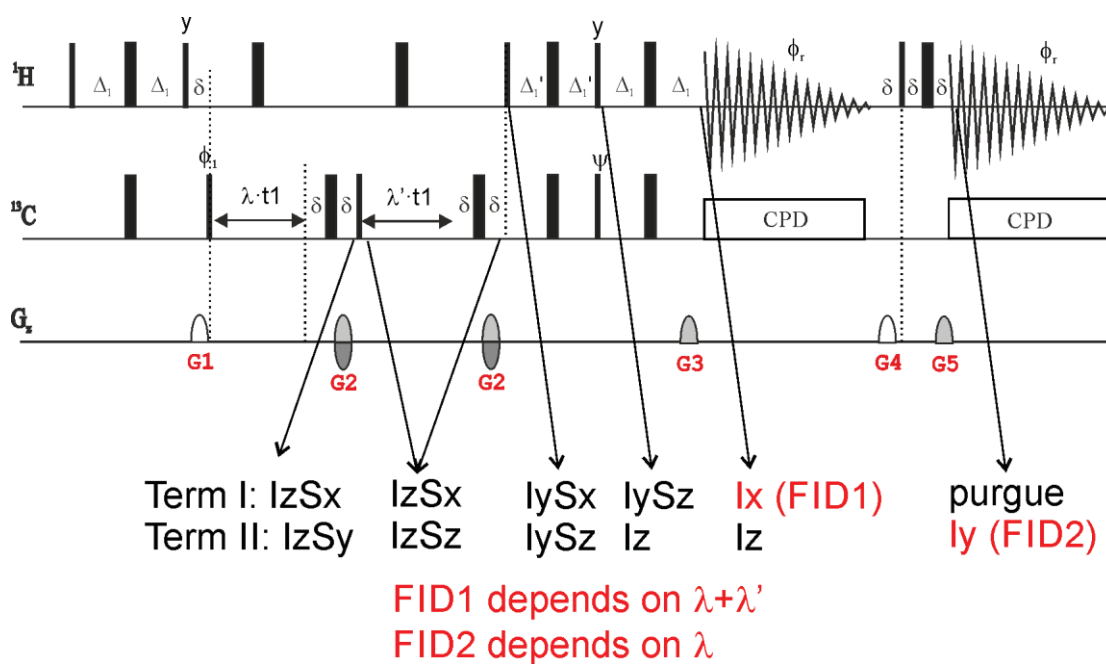


Figure S3: Modified MFA-SA-HSQC pulse scheme to obtain two spectral aliased HSQC spectra. For instance, setting $\lambda=16$ and $\lambda'=0.1616$ in an experiment with a default SW1=160 ppm value would yield 2D HSQC spectra with SW1 of 9.9 ppm (FID1) and 10 ppm (FID2), as recommended in ref. 10 and 19.

Pulse Program

```
;SADA-HSQC
;Simultaneous Acquisition of HSQC and spectral-aliased HSQC
;spectra

#include <Avance.incl>
#include <Grad.incl>
#include <Delay.incl>
#include <De.incl>

"p2=p1*2"
"p4=p3*2"
"d4=1s/(cnst2*4)"
"d24=1s/(cnst2*8)"
"d11=30m"

"d0=3u"
"d20=3u"
"in0=inf1/2"
"in20=cnst20*in0-in0"
"l0=td1/4"

"DELTA=p16+d16+50u+d0*2+p2"
"DELTA1=p16+d16+4u"
"DELTA2=d4-larger(p2,p14)/2"
"DELTA3=p16+d16+50u+d20*2+p2"

"acqt0=0"
baseopt_echo

1 ze
  d11 pl12:f2
2 d1 do:f2
3 d16 st0
                                     ; reset to first buffer memory
  (p1 ph1)
  DELTA2 pl0:f2
  4u
  (center (p2 ph1) (p14:sp3 ph6):f2 )
  4u
  DELTA2 pl2:f2
  p28 ph1
  4u
  (p1 ph2)
  50u UNBLKGRAD
  p16:gp1
  d16
  (p3 ph3):f2

d0
(p2 ph7)
d0
50u
p16:gp2*EA
```

```

d16
(p4 ph4):f2
DELTA
(p3 ph4):f2
d20
(p2 ph7)
d20
50u
p16:gp2*EA
d16
(p4 ph4):f2
DELTA3
(p1 ph1)
d24
(center (p2 ph1) (p4 ph1):f2 )
d24
(center (p1 ph2) (p3 ph5):f2 )
DELTA2 p10:f2
(center (p2 ph1) (p14:sp3 ph1):f2 )
DELTA2

DELTA1
(p2 ph1)
4u p112:f2
p16:gp3
;gradient decoding for 1st magnetization
component
d16 BLKGRAD

goscnp ph31 cpd2:f2 ; 1st FID

d16 do:f2
d16 UNBLKGRAD
p16:gp4 ;purgue gradient
d16 st ;increment buffer memory
(p1 ph1)
DELTA1
(p2 ph1)
4u
p16:gp5 ;gradient decoding for 2nd
magnetization component
d16 BLKGRAD
go=2 ph31 cpd2:f2 ;2nd fid
d1 wr #0 if #0 igrad EA ip5*2
4u do:f2
  lo to 3 times 2
    30u id0
    30u id20
    30u ip3*2
    30u ip6*2
    30u ip31*2
  lo to 3 times 10
50u BLKGRAD
exit
ph1=0
ph2=1

```

```

ph3=0 2
ph4=0 0 2 2
ph5=1 1 3 3
ph6=0
ph7=0 0 2 2
ph10=2
ph28=0
ph29=0 2 2 0
ph30=0
ph31=0 2 2 0

;p10 : 0W
;p11 : f1 channel - power level for pulse (default)
;p12 : f2 channel - power level for pulse (default)
;p13 : f3 channel - power level for pulse (default)
;p112: f2 channel - power level for CPD/BB decoupling
;sp3: f2 channel - shaped pulse 180 degree
;p1 : f1 channel - 90 degree high power pulse
;p2 : f1 channel - 180 degree high power pulse
;p3 : f2 channel - 90 degree high power pulse
;p4 : f2 channel - 180 degree high power pulse
;p14: f2 channel - 180 degree shaped pulse for inversion
;p16: homospoil/gradient pulse
;p22: f3 channel - 180 degree high power pulse
;p28: f1 channel - trim pulse
;d0 : incremented delay (2D) [3 usec]
;d1 : relaxation delay; 1-5 * T1
;d4 : 1/(4J)XH
;d11: delay for disk I/O [30 msec]
;d16: delay for homospoil/gradient recovery
;d24: 1/(8J)XH for all multiplicities
; 1/(4J)XH for XH
;cnst2: = J(XH)
;inf1: 1/SW(X) = 2 * DW(X)
;in0: 1/(2 * SW(X)) = DW(X)
;nd0: 2
;ns: 2 * n
;ds: >= 16
;td1: number of experiments
;FnMODE: echo-antiecho
;cpd2: decoupling according to sequence defined by cpdprg2
;pcpd2: f2 channel - 90 degree pulse for decoupling sequence

;for z-only gradients:
;gpz1: 11%
;gpz2: 40%
;gpz3: 20.1%
;gpz4: -17%
;gpz5: 10.05%
;use gradient files:
;gpnam1: SMSQ10.100
;gpnam2: SMSQ10.100
;gpnam3: SMSQ10.100
;gpnam4: SMSQ10.100
;gpnam5: SMSQ10.100

```

4.3. Publication 3: Interleaved Dual NMR Acquisition of Equivalent Transfer Pathways in TOCSY and HSQC Experiments.

4.3.1. Introduction

The afterglow magnetization used in MFA experiments is a powerful method that can provide the chance to manage and detect the two CTPs components involved in PEP-based experiments. This principle is illustrated using two basic NMR experiments, TOCSY and HSQC. The method allows the use of two different z-filtered TOCSY mixing times (the novel MF-TOCSY/TOCSY experiment) which offers an important advantage in terms of spectrometer time saving and signal sensitive enhancement. Two TOCSY spectra with different mixing times can be simultaneously obtained in a single-shot acquisition.

Following the same approach, this paper also introduces novel MF-HSQC/HSQC experiments where two FIDs are collected into the same scan. For instance, FID1 affords a regular HSQC spectrum and FID2 yields the ^{13}C -coupled version of the same HSQC. A related modification can afford a regular HSQC in F1 and an equivalent pure-shift HSQC version in FID2. These ideas can be easily extended to other combinations involving both HSQC and TOCSY schemes. For instance, an MF-HSQC/HSQC-TOCSY yields a normal HSQC in FID1 and the equivalent HSQC-TOCSY dataset in FID2.

Interleaved Dual NMR Acquisition of Equivalent Transfer Pathways in TOCSY and HSQC Experiments

Pau Nolis,^[a] Kumar Motiram-Corral,^[a] Míriam Pérez-Trujillo,^[a] and Teodor Parella^{*[a]}

A dual NMR data acquisition strategy to handle and detect two active equivalent transfer pathways is presented and discussed. We illustrate the power of this time-efficient approach by collecting two different 2D spectra simultaneously in a single experiment: i) TOCSY or HSQC-TOCSY spectra with different mixing times, ii) F2-¹³C-coupled and decoupled HSQC spectra, iii) conventional and pure-shift HSQC spectra, or iv) complementary HSQC and HSQC-TOCSY spectra.

The overall experimental time of a 2D NMR experiment is defined fundamentally by the imposition of extended recycle delays for a proper T_1 relaxation, of an enough number of recorded t_1 increments to achieve an optimum resolution in the indirect F1 dimension and/or of a minimum number of scans per t_1 increment required to complete a phase cycle for efficient coherence transfer pathways (CTP) selection. This situation is commonly found in modern NMR applications on small molecules, where some milligrams of sample are often more than enough to run the most basic experiments in short experimental times. Possible solutions to economize spectrometer time could be the attempt to speed up data acquisition by some fast NMR method, including shortening the recycle delay, the collection of a moderate number of t_1 increments or the efforts to reduce the needs of long phase cycles by using pulsed field gradient (PFG) CTP selection. Another option relies on the acquisition of multiple NMR spectra using a single pulse sequence which can offer attractive benefits regarding simplicity, efficiency, automation and, in some cases, improved sensitivity per time unit. Some examples of this multiple data acquisition strategy include the collection of multiple FIDs within the same scan (MFA),^[1–3] the recent concept of NOAH based on the interleaved acquisition of various experiments to avoid long recycle delays,^[4,5] the simultaneous acquisition of equivalent ¹³C and ¹⁵N spectra by time-sharing NMR spectroscopy,^[6] or the use of multiple receivers to detect different nuclei in a parallel or interleaved manner.^[7] The simultaneous acquisition of multiple spectra is particularly useful when dealing on complementary NMR experiments having comparable sensitivity (requiring similar scans per t_1 increments, similar

phase cycling), resolution (similar number of t_1 increments) and/or performance (similar parameters settings, the same acquisition mode...) requirements. The success of these time-efficient methods depends on which is the best multiple acquisition strategy (parallel, interleaved, afterglow, separate...) regarding sensitivity, performance and/or spectrometer time savings.

On the other hand, NMR pulse sequences usually monitor a specific CTP by an appropriate phase cycle or PFG coherence selection procedure. However, some sequences have been designed to exploit several CTPs at the same time. A very representative example is the so-called Preservation of Equivalent Pathways (PEP) technique which has been used to add up two different co-existing magnetization components in a single NMR experiment. For instance, PEP has been successfully applied to enhance the sensitivity by a theoretical factor of 2 (signal-to-noise (SNR) ratio by 1.4-fold) during the same total acquisition time in 2D TOCSY,^[8,9] 2D HMQC,^[10,11] 2D HSQC^[12–16] and 2D HSQC-TOCSY^[17–20] experiments or has also been used to generate spin-state selective states in TROSY-type experiments.^[21–24] Both PEP and TROSY elements are standard building blocks in many multidimensional experiments,^[25] but it is worth mentioning that such theoretical sensitivity gains are only achieved for CH and NH spin systems, but not for CH₂ or CH₃ signals.

Here we show how the two CTPs components involved in PEP-based experiments can be managed and detected separately by using the time-optimized MFA technique. As a proof of concept, the features of this method are described, including a discussion about the increased information content, the relative sensitivities for each collected component and the benefits concerning spectrometer times achieved for such an approach. To start, we have chosen the sensitivity-enhanced version of the TOCSY (SE-TOCSY) experiment using a z-filtered DIPSI-2 as the isotropic mixing transfer for propagation between J coupled protons (Figure 1A).^[26] The SE-TOCSY sequence also incorporates gradient-enhanced CTP selection based on the well-known echo/anti-echo acquisition and processing protocols to provide pure absorption lineshapes.^[9] The high sensitivity of the TOCSY experiment makes it suitable for the rapid and successful application on any molecules, only requiring some milligrams of sample and two scans per t_1 increment. Two magnetization components (I_x and I_y) present just before the DIPSI-2 scheme contribute equally to the detected signal after the last 90° ¹H pulse in SE-TOCSY. We propose to insert a simple NMR element consisting of an FID period followed by a purging G2 gradient into the SE-TOCSY sequence to manipulate these orthogonal components selec-

[a] Dr. P. Nolis, K. Motiram-Corral, Dr. M. Pérez-Trujillo, Dr. T. Parella
Servei de Resonància Magnètica Nuclear
Universitat Autònoma de Barcelona
E-08193 Bellaterra, Barcelona, Catalonia
E-mail: Teodor.parella@uab.cat

Supporting information for this article is available on the WWW under
<https://doi.org/10.1002/cphc.201801034>

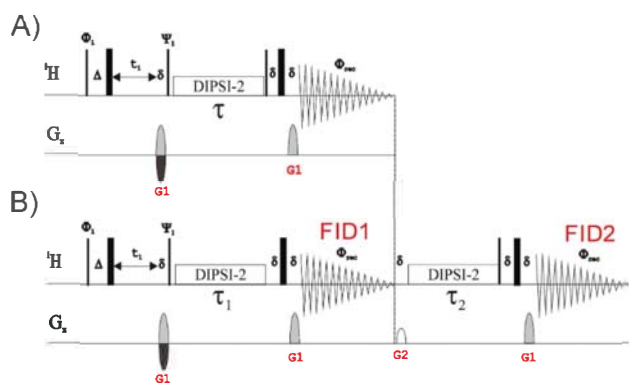


Figure 1. Pulse schemes of the A) conventional 2D sensitivity- and gradient-enhanced TOCSY (SE-TOCSY) and B) MFA-TOCSY/TOCSY experiments.

tively. Figure 1B shows the pulse scheme of the novel MFA-TOCSY/TOCSY experiment which can be used to obtain two 2D TOCSY spectra with different mixing times. The first FID acquisition period (FID1) is designed to observe exclusively transverse I_x components generated during the τ_1 mixing time, whereas the other I_z component remains non-observable. After that, the purging G2 gradient is applied to remove any residual transverse magnetization, and a subsequent 90° pulse flips the unexploited I_z component to the transverse plane to be acquired during a second acquisition period (FID2) inserted after another TOCSY transfer. This method allowed the single-shot dual acquisition of two different TOCSY experiments sharing the same variable t_1 period but recorded with two different mixing times (τ_1 and τ_2 , respectively).

Figure 2 shows the regular SE-TOCSY ($\tau = 60$ ms) acquired in 10 m 28 s, and the two TOCSY spectra both acquired in a total

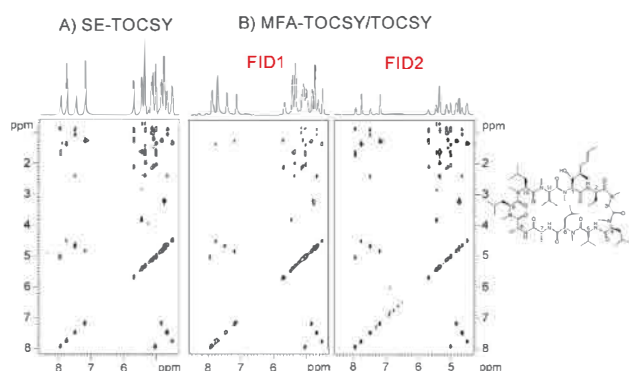


Figure 2. 2D TOCSY spectra of cyclosporine obtained from the A) SE-TOCSY ($\tau = 60$ ms; experimental time = 10 m 28 s) and B) MFA-TOCSY/TOCSY (overall experimental time for both spectra = 11 m 16 s) experiments. Mixing times in the MFA-TOCSY/TOCSY were $\tau_1 = 20$ ms (FID1) and $\tau_2 = 60$ ms (FID2). 1D slices show the internal positive projection for each 2D spectrum.

experimental time of 11 m 16 s (only 7.6% of additional spectrometer time; see Table S1 in SI) with the MFA-TOCSY/TOCSY sequence, with mixing times of $\tau_1 = 20$ ms (FID1) to observe short-range connectivities and $\tau_2 = 60$ ms (FID2) to

trace out longer correlations, respectively. In all these experiments, 1024 points were collected in each acquisition (TD2) giving an acquisition time (AQ) of 102 ms for each FID1 and FID2 periods. As expected, FID1 shows about the 50% of the signal detected in the equivalent SE-TOCSY acquired under identical conditions. The proposed MFA approach can induce two interferences in the second FID2: a relative sensitivity loss due to diffusion effects and the potential presence of NOE and NOE-relayed contributions. In practice, the second TOCSY spectra show a decreased sensitivity due to the diffusion effects generated by the long distance between the defocusing and refocusing gradients. However, the sum of the positive projection FID1 + FID2 only shows a minimum decrease in sensitivity about 15–20% with respect to the maximum expected for the SE-TOCSY (Figure S2). Such losses are negligible for everyday applications, but the TOCSY version without PFG selection^[8] could be used to avoid them. On the other hand, NOE and NOE-relayed contributions could be distinguished by their relative opposite phase but their intensities become not relevant for small molecules in the mentioned conditions.

The separate handling of the PEP components can also be implemented in the sensitivity- and gradient-enhanced HSQC-PEP (SE-HSQC) experiment shown in Figure 3A. Equation (1) summarizes their evolution for an isolated CH spin system after the t_1 period:

$$\begin{aligned} 2I_zS_x + 2I_zS_y &\xrightarrow{90^\circ(H,x)-90^\circ(S,x)} 2I_yS_x + 2I_yS_z \xrightarrow{\Delta-180^\circ(H,x)-180^\circ(S,x)-\Delta} 2I_yS_x + I_x \xrightarrow{90^\circ(H,y)-90^\circ(S,y)} 2I_yS_z + I_z(\text{point a}) \xrightarrow{\Delta-180^\circ(H,x)-180^\circ(S,x)-\Delta} I_x + I_z(\text{point b}) \xrightarrow{90^\circ(H,x)} I_x + I_y(\text{point c}) \end{aligned} \quad (1)$$

There are three key points to highlight in the PEP scheme. In point a, only an anti-phase (AP) term is observable while the other component resides in the z-axis; in point b, only the corresponding in-phase (IP) magnetization remains observable after the subsequent refocusing period; in point c, both signals become observables as orthogonal IP states. The SE-HSQC pulse sequence is specifically designed to generate these two in-phase contributions, which are added up to offer a sensitivity enhancement of 2 compared to the alternative application of a single-echo INEPT refocusing in HSQC. However, this sensitivity gain is not general for all CH_n multiplicities. Only when the inter-pulse Δ_1 and Δ_2 delays are set to $1/4 J$, a maximum theoretical enhancement is expected just for CH spin systems (signal-to-noise (SNR) ratio by 1.4-fold).

The approach followed in this work is different to other previous MFA experiments which use the so-called afterglow magnetization. We explain how these two PEP components can be handled differently, not to mix them in a single acquisition but separating them to provide two different datasets. Figure 3B displays a general MFA-HSQC/HSQC pulse scheme developed to monitor each PEP component. As a first option, only one of the two magnetization components can be selectively detected by activating data acquisition at points a or b, either as AP signals or IP after proper refocusing, respectively,

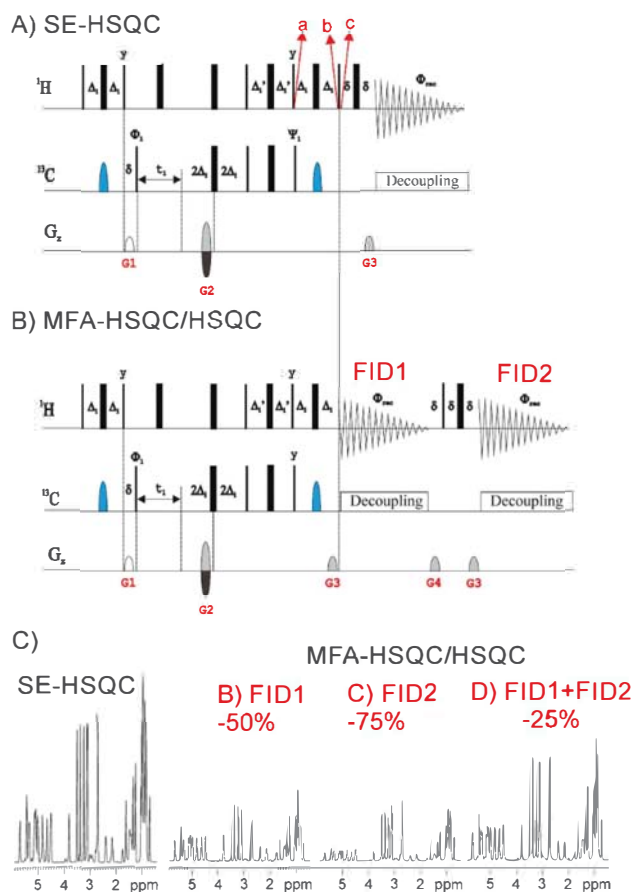


Figure 3. Pulse schemes of the A) conventional sensitivity- and gradient-enhanced HSQC (SE-HSQC) and B) MFA-HSQC/HSQC experiments. C) Relative sensitivities achieved in MFA experiments. Positive projections corresponding to (left) SE-HSQC, (center) FID1 and FID2 of the MFA-HSQC/HSQC spectra, respectively, and (right) the sum of FID1 and FID2.

while the second component remains non-observable as I_z . After this FID1, a purging G_4 gradient is applied to remove any residual transverse magnetization from the first component and followed by a $90^\circ(^1\text{H})$ pulse to create transverse IP magnetization from the unexploited second component. At this new point c, a new acquisition period is inserted (FID2) to detect it after applying a refocusing gradient.

To analyse the performance of our approach, we have applied the MFA-HSQC/HSQC experiment to obtain a 2D HSQC spectrum in both FID1 and FID2 and compare them to SE-HSQC with respect to real sensitivity and percentage of recovered data. As known for SE-HSQC, signal intensity depends on the inter-pulse delays optimization, so in FID1 depends on Δ_1 and in FID2 depends on Δ_1' (simulations are shown in Figure S4). As expected, FID1 affords the 50% of the SE-HSQC signal whereas the averaged intensity achieved in FID2 is about 35% when $\Delta_1' = \Delta_1 = 1/4$ J and about 25% when $\Delta_1' = 1/8$ J and $\Delta_1 = 1/4$ J (Figure 3C). As discussed before, this sensitivity reduction observed in FID2 is attributed to the unavoidable diffusion effects occurring during the duration of the FID1 period (about 100 ms). As shown later, this relative decrease of overall sensitivity concerning SE-HSQC is more than compensated with

the fact of being able to get multiple information into the same acquisition procedure and experimental times. On the other hand, it has been evaluated the diffusion losses as a function of the FID2 duration. In practice, the significant diffusion existing during a FID2 duration of 204 ms ($TD = 2$ K) is partially compensated with the better resolution and linewidths (Figure S5).

Based on these descriptions, a family of new MFA experiments based on the MFA-HSQC/HSQC scheme can be designed. For instance, MFA-HSQCcoupled/HSQC and MFA-HSQC/HSQCcoupled experiments are readily available deactivating the heteronuclear decoupling during the FID1 or FID2, respectively (Figures S6–S9). Regarding overall sensitivity of both coupled and decoupled spectra, it can be recommended to acquire the coupled HSQC spectrum first in FID1 and the more sensitive decoupled HSQC in FID2 (Figures S8–S9). The same general scheme can also be applied for the simultaneous acquisition of a conventional HSQC and a broadband homodecoupled HSQC spectra (Figure 4B,C). Figure 4A shows the MFA-HSQC/psHSQC pulse scheme where the FID2 period is composed by a real-time BIRD-based homodecoupling acquisition scheme.^[27]

PEP has also proven its efficiency to enhance sensitivity in the HSQC-TOCSY experiment,^[17] by implementing an isotropic DIPSI2 mixing scheme at point b in SE-HSQC. The analysis of the involved components follows the same product operators described in Eq. 1, and therefore an MFA-HSQC/HSQC-TOCSY pulse scheme (Figure 5A) is advisable by incorporating the DIPSI2 pulse train before the FID2 period. A 2D HSQC spectrum is collected in FID1 whereas FID2 yields an HSQC-TOCSY spectrum, both with optional heteronuclear decoupling (Figure 5B).

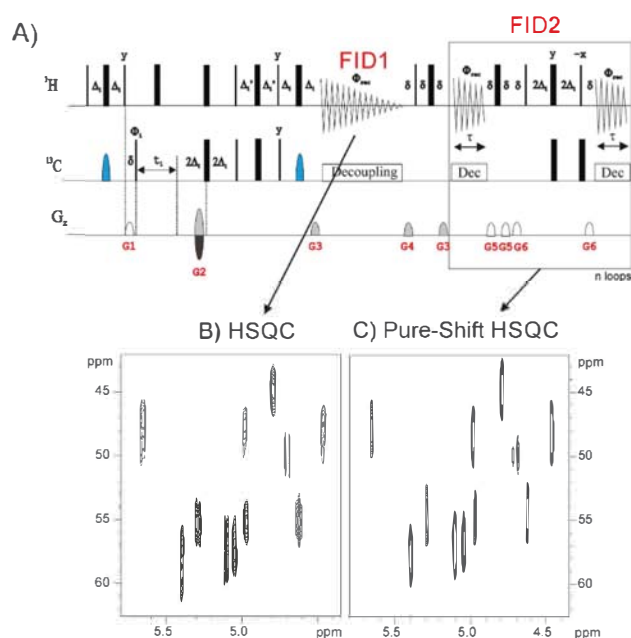


Figure 4. A) Pulse scheme of the MFA-HSQC/psHSQC experiment to acquire both regular and broadband homodecoupled HSQC spectra simultaneously; B–C) Expansions corresponding to the CH_2 region of the B) multiplicity-edited HSQC and C) multiplicity-edited psHSQC spectra of cyclosporine, both acquired under identical conditions.

The relative signal loss observed in the second acquisition by diffusion is of the same order than described before for the HSQC experiment. As a further step, an MFA-HSQC-TOCSY/HSQC-TOCSY experiment is also feasible to collect two HSQC-TOCSY spectra with different mixing times (Figure S10). In this case, TOCSY transfer with DIPSI2 mixing periods of distinct duration is included before both FID1 and FID2 periods. Table S1 compares experimental times between regular HSQC and HSQC-TOCSY experiments and all their MFA counterparts. In general, it can be observed that MFA only extend about 7–12 % the duration of the parent experiment.

In summary, a novel strategy to decipher the two active magnetization components involved in TOCSY and HSQC experiments has been described. The method affords multiple information content while offers optimized spectrometer times. Each magnetization component is monitored by independent FID periods into the same pulse sequence, providing two different NMR datasets with only an extension of 10% in the total acquisition time. The relative loss of signal observed in FID2 by diffusion effects does not affect the effectiveness of the method, which allows us to obtain a second experiment for free. The success of the method can be applied for different purposes, such as obtaining simultaneously two TOCSY or HSQC-TOCSY spectra with different mixing times or to acquire complementary HSQC spectra with various features (coupled vs decoupled; conventional vs pure shift, HSQC vs HSQC-TOCSY...). We anticipate that the combination of MFA methods with other time-optimized, resolution-enhanced and/or fast NMR techniques will further give rise the development of new experiments and better optimization of spectrometer times.

Experimental Section

NMR spectra were recorded on a Bruker AVANCE spectrometer equipped with a 5 mm TBI probehead operating at 600.13 MHz for ^1H at 298 K. The sample used in this work was 25 mM of cyclosporine dissolved in 0.6 ml of CDCl_3 . All MFA experiments were recorded using the same conditions and the echo/anti-echo protocol of the parents SE-TOCSY and SE-HSQC experiments. Basic parameters for the MFA-TOCSY/TOCSY experiment: The pre-scan delay was set to 1 s and 2 scans for each one of the 128 t_1 increments were acquired (1024 points of time domain in the acquisition dimension). The acquisition time of each FID1 and FID2 periods was of 102 ms. A basic two-step phase cycling was applied: $\Phi_1 = x, -x$; $\Phi_{\text{rec}} = x, -x$. The overall duration of the gradient (1 ms) and its recovery delay (δ) was 1.2 ms and the gradient ratio G1:G2 used was 30:23 (gradient shape SINE.100). A DIPSI-2 pulse train was used for TOCSY transfer, with mixing times set to 15 and 60 ms, respectively. All TOCSY experiments were acquired and processed using the echo/anti-echo protocol where the first gradient G1 was inverted for every second FID.

Similar conditions were used for the MFA-HSQC/HSQC and their related experiments. The inter-pulse delays were optimized to 145 Hz ($\Delta_1 = 1.72$ ms and $\Delta_2 = 0.86$ ms) and the gradient ratio G1:G2:G3:G4 was set to 17:80:20.1:33 (gradient shape SINE.100). A basic two-step phase cycling was applied: $\Phi_1 = x, -x$; $\Phi_{\text{rec}} = x, -x$. Real-time BIRD-based homodecoupling in MFA-HSQC/psHSQC was performed using 11.7 ms chunk length and 12 loops (2048 complex points in F_2). All MFA-HSQC experiments were acquired and

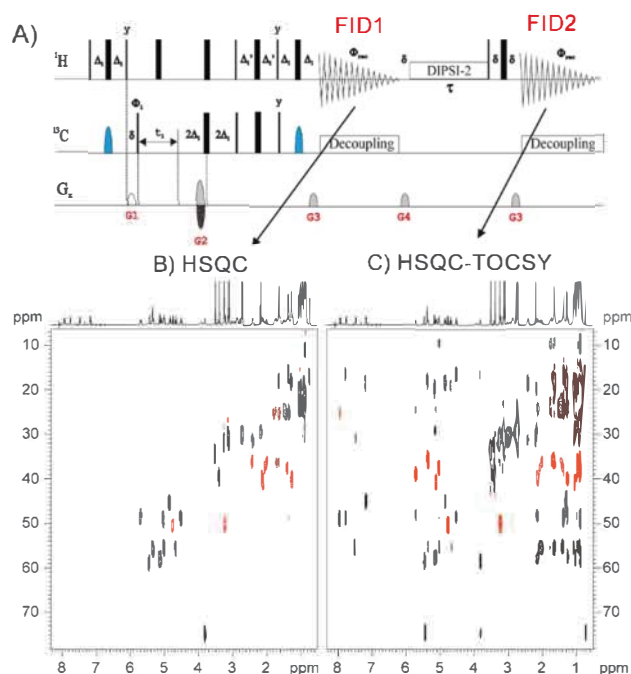


Figure 5. A) Pulse scheme of the MFA-HSQC/HSQC-TOCSY experiment. B) 2D multiplicity-edited HSQC and C) 2D multiplicity-edited HSQC-TOCSY ($\tau = 40$ ms) spectra of cyclosporine simultaneously acquired under identical conditions using the MFA-HSQC/HSQC-TOCSY pulse scheme.

processed using the echo/anti-echo protocol where the gradient G2 was inverted for every second FID.

Experimental times for all conventional and MFA-based TOCSY and HSQC experiments are shown in Table S1. Each FID1/FID2 is allocated in different memory blocks, and therefore all homonuclear and heteronuclear MFA datasets were individually processed in the usual way using the echo/anti-echo protocol. Zero-filling in both F1 and F2 dimensions, up 2048 and 1024 data matrix, respectively, and a non-shifted sine-bell window function in both dimensions were applied before Fourier transformation. All pulse programs are available in the SI.

Acknowledgements

Financial support for this research provided by Spanish MINECO (project CTQ2015-64436-P) is gratefully acknowledged. We also thank the Servei de Resonància Magnètica Nuclear, Universitat Autònoma de Barcelona, for allocating instrument time to this project.

Conflict of Interest

The authors declare no conflict of interest.

Keywords: HSQC • Multiple FID Acquisition • NMR spectroscopy • peptides • TOCSY

- [1] A. Z. Gurevich, I. L. Barsukov, A. S. Arseniev, V. F. Bystrov, *J. Magn. Reson.* **1984**, *56*, 471–478.
- [2] K. Motiram, M. Pérez-Trujillo, P. Nolis, T. Parella, *Chem. Commun.* in press **2018**, *54*, 13507–13510.
- [3] P. Nolis, M. Pérez-Trujillo, T. Parella, *Angew. Chem. Int. Ed.* **2007**, *46*, 7495–7497.
- [4] E. Kupče, T. D. W. Claridge, *Angew. Chem. Int. Ed.* **2017**, *56*, 11779–11783; *Angew. Chem.* **2017**, *129*, 11941–11945.
- [5] E. Kupče, T. D. W. Claridge, *Chem. Commun.* **2018**, *54*, 7139–7142.
- [6] T. Parella, P. Nolis, *Concepts Magn. Reson. Part A* **2010**, *36*, 1–23.
- [7] E. Kupče, *Top. Curr. Chem.* **2013**, *335*, 71–96.
- [8] J. Cavanagh, M. Rance, *J. Magn. Reson.* **1990**, *88*, 72–85.
- [9] K. E. Kövér, D. Uhrin, V. J. Hruby, *J. Magn. Reson.* **1998**, *130*, 162–168.
- [10] G. Zhu, X. Kong, K. Sze, *J. Magn. Reson.* **1998**, *135*, 232–235.
- [11] X. M. Kong, K. H. Sze, G. Zhu, *J. Biomol. NMR* **1999**, *14*, 133–140.
- [12] L. E. Kay, P. Keifer, T. Saarinen, *J. Am. Chem. Soc.* **1992**, *114*, 10663–10665.
- [13] M. Sattler, M. G. Schwendinger, J. Schleucher, C. Griesinger, *J. Biomol. NMR* **1995**, *6*, 11–22.
- [14] J. Cavanagh, M. Rance, *Annu. Reports NMR Spectrosc.* **1993**, *27*, 1–58.
- [15] A. G. Palmer, J. Cavanagh, P. E. Wright, M. Rance, *J. Magn. Reson.* **1991**, *93*, 151–170.
- [16] J. Schleucher, M. Schwendinger, M. Sattler, P. Schmidt, O. Schedletsky, S. J. Glaser, O. W. Sørensen, C. Griesinger, *J. Biomol. NMR* **1994**, *4*, 301–306.
- [17] K. E. Kövér, V. J. Hruby, D. Uhrin, *J. Magn. Reson.* **1997**, *129*, 125–129.
- [18] R. T. Williamson, B. L. Márquez, W. H. Gerwick, *Tetrahedron* **1999**, *55*, 2881–2888.
- [19] S. S. Wijmenga, C. P. M. Van Mierlo, E. Steensma, *J. Biomol. NMR* **1996**, *8*, 319–330.
- [20] V. V. Krishnamurthy, *J. Magn. Reson. Ser. B* **1995**, *106*, 170–177.
- [21] K. Pervushin, R. Riek, G. Wider, K. Wüthrich, *Proc. Natl. Acad. Sci. USA* **1997**, *94*, 12366–12371.
- [22] D. Nietlispach, *J. Biomol. NMR* **2005**, *31*, 161–166.
- [23] J. Weigelt, *J. Am. Chem. Soc.* **1998**, *120*, 10778–10779.
- [24] M. Rance, J. P. Loria, A. G. Palmer, *J. Magn. Reson.* **1999**, *136*, 92–101.
- [25] D. R. Muhandiram, L. E. Kay, *J. Magn. Reson. Ser. B* **1994**, *103*, 203–216.
- [26] S. P. Rucker, A. J. Shaka, *Mol. Phys.* **1989**, *68*, 509–517.
- [27] L. Paudel, R. W. Adams, P. Király, J. A. Aguilar, M. Foroozandeh, M. J. Cliff, M. Nilsson, P. Sándor, J. P. Waltho, G. A. Morris, *Angew. Chem. Int. Ed.* **2013**, *52*, 11616–11619; *Angew. Chem.* **2013**, *125*, 11830–11833.

Manuscript received: November 7, 2018
 Revised manuscript received: November 28, 2018
 Version of record online: December 7, 2018

Supporting Information

© Copyright Wiley-VCH Verlag GmbH & Co. KGaA, 69451 Weinheim, 2019

Interleaved Dual NMR Acquisition of Equivalent Transfer Pathways in TOCSY and HSQC Experiments

Pau Nolis, Kumar Motiram-Corral, Míriam Pérez-Trujillo, and Teodor Parella*

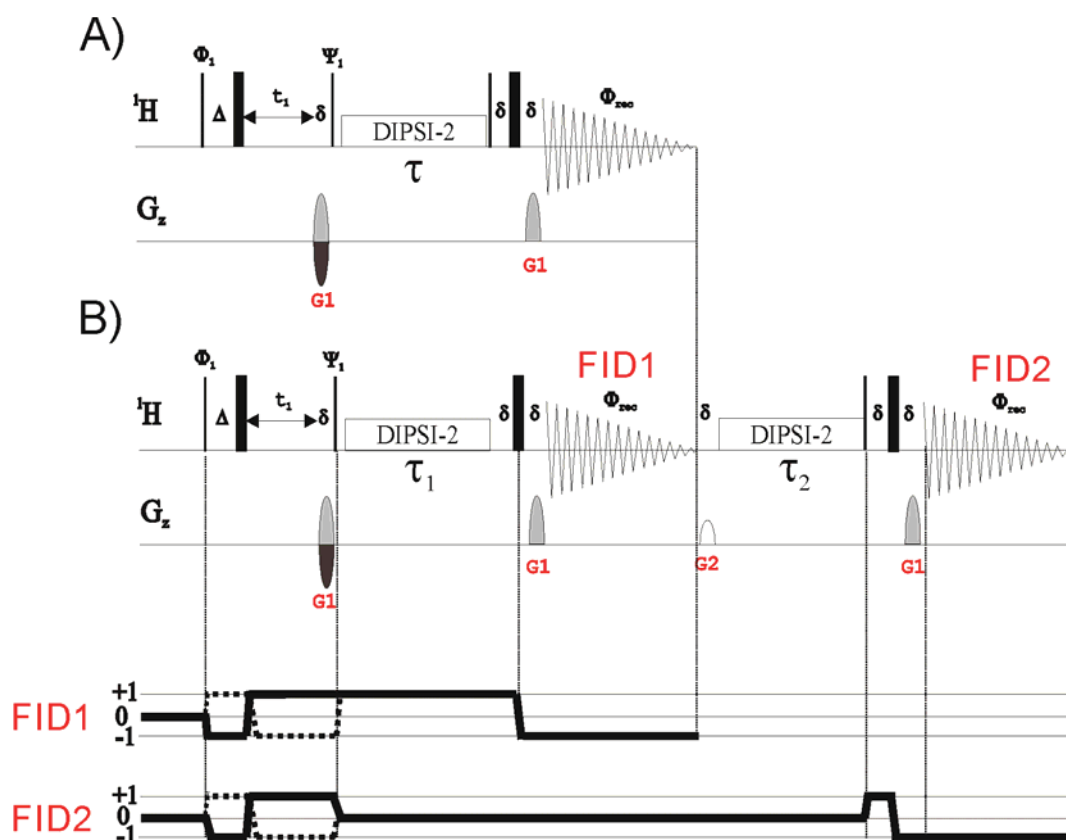


Figure S1: Pulse schemes of the A) conventional 2D sensitivity- and gradient-enhanced TOCSY (SE-TOCSY) and B) MFA-TOCSY/TOCSY experiments. In B), the two active magnetization components individually detected during the FID1 and FID2 periods, respectively, are schematized along their CTPs.

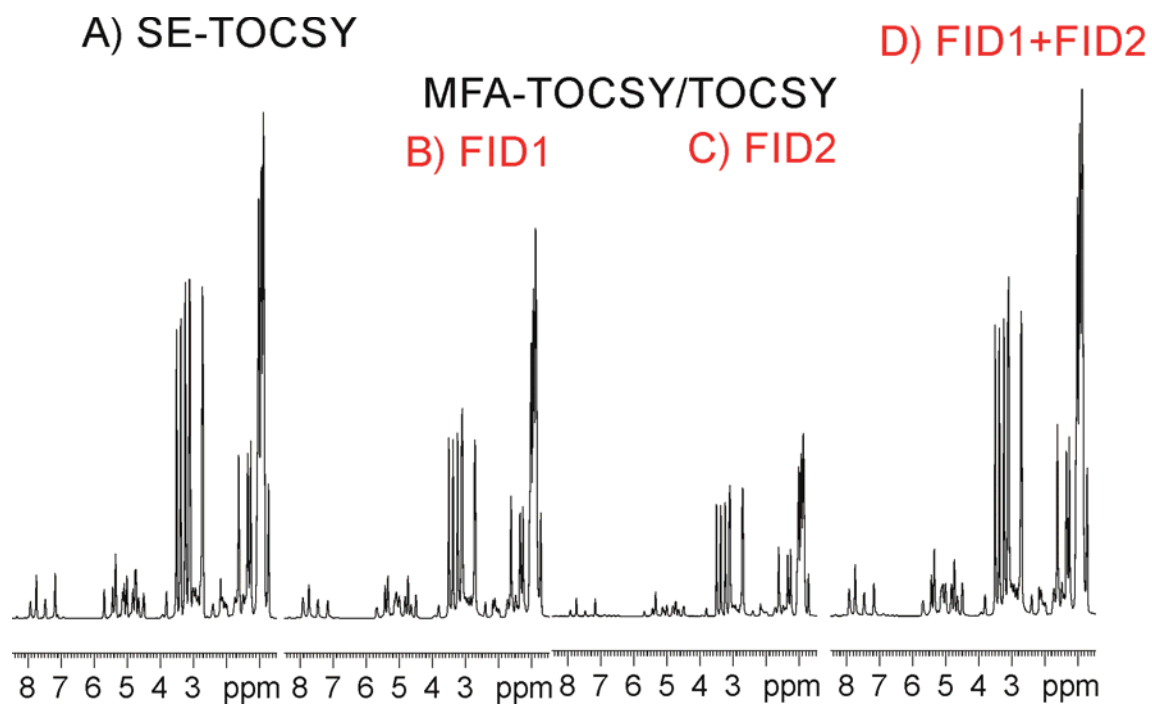


Figure S2: Positive projections corresponding to the A) 2D SE-TOCSY ($\tau = 60$ ms), B-C) FID1 ($\tau = 20$ ms) and FID2 ($\tau = 60$ ms) in 2D MFA-TOCSY/TOCSY experiment, respectively, and D) the sum of FID1 and FID2 (B+C). 2D spectra are shown in Fig. 2 of the main manuscript.

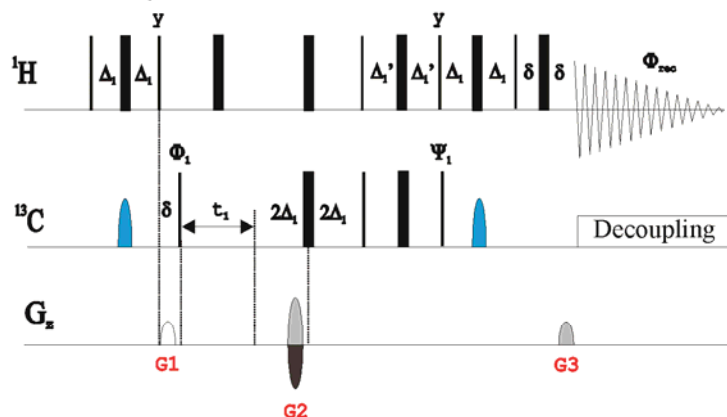
Table S1: Comparison of experimental times for several NMR experiments described in this work.

Pattern Experiment	Experimental time ^a	MFA Experiment	Experimental Time ^a	Extra Duration ^b
SE-TOCSY	10 m 28s	MFA-TOCSY/TOCSY	11 m 16s	7,1%
SE-HSQC	4 m 56s	MFA-HSQC/HSQC	5 m 21s	7,8%
		MFA-HSQC/HSQCTOCSY	5 m 32s	10,8%
		MFA-HSQCTOCSY/HSQCTOCSY	5 m 36s	11,9%
SE-HSQCTOCSY	5 m 8s	MFA-HSQC/HSQCTOCSY	5 m 32s	7,2%
		MFA-HSQCTOCSY/HSQCTOCSY	5 m 36s	8,3%

^a Experimental conditions: TD(F2) = 1K, SW(F2) = 10 ppm, AQ = 100 ms, 128 t₁ increments and ns = 2 per t₁ increment.

^b Percentage in time of the MFA experiment with respect to the pattern experiment.

A) SE-HSQC



B) MFA-HSQC/HSQC

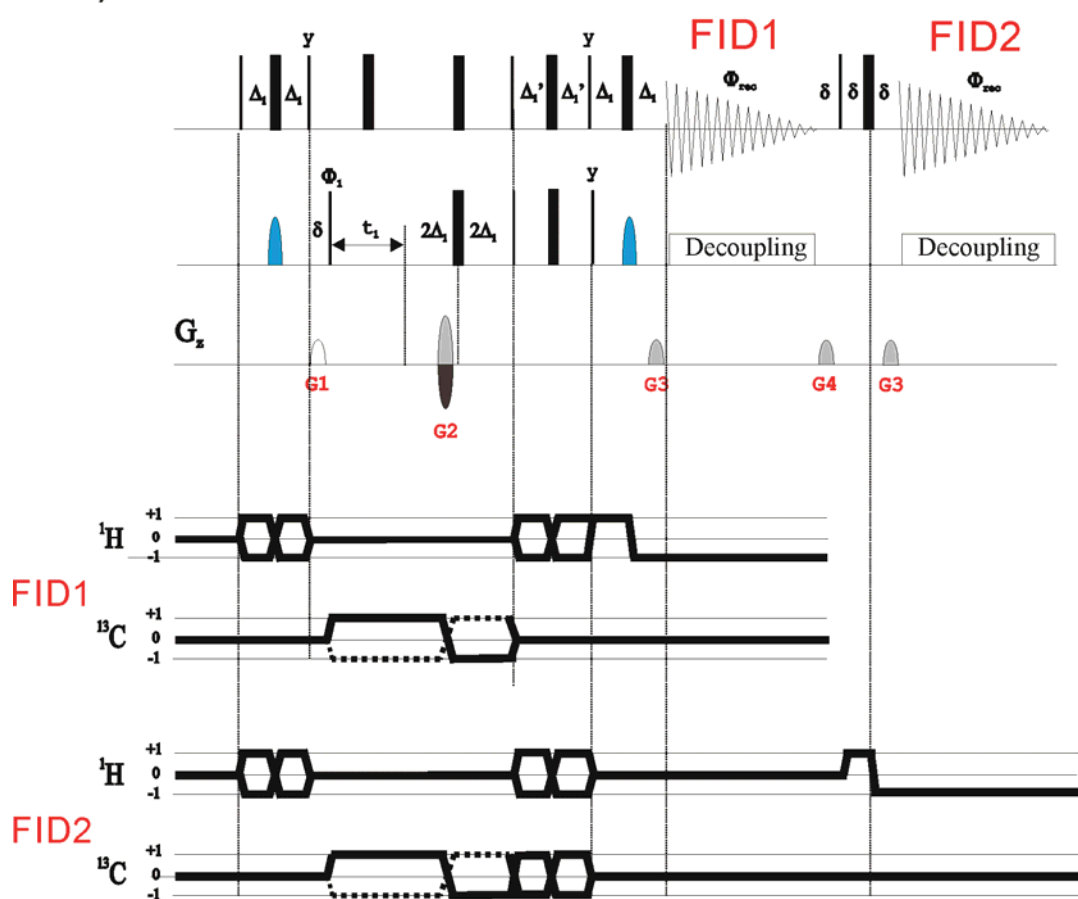


Figure S3: Pulse schemes of the A) conventional sensitivity- and gradient-enhanced HSQC (SE-HSQC) and B) MFA-HSQC/HSQC experiments. In B), the two active magnetization components detected by FID1 and FID2, respectively, are schematized along their CTPs.

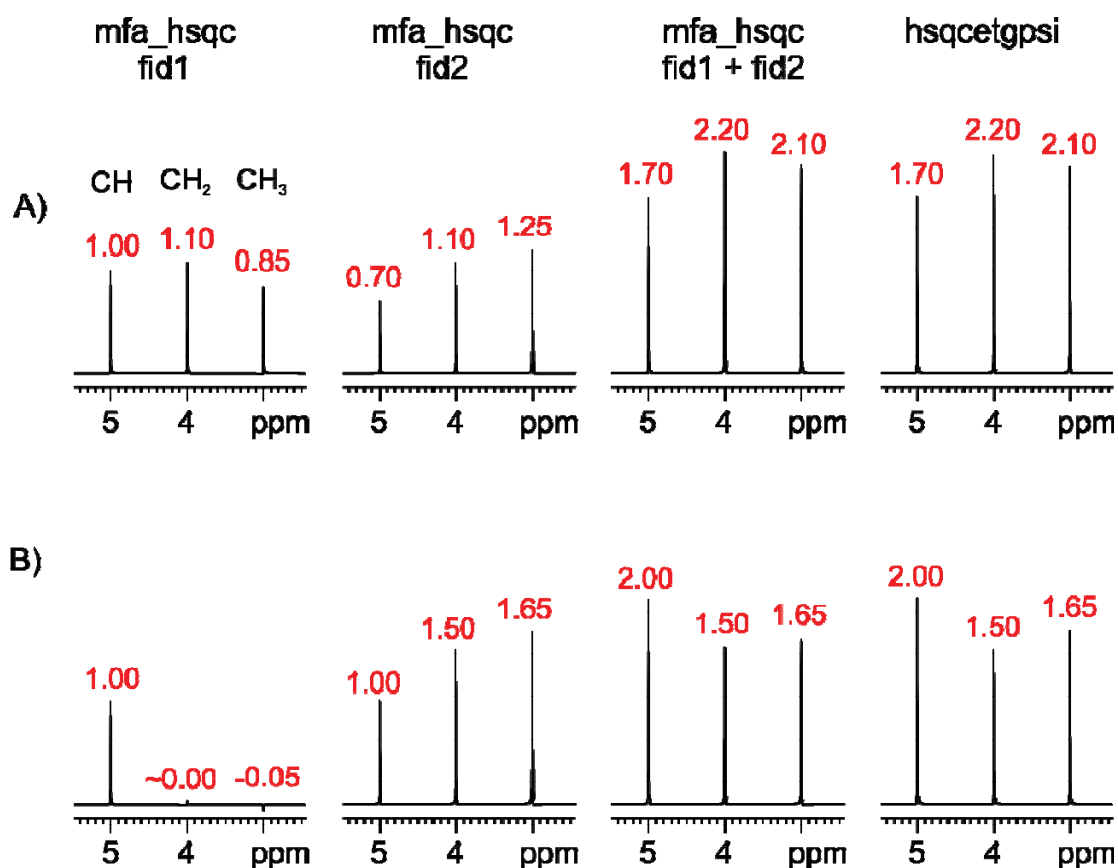


Figure S4: 1D simulations showing signal intensity dependences for all multiplicities using the MFA strategy versus standard acquisition in SE-HSQC experiment. (A) Delay optimization: $\Delta_1'=1/8J$ and $\Delta_1=1/4J$. B) Delay optimization: $\Delta_1'=1/4J$ and $\Delta_1=1/4J$. The spin systems used in the simulation are a CH at 5 ppm, a CH₂ group at 4 ppm, and a CH₃ system at 3 ppm with $^1J_{CH}$ set to 145 Hz in all cases. As expected, FID1+FID2 obtained in the MFA acquisition give rise to the same result as SE-HSQC. With this results in hand, it is highly advisable to avoid (B) delay optimization in MFA strategy due to the complete loss of signal for CH₂ and CH₃ groups in FID1. The experimental signal lost observed at FID2 due to diffusion phenomena is not considered along simulations.

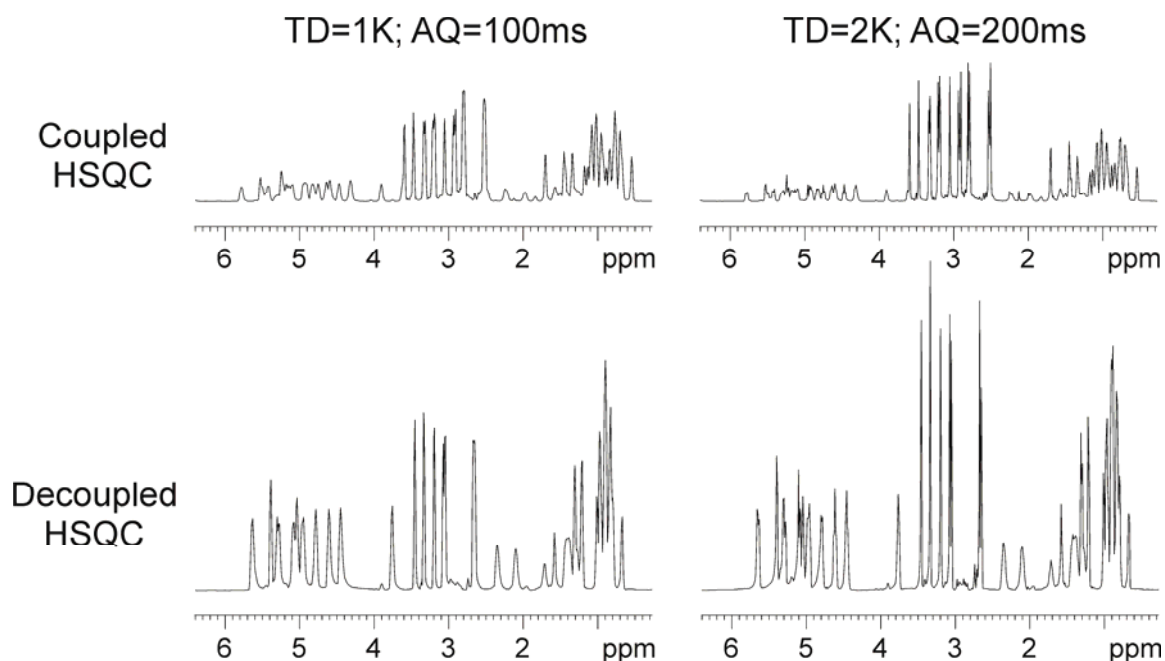
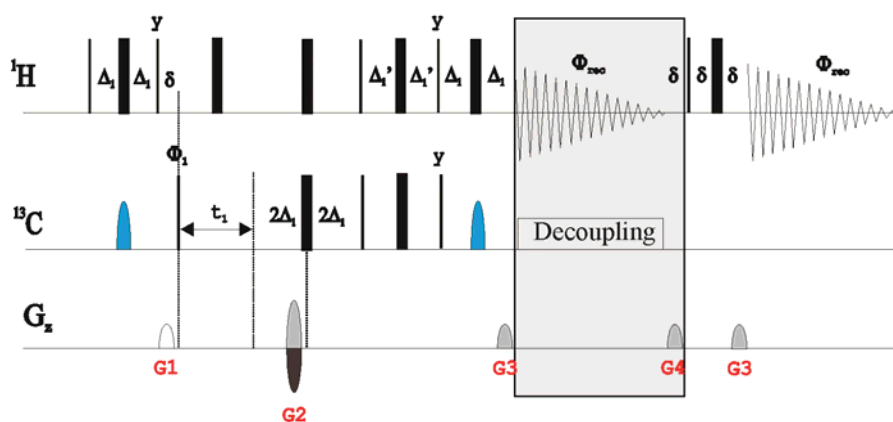
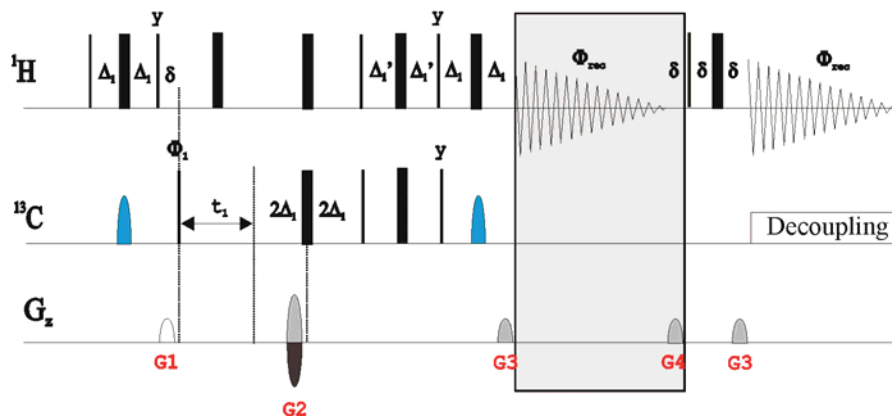


Figure S5: Relative sensitivities in decoupled and coupled HSQC spectra acquired simultaneously with the MFA-HSQC/coupledHSQC pulse scheme as a function of the FID1 and FID2 durations. IN the decoupled HSQC spectrum (FID1), it can be observed that the improved resolution affords better linewidths and therefore better sensitivity. However, despite the best resolution, sensitivity is decreased due to more pronounced diffusion effects in the coupled HSQC spectrum (FID2).

A) MFA-HSQC/CoupledHSQC



B) MFA-CoupledHSQC/HSQC



C) MFA-CoupledHSQC/HSQC

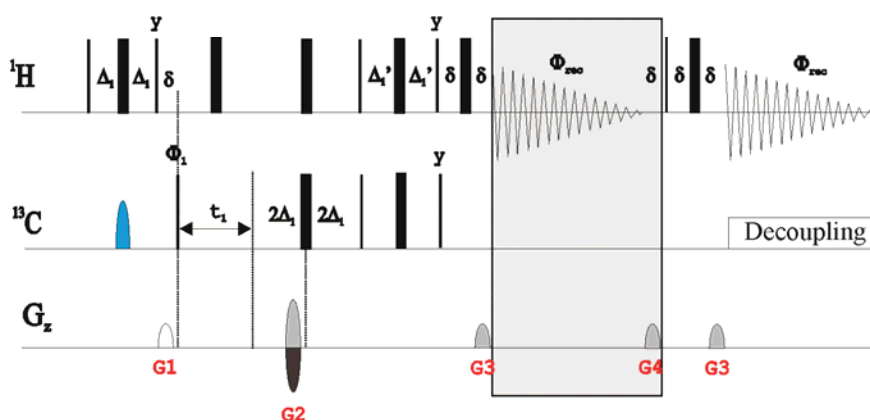


Figure S6: Several pulse schemes based on the MFA-HSQC/HSQC experiment to record simultaneously F2- ^{13}C -coupled and decoupled HSQC spectra.

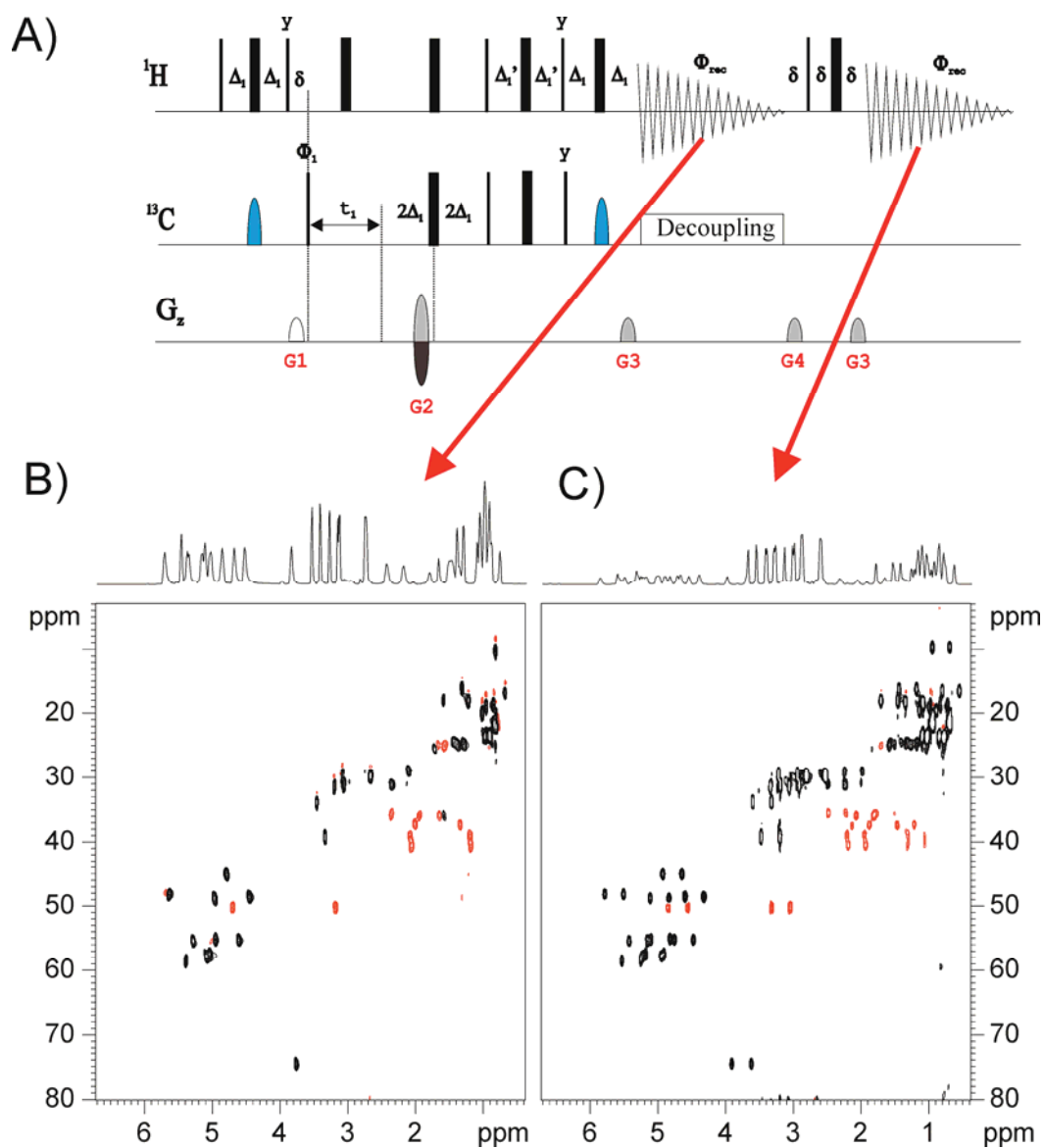


Figure S7: F2- ^{13}C -decoupled (left) and coupled (right) 2D HSQC spectra of cyclosporine acquired with the MFA-HSQC/coupledHSQC pulse scheme. 1D slices correspond to the internal positive projection of each 2D spectrum.

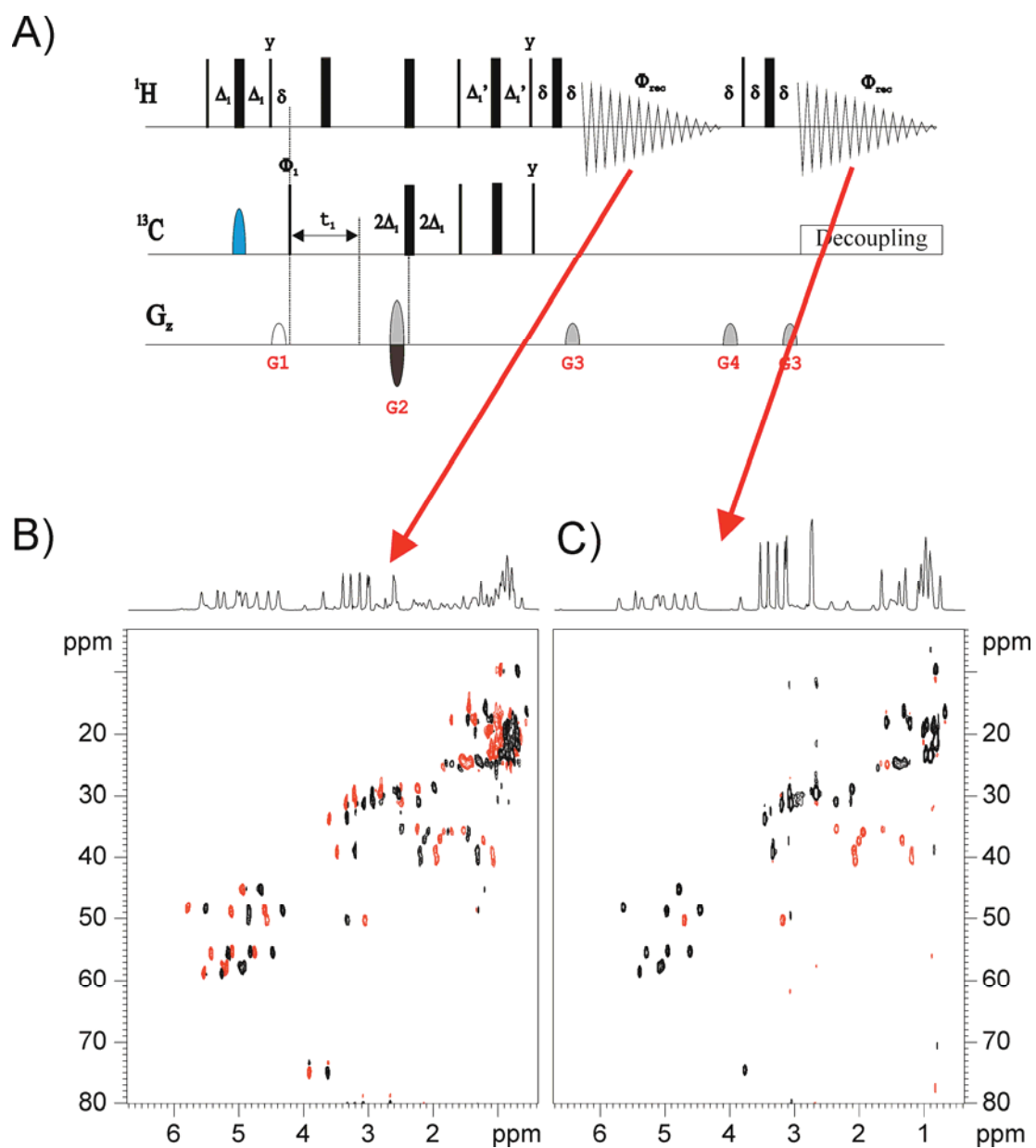


Figure S8: F2- ^{13}C -coupled (left) and decoupled (right) 2D HSQC spectra of cyclosporine acquired with the MFA-coupledHSQC/HSQC pulse scheme shown in A). 1D slices correspond to the internal positive projection of each 2D spectrum.

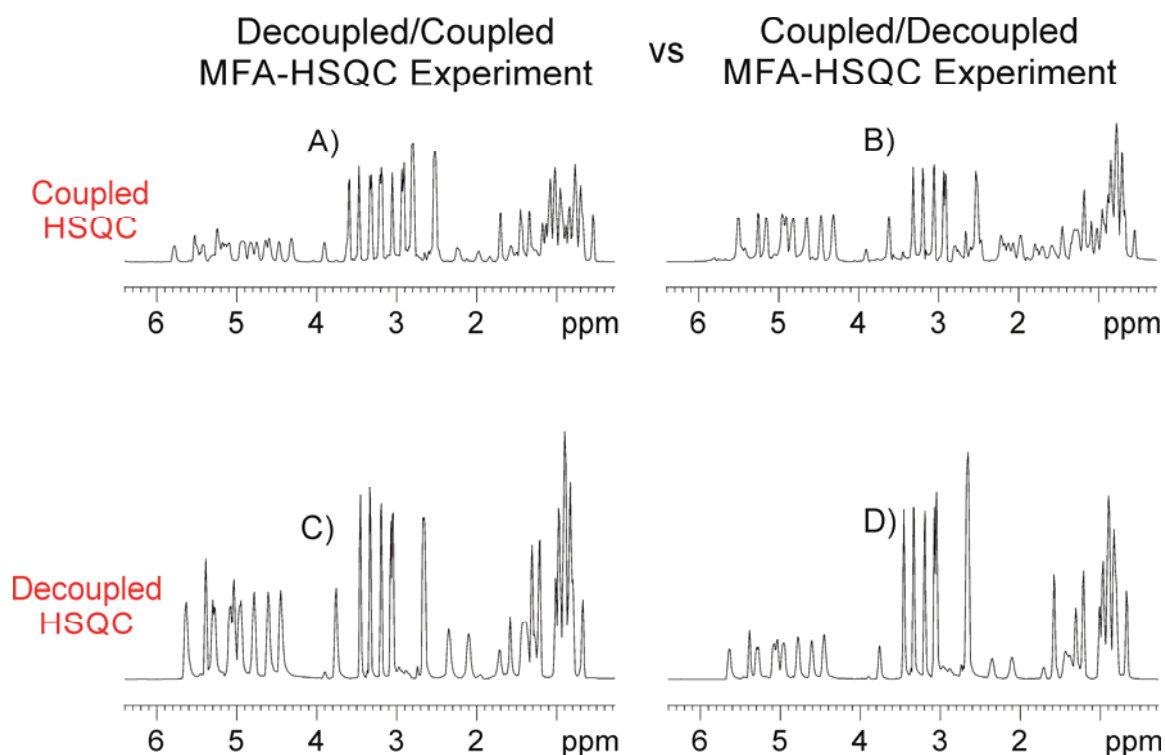


Figure S9: Relative sensitivities in decoupled (bottom) and coupled (top) HSQC spectra acquired simultaneously with the MFA-HSQC/coupledHSQC (left) and MFA-coupledHSQC/HSQC (right) pulse schemes as a function of the FID1 and FID2 durations. Note that the sensitivity of both decoupled and coupled HSQC spectra are best balanced using the MFA-coupledHSQC/HSQC experiment. Spectrum B (coupled HSQC) only shows the positive component of the anti-phase doublet.

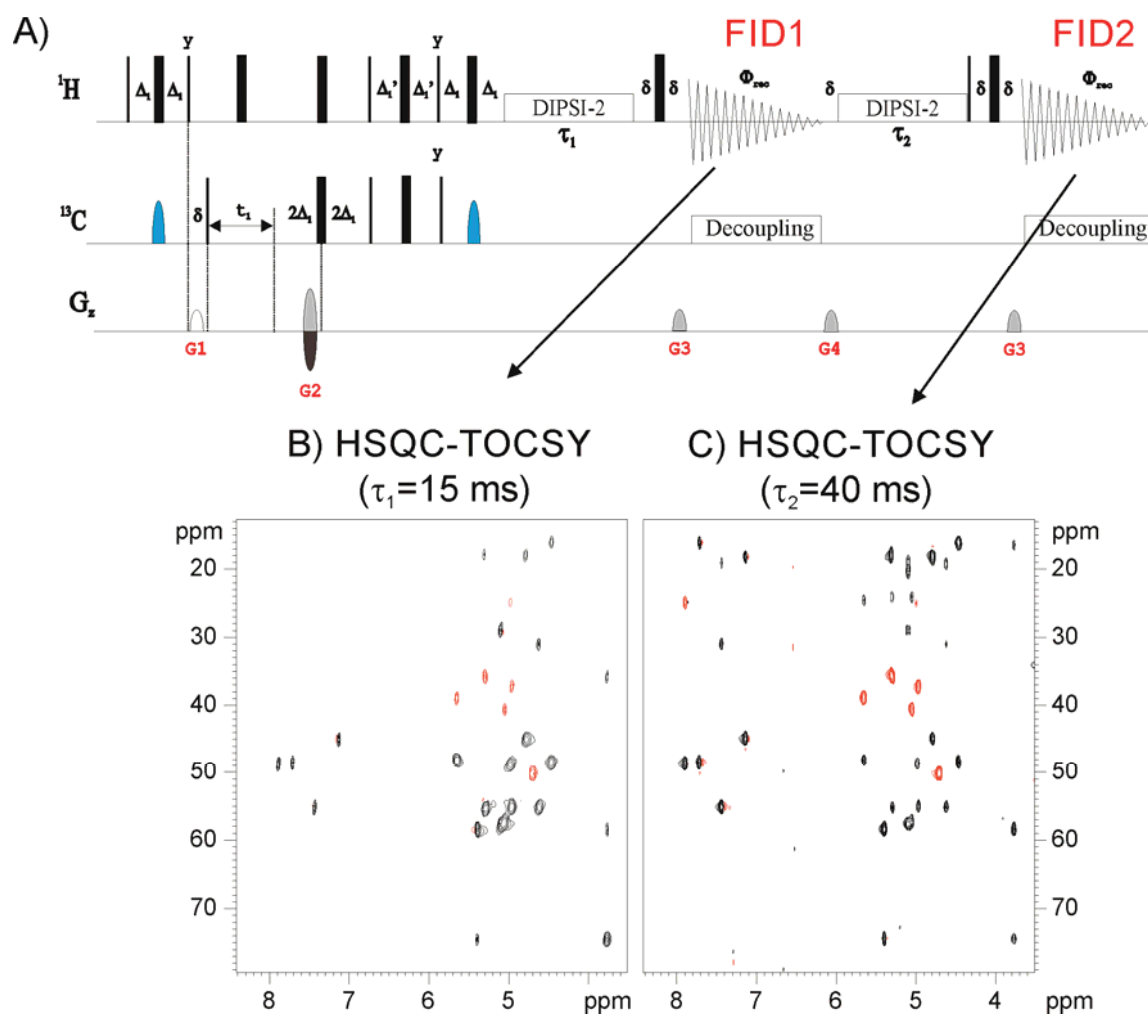


Figure S10: A) Pulse scheme of the MFA-HSQC-TOCSY/HSQC-TOCSY experiment. B-C) 2D HSQC-TOCSY spectra of cyclosporine simultaneous acquired using the MFA-HSQC/HSQC-TOCSY pulse scheme with mixing times of $\tau_1=15$ ms and $\tau_1=40$ ms, respectively.

Pulse Program of the MFA-TOCSY/TOCSY experiment

```
;mfa-toto
;derived from dipsi2etgps
;MFA-TOCSY/TOCSY

#include <Avance.incl>
#include <Grad.incl>
#include <Delay.incl>

"p2=p1*2"
"d0=3u"
"d11=30m"

"DELTA=p16+d16+d0"
"DELTA1=p16+d16+8u"
"l0=td1/2"

"FACTOR1=(d9/(p6*115.112))/2+0.5"
"FACTOR2=(d10/(p6*115.112))/2+0.5"
"l1=FACTOR1*2"
"l2=FACTOR2*2"

1 ze
  d11
2 d1 p11:f1
3 50u UNBLKGRAD
  p1 ph1
  DELTA
  p2 ph2
  d0
  p16:gp1*EA
  d16
  p1 ph3
  d12 p110:f1
                                     ;begin DIPSI2
4 p6*3.556 ph23
  p6*4.556 ph25
  p6*3.222 ph23
  p6*3.167 ph25
  p6*0.333 ph23
  p6*2.722 ph25
  p6*4.167 ph23
  p6*2.944 ph25
  p6*4.111 ph23
  p6*3.556 ph25
  p6*4.556 ph23
  p6*3.222 ph25
  p6*3.167 ph23
  p6*0.333 ph25
```

```

p6*2.722 ph23
p6*4.167 ph25
p6*2.944 ph23
p6*4.111 ph25
p6*3.556 ph25
p6*4.556 ph23
p6*3.222 ph25
p6*3.167 ph23
p6*0.333 ph25
p6*2.722 ph23
p6*4.167 ph25
p6*2.944 ph23
p6*4.111 ph25
p6*3.556 ph23
p6*4.556 ph25
p6*3.222 ph23
p6*3.167 ph25
p6*0.333 ph23
p6*2.722 ph25
p6*4.167 ph23
p6*2.944 ph25
p6*4.111 ph23
lo to 4 times 11

;end DIPSI2

DELTA1 pl1:f1
p2 ph2
4u
p16:gp1
d16
4u BLKGRAD
goscnp ph31
d12 wr #1

50u UNBLKGRAD
p16:gp2
d16
d12 pl10:f1

;begin DIPSI2
5 p6*3.556 ph23
p6*4.556 ph25
p6*3.222 ph23
p6*3.167 ph25
p6*0.333 ph23
p6*2.722 ph25
p6*4.167 ph23
p6*2.944 ph25
p6*4.111 ph23
p6*3.556 ph25
p6*4.556 ph23
p6*3.222 ph25
p6*3.167 ph23
p6*0.333 ph25

```

```

p6*2.722 ph23
p6*4.167 ph25
p6*2.944 ph23
p6*4.111 ph25
p6*3.556 ph25
p6*4.556 ph23
p6*3.222 ph25
p6*3.167 ph23
p6*0.333 ph25
p6*2.722 ph23
p6*4.167 ph25
p6*2.944 ph23
p6*4.111 ph25
p6*3.556 ph23
p6*4.556 ph25
p6*3.222 ph23
p6*3.167 ph25
p6*0.333 ph23
p6*2.722 ph25
p6*4.167 ph23
p6*2.944 ph25
p6*4.111 ph23
lo to 5 times 12

;end DIPSI2

d12 pl1:f1
p1 ph4
DELTA1
p2 ph2
4u
p16:gpl
d16
4u BLKGRAD
gosc ph31
d1 wr #2
lo to 3 times 2

d12 if #1
d12 zd
d12 if #2
30u igrad EA
30u ip3*2
lo to 3 times 2
30u ip1*2
30u ip31*2
30u id0
lo to 3 times 10
exit

ph1=0 2
ph2=0
ph3=0 0 2 2
ph4=2 2 0 0

```

```

ph23=3
ph25=1
ph31=0 2

;p11 : f1 channel - power level for pulse (default)
;p110: f1 channel - power level for TOCSY-spinlock
;p1 : f1 channel - 90 degree high power pulse
;p2 : f1 channel - 180 degree high power pulse
;p6 : f1 channel - 90 degree low power pulse
;p16: homospoil/gradient pulse
;d0 : incremented delay (2D) [3 usec]
;d1 : relaxation delay; 1-5 * T1
;d9 : TOCSY mixing time
;d10 : TOCSY mixing time
;d11: delay for disk I/O [30 msec]
;d16: delay for homospoil/gradient recovery
;l1: loop for DIPSI cycle: ((p6*115.112) * l1) = mixing time
;l2: loop for DIPSI cycle: ((p6*115.112) * l2) = mixing time
;in0: 1/(1 * SW) = 2 * DW
;nd0: 1
;NS: 2 * n
;DS: 8
;td1: number of experiments
;FnMODE: echo-antiecho

;use gradient ratio: gp 1 : gp 2
; 30 : 23
;for z-only gradients:
;gpz1: 30%
;gpz2: 23%
;use gradient files:
;gpnam1: SINE.100
;gpnam2: SINE.100

```

Pulse Program: MFA-HSQC/HSQC

```
;mf_hsqc
;derived from hsqcedetgpsisp2
;MFA-HSQC/HSQC

#include <Avance.incl>
#include <Grad.incl>
#include <Delay.incl>

"p2=p1*2"
"p4=p3*2"
"d0=3u"
"d4=1s/(cnst2*4)"
"d11=30m"

"DELTA1=p16+d16+8u"
"DELTA2=d4-larger(p2,p14)/2"
"DELTA3=d24-p19-d16"
"DELTA4=d4-larger(p2,p14)/2-p16-d16"
"DELTA5=d4-larger(p2,p14)/2-p16-d16-p16-d16"
"DELTA=d21-p16-d16-p2-d0*2"
"l0=td1/2"

1 ze
  d11 p112:f2
2 d1 do:f2
3 (p1 ph1)
  DELTA2 p10:f2
  4u
  (center (p2 ph1) (p14:sp3 ph6):f2 )
  4u
  DELTA2 p12:f2 UNBLKGRAD
  (p1 ph2) (p3 ph3):f2
  d0
  (p2 ph7)
  d0
  p16:gp1*EA
  d16
  DELTA
  (center (p2 ph1) (p4 ph4):f2 )
  d21
  (center (p1 ph1) (p3 ph4):f2 )
  p19:gp3
  d16
  DELTA3
  (center (p2 ph1) (p4 ph1):f2 )
  DELTA3
  p19:gp3
  d16
```

```

(center (p1 ph2) (p3 ph5):f2 )
p16:gp4
d16
DELTA4 p10:f2
(center (p2 ph1) (p14:sp3 ph1):f2 )
DELTA4
p16:gp6
d16 p112:f2
4u BLKGRAD
goscnp ph31 cpd2:f2
d12 do:f2
d12 wr #1

4u UNBLKGRAD
p16:gp5
d16
p1 ph1
DELTA1
(p2 ph1)
50u p112:f2
p16:gp2
d16 BLKGRAD

gosc ph31 cpd2:f2
d12 do:f2
d1 wr #2
lo to 3 times 2

d12 if #1
d12 zd
d12 if #2
30u igrad EA
30u ip3*2
30u ip6*2
30u ip31*2
lo to 3 times 2

30u id0
lo to 3 times 10
exit

ph1=0
ph2=1
ph3=0 2
ph4=0 0 2 2
ph5=1 1 3 3
ph6=0
ph7=0 0 2 2
ph8=3
ph9=2
ph31=2 0 0 2

```

```

;p10 : 120dB
;p11 : f1 channel - power level for pulse (default)
;p12 : f2 channel - power level for pulse (default)
;p13 : f3 channel - power level for pulse (default)
;p112: f2 channel - power level for CPD/BB decoupling
;sp3: f2 channel - shaped pulse 180 degree
;p1 : f1 channel - 90 degree high power pulse
;p2 : f1 channel - 180 degree high power pulse
;p3 : f2 channel - 90 degree high power pulse
;p4 : f2 channel - 180 degree high power pulse
;p14: f2 channel - 180 degree shaped pulse for inversion
;p16: homospoil/gradient pulse
;p19: gradient pulse 2 [500 usec]
;p22: f3 channel - 180 degree high power pulse
;p28: f1 channel - trim pulse
;d0 : incremented delay (2D) [3 usec]
;d1 : relaxation delay; 1-5 * T1
;d4 : 1/(4J)XH
;d11: delay for disk I/O [30 msec]
;d16: delay for homospoil/gradient recovery
;d21: set d21 according to multiplicity selection
;      1/(2J(XH)) XH, XH3 positive, XH2 negative
;d24: 1/(8J)XH for all multiplicities
;      1/(4J)XH for XH
;cnst2: = J(XH)
;in0: 1/(2 * SW(X)) = DW(X)
;nd0: 2
;NS: 2 * n
;DS: >= 16
;td1: number of experiments
;FnMODE: echo-antiecho
;cpd2: decoupling according to sequence defined by cpdprg2
;pcpd2: f2 channel - 90 degree pulse for decoupling sequence

;for z-only gradients:
;gpz1: 80%
;gpz2: 20.1%
;gpz3: 11%
;gpz4: -5%
;gpz5: 33%
;gpz6: 15.1%

```


Pulse Program: MFA-HSQC/psHSQC

```
;mfa-hs qc-pshsqc

#include <Avance.incl>
#include <Grad.incl>
#include <Delay.incl>
#include <De.incl>

#define ps

#ifdef ps
dwellmode explicit
;"d2=aq/2*12"
"d2=aq/2*12*1.1" ;for a different aliasing
#else
#endif

"p2=p1*2"
"p4=p3*2"
"d4=1s/(cnst2*4)"
"d11=30m"
"d0=3u"
"in0=infl/2"
"l0=td1/4"

"DELTA1=p16+d16+4u"
"DELTA2=d4-larger(p2,p14)/2"
"DELTA5=d4*2-larger(p2,p14)/2"
"TAU=p4"
"DELTA=p16+d16+50u+p2+d0*2"

"acqt0=0"
baseopt_echo

1 ze
  d11 p112:f2
2 d1 do:f2
3 d16 st0
                                     ; reset to first buffer memory
block
  (p1 ph1)
  DELTA2 p10:f2
  4u
  (center (p2 ph1) (p14:sp3 ph6):f2 )
  4u
  DELTA2 p12:f2
  p28 ph1
  4u
  (p1 ph2) (p3 ph3):f2
  d0
```

```

(p2 ph7)

d0
50u UNBLKGRAD
p16:gp1*EA
d16
(p4 ph4):f2
DELTA
(center (p1 ph1) (p3 ph4):f2 )
d24
(center (p2 ph1) (p4 ph1):f2 )
d24
(center (p1 ph2) (p3 ph5):f2 )
DELTA2 p10:f2
(center (p2 ph1) (p14:sp3 ph1):f2 )
DELTA2

DELTA1
(p2 ph1)
4u
p16:gp2
;gradient decoding for 1st magnetization component

d16 pl12:f2
goscnp ph31 cpd2:f2 ; 1st FID
d16 do:f2
p16:gp3 ;purgue gradient
d16 st ;increment buffer memory
block (into same file)
(p1 ph1)
;PEP here

DELTA1
(p2 ph1)
4u
p16:gp2 ;gradient decoding for 2nd
magnetization component
d16 BLKGRAD

#ifdef ps
ACQ_START(ph30,ph31)
4u cpd2:f2
0.1u REC_UNBLK
0.05u DWL_CLK_ON
d2*0.5
0.05u DWL_CLK_OFF
0.1u REC_BLK

5u UNBLKGRAD
5u do:f2
p29:gp5
d16
TAU p12:f2

```

```

(p1 ph1)
DELTA5
(center (p2 ph2) (p4 ph1):f2 )
DELTA5
(p1 ph10)
(p4 ph1):f2
p29:gp5
d16 p112:f2
20u
p29:gp6
d16
4u
(p2 ph1)
4u
p29:gp6
d16 BLKGRAD
10u cpd2:f2

4 0.1u REC_UNBLK
0.05u DWL_CLK_ON
d2
0.05u DWL_CLK_OFF
0.1u REC_BLK

5u UNBLKGRAD
5u do:f2
p29:gp5
d16
TAU p12:f2
(p1 ph1)
DELTA5
(center (p2 ph2) (p4 ph1):f2 )
DELTA5
(p1 ph10)
(p4 ph1):f2
p29:gp5
d16 p112:f2
20u
p29:gp6
d16
4u
(p2 ph1)
4u
p29:gp6
d16 BLKGRAD
10u cpd2:f2

lo to 4 times l2

0.1u REC_UNBLK
0.05u DWL_CLK_ON
d2*10

```

```

0.05u DWL_CLK_OFF
0.1u REC_BLK
4u BLKGRAD
rcyc=2

#else
    go=2 ph31 cpd2:f2                ;2nd fid
#endif
    d1 wr #0 if #0 igrad EA
    4u do:f2

        lo to 2 times 2
        30u id0
        30u ip3*2
        30u ip6*2
        30u ip31*2
        lo to 3 times 10
    50u BLKGRAD
    exit

ph1=0
ph2=1
ph3=0 2
ph4=0 0 2 2
ph5=1 1 3 3
ph6=0
ph7=0 0 2 2
ph10=2
ph30=0
ph31=0 2 2 0

;p10 : 0W
;p11 : f1 channel - power level for pulse (default)
;p12 : f2 channel - power level for pulse (default)
;p13 : f3 channel - power level for pulse (default)
;p112: f2 channel - power level for CPD/BB decoupling
;sp3: f2 channel - shaped pulse 180 degree
;p1 : f1 channel - 90 degree high power pulse
;p2 : f1 channel - 180 degree high power pulse
;p3 : f2 channel - 90 degree high power pulse
;p4 : f2 channel - 180 degree high power pulse
;p14: f2 channel - 180 degree shaped pulse for inversion
;p16: homospoil/gradient pulse
;p22: f3 channel - 180 degree high power pulse
;p28: f1 channel - trim pulse
;d0 : incremented delay (2D)                [3 usec]
;d1 : relaxation delay; 1-5 * T1
;d4 : 1/(4J)XH
;d11: delay for disk I/O                    [30 msec]
;d16: delay for homospoil/gradient recovery
;d24: 1/(8J)XH for all multiplicities
;      1/(4J)XH for XH

```

```

;cnst2: = J(XH)
;inf1:  $1/SW(X) = 2 * DW(X)$ 
;in0:  $1/(2 * SW(X)) = DW(X)$ 
;nd0: 2
;ns: 1 * n
;ds: >= 16
;td1: number of experiments
;FnMODE: echo-antiecho
;cpd2: decoupling according to sequence defined by cpdprg2
;pcpd2: f2 channel - 90 degree pulse for decoupling sequence

;for z-only gradients:
;gpz1: 80%
;gpz2: 20.1%
;gpz3: 17%
;gpz5: 11%
;gpz6: 15%

```

Pulse Program: MFA-HSQC/HSQC-TOCSY

```
; mfa_hsqctocsy
;MFA-HSQC/HSQCTOCSY

#include <Avance.incl>
#include <Grad.incl>
#include <Delay.incl>

"p2=p1*2"
"p4=p3*2"
"d0=3u"
"d4=1s/(cnst2*4)"
"d11=30m"

"DELTA1=p16+d16+8u"
"DELTA2=d4-larger(p2,p14)/2"
"DELTA3=d24-p19-d16"
"DELTA4=d4-larger(p2,p14)/2-p16-d16"
"DELTA5=d4-larger(p2,p14)/2-p16-d16-p16-d16"
"DELTA=d21-p16-d16-p2-d0*2"
"l0=td1/2"

"FACTOR1=(d9/(p6*115.112))/2+0.5"
"l1=FACTOR1*2"

1 ze
  d11 p112:f2
2 d1 do:f2
3 (p1 ph1)
  DELTA2 p10:f2
  4u
  (center (p2 ph1) (p14:sp3 ph6):f2 )
  4u
  DELTA2 p12:f2 UNBLKGRAD
  (p1 ph2) (p3 ph3):f2
  d0
  (p2 ph7)
  d0
  p16:gp1*EA
  d16
  DELTA
  (center (p2 ph1) (p4 ph4):f2 )
  d21
  (center (p1 ph1) (p3 ph4):f2 )
  p19:gp3
  d16
  DELTA3
  (center (p2 ph1) (p4 ph1):f2 )
  DELTA3
```

```

p19:gp3
d16
(center (p1 ph2) (p3 ph5):f2 )
p16:gp4
d16
DELTA4 p10:f2
(center (p2 ph1) (p14:sp3 ph1):f2 )
DELTA4
p16:gp6
d16 p112:f2
4u BLKGRAD
goscnp ph31 cpd2:f2
d12 do:f2
d12 wr #1

4u UNBLKGRAD
p16:gp5
d16 p110:f1

;begin DIPSI2
4 p6*3.556 ph22
p6*4.556 ph24
p6*3.222 ph22
p6*3.167 ph24
p6*0.333 ph22
p6*2.722 ph24
p6*4.167 ph22
p6*2.944 ph24
p6*4.111 ph22
p6*3.556 ph24
p6*4.556 ph22
p6*3.222 ph24
p6*3.167 ph22
p6*0.333 ph24
p6*2.722 ph22
p6*4.167 ph24
p6*2.944 ph22
p6*4.111 ph24
p6*3.556 ph24
p6*4.556 ph22
p6*3.222 ph24
p6*3.167 ph22
p6*0.333 ph24
p6*2.722 ph22
p6*4.167 ph24
p6*2.944 ph22
p6*4.111 ph24
p6*3.556 ph22
p6*4.556 ph24
p6*3.222 ph22
p6*3.167 ph24
p6*0.333 ph22
p6*2.722 ph24

```

```

p6*4.167 ph22
p6*2.944 ph24
p6*4.111 ph22
lo to 4 times l1

;end DIPSI2

4u pl1:f1
p1 ph1
DELTA1
(p2 ph1)
50u pl12:f2
p16:gp2
d16 BLKGRAD

gosc ph31 cpd2:f2
d12 do:f2
d1 wr #2
lo to 3 times 2

d12 if #1
d12 zd
d12 if #2
30u igrad EA
30u ip3*2
30u ip6*2
30u ip31*2
lo to 3 times 2

30u id0
lo to 3 times l0
exit

ph1=0
ph2=1
ph3=0 2
ph4=0 0 2 2
ph5=1 1 3 3
ph6=0
ph7=0 0 2 2
ph8=3
ph9=2
ph22=3
ph24=1
ph31=2 0 0 2

;p10 : 120dB
;p11 : f1 channel - power level for pulse (default)
;p12 : f2 channel - power level for pulse (default)
;p13 : f3 channel - power level for pulse (default)
;p112: f2 channel - power level for CPD/BB decoupling
;sp3: f2 channel - shaped pulse 180 degree
;p1 : f1 channel - 90 degree high power pulse
;p2 : f1 channel - 180 degree high power pulse

```



```

;p3 : f2 channel - 90 degree high power pulse
;p4 : f2 channel - 180 degree high power pulse
;p14: f2 channel - 180 degree shaped pulse for inversion
;p16: homospoil/gradient pulse
;p19: gradient pulse 2 [500 usec]
;p22: f3 channel - 180 degree high power pulse
;p28: f1 channel - trim pulse
;d0 : incremented delay (2D) [3 usec]
;d1 : relaxation delay; 1-5 * T1
;d4 : 1/(4J)XH
;d11: delay for disk I/O [30 msec]
;d16: delay for homospoil/gradient recovery
;d21: set d21 according to multiplicity selection
;      1/(2J(XH)) XH, XH3 positive, XH2 negative
;d24: 1/(8J)XH for all multiplicities
;      1/(4J)XH for XH
;cnst2: = J(XH)
;in0: 1/(2 * SW(X)) = DW(X)
;nd0: 2
;NS: 2
;DS: >= 16
;td1: number of experiments
;FnMODE: echo-antiecho
;cpd2: decoupling according to sequence defined by cpdprg2
;pcpd2: f2 channel - 90 degree pulse for decoupling sequence

;for z-only gradients:
;gpz1: 80%
;gpz2: 20.1%
;gpz3: 11%
;gpz4: -5%
;gpz5: 33%
;gpz6: 15.1%

```

Pulse Program: MFA-HSQC-TOCSY/HSQC-TOCSY

```
;teo_mf_hsqcto
;MFA-HSQCTOCSY/HSQCTOCSY

#include <Avance.incl>
#include <Grad.incl>
#include <Delay.incl>

"p2=p1*2"
"p4=p3*2"
"d0=3u"
"d4=1s/(cnst2*4)"
"d11=30m"

"DELTA1=p16+d16+8u"
"DELTA2=d4-larger(p2,p14)/2"
"DELTA3=d24-p19-d16"
"DELTA4=d4-larger(p2,p14)/2-p16-d16"
"DELTA5=d4-larger(p2,p14)/2-p16-d16-p16-d16"
"DELTA=d21-p16-d16-p2-d0*2"
"l0=td1/2"

"FACTOR1=(d9/(p6*115.112))/2+0.5"
"l1=FACTOR1*2"
"FACTOR2=(d10/(p6*115.112))/2+0.5"
"l2=FACTOR2*2"

1 ze
  d11 pl12:f2
2 d1 do:f2
3 (p1 ph1)
  DELTA2 pl0:f2
  4u
  (center (p2 ph1) (p14:sp3 ph6):f2 )
  4u
  DELTA2 pl2:f2 UNBLKGRAD
  (p1 ph2) (p3 ph3):f2
  d0
  (p2 ph7)
  d0
  p16:gp1*EA
  d16
  DELTA
  (center (p2 ph1) (p4 ph4):f2 )
  d21
  (center (p1 ph1) (p3 ph4):f2 )
  p19:gp3
  d16
  DELTA3
  (center (p2 ph1) (p4 ph1):f2 )
  DELTA3
```

```

p19:gp3
d16
(center (p1 ph2) (p3 ph5):f2 )
p16:gp4
d16
DELTA4 p10:f2
(center (p2 ph1) (p14:sp3 ph1):f2 )
DELTA4
p16:gp4
d16
d12 p110:f1

;begin DIPSI2
4 p6*3.556 ph22
  p6*4.556 ph24
  p6*3.222 ph22
  p6*3.167 ph24
  p6*0.333 ph22
  p6*2.722 ph24
  p6*4.167 ph22
  p6*2.944 ph24
  p6*4.111 ph22
  p6*3.556 ph24
  p6*4.556 ph22
  p6*3.222 ph24
  p6*3.167 ph22
  p6*0.333 ph24
  p6*2.722 ph22
  p6*4.167 ph24
  p6*2.944 ph22
  p6*4.111 ph24
  p6*3.556 ph22
  p6*4.556 ph24
  p6*3.222 ph24
  p6*3.167 ph22
  p6*0.333 ph24
  p6*2.722 ph24
  p6*4.167 ph22
  p6*2.944 ph24
  p6*4.111 ph22
  lo to 4 times 11

;end DIPSI2

4u p11:f1

```

```

DELTA1
(p2 ph1)
50u pl12:f2
p16:gp2
d16 BLKGRAD

goscnp ph31 cpd2:f2
d12 do:f2
d12 wr #1

4u UNBLKGRAD
p16:gp5
d16 pl10:f1

;begin DIPSI2
5 p6*3.556 ph22
  p6*4.556 ph24
  p6*3.222 ph22
  p6*3.167 ph24
  p6*0.333 ph22
  p6*2.722 ph24
  p6*4.167 ph22
  p6*2.944 ph24
  p6*4.111 ph22
  p6*3.556 ph24
  p6*4.556 ph22
  p6*3.222 ph24
  p6*3.167 ph22
  p6*0.333 ph24
  p6*2.722 ph22
  p6*4.167 ph24
  p6*2.944 ph22
  p6*4.111 ph24
  p6*3.556 ph24
  p6*4.556 ph22
  p6*3.222 ph24
  p6*3.167 ph22
  p6*0.333 ph24
  p6*2.722 ph22
  p6*4.167 ph24
  p6*2.944 ph22
  p6*4.111 ph24
  p6*3.556 ph22
  p6*4.556 ph24
  p6*3.222 ph22
  p6*3.167 ph24
  p6*0.333 ph22
  p6*2.722 ph24
  p6*4.167 ph22
  p6*2.944 ph24
  p6*4.111 ph22
lo to 5 times 12

```

```

                                ;end DIPSI2

4u p11:f1
p1 ph1
DELTA1
(p2 ph1)
50u p112:f2
p16:gp2
d16 BLKGRAD

gosc ph31 cpd2:f2
d12 do:f2
d1 wr #2
lo to 3 times 2

d12 if #1
d12 zd
d12 if #2
30u igrad EA
lo to 3 times 2
30u ip3*2
30u ip6*2
30u ip31*2
30u id0
lo to 3 times 10
exit

ph1=0
ph2=1
ph3=0 2
ph4=0 0 2 2
ph5=1 1 3 3
ph6=0
ph7=0 0 2 2
ph8=3
ph9=2
ph22=3
ph24=1
ph31=2 0 0 2

;p10 : 120dB
;p11 : f1 channel - power level for pulse (default)
;p12 : f2 channel - power level for pulse (default)
;p13 : f3 channel - power level for pulse (default)
;p112: f2 channel - power level for CPD/BB decoupling
;sp3: f2 channel - shaped pulse 180 degree
;p1 : f1 channel - 90 degree high power pulse
;p2 : f1 channel - 180 degree high power pulse
;p3 : f2 channel - 90 degree high power pulse
;p4 : f2 channel - 180 degree high power pulse
;p14: f2 channel - 180 degree shaped pulse for inversion
;p16: homospoil/gradient pulse

```

```

;p19: gradient pulse 2 [500 usec]
;p22: f3 channel - 180 degree high power pulse
;p28: f1 channel - trim pulse
;d0 : incremented delay (2D) [3 usec]
;d1 : relaxation delay; 1-5 * T1
;d4 : 1/(4J)XH
;d11: delay for disk I/O [30 msec]
;d16: delay for homospoil/gradient recovery
;d21: set d21 according to multiplicity selection
;      1/(2J(XH)) XH, XH3 positive, XH2 negative
;d24: 1/(8J)XH for all multiplicities
;      1/(4J)XH for XH
;cnst2: = J(XH)
;in0: 1/(2 * SW(X)) = DW(X)
;nd0: 2
;NS: 1 * n
;DS: >= 16
;td1: number of experiments
;FnMODE: echo-antiecho
;cpd2: decoupling according to sequence defined by cpdprg2
;pcpd2: f2 channel - 90 degree pulse for decoupling sequence

;for z-only gradients:
;gpz1: 80%
;gpz2: 20.1%
;gpz3: 11%
;gpz4: -5%
;gpz5: 33%
;gpz6: 15.1%

```

4.4. Publication 4: Broadband homodecoupled time-shared ^1H - ^{13}C and ^1H - ^{15}N HSQC experiments.

4.4.1. Introduction

In this article, the benefits of merging the complementary concepts of pure-shift NMR and time-sharing into a single NMR experiment are described. Novel time-shared BIRD and perfect BIRD elements have been designed to achieve broadband homodecoupling simultaneously for ^{13}C and ^{15}N . The impact of this approach in economizing spectrometer time, to improve sensitivity per time unit, to enhance spectral resolution along the ^1H dimension or in the simultaneous measurement of $^1J_{\text{CH}}$ and $^1J_{\text{NH}}$ coupling constants is shown with illustrative examples.



Broadband homodecoupled time-shared ^1H - ^{13}C and ^1H - ^{15}N HSQC experiments

Pau Nolis, Kumar Motiram-Corral, Míriam Pérez-Trujillo, Teodor Parella*

Servei de Ressonància Magnètica Nuclear, Universitat Autònoma de Barcelona, E-08193, Bellaterra, Barcelona, Catalonia, Spain

ARTICLE INFO

Article history:

Received 24 October 2018

Revised 19 November 2018

Accepted 20 November 2018

Available online 22 November 2018

Keywords:

NMR

Time-shared NMR

Pure-shift HSQC

HSQC

J -resolved HSQC

Proton-carbon coupling constants

Proton-nitrogen coupling constants

ABSTRACT

The concepts of pure-shift NMR and time-shared NMR are merged in a single experiment. A $^{13}\text{C}/^{15}\text{N}$ time-shared version of the real-time BIRD-based broadband homodecoupled HSQC experiment is described. This time-efficient approach affords simultaneously ^1H - ^{13}C and ^1H - ^{15}N pure-shift HSQC spectra in a single acquisition, while achieving substantial gains in both sensitivity and spectral resolution. We also present a related $^{13}\text{C}/^{15}\text{N}$ -F2-coupled homodecoupled version of the CLIP-HSQC experiment for the simultaneous measurement of $^1J_{\text{CH}}$ and $^1J_{\text{NH}}$ from the simplified doublets observed along the direct dimension. Finally, a novel J -resolved HSQC experiment has been designed for the simple and automated determination of both $^1J_{\text{CH}}/^1J_{\text{NH}}$ from a 2D J -resolved spectrum.

© 2018 Elsevier Inc. All rights reserved.

1. Introduction

In the last years, the development of powerful broadband homodecoupling techniques and their implementation in a broad range of existing and novel experiments has emerged as a useful tool in modern small-molecule NMR spectroscopy [1]. This concept of pure-shift (ps) NMR affords a spectacular increase in spectral resolution because the typical wide J multiplet structures are simplified to singlets, minimizing signal overlap and making data analysis and interpretation much easier. Many different ps techniques are currently available, but we want to highlight two relevant contributions. The PSYCHE element [2] improves the sensitivity and performance of the original Zangger-Sterk experiment [3], allowing its successful implementation in many interferogram-based 1D and 2D NMR experiments [4]. A second relevant contribution was the real-time broadband homodecoupling scheme based on BIRD (Bilinear Rotation Decoupling) elements [5,6] applied during ^1H acquisition in heteronuclear HSQC-type experiments [7,8]. The HSQC pulse train acts as a ^1H - ^{13}C selection filter, and it is specifically designed to suppress the large ^1H - ^{12}C contribution. In contrast to PSYCHE that is related to important sensitivity losses and longer acquisitions, the sensitivity and duration of the real-time pure-shift HSQC (psHSQC) is not affected when compared to the

parent HSQC experiment. Recently, an excellent description on the practical aspects involved in real-time homodecoupled HSQC experiments has been reported. [9] For instance, the generation of artefacts or sidebands, the line broadening caused by transverse relaxation between data chunks and/or by the mismatch between BIRD timing and $^1J_{\text{CH}}$ values, or the effects of imperfect pulses are some of the issues to consider when implementing this technique.

Time-Shared (TS) NMR experiments allows the simultaneous acquisition of ^1H - ^{13}C and ^1H - ^{15}N spectra in spectrometers having a triple-channel hardware configuration [10,11]. These methods are particularly useful for molecules containing both carbon and nitrogen because two experiments that use the same pulse train can be concentrated in a single sequence. The performance of TS experiments relies in the fact that the evolution of ^1H s attached to ^{13}C and ^1H s attached to ^{15}N do not interfere between them. These contributions can be successfully manipulated by designing pulse sequences that involve integrated $^{13}\text{C}/^{15}\text{N}$ pulses and shared delays to achieve similar effects in both nuclei at the same time. Several TS applications have been provided for the most common 2D heteronuclear experiments, such as CN-HSQC, CN-HSQC-TOCSY and CN-HMBC for small molecules [12–15], and also for multi-dimensional protein NMR [16–25]. The main advantage of the simultaneous TS acquisition compared to the conventional sequential acquisition of the two separate experiments is a considerable sensitivity-gain per time unit.

* Corresponding author.

E-mail address: teodor.parella@uab.cat (T. Parella).

In this article we show how the features offered by pure-shift NMR and time-shared NMR can be merged in a single NMR experiment. Thus, a $^{13}\text{C}/^{15}\text{N}$ time-shared version of the real-time BIRD-based broadband homodecoupled HSQC experiment is presented. This novel CN-psHSQC experiment affords simultaneously both pure-shift ^1H - ^{13}C and ^1H - ^{15}N HSQC spectra in a unique measurement, affording a substantial sensitivity gain per time unit when compared to the separate recording of each experiment. We also provide the $^{13}\text{C}/^{15}\text{N}$ -F2-coupled homodecoupled version of the CLIP-HSQC experiment (CN-psCLIPHSQC) for the simultaneous measurement of $^1J_{\text{CH}}$ and $^1J_{\text{NH}}$ from the simplified doublets obtained along the direct dimension. We also show how other resolution-enhanced techniques, such as non-uniform sampling (NUS) or J -spectroscopy, can be incorporated into these experiments. Thus, a novel J -resolved HSQC experiment (referred to as CN- J -psHSQC) has been created for the easy and automated determination of both $^1J_{\text{CH}}/^1J_{\text{NH}}$ coupling values from the indirect dimension of a 2D J -resolved spectrum.

2. Results and discussion

The TS experiments proposed in this article use several criss-crossed NMR building blocks, such as mixed INEPT (CN-INEPT), BIRD $^{\text{d},\text{x}}$ (CN-BIRD $^{\text{d},\text{x}}$), BIRD $^{\text{d}}$ (CN-BIRD $^{\text{d}}$) and perfectBIRD (CN-perfectBIRD) elements (Fig. 1). Note that the number of carbon (nitrogen) pulses in these CN-based elements are the same found in the original single-nucleus ^{13}C (^{15}N) analogues. In terms of delays, the N-INEPT transfer ($\Delta_2 = 1/(4 * ^1J_{\text{NH}}) = 2.78$ ms for 90 Hz) is longer than C-INEPT ($\Delta_1 = 1/(4 * ^1J_{\text{CH}}) = 1.85$ ms for 135 Hz) due to the lower magnitude of $^1J_{\text{NH}}$ vs $^1J_{\text{CH}}$. Thus, the CN-INEPT block which has the same duration than N-INEPT can generate some ^{13}C sensitivity loss by additional T_2 relaxation. This loss is bigger for the rest of CN-BIRD elements because delays are twice as long. However, ^{15}N is the limiting experiment in terms of sensitivity and therefore this expected ^{13}C signal loss becomes not critical. A detailed description of the main features of the basic BIRD $^{\text{d},\text{x}}$ and BIRD $^{\text{d}}$ elements can be found in Refs. [5,6] and those of perfectBIRD

in Refs. [30,34], and their effects on coupling constants and chemical shifts are summarized in Table S1.

The CN-psHSQC scheme depicted in Fig. 2 is derived from the original CN-HSQC experiment which already included CN-INEPT transfer elements and sensitive-enhancement PEP [26] to maximize signal intensities for both CH and NH spin systems. Basically, it is the pulse sequence shown in Fig. 1d of the reference [10] up to the detection period. Real-time BIRD-based homodecoupling is inserted during ^1H acquisition using the data chunk strategy described in the psHSQC experiment based on the G_7 - $180^\circ(^1\text{H})$ - G_7 - G_8 -CN-BIRD- G_8 cluster, where G_7 and G_8 stands for gradients plus their recovery delays. As a major novelty, we use the adapted CN-BIRD $^{\text{d}}$ element introduced in Fig. 1C for the simultaneous homodecoupling of all detected ^1H - ^{13}C and ^1H - ^{15}N signals with respect to the passive ^1H - ^{12}C and ^1H - ^{14}N proton [8,9] instead of the BIRD $^{\text{d},\text{x}}$ element [7].

The resulting 2D CN-psHSQC spectrum shows all ^1H signals as singlets, except those from prochiral CH_2 and NH_2 groups that will show an additional splitting due to $^2J_{\text{HH}}$. The performance of this scheme has been tested on a standard sample of cyclosporine, a typical peptide containing all NH and CH_n ($n = 1-3$) multiplicities (Fig. 3). The relative positive/negative intensity of CH and NH cross-peaks in CN-psHSQC spectra results of the relative phase between the $90^\circ(^{13}\text{C})$ and $90^\circ(^{15}\text{N})$ pulses applied prior to the t_1 and t_1' periods, respectively. By default, we apply $\phi_1 = x$ and $\phi_2 = -x$ to differentiate them as positive (CH) and negative (NH) cross-peaks. We have recorded a complete set of HSQC experiments under identical experimental and time conditions to analyze the experimental sensitivity ratios achieved per time unit: C-HSQC (4 scans per t_1 increment), N-HSQC (4 scans per t_1 increment), C-psHSQC (4 scans per t_1 increment), N-psHSQC (4 scans per t_1 increment), CN-HSQC (8 scans per t_1 increment) and CN-psHSQC (8 scans per t_1 increment). As already reported for the original CN-HSQC experiment, the simultaneous acquisition of ^{13}C and ^{15}N data by CN-psHSQC affords an averaged signal-to-noise (SNR) per time unit enhancement about 15–20% and 40% when compared to the individual C-psHSQC and N-psHSQC, respectively (Fig. 3B). This

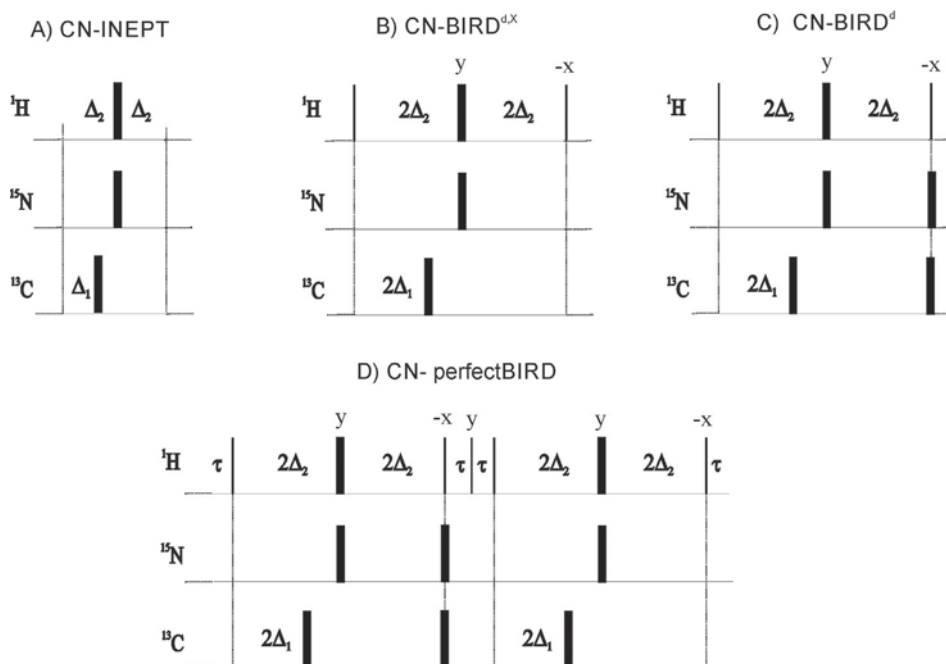


Fig. 1. Schematic representation of several NMR building blocks used in time-shared pure-shift NMR experiments: (A) CN-INEPT; (B) CN-BIRD $^{\text{d},\text{x}}$; (C) CN-BIRD $^{\text{d}}$ and (D) CN-perfectBIRD. Narrow and wide rectangular pulses refer to 90° and 180° pulses, respectively, along the x-axis unless indicated otherwise. The delays Δ_1 and Δ_2 are set to $1/(4 * ^1J_{\text{CH}})$ and $1/(4 * ^1J_{\text{NH}})$, respectively. 2τ is the echo period in the CN-perfectBIRD element.

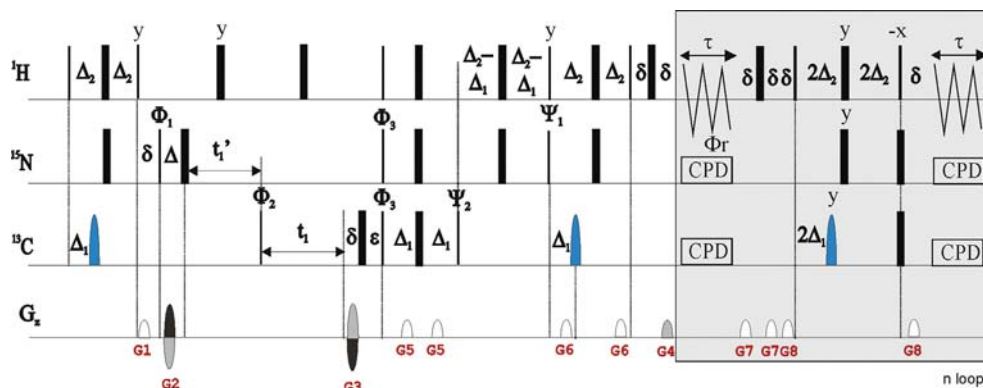


Fig. 2. Two-dimensional CN-psHSQC pulse sequence employing a pure-shift acquisition module using CN-BIRD^d. Narrow and wide rectangular pulses refer to 90° and 180° pulses, respectively, along the x-axis unless indicated otherwise. The inter-pulse delays are optimized according to $\Delta_1 = 1/(4^*J_{CH})$ and $\Delta_2 = 1/(4^*J_{NH})$, for maximizing CH and NH signals, respectively. The periods ε and Δ compensate evolution during the variable t_1 and t_1' periods and the time increments are set to $\Delta t_1 = 1/SW(^{13}C)$ and $\Delta t_1' = 1/SW(^{15}N)-1/SW(^{13}C)$. Phase cycle: $\phi_1 = (-x, x)$, $\phi_2 = (x, -x)$, $\phi_3 = (x, x, -x, -x)$, $\phi_r = (x, -x, -x, x)$. More information about gradients and other details can be found in the experimental section.

sensitivity gain can be reinforced by the signal collapsing achieved by homodecoupling which depends on the J coupling multiplet structure of each 1H signal. Thus, whereas the intensities of singlets belonging to N-Me groups are obviously not enhanced by homodecoupling, substantial sensitivity enhancements up to 50–100% can be observed additionally for the more complex CH_x multiplets. On the other hand, the duration of the homodecoupling block (overall duration of the G_7 -180°(1H)- G_7 - G_8 -BIRD- G_8 cluster) is around 10.5 ms in C-psHSQC and 14.2 ms in N-psHSQC and CN-psHSQC experiments. This longer duration could introduce an additional line broadening factor caused by transverse relaxation between data chunks but, in practice, this effect is negligible for cyclosporine. In addition to all the advantages described above, CN-psHSQC dramatically improves the levels of spectral resolution, greatly avoiding signal overlap and expediting spectral analysis. Regarding spectrometer economy, all TS method also can take profit of the advantages of other resolution-enhanced methods, such as NUS, to increase the levels of F1 digital resolution per time unit or to speed up even more data acquisition. [27] Fig. S3 shows the practical implementation of 25% of NUS to improve the performance of CN-psHSQC, similarly as done in regular HSQC data, [28] obtaining both ^{13}C and ^{15}N data in shorter experimental times and/or improved digital resolution.

The measurement of J_{CH} values from interferogram-based [29–31] and real-time [32] BIRD-based homodecoupled HSQC spectra has also received great interest for several research groups. As an extension of its applicability, the same pulse scheme of Fig. 2 can be slightly modified to obtain the F2-coupled CN-psHSQC spectrum, by omitting the broadband heteronuclear decoupling in both ^{13}C and ^{15}N channels during the FID acquisition and adding 90° ($^{13}C/^{15}N$) CLIP pulses prior to acquisition (Fig. S2). All 1H signals in CN-psCLIPHSQC spectra appear as reduced doublet patterns from which the magnitude of both J_{CH} and J_{NH} can be easily determined along the F2 dimension (Fig. 4A). As discussed above, the major gains in resolution and sensitivity by signal multiplet collapsing are observed for CH cross-peaks. Besides, simplified peaks can expedite the measurement when accidental overlap occurs, as shown from $H_{\alpha-4}$ and $H_{\alpha-6}$ signals (Fig. 4B). As recently reported in Ref. [32], more accurate measurements could be performed cycling the radiofrequency pulses involved in the homodecoupling block both from chunk to chunk acquisition and from scan to scan during time averaging. These supercycle requirements lengthen the minimum phase cycle to be applied and therefore requires accumulating more scans per increment, increasing the

acquisition time. It is also important to note that the real-time broadband homodecoupling technique fails to measure accurately J_{CH} when strong coupling effects are present. One example is the strong coupling effects shown by the olefinic H_{1E} and H_{1Z} protons resonating at 5.63 and 5.52 ppm, respectively ($^3J_{HH} = 15.5$ Hz and separated by only 65 Hz). The two satellite components show a characteristic non-symmetrical pattern in all CLIPHSQC spectra that makes difficult a precise measurement of J_{CH} in both conventional and homodecoupled signals (Fig. S4) [32].

The measurement of J_{CH} from the indirect dimension of HSQC and J -resolved HSQC experiments has shown its utility for measuring scalar and residual dipolar couplings (RDCs) in small- and biomolecules. [33–38] Here we propose a novel time-shared J -resolved pure-shift HSQC (CN- J -psHSQC) experiment to perform the simultaneous measurement of J_{CH} and J_{NH} along the F1 dimension of a J -resolved spectrum (Fig. 5A). Data 1H acquisition is performed using the mentioned real-time homodecoupling scheme based on the CN-BIRD^d cluster [8,9]. The major modifications are the replacement of the variable $^{13}C/^{15}N$ chemical shift t_1 and t_1' evolution periods in the CN-psHSQC scheme by a fixed minimum period to allocate only the defocusing gradients, whereas the indirect dimension is generated by a J -coupling t_1 evolution period that substitutes the initial CN-INEPT transfer. As a basic implementation, a CN-BIRD^{d,x} element flanked by two purging gradients can be used as a central refocusing element in this t_1 period to avoid unwanted J_{HH} and long-range $^nJ_{CH}$ and $^nJ_{NH}$ contributions (Fig. S6A). However, $^2J_{HH}$ is modulated by both CN-BIRD^d and CN-BIRD^{d,x} clusters and therefore prochiral CH_2/NH_2 protons display doublets in both dimensions (Fig. S6B). We propose to use a CN-perfectBIRD as a refocusing element (Fig. 1D) to remove the $^2J_{HH}$ splitting in the F1 dimension. The CN-perfectBIRD consists of a longer $t_1/2$ -CN-BIRD^d- $t_1/2$ -90°(1H)- $t_1/2$ -CN-BIRD^{d,x}- $t_1/2$ cluster [30,34] which can introduce some sensitivity penalty when short T_2 relaxation times are present but it works for all multiplicities (Fig. 5B). Because of the small $SW(F1)$ used in the CN- J -psHSQC experiment (about 400–500 Hz), the incremented Δt_1 period becomes relatively long and therefore it is advisable to shorten the overall duration of the sequence to minimize deleterious T_2 effects. This is the main reason because the refocusing PEP scheme has been reduced to a shorter single echo CN-INEPT. It's worth mentioning that the homodecoupling properties of the perfectBIRD can be exploited only in the indirect dimension of a multidimensional experiment, as shown in Fig. 5A, [34] or in interferogram-based acquisition techniques, as reported in Ref. [30].

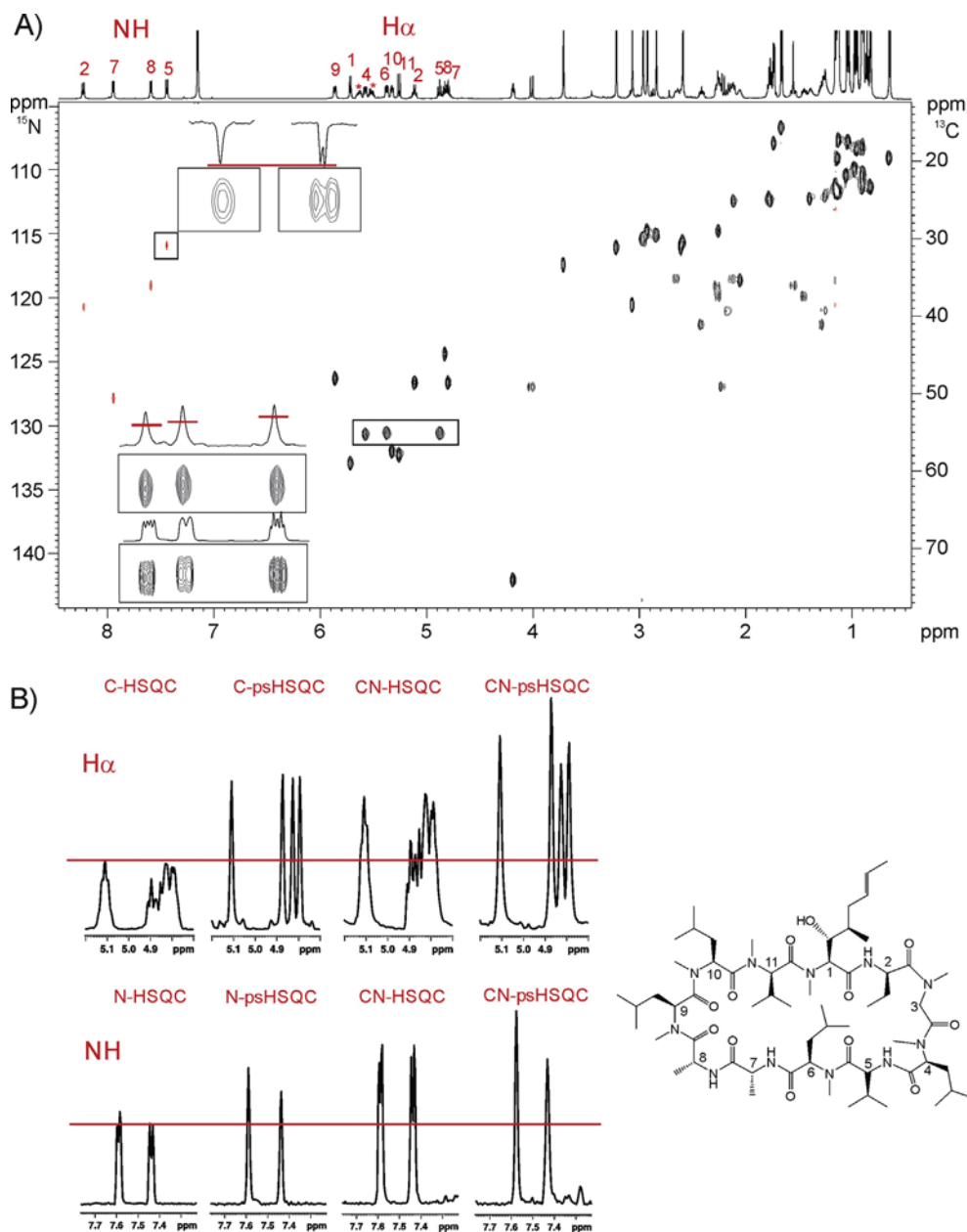


Fig. 3. (A) 2D CN-psHSQC spectrum of cyclosporine in benzene d_6 . The expanded areas compare the relative sensitivity, multiplet simplification and linewidths obtained for some CH and NH cross-peaks using conventional and broadband homodecoupled ^1H acquisition. (B) Comparison of some CH and NH signal intensities and multiplet patterns obtained in C-HSQC (4 scans per t_1); N-HSQC (4 scans per t_1); C-psHSQC (4 scans per t_1); N-psHSQC (4 scans per t_1); CN-HSQC (8 scans per t_1) and CN-psHSQC (8 scans per t_1) experiments acquired in equivalent experimental times.

The benefits of the CN-J-psHSQC spectrum rely on its user-friendly J-resolved representation, yielding simplified singlets for both CH and NH signals along the detected dimension and clean symmetrical doublets due to $^1J_{\text{CH}}$ and $^1J_{\text{NH}}$ along the indirect dimension for all multiplicities (Fig. 4B). Signals in CN-J-psHSQC spectra show an antiphase coupling pattern along F1 which does not affect the easy $^1J_{\text{CH}}/^1J_{\text{NH}}$ measurement. The phases ϕ_1 and ϕ_2 determine the relative up-down (CH) or down-up (NH) phase of cross-peaks. Fig. 6 illustrates the advantages in terms of sensitivity-enhancement and spectral resolution achieved by broadband homodecoupling over the conventional acquisition mode in CN-J-psHSQC. The high resolution available in F1 (0.4 Hz/pt using 128 t_1 increments before data processing) allows the accurate extraction of $^1J_{\text{CH}}/^1J_{\text{NH}}$ for each cross-peak by only determining their y-axis coordinate. The excellent spectral

sharpness affords valuable user-friendly $^1J_{\text{CH}}$ and $^1J_{\text{NH}}$ NMR profiles (Fig. 7), that identify each individual cross-peak and allows a rapid visualization of their coupling values for CHs (magnitudes around 135–142 Hz) and NHs (values around 92–94 Hz).

3. Conclusions

In summary, a set of time-shared pure-shift NMR experiments has been presented for the acquisition of homodecoupled ^{13}C and ^{15}N 2D HSQC spectra. Several CN-BIRD elements have been described for simultaneous ^1H - ^{13}C and ^1H - ^{15}N homodecoupling. It has been shown that the proposed experiments retain the known “sensitivity per time unit” benefits of the parallel TS acquisition of two different nuclei. Moreover, the full compatibility between sensitivity-enhanced PEP strategy and BIRD-based broadband

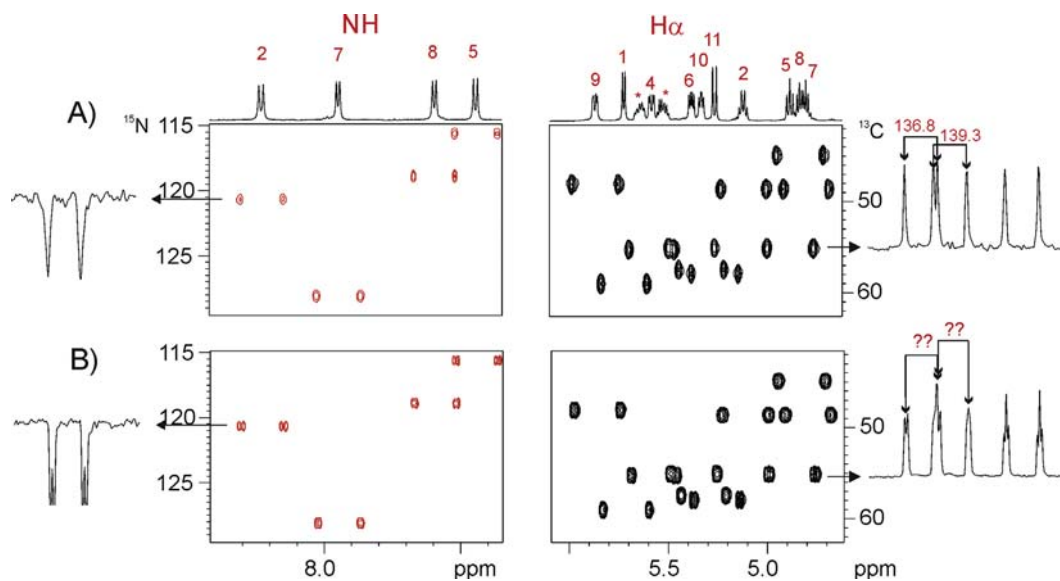


Fig. 4. Expansions corresponding to the (left) NH and (right) CH α regions of the (A) CN-psCLIPHSQC and (B) CN-CLIPHSQC spectra of cyclosporine. 1D slices show specific rows in conventional and homodecoupled spectra.

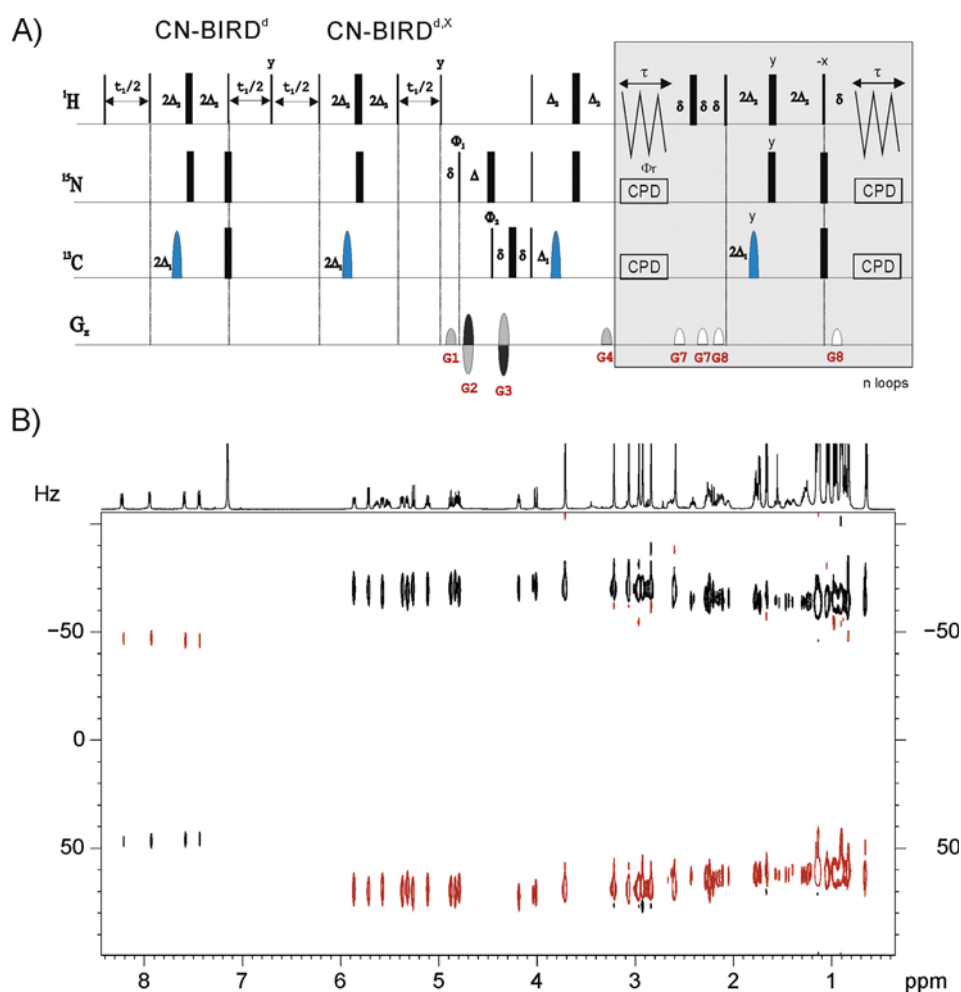


Fig. 5. (A) Pulse scheme of the CN-J-psHSQC experiment employing a CN-perfectBIRD element as a refocusing in t_1 and a pure-shift acquisition module using CN-BIRD^d. (B) 2D CN-J-psHSQC spectrum of cyclosporine, showing all NH (down-up multiplets) and CH (up-down multiplets) signals as clean doublet splittings along F1, irrespective of their multiplicities.

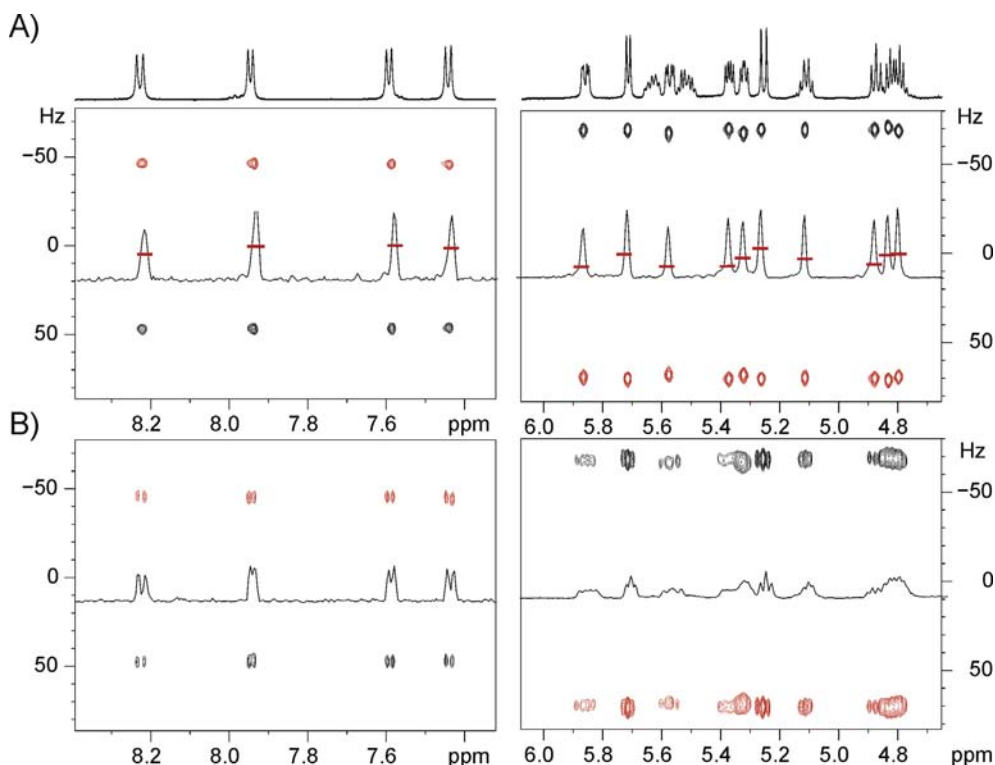


Fig. 6. Expansion of the NH and CH α region of the (A) CN-J-psHSQC and (B) CN-J-HSQC spectra. Both spectra have been acquired under identical parameters and overall experimental times. 1D internal projections are displayed for a real comparison about relative sensitivities and spectral resolution achieved in both experiments.

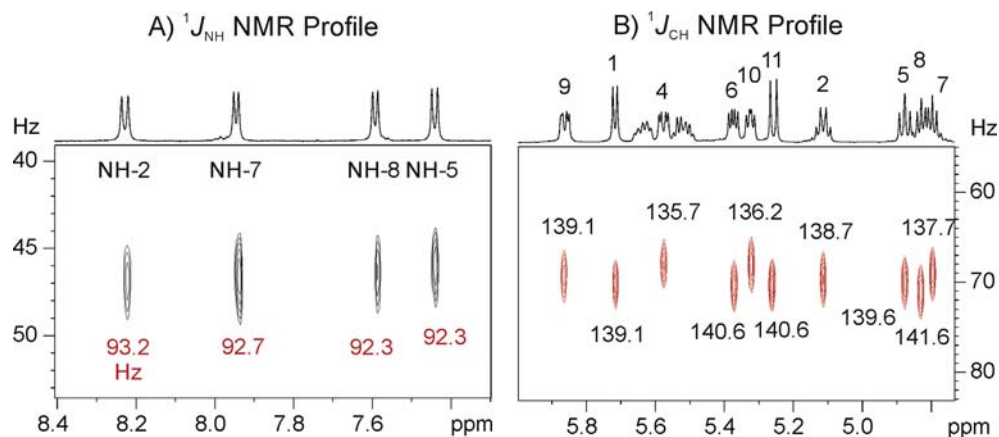


Fig. 7. Representative $^1J_{\text{NH}}$ and $^1J_{\text{CH}}$ NMR profiles of cyclosporine, displaying $\delta(^1\text{H})$ in F2 and $^1J_{\text{NH}}/2$ and $^1J_{\text{CH}}/2$ in F1. The magnitude of the coupling constants can be extracted from the y coordinate of each cross-peak or using a simple python applet after conventional peak picking.

homodecoupling affords maximum levels of attainable sensitivity while spectral resolution is increased by J multiplet simplification. In practice, the longer evolution delays involved in the described concatenated NMR elements affects minimally to the ^{13}C signal intensities and linewidths. Two different methods to measure $^1J_{\text{CH}}$ and $^1J_{\text{NH}}$ simultaneously along the F1 or F2 dimension have been described. Of interest is the CN-J-psHSQC experiment that allows an accurate and automated determination of both $^1J_{\text{CH}}$ and $^1J_{\text{NH}}$ coupling values in a user-friendly J -resolved spectrum. This is an example showing how two resolution-enhanced techniques, such as pure-shift and J -resolved spectroscopy, can be efficiently combined with time-optimized time-sharing evolution in a single NMR experiment.

4. Experimental part

NMR experiments were recorded on a 600 MHz spectrometer equipped with a triple-resonance $^1\text{H}/^{13}\text{C}/^{15}\text{N}$ inverse probe. The sample used was 25 mM of cyclosporine dissolved in benzene d_6 and the temperature for all measurements was set to 300 K.

All spectra were recorded with proton 90° pulses of 8.3 μs and carbon 90° pulses of 21.5 μs . For broadband carbon inversion, 0.5 ms smoothed Chirp pulses sweeping over a frequency band of 60 kHz was used. ^{15}N heteronuclear decoupling was performed using GARP and ^{13}C heteronuclear decoupling using the adiabatic decoupling p5m4sp180.2 scheme. The ^1H , ^{13}C , ^{15}N carriers were centred at 5 ppm, 55 ppm and 120 ppm, respectively. For all exper-

iments, the duration of the pre-scan delay was 1s, the inter-pulse delays were optimized according to $\Delta_1 = 1/(4^*J_{CH}) = 1.85$ ms ($J_{CH} = 140$ Hz) and $\Delta_2 = 1/(4^*J_{NH}) = 2.78$ ms ($J_{NH} = 90$ Hz). Gradient ratios were set-up as percentage of the absolute gradient strength of 53.5 G/cm. All gradients had a rectangular shape with smoothed edges (SMSQ10.100 in Bruker nomenclature) and their durations (δ in ms) and strengths (%) were: G1 = (800 μ s, 80), G2 = (1 ms, -47.63), G3 = (1 ms, 32.37), G4 = (1 ms, 8.14), G5 = (800 μ s, 11.0), G6 = (800 μ s, -5.0), G7 = (800 μ s, 13.0), G8 = (800 μ s, 17.0). Basic phase cycle: $\phi_1 = -x, x$; $\phi_2 = x, -x$; $\phi_3 = x, x, -x, -x$; $\Psi_1 = y, y, -y, -y$; $\Psi_2 = -y, -y, y, y$; $\phi_r = x, -x, -x, x$. All experiments were acquired and processed using the echo/anti-echo protocol where the echo and anti-echo signals were collected separately by inverting the sign of gradients G2 and G3 together with the inversion of Ψ_1 and Ψ_2 . Real-time BIRD-based homodecoupling was performed using 14.97 ms chunk length (τ) and 6 loops, giving an acquisition time of 179 ms (2048 complex points in F2).

Experimental conditions of the CN-psHSQC experiments: 8 scans were accumulated for each one of the 128 t_1 increments and the number of complex data points in t_2 was set to 2048. Prior to Fourier-transformation of each data, zero filling to 1024 in ω_1 and a $\pi/2$ -shifted squared sine bell window function (QSINE, SSB: 2) in both dimensions were applied. The Δt_1 and $\Delta(t_1 + t_1')$ times were 23.7 μ s and 189.3 μ s, respectively, that correspond to spectral widths of 21128 Hz and 5283 Hz for ^{13}C and ^{15}N , respectively. The experimental conditions of the CN-psCLIPHSQC experiments were the same as described for the analog CN-psHSQC. We have not used the time-consuming chunk-to-chunk phase supercycle described in Ref. [32] because it lengthens the acquisition time very much. For accurate measurements, we strongly recommend the CN-J-psHSQC experiment.

Experimental conditions of the CN-J-psHSQC: 8 scans were accumulated for each one of the 128 t_1 increments and the number of complex data points in t_2 was set to 2048. Spectra were acquired with spectral widths of 5699 Hz (in F₂) and 500 Hz (in F₁), respectively. Prior to Fourier-transformation of each data, zero filling to 1024 in F1 and a $\pi/2$ -shifted squared sine bell window function (QSINE, SSB: 2) in both dimensions were applied. After applying zero filling, the digital resolution was of 0.48 Hz in F1. An error of ± 0.5 Hz in the determination of J_{CH} and J_{NH} is assumed as a conservative estimate.

The java applet jmeasurement.jar described in the SI for extracting J_{CH} automatically is available on request. Pulse programs are available in the supporting information.

Acknowledgments

Financial support for this research provided by Spanish MINECO (project CTQ2015-64436-P) is gratefully acknowledged. We also thank the Servei de Resonància Magnètica Nuclear, Universitat Autònoma de Barcelona, for allocating instrument time to this project.

Appendix A. Supplementary material

Supplementary data associated with this article can be found, in the online version, at <https://doi.org/10.1016/j.jmr.2018.11.005>.

References

- [1] L. Castañar, T. Parella, Broadband 1H homodecoupled NMR experiments: recent developments, methods and applications, *Magn. Reson. Chem.* 53 (2015) 399–426.
- [2] M. Foroozandeh, R.W. Adams, N.J. Meharry, D. Jeannerat, M. Nilsson, G.A. Morris, Ultrahigh-resolution NMR spectroscopy, *Angew. Chemie – Int. Ed.* 53 (2014) 6990–6992.

- [3] K. Zangger, H. Sterk, Homonuclear broadband-decoupled NMR spectra, *J. Magn. Reson.* 489 (1997) 486–489.
- [4] M. Foroozandeh, R.W. Adams, M. Nilsson, G.A. Morris, Ultrahigh-resolution total correlation NMR spectroscopy, *J. Am. Chem. Soc.* 136 (2014) 11867–11869.
- [5] J.P. Garbow, D.P. Weitekamp, A. Pines, Bilinear rotation decoupling of homonuclear scalar interactions, *Chem. Phys. Lett.* 93 (1982) 504–509.
- [6] D. Uhrin, T. Liptaj, K.E. Kövér, Modified BIRD pulses and design of heteronuclear pulses sequences, *J. Magn. Reson.* 101 (1993) 41–46.
- [7] L. Paudel, R.W. Adams, P. Király, J.A. Aguilar, M. Foroozandeh, M.J. Cliff, M. Nilsson, P. Sándor, J.P. Waltho, G.A. Morris, Simultaneously enhancing spectral resolution and sensitivity in heteronuclear correlation NMR spectroscopy, *Angew. Chemie – Int. Ed.* 52 (2013) 11616–11619.
- [8] P. Király, R.W. Adams, L. Paudel, M. Foroozandeh, J.A. Aguilar, I. Timári, M.J. Cliff, M. Nilsson, P. Sándor, G. Batta, J.P. Waltho, K.E. Kövér, G.A. Morris, Real-time pure shift ^{15}N HSQC of proteins: a great improvement in resolution and sensitivity, *J. Biomol. NMR.* 62 (2015) 43–52.
- [9] P. Király, M. Nilsson, G.A. Morris, Practical aspects of real-time pure shift HSQC experiments, *Magn. Reson. Chem.* 56 (2018) 993–1005.
- [10] M. Sattler, M. Maurer, J. Schleucher, C. Griesinger, A simultaneous ^{15}N , ^1H - and ^{13}C , ^1H -HSQC with sensitivity enhancement and a heteronuclear gradient echo, *J. Biomol. NMR* 5 (1995) 97–102.
- [11] T. Parella, P. Nolis, Time-shared NMR experiments, *Concepts Magn. Reson. Part A Bridg. Educ. Res.* 36 (2010) 1–23.
- [12] M. Pérez-Trujillo, P. Nolis, W. Berner, T. Parella, Optimizing sensitivity and resolution in time-shared NMR experiments, *Magn. Reson. Chem.* 45 (2007) 325–329.
- [13] P. Nolis, T. Parella, Simultaneous α/β spin-state selection for ^{13}C and ^{15}N from a time-shared HSQC-IPAP experiment, *J. Biomol. NMR* 37 (2007) 65–77.
- [14] P. Nolis, M. Pérez-Trujillo, T. Parella, Multiple FID acquisition of complementary HMBC data, *Angew. Chem. Int. Ed. Engl.* 46 (2007) 7495–7497.
- [15] Nolis P, Pérez-Trujillo M, Parella T. Time-sharing evolution and sensitivity enhancements in 2D HSQC-TOCSY and HSQMBC experiments, 44 (2006) 1031–1036.
- [16] D.A. Snyder, Y. Xu, D. Yang, R. Brüschweiler, Resolution-enhanced 4D $^{15}\text{N}/^{13}\text{C}$ NOESY protein NMR spectroscopy by application of the covariance transform, *J. Am. Chem. Soc.* 129 (2007) 14126–14127.
- [17] D.P. Frueh, H. Arthanari, G. Wagner, Unambiguous assignment of NMR protein backbone signals with a time-shared triple-resonance experiment, *J. Biomol. NMR* 33 (2005) 187–196.
- [18] D.P. Frueh, D.A. Vosburg, C.T. Walsh, G. Wagner, Determination of all nOes in ^1H - ^{13}C -Me-ILV-U-2H- ^{15}N proteins with two time-shared experiments, *J. Biomol. NMR* 34 (2006) 31–40.
- [19] P. Würtz, O. Aitio, M. Hellman, P. Permi, Simultaneous detection of amide and methyl correlations using a time shared NMR experiment: application to binding epitope mapping, *J. Biomol. NMR* 39 (2007) 97–105.
- [20] S.H. Mishra, B.J. Harden, D.P. Frueh, A 3D time-shared NOESY experiment designed to provide optimal resolution for accurate assignment of NMR distance restraints in large proteins, *J. Biomol. NMR* 60 (2014) 265–274.
- [21] M. Burgering, R. Boelens, R. Kaptein, Observation of intersubunit NOEs in a dimeric P22 Mnt repressor mutant by a time-shared [^{15}N , ^{13}C] double half-filter technique, *J. Biomol. NMR* 3 (1993) 709–714.
- [22] R. Boelens, M. Burgering, R.H. Fogh, R. Kaptein, Time-saving methods for heteronuclear multidimensional NMR of (^{13}C , ^{15}N) doubly labeled proteins, *J. Biomol. NMR* 4 (1994) 201–213.
- [23] L.E. Kay, M. Wittekind, M.A. McCoy, M.S. Friedrichs, L. Mueller, 4D NMR triple-resonance experiments for assignment of protein backbone nuclei using shared constant-time evolution periods, *J. Magn. Reson.* 98 (1992) 443–450.
- [24] Y. Xu, D. Long, D. Yang, Rapid data collection for protein structure determination by NMR spectroscopy, *J. Am. Chem. Soc.* 129 (2007) 7722–7723.
- [25] C. Guo, D. Zhang, V. Tugarinov, An NMR experiment for simultaneous TROSY-based detection of amide and methyl groups in large proteins, *J. Am. Chem. Soc.* 130 (2008) 10872–10873.
- [26] L.E. Kay, P. Keifer, T. Saarinen, Pure absorption gradient enhanced heteronuclear single quantum correlation spectroscopy with improved sensitivity, *J. Am. Chem. Soc.* 114 (1992) 10663–10665.
- [27] S.G. Hyberts, H. Arthanari, G. Wagner, Applications of non-uniform sampling and processing, *Top. Curr. Chem.* 316 (2012) 125–148.
- [28] A. Le Guennec, J.-N. Dumez, P. Giraudeau, S. Caldarelli, Resolution-enhanced 2D NMR of complex mixtures by non-uniform sampling, *Magn. Reson. Chem.* 53 (2015) 913–920.
- [29] I. Timári, L. Kaltschnee, A. Kolmer, R.W. Adams, M. Nilsson, C.M. Thiele, G.A. Morris, K.E. Kövér, Accurate determination of one-bond heteronuclear coupling constants with “pure shift” broadband proton-decoupled CLIP/CLAP-HSQC experiments, *J. Magn. Reson.* 239 (2014) 130–138.
- [30] L. Kaltschnee, A. Kolmer, I. Timári, V. Schmidts, R.W. Adams, M. Nilsson, K.E. Kövér, G.A. Morris, C.M. Thiele, K.E. Kövér, Real-time broadband proton-homodecoupled CLIP/CLAP-HSQC for automated measurement of heteronuclear one-bond coupling constants, *RSC Adv.* 6 (2016) 87848–87855.

- [33] T. Parella, Current developments in homonuclear and heteronuclear J - resolved NMR experiments, *Magn. Reson. Chem.* 56 (2018) 230–250.
- [34] N. Marcó, A.A.A. Souza, P. Nolis, R.R. Gil, T. Parella, Perfect $^1J_{CH}$ -resolved HSQC: Efficient measurement of one-bond proton-carbon coupling constants along the indirect dimension, *J. Magn. Reson.* 276 (2017) 37–42.
- [35] L. Castañar, M. Garcia, E. Hellemann, P. Nolis, R.R. Gil, T. Parella, One-shot determination of residual dipolar couplings: application to the structural discrimination of small molecules containing multiple stereocenters, *J. Org. Chem.* 81 (2016) 11126–11131.
- [36] B. Luy, J.P. Marino, JE-TROSY: combined J - and TROSY-spectroscopy for the measurement of one-bond couplings in macromolecules, *J. Magn. Reson.* 163 (2003) 92–98.
- [37] J. Furrer, M. John, H. Kessler, B. Luy, J-Spectroscopy in the presence of residual dipolar couplings: determination of one-bond coupling constants and scalable resolution, *J. Biomol. NMR* 37 (2007) 231–243.
- [38] J.D. Snider, E. Troche-Pesqueira, S.R. Woodruff, C. Gayathri, N.V. Tsarevsky, R.R. Gil, New strategy for RDC-assisted diastereotopic proton assignment using a combination of J -scaled BIRD HSQC and J -scaled BIRD HMQC/HSQC, *Magn. Reson. Chem.* 50 (2012) S86–S91.

Supporting Information

Broadband homodecoupled Time-Shared ^1H - ^{13}C and ^1H - ^{15}N HSQC experiments

Pau Nolis, Kumar Motiram-Corral, Míriam Pérez-Trujillo and Teodor Parella*

Servei de Ressonància Magnètica Nuclear,

Universitat Autònoma de Barcelona, E-08193, Bellaterra, Barcelona, Catalonia, Spain.

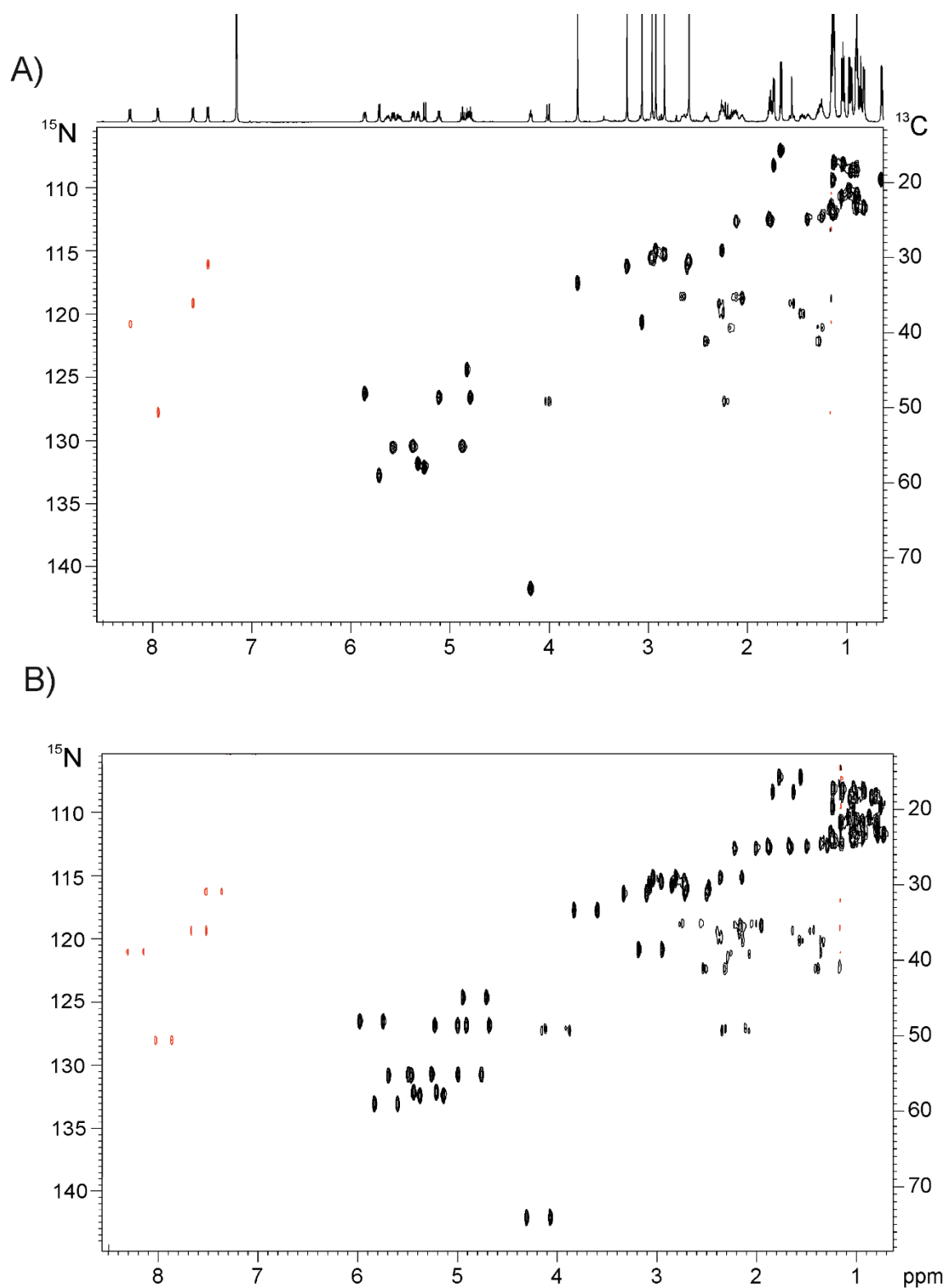


Figure S1: Two-dimensional A) CN-psHSQC and B) CN-psCLIPHSQC spectra of cyclosporine recorded under identical conditions using the pulse sequences of Figure 2 of the main manuscript and Figure S2, respectively.

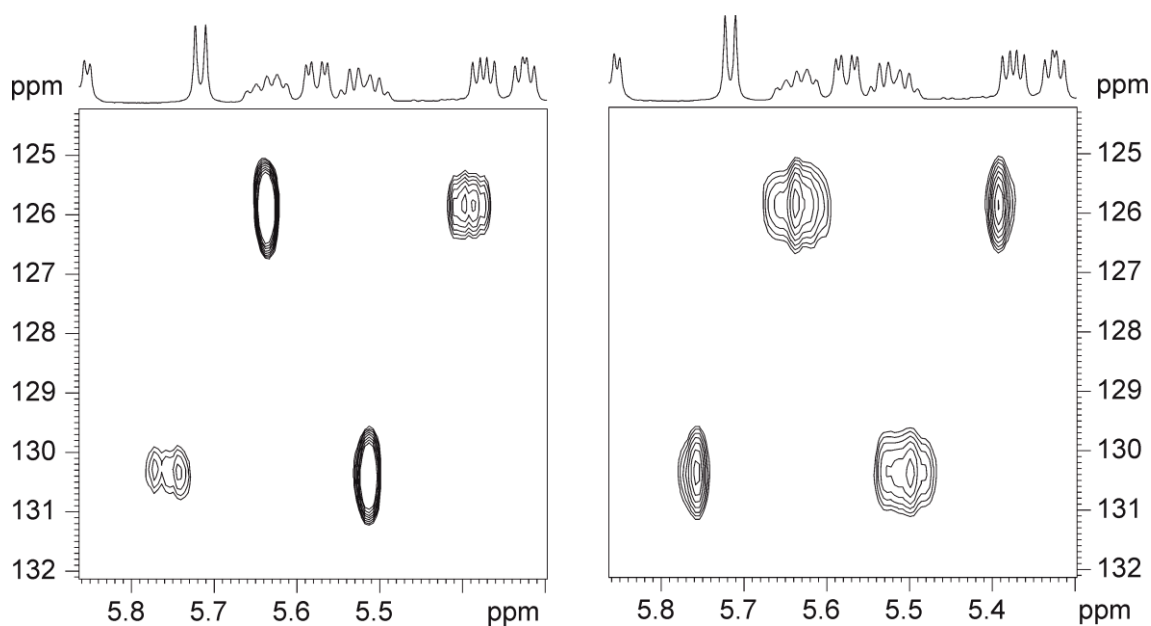


Figure S4: Strong coupling effects in the form of assimetric doublets observed for protons $H_{1\epsilon}$ and $H_{1\zeta}$ in (left) CN-CLIPHSQC and (right) CN-psCLIPHSQC spectra, respectively. These protons are separated by just 65 Hz and present a mutual $^3J_{HH}$ coupling of 15.5 Hz. Tentative $^1J_{CH}$ coupling values are about 140 Hz.

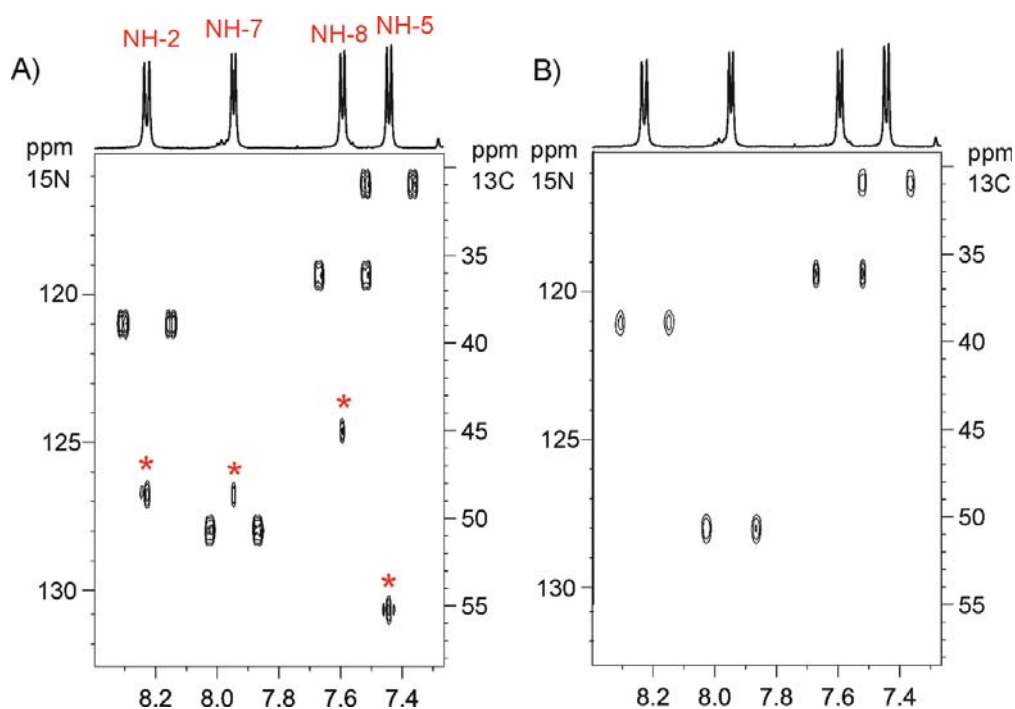


Figure S5: NH area corresponding to the CN-CLIPHSQC spectra of cyclosporine acquired A) without and B) with homodecoupling. Note that all COSY-type cross-peaks generated by the PEP scheme and observed in the conventional spectrum (marked with *) are absents in the homodecoupled spectrum.

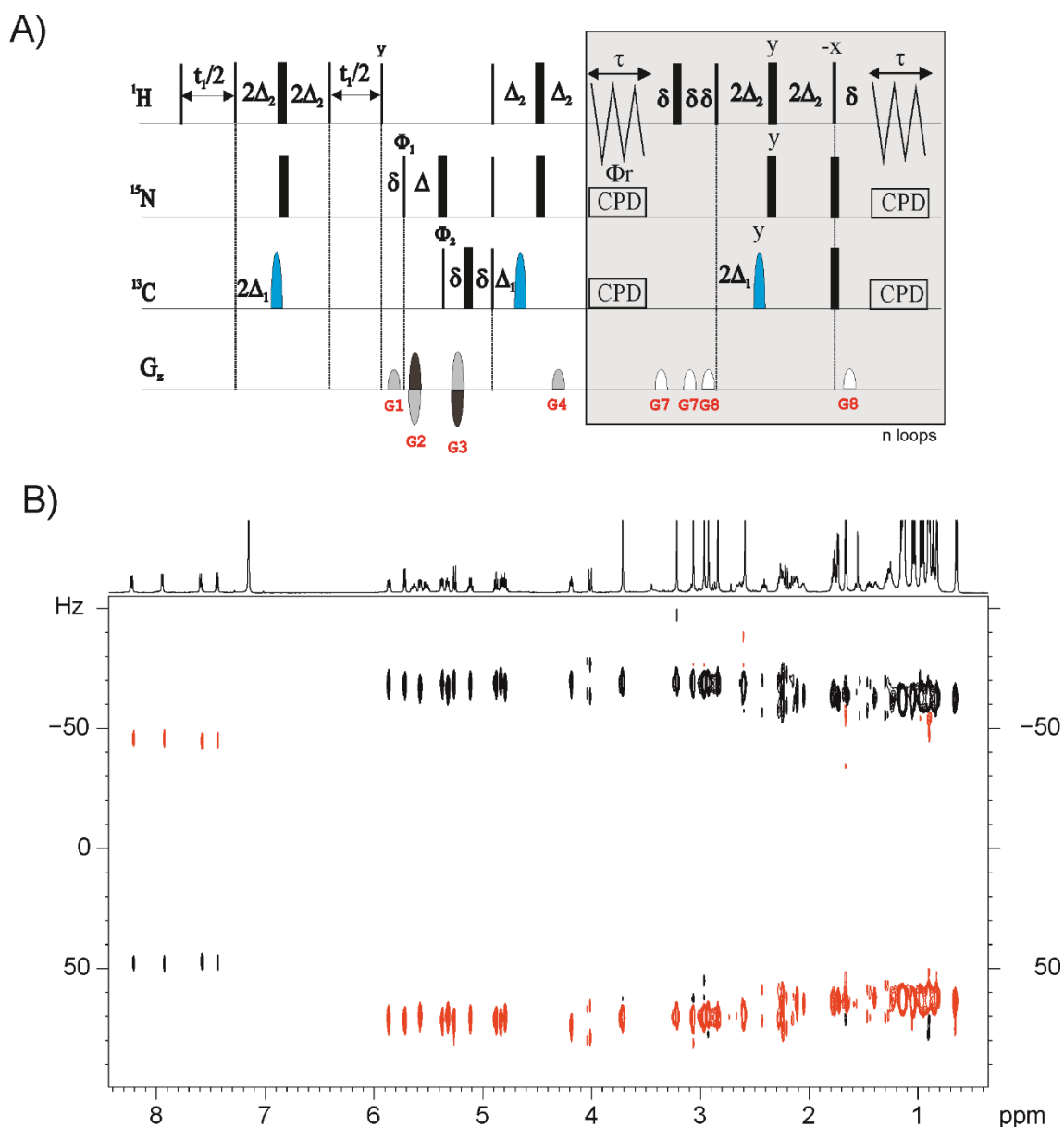


Figure S6: A) Pulse scheme of the CN-*J*-psHSQC experiment using a CN-perfectBIRD as a refocusing element. A single refocusing CN-INEPT period instead of the double PEP block was used prior to acquisition to minimize the overall duration of the experiment. B) CN-*J*-psHSQC spectrum of cyclosporine. Experimental details as described in Fig. 5 of the main manuscript.

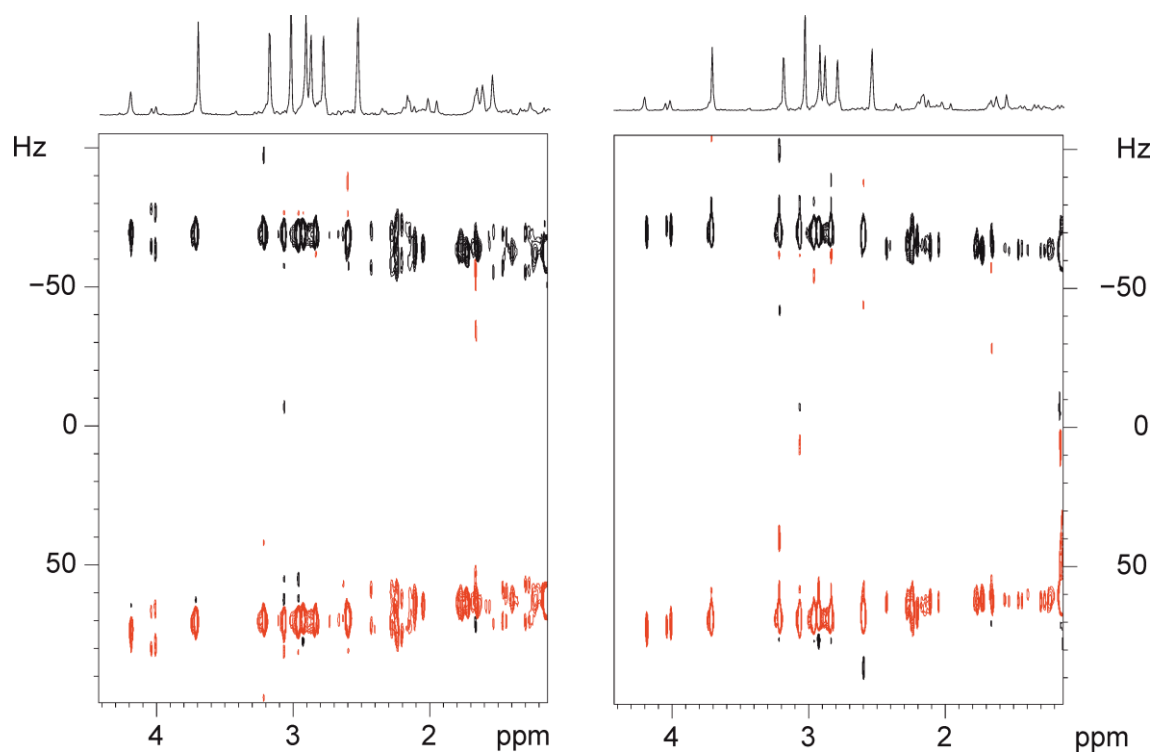


Figure S7. Comparison of CN-*J*-psHSQC spectra using (left) CN-BIRD and (right) CN-perfectBIRD as refocusing elements. Note that the splitting due to $^2J_{\text{HH}}$ along F1 are perfectly removed using the CN-perfectBIRD element.

Table S1: Effect of several BIRD elements in the most relevant ^{13}C and ^{15}N NMR parameters.^a

	Inversion Element	J_{HH}	$^2J_{\text{HH}}$	$^1J_{\text{CH}}$ Or $^1J_{\text{NH}}$	$^nJ_{\text{CH}}$ or $^nJ_{\text{NH}}$	$\delta(^1\text{H}\{^{13}\text{C}\})$ or $\delta(^1\text{H}\{^{15}\text{N}\})$	$\delta(^1\text{H}\{^{12}\text{C}\})$ or $\delta(^1\text{H}\{^{14}\text{N}\})$	$\delta(^{13}\text{C})$ or $\delta(^{15}\text{N})$
G	BIRD ^d	0	1	0	1	0	1	1
H	BIRD ^{d,X}	0	1	1	0	0	1	0
K	G-90(y)-H	0	0	1	1	0	1	0.5

^a 1 represents full evolution during the entire echo; 0 means that the corresponding modulation is refocused; 0.5 means that modulation only occurs during half of the corresponding PE element.

Table S2: $^1J_{CH}$ and $^1J_{NH}$ coupling constants of cyclosporine measured using several NMR experiments.

	CN-CLIPHSQC	CN- psCLIPHSQC	CN-J-HSQC	CN-J-psHSQC
	$^1J_{NH}$			
NH2	93.3	94.6	93.2	93.3
NH7	93.9	94.4	94.0	93.8
NH8	92.3	91.7	92.3	92.3
NH5	92.0	92.3	92.1	91.8
	$^1J_{CH}$			
H9	139.5	139.5	138.2	139.1
H1	139.1	138.9	139.2	139.1
H4	overlapping	136.4	135.6	135.7
H6	overlapping	140.1	139.7	140.6
H10	136.2	136.4	136.4	136.2
H11	140.3	141.8	140.2	140.6
H2	139.3	138.9	139.0	138.7
H5	139.4	139.9	139.5	139.6
H8	141.8	141.8	overlapping	141.6
H7	138.3	137.1	overlapping	137.7

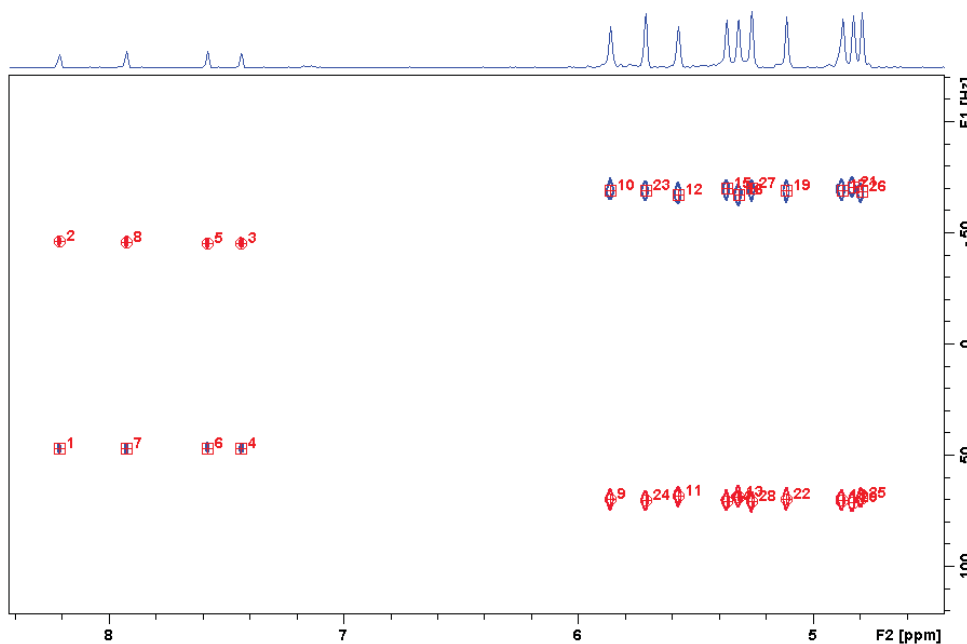
1J automated analysis

A Jython script, named CN-1J-psHSQC.py, is provided for the automated analysis of simultaneous $^1J_{CH}$ and $^1J_{NH}$ values from the proposed CN-J-psHSQC NMR experiment. For those not familiar, Jython is the java implementation of the Python programming language and it runs directly in Bruker software.

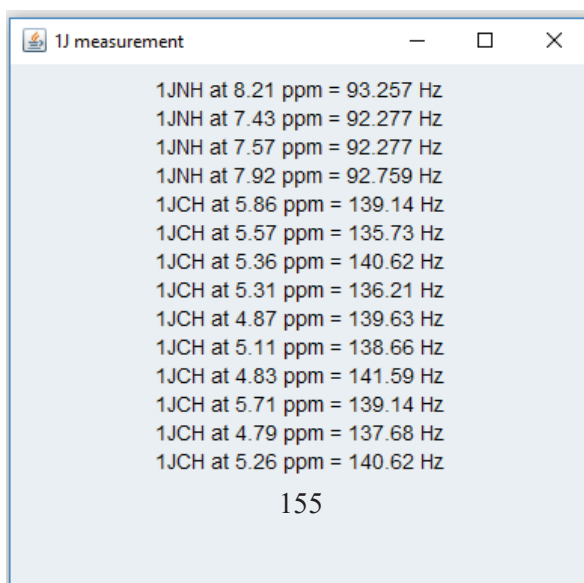
The provided script must be saved in the following working directory:

<TopSpin installation directory>/exp/stan/nmr/py/user

First, the user must perform peak picking taking into account positive and negative peaks as exemplified in the figure below. Notice, that this procedure, due to Pure Shift nature of the experiment is extra clean, therefore facilitating the automated extraction of 1J values along the indirect dimension.



Next step is just run the script from the TopSpin command line and a new window is launched providing $^1J_{NH}$ and $^1J_{CH}$ list extracted from F1 doublets automatically (see figure below).



BRUKER Pulse Programs for the CN-psHSQC experiment.

```
; 2D CN-psHSQC

prosol relations=<triple>

#include <Avance.incl>
#include <Grad.incl>
#include <Delay.incl>
#include <De.incl>

#define ps

#ifdef ps
dwellmode explicit
"d2=aq/2*12"
#else
#endif

"p2=p1*2"
"p4=p3*2"
"p22=p21*2"
"d4=1s/(cnst2*4)"
"d11=30m"
"d12=20u"
"d26=1s/(cnst4*4)"
"d24=d4/2"

"d0=3u"
"d28=3u"
"in0=inf1/2"
"in28=in20/2-in0"

"DELTA=d4-p8/2"
"DELTA1=d26-d4-p8/2"
"DELTA2=p16+d16+d28*2+p2+p3*2+p4+d0*4+p2*2"
"DELTA3=p16+d16+d0*2+p2"
"DELTA4=d4+p21+p1-p2-p22-p19-d16"
"DELTA5=d26-d4-p2-p22+p3-p4-(p21*0.27)"
"DELTA6=(p21*0.27)-(p1*0.27)"
"DELTA7=d26-d4"
"DELTA8=p16+d16+4u"
"DELTA9=d4-p19-d16"
"DELTA10=d4-p8/2-p19-d16"
"DELTA11=d26-p19-d16"
"DELTA12=d26*2-larger(p2,p22)/2"
"DELTA13=d4*2-p8/2"
"DELTA14=d26*2-d4*2-p8/2-larger(p2,p22)/2"
"TAU=larger(p2,p22)"

"spoff13=0"

1 ze
  d11 p112:f2 p116:f3
```

2 d1 do:f2 do:f3
 3 d12 pl2:f2 pl3:f3

(p1 ph1)
 DELTA
 (p8:sp13 ph6):f2
 DELTA1
 (center (p2 ph1) (p22 ph7):f3)
 d26 UNBLKGRAD
 (p28 ph1)
 4u
 (p1 ph2)

4u
 p16:gp1
 d16 pl2:f2

(p21 ph8):f3
 4u
 p16:gp2*EA
 d16
 DELTA2
 (p22 ph8):f3
 d28
 p2 ph1
 d28
 (p3 ph3):f2
 d0
 p2 ph2
 d0
 p16:gp3*EA
 d16
 (p4 ph4):f2
 DELTA3
 (p3 ph4):f2
 (p21 ph10):f3

(p1 ph1)
 p19:gp5
 d16
 DELTA9
 (p4 ph1):f2
 (p2 ph1)
 (p22 ph1):f3
 DELTA4
 p19:gp5
 d16
 (p3 ph5):f2
 DELTA7
 (p2 ph1)
 (p22 ph1):f3
 DELTA5
 (p21 ph11):f3
 DELTA6
 (p1 ph2)
 p19:gp6

```

d16
DELTA10
(p8:sp13 ph1):f2
DELTA1
(center (p2 ph1) (p22 ph1):f3 )
DELTA11
p19:gp6
d16
(p1 ph1)
DELTA8
p2 ph1
4u
p16:gp4
d16
4u p112:f2 p116:f3
;initial chunk
#ifdef ps

4u cpd2:f2 cpd3:f3
ACQ_START(ph30,ph31)
0.1u REC_UNBLK
0.05u DWL_CLK_ON
d2*0.5
0.05u DWL_CLK_OFF
0.1u REC_BLK

;BIRD
10u do:f2 do:f3
p29:gp7
d16
TAU
(p1 ph1)
DELTA13 p10:f2 p13:f3
(p8:sp13 ph2):f2
DELTA14
(center (p2 ph2) (p22 ph2):f3 )
DELTA12 p12:f2
(p1 ph17)
(center (p4 ph1):f2 (p22 ph1):f3)
d16
p29:gp7
10u
;chem. shift refoc.
10u
p29:gp8
d16 p112:f2 p116:f3
4u
(p2 ph1):f1
4u
d16
p29:gp8
10u cpd2:f2 cpd3:f3

5 0.1u REC_UNBLK
0.05u DWL_CLK_ON
d2

```

```

0.05u DWL_CLK_OFF
0.1u REC_BLK

;BIRD
10u do:f2 do:f3
p29:gp7
d16
TAU
(p1 ph1)
DELTA13 p10:f2 p13:f3
(p8:sp13 ph2):f2
DELTA14
(center (p2 ph2) (p22 ph2):f3 )
DELTA12 p12:f2
(p1 ph17)
(center (p4 ph1):f2 (p22 ph1):f3)
d16 p112:f2 p116:f3
p29:gp7
10u
;chem. shift refoc.
10u
p29:gp8
d16
4u
(p2 ph1):f1
4u
d16
p29:gp8
10u cpd2:f2 cpd3:f3
lo to 5 times l2

0.1u REC_UNBLK
0.05u DWL_CLK_ON
d2*10
0.05u DWL_CLK_OFF
0.1u REC_BLK
rcyc=2

#else
go=2 ph31 cpd2:f2 cpd3:f3
#endif
d1 do:f2 do:f3 mc #0 to 2
FlEA(calgrad(EA) & calph(ph5, +180) & calph(ph11, +180),
caldel(d0, +in0) & caldel(d28, +in28) & calph(ph3, +180) &
calph(ph6, +180) & calph(ph7, +180) & calph(ph8, +180) &
calph(ph31, +180))
exit

ph1=0
ph2=1
ph3=0 2
ph4=0 0 2 2
ph5=3 3 1 1
ph6=0
ph7=0
ph8=2 0

```

```

ph10=0 0 2 2
ph11=1 1 3 3
ph17=2
ph30=0
ph31=0 2 2 0

;p11 : f1 channel - power level for pulse (default)
;p12 : f2 channel - power level for pulse (default)
;p13 : f3 channel - power level for pulse (default)
;p112: f2 channel - power level for CPD/BB decoupling
;p116: f3 channel - power level for CPD/BB decoupling
;sp13: f2 channel - shaped pulse 180 degree (adiabatic)
;p1 : f1 channel - 90 degree high power pulse
;p2 : f1 channel - 180 degree high power pulse
;p3 : f2 channel - 90 degree high power pulse
;p4 : f2 channel - 180 degree high power pulse
;p8 : f2 channel - 180 degree shaped pulse for inversion
(adiabatic)
;p16: homospoil/gradient pulse
;p19: gradient pulse 2 [500
usec]
;p21: f3 channel - 90 degree high power pulse
;p22: f3 channel - 180 degree high power pulse
;p28: f1 channel - trim pulse [1 msec]
;d0 : incremented delay [3 usec]
;d1 : relaxation delay; 1-5 * T1
;d4 : 1/(4J(CH))
;d11: delay for disk I/O [30 msec]
;d12: delay for power switching [20 usec]
;d16: delay for homospoil/gradient recovery
;d24: = d4 / 2
;d26: 1/(4J(NH))
;d28: incremented delay [3 usec]
;cnst2: = J(CH)
;cnst4: = J(NH)
;inf1: 1/SW(C) = 2 * DW(C)
;in0: 1/(2 * SW(C)) = DW(C)
;nd0: 2
;in20: 1/SW(N) = 2 * DW(N)
;in28: in20/2 - in0
;NS: 4 * n
;DS: >= 16
;td1: number of experiments
;FnMODE: echo-antiecho
;cpd2: decoupling according to sequence defined by cpdprg2
;cpd3: decoupling according to sequence defined by cpdprg3
;pcpd2: f2 channel - 90 degree pulse for decoupling sequence
;pcpd3: f3 channel - 90 degree pulse for decoupling sequence

;use gradient ratio: gp 1 : gp 2 : gp 3 : gp 4 : gp 5 : gp
6 : gp 7 : gp 8

; 80 : -47.63 : 32.37 : 8.14 : 11 :
-5 : 13 : 17

```

```
;for z-only gradients:  
;gpz1: 80%  
;gpz2: -47.63%  
;gpz3: 32.37%  
;gpz4: 8.14%  
;gpz5: 11%  
;gpz6: -5%  
;gpz7: 13%  
;gpz8: 17%
```

```
;use gradient files:  
;gpnam1: SMSQ10.100  
;gpnam2: SMSQ10.100  
;gpnam3: SMSQ10.100  
;gpnam4: SMSQ10.100  
;gpnam5: SMSQ10.100  
;gpnam6: SMSQ10.100  
;gpnam7: SMSQ10.100  
;gpnam8: SMSQ10.100
```

BRUKER Pulse Programs for the CN-J-psHSQC experiment.

```
; CN-J-psHSQC.2

prosol relations=<triple>

#include <Avance.incl>
#include <Grad.incl>
#include <Delay.incl>
#include <De.incl>

#define ps

#ifdef ps
dwellmode explicit
"d2=aq/2*12"
#else
#endif

"p2=p1*2"
"p4=p3*2"
"p22=p21*2"
"d4=1s/(cnst2*4)"
"d11=30m"
"d12=20u"
"d26=1s/(cnst4*4)"
"d24=d4/2"

"d0=3u"
"d28=3u"
"in0=inf1/2"
"in28=in20/2-in0"

"DELTA=d4-p8/2"
"DELTA1=d26-d4-p8/2"
"DELTA2=p4+p16+d16+4u"
"DELTA3=p16+d16+4u"
"DELTA4=d4+p21+p1-p2-p22-p19-d16"
"DELTA5=d26-d4-p2-p22+p3-p4-(p21*0.27)"
"DELTA6=(p21*0.27)-(p1*0.27)"
"DELTA7=d26-d4"
"DELTA8=p16+d16+8u"
"DELTA9=d4-p19-d16"
"DELTA10=d4-p4/2-p19-d16"
"DELTA11=d26-p19-d16"
"DELTA12=d26*2-larger(p2,p22)/2"
"DELTA13=d4*2-p8/2"
"DELTA14=d26*2-d4*2-p8/2-larger(p2,p22)/2"
"DELTA15=d26-p16-d16-4u"
"TAU=larger(p4,p22)"

"spoff13=0"

1 ze
  d11 p112:f2 p116:f3
2 d1 do:f2 do:f3
```

```

3 d12 p12:f2 p13:f3

(p1 ph1)
d0
;BIRD

(p1 ph1)
DELTA13 p10:f2
(p8:sp13 ph1):f2
DELTA14
(center (p2 ph2) (p22 ph1):f3 )
DELTA12
(p1 ph17)

;BIRD finish
d0
(p1 ph2)

4u UNBLKGRAD
p16:gp1
d16 p12:f2

(p21 ph8):f3
4u
p16:gp2*EA
d16
DELTA2
(center (p3 ph3):f2 (p22 ph1):f3)
4u
p16:gp3*EA
d16
(p4 ph4):f2
DELTA3

(ralign (p1 ph1) (p3 ph4):f2 (p21 ph10):f3)
DELTA p10:f2
(p8:sp13 ph1):f2
DELTA1
(center (p2 ph1) (p22 ph1):f3 )
DELTA15
4u
p16:gp4
d16 p112:f2 p116:f3

;initial chunk
#ifdef ps

4u cpd2:f2 cpd3:f3
ACQ_START(ph30,ph31)
0.1u REC_UNBLK
0.05u DWL_CLK_ON
d2*0.5
0.05u DWL_CLK_OFF
0.1u REC_BLK

;BIRD

```



```

10u do:f2 do:f3
p29:gp7
d16
TAU
(p1 ph1)
DELTA13 p10:f2 p13:f3
(p8:sp13 ph1):f2
DELTA14
(center (p2 ph2) (p22 ph1):f3 )
DELTA12 p12:f2
(p1 ph17)
(center (p4 ph1):f2 (p22 ph1):f3)
d16 p112:f2 p116:f3
p29:gp7
10u
;chem. shift refoc.
10u
p29:gp8
d16
4u
(p2 ph1):f1
4u
d16
p29:gp8
10u cpd2:f2 cpd3:f3

5 0.1u REC_UNBLK
0.05u DWL_CLK_ON
d2
0.05u DWL_CLK_OFF
0.1u REC_BLK

;BIRD
10u do:f2 do:f3
p29:gp7
d16
TAU
(p1 ph1)
DELTA13 p10:f2 p13:f3
(p8:sp13 ph1):f2
DELTA14
(center (p2 ph2) (p22 ph1):f3 )
DELTA12 p12:f2
(p1 ph17)
(center (p4 ph1):f2 (p22 ph1):f3)
d16 p112:f2 p116:f3
p29:gp7
10u
;chem. shift refoc.
10u
p29:gp8
d16
4u
(p2 ph1):f1
4u
d16

```

```

    p29:gp8
    10u cpd2:f2 cpd3:f3
lo to 5 times l2

    0.1u REC_UNBLK
    0.05u DWL_CLK_ON
    d2*10
    0.05u DWL_CLK_OFF
    0.1u REC_BLK
    rcyc=2

#else
go=2 ph31 cpd2:f2 cpd3:f3
#endif
    d1 do:f2 do:f3 mc #0 to 2
    FlEA(calgrad(EA) & calph(ph5, +180) & calph(ph11, +180),
caldel(d0, +in0) & calph(ph3, +180) & calph(ph6, +180) &
calph(ph7, +180) & calph(ph8, +180) & calph(ph31, +180))
exit

ph1=0
ph2=1
ph3=0 2
ph4=0 0 2 2
ph5=3 3 1 1
ph6=0
ph7=0
ph8=2 0
ph10=0 0 2 2
ph11=1 1 3 3

ph17=2

ph30=0
ph31=0 2 2 0

;p11 : f1 channel - power level for pulse (default)
;p12 : f2 channel - power level for pulse (default)
;p13 : f3 channel - power level for pulse (default)
;p112: f2 channel - power level for CPD/BB decoupling
;p116: f3 channel - power level for CPD/BB decoupling
;sp13: f2 channel - shaped pulse 180 degree (adiabatic)
;p1 : f1 channel - 90 degree high power pulse
;p2 : f1 channel - 180 degree high power pulse
;p3 : f2 channel - 90 degree high power pulse
;p4 : f2 channel - 180 degree high power pulse
;p8 : f2 channel - 180 degree shaped pulse for inversion
(adiabatic)
;p16: homospoil/gradient pulse
;p19: gradient pulse 2 [500
uSec]
;p21: f3 channel - 90 degree high power pulse
;p22: f3 channel - 180 degree high power pulse
;p28: f1 channel - trim pulse [1 msec]

```

```

;d0 : incremented delay [3 usec]
;d1 : relaxation delay; 1-5 * T1
;d4 : 1/(4J(CH))
;d11: delay for disk I/O [30 msec]
;d12: delay for power switching [20 usec]
;d16: delay for homospoil/gradient recovery
;d24: = d4 / 2
;d26: 1/(4J(NH))
;d28: incremented delay [3 usec]
;cnst2: = J(CH)
;cnst4: = J(NH)
;inf1: 1/SW(C) = 2 * DW(C)
;in0: 1/(2 * SW(C)) = DW(C)
;nd0: 2
;in20: 1/SW(N) = 2 * DW(N)
;in28: in20/2 - in0
;NS: 4 * n
;DS: >= 16
;td1: number of experiments
;FnMODE: echo-antiecho
;cpd2: decoupling according to sequence defined by cpdprg2
;cpd3: decoupling according to sequence defined by cpdprg3
;pcpd2: f2 channel - 90 degree pulse for decoupling sequence
;pcpd3: f3 channel - 90 degree pulse for decoupling sequence

;use gradient ratio: gp 1 : gp 2 : gp 3 : gp 4 : gp 7 : gp
8
; 80 : -47.63 : 32.37 : 8.14 : 13 :
17

;for z-only gradients:
;gpz1: 80%
;gpz2: -47.63%
;gpz3: 32.37%
;gpz4: 8.14%
;gpz7: 13%
;gpz8: 17%

;use gradient files:
;gpnam1: SMSQ10.100
;gpnam2: SMSQ10.100
;gpnam3: SMSQ10.100
;gpnam4: SMSQ10.100
;gpnam7: SMSQ10.100
;gpnam8: SMSQ10.100

```

4.5. Publication 5: LR-selHSQMBC: Simultaneous Detection and Quantification of Very Weak Long-Range Heteronuclear NMR Correlations.

4.5.1. Introduction

In this article, the concepts of time-sharing and detection of ultra-long-range heteronuclear correlations are combined in a single NMR experiment. The TS version of the selHSQMBC affords the possibility to detect and measure simultaneously J_{CH} and J_{NH} in a single spectrum. Direct measurements in simple multiplets or the IPAP approach in more complex coupling patterns are both feasible. On the other hand, the re-optimization of the interpulse delay in this novel TS-selHSQMBC to smaller nJ values offers the possibility to detect and quantify ultra-long-range heteronuclear correlations, for both carbon and nitrogen. In addition, the compatibility of an extended TOCSY transfer also allows the determination of the sign of heteronuclear couplings over four, five and six bonds away with excellent accuracy.

LR-selHSQMBC: Simultaneous Detection and Quantification of Very Weak Long-Range Heteronuclear NMR Correlations

Kumar Motiram-Corral,^[a] Alexandre A. Souza,^[b] Josep Saurí,^[c] Pau Nolis,^[a] and Teodor Parella*^[a]

The optimum detection and accurate measurement of longer-range (4J and higher) heteronuclear NMR correlations is described. The magnitude and/or the sign of a wide range of large and small long-range couplings can be simultaneously determined for protonated and non-protonated ^{13}C and ^{15}N nuclei using the LR-selHSQMBC experiment.

Two-dimensional HMBC and HSQMBC experiments are fundamental NMR techniques to trace out through-bond long-range proton-carbon ($^nJ_{\text{CH}}$) connectivities in structural elucidation studies of small and medium-sized molecules.^[1–3] The interpulse evolution delays in these experiments are routinely optimized to $J^{\text{opt}} = 6\text{--}10\text{ Hz}$ to observe most of the short-range two-bond and three-bond heteronuclear correlations. A simple strategy to try detecting weaker $^nJ_{\text{CH}}$ correlations is to fix these delays to longer values, for instance to $J^{\text{opt}} = 2\text{--}4\text{ Hz}$. Under these conditions, the success of the method is limited to proton signals having long T_2 relaxation times. Besides, the evolution of J_{HH} during these long periods can introduce unwanted phase and signal intensity modulations, affording complex multiplets that show mixtures of In-Phase (IP) and Anti-Phase (AP) contributions. The resulting phase anomalies complicate the analysis of distorted cross-peaks; partial or complete signal cancellation can arise due to the AP character of both $^nJ_{\text{CH}}$ and J_{HH} splittings. The use of refocused versions of these experiments has been reported to improve the observation of IP magnetization components that can be detected under heteronuclear decoupling. Recently, a comparative study focusing on the effects of J_{HH} modulation in D-HMBC^[4] versus LR-HSQMBC^[5–6] pulse schemes concluded that more cross-peaks are expected to show up in an LR-HSQMBC spectrum compared with a D-HMBC spectrum.^[7–8] In particular, the use of ultra-long-

range correlations observed in LR-HSQMBC spectra has shown its usefulness in computer-assisted structure elucidation (CASE) analysis of proton-deficient natural products.^[9] On the other hand, HSQMBC-TOCSY^[10] and ADEQUATE experiments^[11–12] are alternative NMR tools to detect such longer-range correlations, although the limitations in sensitivity due to additional relaxation effects or the required ^{13}C - ^{13}C selection at natural abundance are challenges to overcome.

The advantages of using a ^1H frequency-selective version of the HSQMBC experiment (selHSQMBC) that has been previously reported to measure $^nJ_{\text{CH}}$ coupling constants from pure absorption IP coupling J patterns is analyzed herein.^[13–19] We want to explore experimental solutions in which only the intensity modulation of $^nJ_{\text{CH}}$ exclusively survives, while at the same time unwanted AP contributions due to both $^nJ_{\text{CH}}$ and J_{HH} phase modulations are efficiently suppressed. We intend to evaluate the performance of the selHSQMBC experiment for observing cross-peaks corresponding to very small $^nJ_{\text{CH}}$ coupling values, to measure them robustly, simultaneously determining their positive/negative sign.^[20]

Figure 1 shows the time-shared ^1H - ^{13}C and ^1H - ^{15}N version of the selHSQMBC experiment used in this study, which allows the simultaneous determination of both proton-carbon and proton-nitrogen coupling constants.^[21–26] The pulse sequence follows a similar coherence transfer pathway to the original selHSQMBC

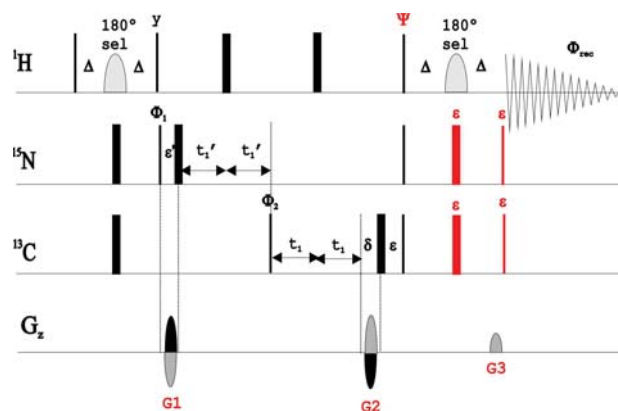


Figure 1. Pulse scheme of the $^{13}\text{C}/^{15}\text{N}$ -selHSQMBC experiment. The interpulse delay is set to $\Delta = 1/(4^*J_{\text{HH}})$. The selective 180° ^1H is applied to the selected proton resonances. Editing for ^{13}C (positive cross-peaks) and ^{15}N (negative cross-peaks) is achieved from a basic two-step phase cycle: $\phi_1 = x, -x$, $\phi_2 = -x, x$ and $\phi_{\text{rec}} = x, -x$. IP/AP datasets can be collected using $\Psi = y/x$ and $\epsilon = \text{on/off}$, respectively. Simultaneous ^{13}C and ^{15}N coherence selection is achieved by setting the relative G1:G2:G3 gradient strengths to a $-47.63:32.37:8.14$ ratio. Other sequence details can be found in the experimental section.

[a] K. Motiram-Corral, Dr. P. Nolis, Dr. T. Parella
Servei de Resonància Magnètica Nuclear
Universitat Autònoma de Barcelona
E-08193 Bellaterra, Barcelona (Catalonia) Spain
E-mail: Teodor.parella@uab.cat

[b] Dr. A. A. Souza
Departamento de Química
Universidade Federal de Piauí
64049-550 Teresina, PI, Brazil

[c] Dr. J. Saurí
Structure Elucidation Group
Analytical Research & Development, Merck & Co., Inc.
33 Av. Louis Pasteur, Boston, MA, 02215, USA

Supporting information for this article is available on the WWW under <https://doi.org/10.1002/cphc.201901142>

scheme (see Figure S1A in the Supporting Information) where simultaneous pulses on both ^{13}C and ^{15}N channels are applied (triple channel configuration is required) whereas a redistribution of the indirect t_1 and $t_{1'}$ periods monitor ^{13}C and ^{15}N chemical shift evolution. Because the size of $^nJ_{\text{CH}}$ and $^nJ_{\text{NH}}$ are of the same magnitude (0–15 Hz), the defocusing and refocusing effects during the Δ periods act at the same time and in an independent way for both coupling pathways. The central selective 180° ^1H pulses applied to selected resonances avoids J_{HH} modulation during the echo periods ($2\Delta = 1/(2^*J^{\text{opt}})$) and the 90° $^{13}\text{C}/^{15}\text{N}$ purge pulses before data acquisition remove any residual AP $^nJ_{\text{XH}}$ contribution, providing pure IP cross-peaks irrespective the J^{opt} utilized for the experimental $^nJ_{\text{XH}}$ values.

The implementation of time-sharing into selHSQMBC achieves at least a 50% reduction of spectrometer time because both C- and N-selHSQMBC datasets are collected jointly without sensitivity losses compared to the traditional sequential acquisition mode (Figure S2). ^{13}C and ^{15}N cross-peaks are distinguished according to their relative opposite IP phases, which are defined by the phase of the 90° pulses preceding the t_1 and t_1' evolution periods (ϕ_1 and ϕ_2 , respectively). To start, we have chosen a simple model spin system to evaluate the performance of selHSQMBC. As a proof of concept, we chose the H2 proton of 1,2,4-triazolo[1,5-a]pyrimidine (1) that resonates at 8.51 ppm as a well-isolated singlet in the conventional ^1H NMR spectrum. Four different cross-peaks are observed as resolved doublets at the detected F2 frequency of H2 in selHSQMBC with $J^{\text{opt}} = 8$ Hz (Figure 2A). The simplicity of the IP doublet pattern for all cross-peaks and the excellent FID resolution achieved at the F2 dimension allows a direct and accurate J extraction for each cross-peak. Two negative (red) IP peaks are observed corresponding to $^2J_{\text{N1-H2}}$ (11.9 Hz) and $^3J_{\text{N7a-H2}}$ (5.4 Hz), respectively, whereas the two positive (black) cross-peaks corresponds to the large $^1J_{\text{C2-H2}}$ (207.7 Hz) and the vicinal $^3J_{\text{C3a-H2}}$ (10.3 Hz) correlations. The same selHSQMBC experiment optimized to a shorter value, $J^{\text{opt}} = 3$ Hz (referred to as LR-selHSQMBC), affords complementary information, as shown for the three new cross-peaks observed in Figure 2B: one negative doublet corresponding to $^2J_{\text{N3-H2}}$ (15.7 Hz) and two non-resolved singlets corresponding to the remote $^4J_{\text{C7-H2}}$ and $^5J_{\text{C6-H2}}$ connectivities (smaller than line-widths, < 2 Hz). Signal intensity in selHSQMBC experiments depends exclusively on $\sin^2(\pi J_{\text{XH}} 2\Delta) \cdot \exp(-4\Delta/T_2)$, so null points can be accidentally reached for couplings near to $\kappa \cdot J^{\text{opt}}$ ($\kappa = 0, 2, 4, \dots$). This explains why $^2J_{\text{N3-H2}}$ of 15.6 Hz was not observed when $J^{\text{opt}} = 8$ Hz and NH cross-peaks corresponding to couplings around 6 and 12 Hz are practically not detected when $J^{\text{opt}} = 3$ Hz.

The IPAP strategy is recommended for the analysis of complex multiplets and for the measurement of small J_{KH} values. Two complementary IP ($\Psi=\text{y}$ and $\epsilon=\text{on}$) and AP ($\Psi=\text{x}$ and $\epsilon=\text{off}$) datasets are collected using the pulse scheme of Figure 1 and co-processed (IP \pm AP) to afford separate spin-selected α/β spectra. The relative signal displacement along the F2 dimension affords the extraction of coupling values, even smaller than the linewidth (for instance, 1.4 Hz is measured for $^4J_{\text{C7-H2}}$ and 1.3 Hz for $^5J_{\text{C6-H2}}$) (Figure 2C). The theoretical signal intensity dependence for IP and AP datasets as a function of J^{opt}

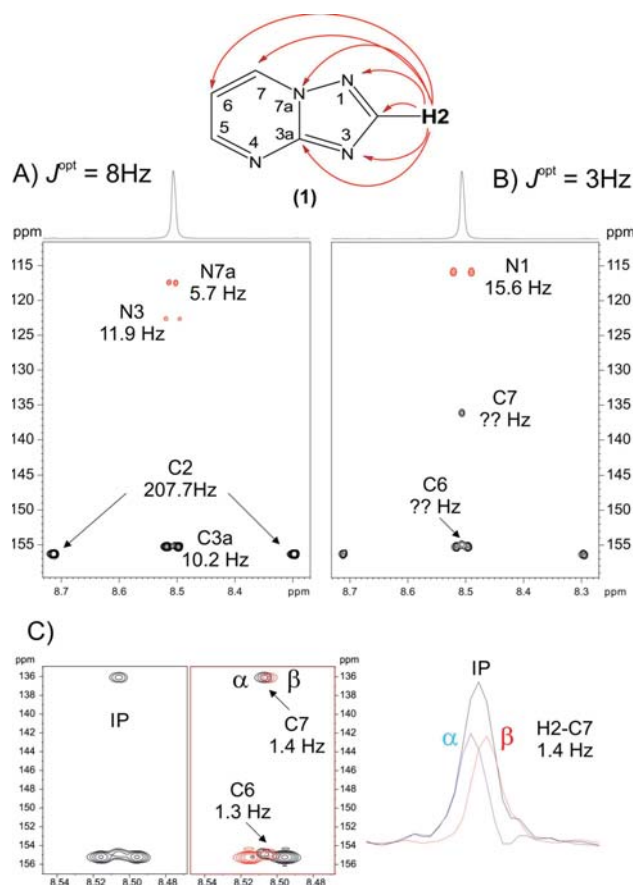


Figure 2. A) 8-Hz selHSQMBC and B) 3-Hz LR-selHSQMBC spectra of 1,2,4-triazolo[1,5-a]pyrimidine (**1**) after selective refocusing of the H-2 proton with a 10 ms Gaussian-shaped 180° ^1H pulse. C) Expansion showing the performance of the IPAP strategy to measure the non-resolved four-bond H2-C7 coupling of 1.4 Hz.

versus $^nJ_{\text{CH}}$ are shown in Figure S3, whereas the percentage of cross-talk in IPAP is defined by $[\sin(\pi J_{\text{XH}}2\Delta) - \sin^2(\pi J_{\text{XH}}2\Delta)] / [\sin(\pi J_{\text{XH}}2\Delta) + \sin^2(\pi J_{\text{XH}}2\Delta)]$.

Although selHSQMBC is a non-broadband, frequency-selective NMR experiment, its success is not limited to a single-frequency excitation. One experiment can cover different proton signals by using region-selective excitation, frequency-modulated pulses, extended TOCSY transfer or time-efficient, sensitivity-improved Hadamard encoding. Figure 3A shows the 8-Hz optimized selHSQMBC spectrum after simultaneous selective refocusing of the two resonances in close spectral proximity H2 and H8 protons of 1,7-phenanthroline (**2**). Both H2 and H8 signals show a clear double-doublet J_{HH} coupling pattern in the conventional ^1H spectrum. Because these protons are not mutually coupled, there is no interference of $J_{\text{H2-H8}}$ evolution in selHSQMBC cross-peaks in the form of phase distortion. The large $^1J_{\text{CH}}$, as well as $^2J_{\text{CH}}$, $^3J_{\text{CH}}$ and $^2J_{\text{NH}}$ connectivities, are observed when $J^{\text{opt}}=8\text{ Hz}$. This is an illustrative example showing how in simple multiplets, the size of $^nJ_{\text{CH}}$ and $^nJ_{\text{NH}}$ in the order of 5–12 Hz can be determined directly from the additional splitting or the multiplet widths observed in each F2 cross-peak. Additional cross-peaks corresponding to remote

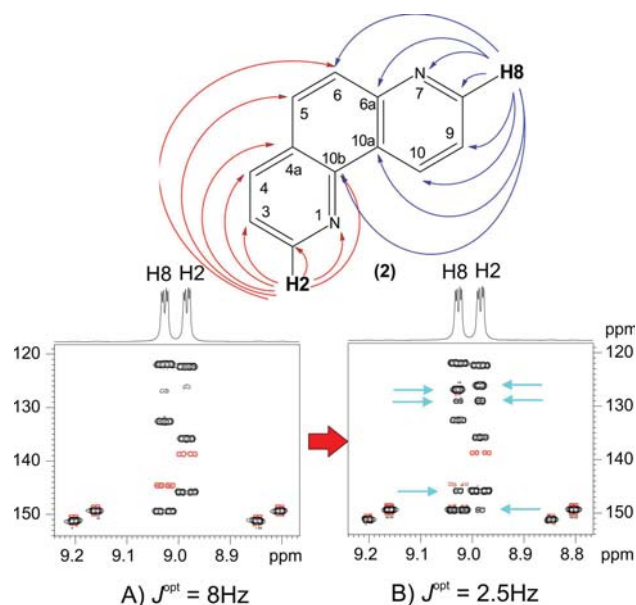


Figure 3. Comparison of A) 8-Hz selHSQMBC versus B) 2.5-Hz LR-selHSQMBC spectra after selective refocusing of both H2/H8 protons in **2**. Positive (black) and negative (red) IP cross-peaks represent ^{13}C and ^{15}N , respectively. The arrows in Figure 3B stand for the new cross-peaks observed in the LR-selHSQMBC spectrum. The coupling value of each cross-peak can be determined as shown in Figure 4.

range $^4J_{\text{CH}}$ and $^5J_{\text{CH}}$ connectivities are visualised when $J^{\text{opt}} = 2.5$ Hz (Figure 3B). Figure 4 shows the excellent performance of the IPAP strategy to obtain a complete range of couplings, including measurements of small values below 1.5–2 Hz.

The complementarity of LR-selHSQMBC versus selHSQMBC is strongly supported by the major number of couplings able to

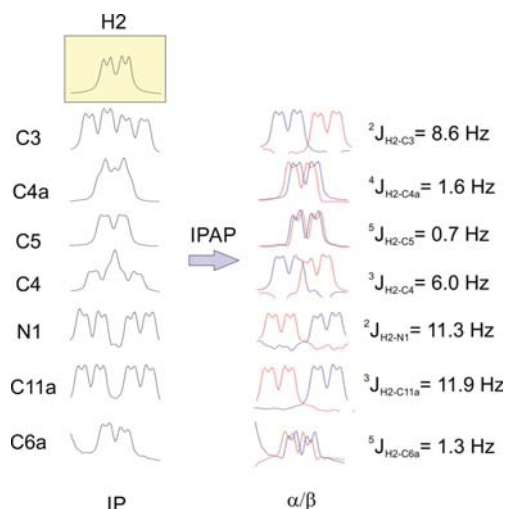


Figure 4. 1D slices showing (left) IP and (right) IPAP multiplets corresponding to the H2 cross-peaks along F2 in Figure 3B. The magnitude of the active coupling can be extracted directly from the well-resolved IP cross-peaks or from the relative displacement between α/β multiplets measured along F2. Note the minimum cross-talk interference for a wide range of coupling values. At the top, the reference doublet multiplicity of H2 extracted from the conventional ^1H spectrum.

be observed and measured. Thus, while only six correlations are observed in the 8-Hz selHSQMBC spectrum (Figure 5A), up to twelve connectivities are detected in the complementary 2.5-Hz LR-selHSQMBC (Figure 5B), they all provide couplings exclusively from the two selected H3/H9 signals of **2**. The features of LR-selHSQMBC can be further enhanced by using an extended TOCSY transfer. The resulting LR-selHSQMBC-TOCSY enables the measurement of $^nJ_{\text{CH}}$ and $^nJ_{\text{NH}}$ to many other protons, including those where selective refocusing is not feasible (for instance, overlapped signals) or those having coupling values near 0 Hz. Thus, the 8-Hz selHSQMBC-TOCSY (Figure 5C) provides eighteen cross-peaks whereas forty-one correlations are observed in the complementary 2.5-Hz LR-selHSQMBC-TOCSY (Figure 5D), they all providing couplings from the two chosen protons as well as for the relayed H2/H4 and H7/H8 protons. Theoretically, the intensity of a relayed ultra-long-range C–H1 cross-peak in a C (H1)–H2 three-spin system does not depend on $\sin^2(\pi J_{\text{C-H2}}2\Delta)$ but the efficiency of the TOCSY transfer as a function of $\sin^2(\pi J_{\text{C-H1}}2\Delta) \cos(\pi J_{\text{H1-H2}}\tau)$. Thus, selHSQMBC-TOCSY allows the accurate measurement of couplings smaller than the linewidth as well as of the corresponding sign if IPAP is applied. In Figure 5E it is

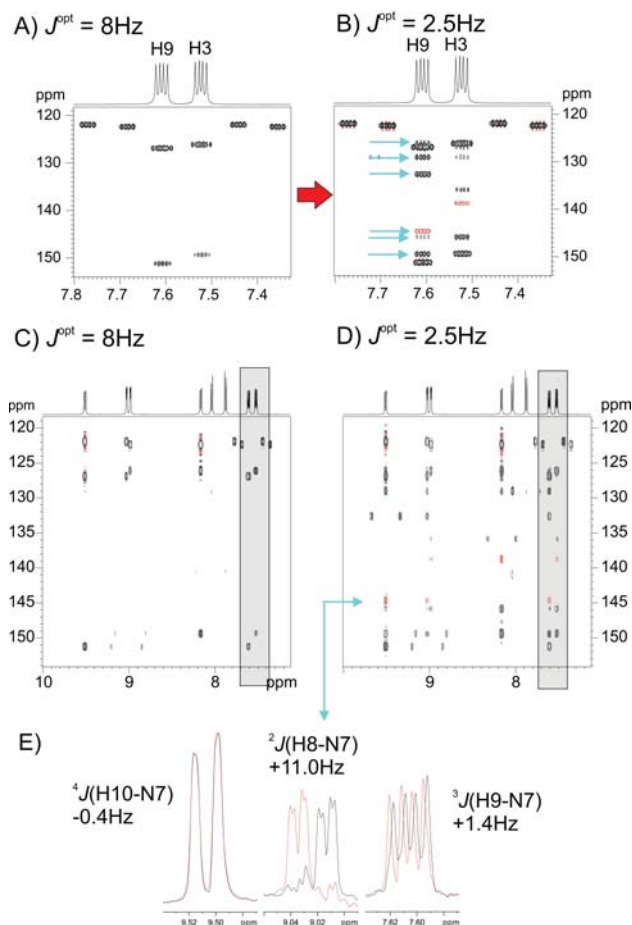


Figure 5. A) 8-Hz selHSQMBC versus B) 2.5-Hz LR-selHSQMBC of H3/H9 protons of **2** resonating at 7.56 ppm; Related C) 8-Hz selHSQMBC-TOCSY versus D) 2.5-Hz LR-selHSQMBC-TOCSY spectra using an extended TOCSY mixing time of 40 ms. E) Coupling sizes and signs extracted from the analysis of the 1D α/β slices taken at the N7 nitrogen frequency in spectrum 5D.

shown how J values for the N7 nitrogen from 0.4 to 11.0 Hz can be measured with accuracy as well as their signs.

In summary, it has been shown that the utility of time-sharing NMR spectroscopy combined with the proper delay optimization in selHSQMBC allows the detection and accurate measurement of a wide range of couplings (1J , 2J , 3J , 4J and 5J) for both protonated and non-protonated ^{13}C and ^{15}N hetero-nuclei. Several methods are feasible for efficient J extraction: direct measurement or multiplet width analysis of IP data, IPAP data combination and TOCSY extension. The robustness of the IPAP strategy in selHSQMBC experiments optimized at 2.5–3 Hz has been demonstrated for the measurement of J smaller than the linewidth and for determining the positive/negative sign in related LR-selHSQMBC-TOCSY experiments. In practice, the execution of the selHSQMBC experiment with J^{opt} of 8 and 2–3 Hz is therefore recommended to avoid missed cross-peaks due to the null-point condition.

Acknowledgements

Financial support for this research provided by Spanish MINECO (project PGC2018-095808-B-I00) is gratefully acknowledged. A.A.S. gratefully acknowledges support from the Brazilian agency CAPES (BEX 5382/15-7) and K.M.C. from the Spanish MINECO (BES-2016-078903). We also thank the Servei de Ressonància Magnètica Nuclear, Universitat Autònoma de Barcelona, for allocating instrument time to this project.

Keywords: heteronuclear coupling constants • long-range heteronuclear connectivities • NMR spectroscopy • proton-deficient molecules structure elucidation • time-sharing NMR

[1] J. Furrer, *Concepts Magn. Reson. Part A* **2012**, 40A, 101–127.

[2] J. Furrer, *Concepts Magn. Reson. Part A* **2012**, 40A, 146–169.

[3] J. Furrer, *Concepts Magn. Reson. Part A* **2015**, 43, 177–206.

[4] K. Furihata, H. Seto, *Tetrahedron Lett.* **1995**, 36, 2817–2820.

[5] R. T. Williamson, A. V. Buevich, G. E. Martin, T. Parella, *J. Org. Chem.* **2014**, 79, 3887–3894.

[6] K. A. Blinov, A. V. Buevich, R. T. Williamson, G. E. Martin, *Org. Biomol. Chem.* **2014**, 12, 9505–9509.

[7] P. Bigler, J. Furrer, *Magn. Reson. Chem.* **2018**, 56, 1101–1116.

[8] P. Bigler, J. Furrer, *Magn. Reson. Chem.* **2019**, 57, 129–143.

[9] J. Saurí, S. Chan, A. Buevich, K. Gustafson, R. Williamson, G. Martin, *Planta Med.* **2015**, 81, PQ32.

[10] J. Saurí, N. Marcó, R. T. Williamson, G. E. Martin, T. Parella, *J. Magn. Reson. J. Magn. Reson.* **2015**, 258, 25–32.

[11] J. Saurí, I. E. Ndukwe, M. Reibarkh, Y. Liu, R. T. Williamson, G. E. Martin, *Annu. Reports NMR Spectrosc.* **2019**, 98, 1–56.

[12] J. Saurí, W. Bermel, A. V. Buevich, E. C. Sherer, L. A. Joyce, M. H. M. Sharaf, P. L. Schiff, T. Parella, R. T. Williamson, G. E. Martin *Angew. Chemie Int. Ed.* **2015**, 54, 10160–10164.

[13] J. Saurí, P. Nolis, T. Parella, *J. Magn. Reson.* **2013**, 236, 66–69.

[14] J. Saurí, E. Sistaré, R. T. Williamson, G. E. Martin, T. Parella, *J. Magn. Reson.* **2015**, 252, 170–175.

[15] J. Saurí, P. Nolis, T. Parella, *Magn. Reson. Chem.* **2015**, 53, 427–432.

[16] J. F. Espinosa, P. Vidal, T. Parella, S. Gil, *Magn. Reson. Chem.* **2011**, 49, 502–507.

[17] J. Saurí, M. Frédérich, A. T. Tchinda, T. Parella, R. T. Williamson, G. E. Martin, *J. Nat. Prod.* **2015**, 78, 2236–2241.

[18] L. Castañar, J. Saurí, P. Nolis, A. Virgili, T. Parella, *J. Magn. Reson.* **2014**, 238, 63–69.

[19] J. Saurí, T. Parella, J. F. Espinosa, *Org. Biomol. Chem.* **2013**, 11, 4473–8.

[20] T. Parella, J. F. Espinosa, *Prog. Nucl. Magn. Reson. Spectrosc.* **2013**, 73, 17–55.

[21] M. Sattler, M. Maurer, J. Schleucher, C. Griesinger, *J. Biomol. NMR* **1995**, 5, 97–102.

[22] M. Pérez-Trujillo, P. Nolis, W. Bermel, T. Parella, *Magn. Reson. Chem.* **2007**, 45, 325–329.

[23] T. Parella, P. Nolis, *Concepts Magn. Reson. Part A* **2010**, 36, 1–23.

[24] P. Nolis, T. Parella, *J. Biomol. NMR* **2007**, 37, 65–77.

[25] P. Nolis, M. Pérez-Trujillo, T. Parella, *Angew. Chem. Int. Ed. Engl.* **2007**, 46, 7495–7497.

[26] P. Nolis, P. Miriam, T. Parella, *Magn. Reson. Chem.* **2006**, 44, 1031–1036.

Manuscript received: December 3, 2019

Revised manuscript received: January 10, 2020

Accepted manuscript online: January 17, 2020

Version of record online: January 22, 2020

LR-selHSQMBC: Simultaneous Detection and Quantification of Very Weak Long-Range Heteronuclear NMR Correlations

Kumar Motiram-Corral, Alexandre A. Souza, Josep Saurí, Pau Nolis, and Teodor Parella*

Experimental Section

All NMR spectra were recorded on a Bruker AVANCE spectrometer operating at 500.13 MHz for ^1H and equipped with a cryogenically cooled triple-resonance TCI $^1\text{H}/^{13}\text{C}/^{15}\text{N}$ probe. The temperature for all measurements was set to 298 K. The samples used were 25 mg of triazolo-pyrimidine (**1**) and 30 mg of 1,7-phenanthroline (**2**), both dissolved in 0.6 ml of CDCl_3 .

All spectra were recorded with proton 90° pulses of 8.0 μs and carbon 90° pulses of 15.0 μs . For broadband carbon inversion, 0.5 ms smoothed Chirp pulses sweeping over a frequency band of 60 kHz were used. The ^1H , ^{13}C , ^{15}N carriers were centred at 8.0 ppm, 135 ppm and 299 ppm, respectively. Gradient ratios were set-up as percentage of the absolute gradient strength of 53.5 G/cm. All gradients have a SINE.100 shape and their durations (δ in ms) and strengths (G/cm) are: $G1 = (1 \text{ ms}, -47.63)$, $G2 = (1 \text{ ms}, 32.37)$, $G3 = (1 \text{ ms}, 8.14)$.

SeIHSQMBC experiments were collected using 4 scans for each one of the 128 t_1 increments and the number of complex data points in t_2 was set to 4096. The maximum t_1 and t_1' times were 10.2 ms and 25.6 ms, respectively, that correspond to spectral widths of 25153 Hz and 10274 Hz for ^{13}C and ^{15}N , respectively. The inter-pulse delays were set to optimized to $1/(4 \cdot J)$; for instance, 30 ms for $J^{\text{opt}} = 8 \text{ Hz}$. The FID resolution in F2 was 0.7 Hz/pt. The experimental time was about 15-17 min, as a function of J^{opt} . SeIHSQMBC-TOCSY experiments were collected using the same conditions but with 16 scans per t_1/t_1' increment. The homonuclear TOCSY transfer was achieved by a 7 KHz DIPSI-2 pulse train of duration 40 ms. The experimental time of each dataset was about 1h. 10m., as a function of J^{opt} .

All experiments were acquired and processed using the echo/anti-echo protocol where the echo and anti-echo signals were collected separately by inverting the sign of gradients G1 and G2 together. Prior to Fourier-transformation of each set of data, zero filling to 1024 in ω_1 , 8K in ω_2 and a $\pi/2$ -shifted squared cosine window function (SINE, SSB: 2) was applied in both dimensions. Spectral digital resolution along the F2 dimension was 0.36 Hz/pt.

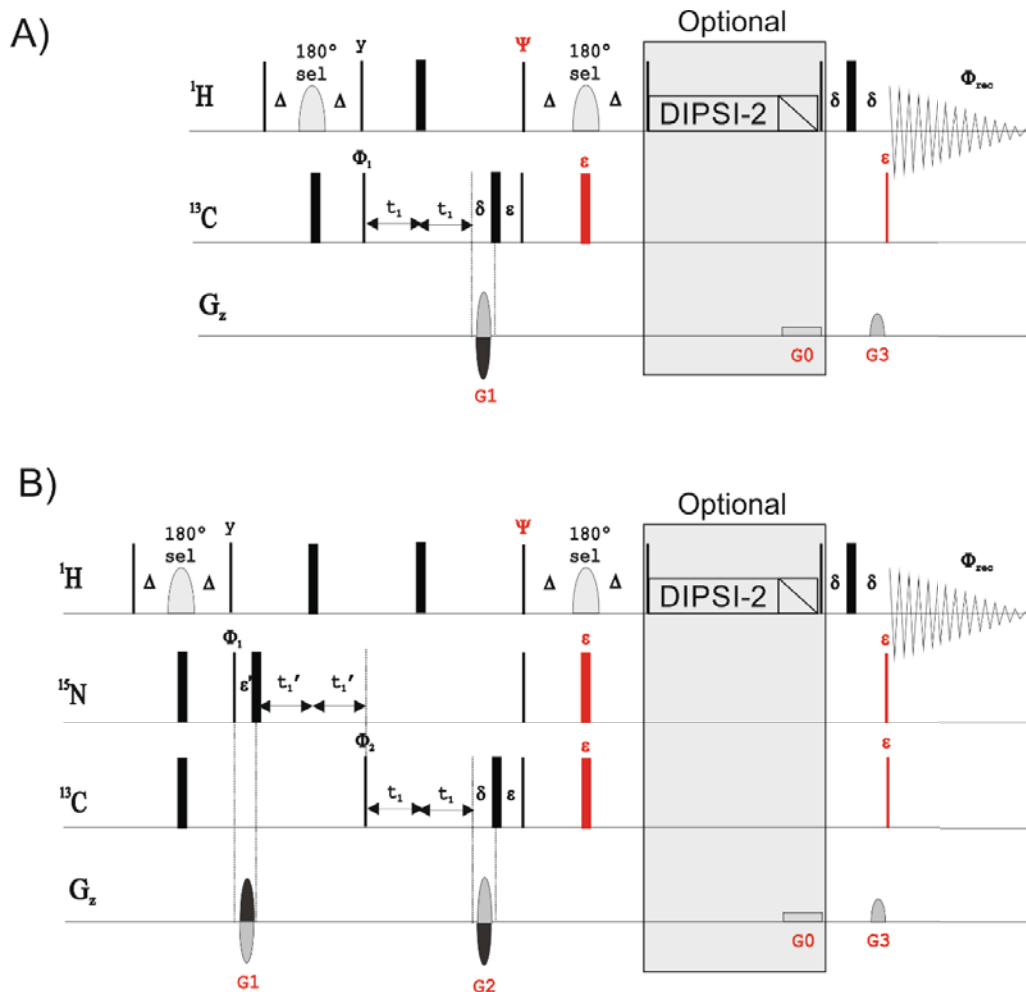


Figure S1: Pulse schemes of the A) conventional and B) time-shared selHSQMBC experiments. Optionally, a TOCSY transfer can be included to generate selHSQMBC-TOCSY spectra.^[17] Thin and thick bars represent 90° and 180° non-selective pulses and are applied along the x-axis unless otherwise stated. The frequency-selective 180 ¹H is applied to the selected proton resonance. ¹³C (positive cross-peaks) and ¹⁵N (negative cross-peaks) editing is achieved from a basic two-step phase cycle: $\phi_1=x,-x$, $\phi_2=-x,x$ and $\phi_{rec}=x,-x$; and quadrature in the F1 dimension was achieved applying an Echo/Anti-echo protocol. The delays ε and ε' compensate for evolution during the variable t_1 and t_1' periods and the time increments were set to $\Delta t_1=1/SW(C)$ and $\Delta t_1'=1/(SW(N)-1/SW(C))$. The inter-pulse delays are set to $\Delta=1/(4^n J(XH))$. For IPAP measurements, the different α,β -spin-state edited spectra were generated by addition/subtraction of the in-phase (IP: $\Psi=y$ and $\varepsilon=on$) and anti-phase (AP: $\Psi=x$ and $\varepsilon=off$) data collected separately.

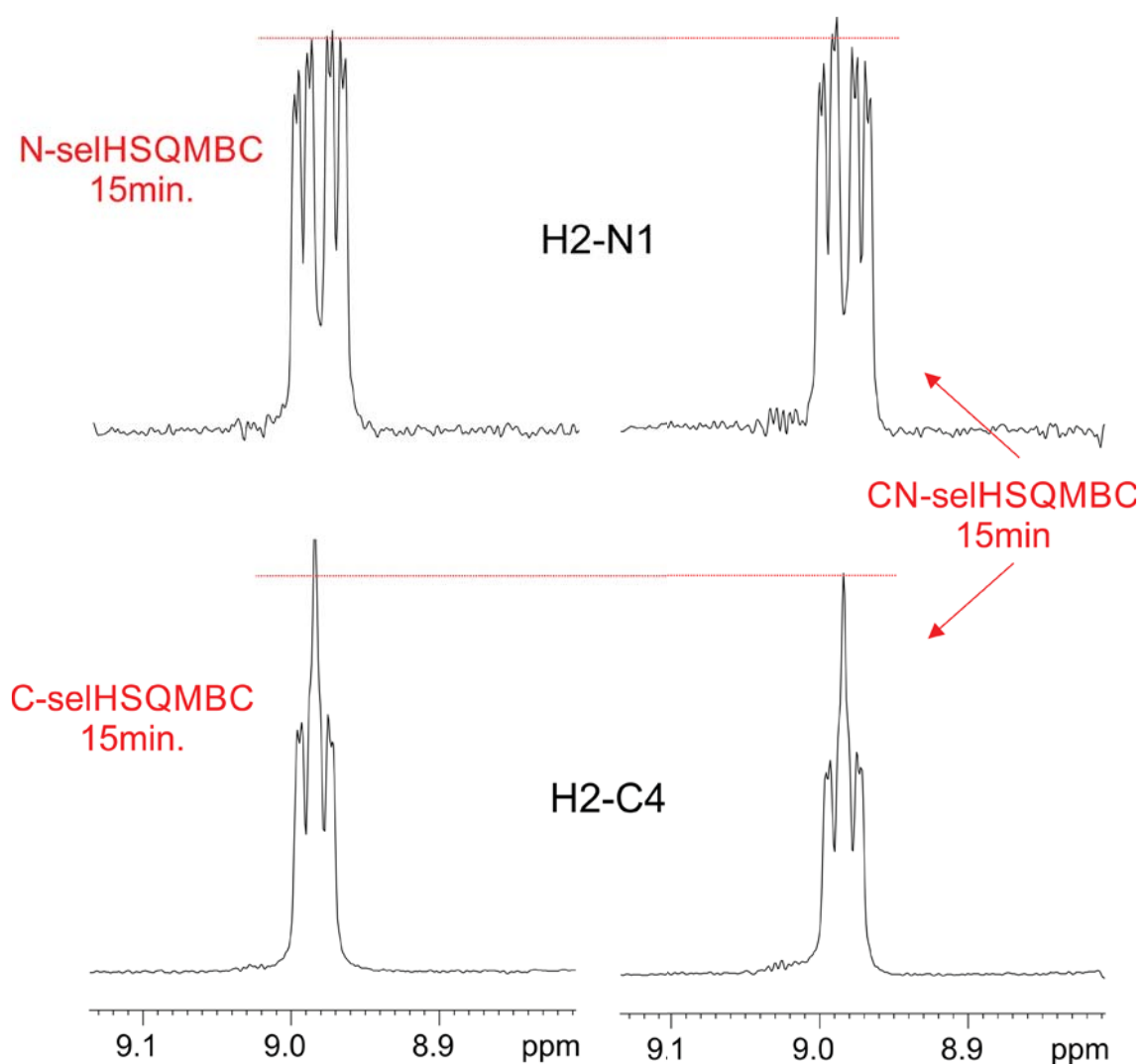
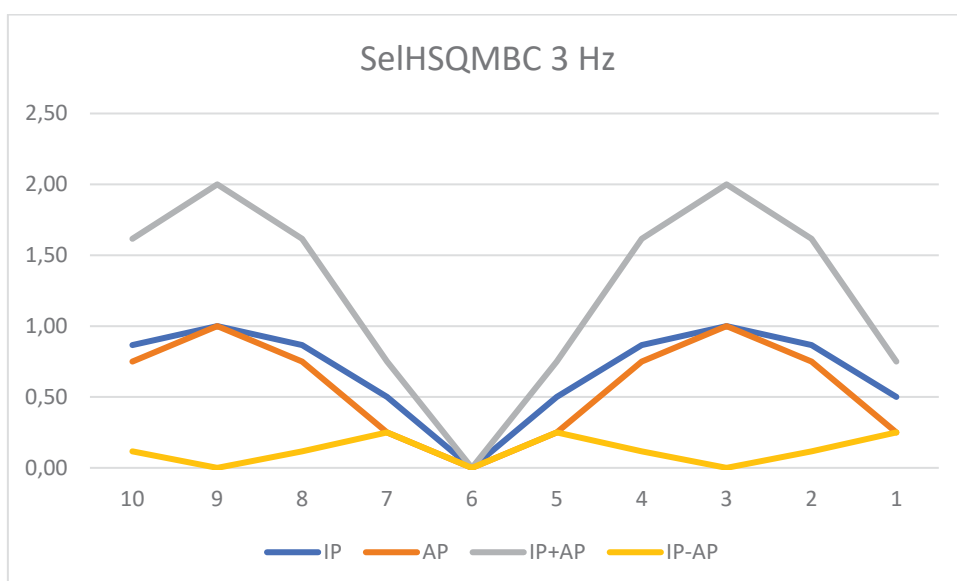
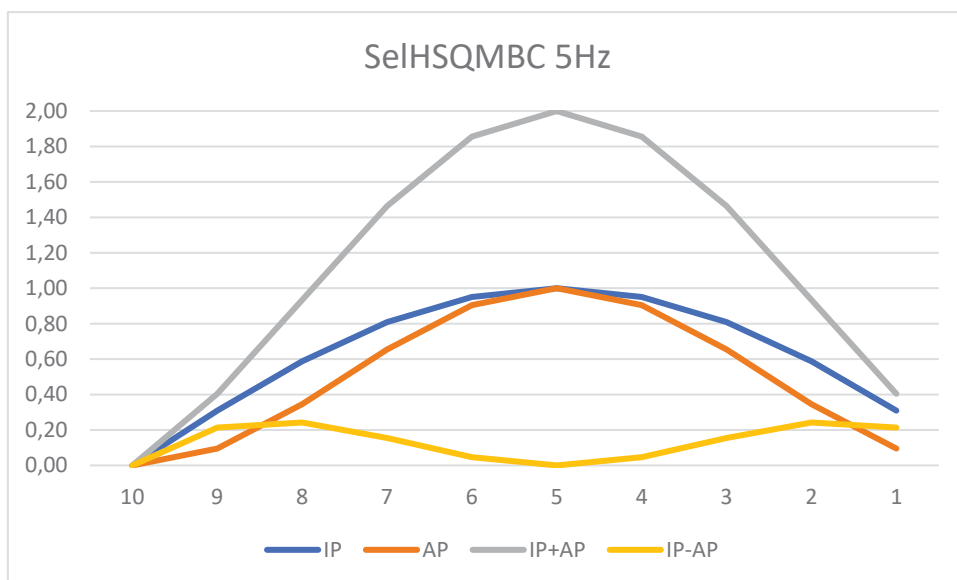
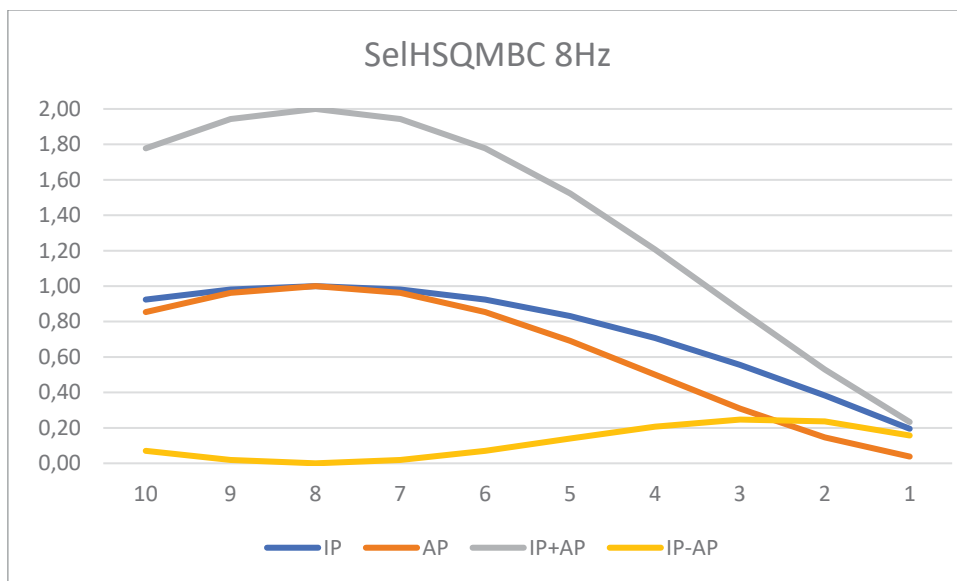


Figure S2: Relative sensitivity of the C- and N-selHSQMBC vs the time-shared CN-selHSQMBC experiment. (left) ^{15}N and ^{13}C cross-peaks corresponding to the two-bond H2-N1 and the three-bond H2-C4 correlations of (2), respectively, acquired separately using the corresponding selHSQMBC scheme. The experimental times were 15 min and 15 min for the N and C-selHSQMBC experiments. (right) the same projections obtained from a single CN-selHSQMBC acquired in 15 min. Note that SNR are of the same order, confirming the 50% save in spectrometer time of the TS experiment.



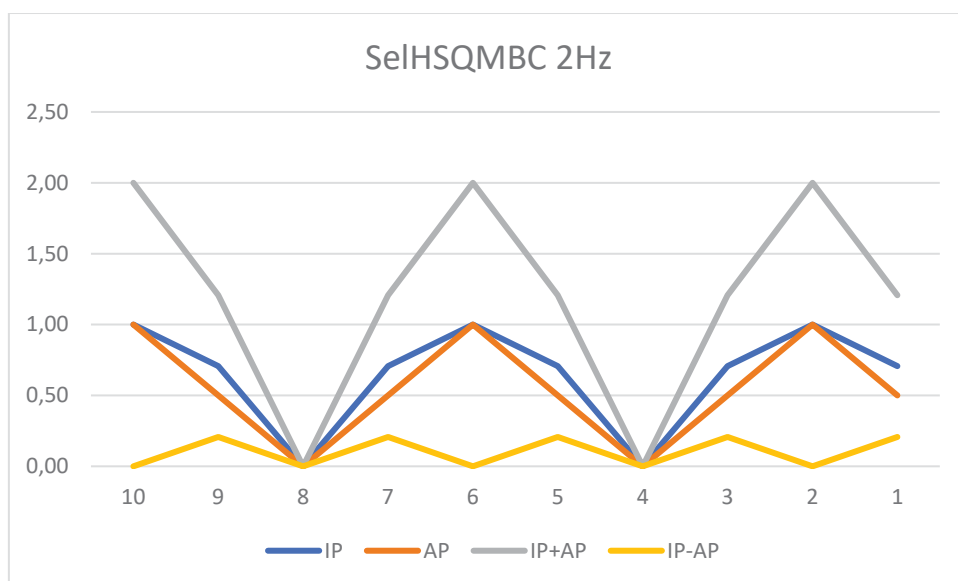


Figure S3. Theoretical signal intensity dependence (IP, AP, IP+AP and IP-AP) in selHSQMBC experiments optimized to 8 Hz, 5 Hz, 3 Hz and 2 Hz.

Pulse Program (TS 1.3)

```
;teo_selhsqmbcto_ts

prosol relations=<triple>

#include <Avance.incl>
#include <Grad.incl>
#include <Delay.incl>

"p2=p1*2"
"p4=p3*2"
"p22=p21*2"
"d0=3u"
"d11=30m"
"d12=20u"
"d26=1s/(cnst13*4)"

"d28=3u"
"in28=in20-in0"
"DELTA2=p16+d16+d28*2+p2+p3*2+p4+d0*4+p2*2+p1*6+16u"
"DELTA3=p16+d16+d0*2+p2+p1*2+6u"
"DELTA6=(p21*0.27)-(p1*0.27)"
"DELTA8=p16+d16+8u"
"DELTA=d26-p12/2-d12-50u"

"FACTOR1=(d9/(p6*115.112))/2+0.5"
"l1=FACTOR1*2"

1 ze
2 d12
  d1 p11:f1
3 d12 p12:f2 p13:f3
  (p1 ph1)
  50u UNBLKGRAD
  DELTA
  d12 p10:f2 p10:f1
  (center (p12:sp1 ph1) (p22 ph7):f3 (p8:sp13 ph6):f2)
  DELTA p12:f2 p11:f1
  50u
  d12

  p28 ph1
  (p1 ph2)

  (p21 ph8):f3

  4u
  p16:gp1*EA
  d16
  DELTA2
  (p22 ph8):f3
  d28
```

```

(p2 ph1)
d28
(p3 ph3):f2
d0
(p2 ph2)
d0
p16:gp2*EA
d16
(p4 ph1):f2
DELTA3

(center (p3 ph4):f2 (p21 ph10):f3 )
d13
(p1 ph2)

DELTA
50u
d12 p10:f2 p10:f1

if "cnst25==0"
{
  (center (p8:sp13 ph1):f2 (p12:sp1 ph1) (p22 ph1):f3 )
}
else
{
  (p12:sp1 ph1)
}

DELTA p12:f2 p11:f1
50u
d12

;starts tocsy

if "cnst24==0"

{
  (p1 ph1):f1

  d12 p110:f1

;begin DIPSI2
4 p6*3.556 ph22
  p6*4.556 ph24
  p6*3.222 ph22
  p6*3.167 ph24
  p6*0.333 ph22
  p6*2.722 ph24
  p6*4.167 ph22
  p6*2.944 ph24
  p6*4.111 ph22

  p6*3.556 ph24

```



```

p6*4.556 ph22
p6*3.222 ph24
p6*3.167 ph22
p6*0.333 ph24
p6*2.722 ph22
p6*4.167 ph24
p6*2.944 ph22
p6*4.111 ph24

p6*3.556 ph24
p6*4.556 ph22
p6*3.222 ph24
p6*3.167 ph22
p6*0.333 ph24
p6*2.722 ph22
p6*4.167 ph24
p6*2.944 ph22
p6*4.111 ph24

p6*3.556 ph22
p6*4.556 ph24
p6*3.222 ph22
p6*3.167 ph24
p6*0.333 ph22
p6*2.722 ph24
p6*4.167 ph22
p6*2.944 ph24
p6*4.111 ph22
lo to 4 times ll

;end DIPSI2

5u pl0:f1
300u gron0
pl3:sp4:f1 ph7
100u groff
dl6

4u pl1:f1
pl ph1
}
else
{
}
;end tocsy

DELTA8
(p2 ph1)
4u
pl6:gp3
dl6
4u BLKGRAD

if "cnst25==0"
{
(center (p3 ph1):f2 (p21 ph1):f3 )
}

```

```

        else
        {

        }

go=2 ph31
d12 mc #0 to 2
F1EA(igrad EA, id0 & id28 & ip3*2 & ip6*2 & ip7*2 & ip8*2 &
ip31*2)
exit

ph1=0
ph2=1
ph3=0 2
ph4=0
ph6=0
ph7=0
ph8=2 0
ph10=0
ph22=3
ph24=1
ph31=0 2

;p11 : f1 channel - power level for pulse (default)
;p12 : f2 channel - power level for pulse (default)
;p13 : f3 channel - power level for pulse (default)
;p112: f2 channel - power level for CPD/BB decoupling
;p116: f3 channel - power level for CPD/BB decoupling
;sp13: f2 channel - shaped pulse 180 degree (adiabatic)
;p1 : f1 channel - 90 degree high power pulse
;p2 : f1 channel - 180 degree high power pulse
;p3 : f2 channel - 90 degree high power pulse
;p4 : f2 channel - 180 degree high power pulse
;p8 : f2 channel - 180 degree shaped pulse for inversion
(adiabatic)
;p16: homospoil/gradient pulse
;p21: f3 channel - 90 degree high power pulse
;p22: f3 channel - 180 degree high power pulse
;p28: f1 channel - trim pulse [1 msec]
;id0 : incremented delay (F1 in 3D) [3 usec]
;d1 : relaxation delay; 1-5 * T1
;d11: delay for disk I/O [30 msec]
;d12: delay for power switching [20 usec]
;d16: delay for homospoil/gradient recovery
;d24: = d4 / 2
;d26: 1/(4J(NH))
;cnst13: = J(XH)
;cnst25: = 0 IP, 1 AP
;cnst24: = 0 TOCSY, 1 no-TOCSY applied
;in0: 1/(2 * SW(C)) = DW(C)
;nd0: 2
;in20: 1/(2 * SW(N)) = DW(N)
;in28: in20 - in0

```

```

;NS: 2 * n
;DS: >= 4
;td1: number of experiments in F1
;FnMODE: echo-antiecho in F1

;use gradient ratio:      gp 1 :    gp 2 :    gp 3
;                          -47.63 : 32.37 : 8.14

;for z-only gradients:
;gpz1: -47.63%
;gpz2: 32.37%
;gpz3: 8.14%

;use gradient files:
;gpnam1: SINE.100
;gpnam2: SINE.100
;gpnam3: SINE.100

```

4.6. Publication 6: LR-HSQMBC versus LR-selHSQMBC: Enhancing the Observation of Tiny Long-Range Heteronuclear NMR Correlations.

4.6.1. Introduction

In the previous article, the LR-selHSQMBC experiment has shown its efficiency to measure long-range coupling constants with excellent accuracy. As a proof of concept, a comparative study between this novel LR-selHSQMBC experiment with the original LR-HSQMBC experiment is made here. The important and unwanted effects of J_{HH} evolution in the long delays involved in long-range correlation experiments are evaluated in detail and discussions about how to minimize and/or remove them is made. Experimental data completely agree with simulations, and examples are given to ensure the robustness of the proposal. Ultra long-range correlations can be detected under improved experimental conditions and with optimum accuracy and sensitivity.

LR-HSQMBC versus LR-selHSQMBC: Enhancing the Observation of Tiny Long-Range Heteronuclear NMR Correlations

Kumar Motiram-Corral, Pau Nolis, Josep Saurí, and Teodor Parella*

Cite This: *J. Nat. Prod.* 2020, 83, 1275–1282

Read Online

ACCESS |



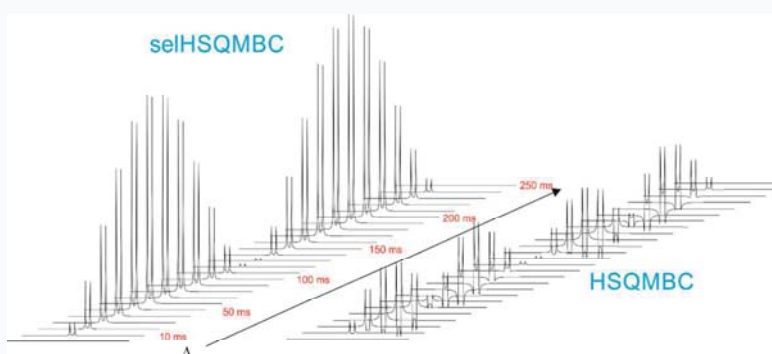
Metrics & More



Article Recommendations



Supporting Information



ABSTRACT: The detection of ultra-long-range ($^4J_{\text{CH}}$ and higher) heteronuclear connectivities can complement the conventional use of HMBC/HSQMBC data in structure elucidation NMR studies of proton-deficient natural products, where two-bond and three-bond correlations are usually observed. The performance of the selHSQMBC experiment with respect to its broadband HSQMBC counterpart is evaluated. Despite its frequency-selectivity nature, selHSQMBC efficiently prevents any unwanted signal phase and intensity modulations due to passive proton–proton coupling constants typically involved in HSQMBC. As a result, selHSQMBC offers a significant sensitivity enhancement and provides pure in-phase multiplets, improving the detection levels for short- and long-range cross-peaks corresponding to small heteronuclear coupling values. This is particularly relevant for experiments optimized to small $^nJ_{\text{CH}}$ values (2–3 Hz), referred to as LR-selHSQMBC, where key cross-peaks that are not visible in the equivalent broadband LR-HSQMBC spectrum can become observable in optimum conditions.

Cross-peak intensities in long-range heteronuclear NMR correlation experiments, such as the heteronuclear multiple bond correlation (HMBC)^{1,2} and heteronuclear single-quantum multiple bond correlation (HSQMBC)^{3,4} pulse schemes, depend on the magnitude of the active coupling ($^nJ_{\text{CH}}$; $n > 1$) and the corresponding interpulse delay optimization (Δ), according to the $\sin(\pi^n J_{\text{CH}} \Delta)$ and $\sin^2(\pi^n J_{\text{CH}} \Delta)$ functions in non-refocused and refocused versions, respectively. Therefore, the effective observation of these correlations depends on the optimum matching between $^nJ_{\text{CH}}$ and Δ . The Δ period is experimentally set to $1/(2 \cdot ^n J_{\text{CH}})$ and, unfortunately, null points appear when Δ satisfies the condition $\Delta = k/{}^n J_{\text{CH}}$, $k = 1, 2, \dots$. In practice, conventional recording of 8 Hz optimized HMBC or HSQMBC experiments (Δ is set to 62.5 ms) yields two-bond ($^2J_{\text{CH}}$) and three-bond ($^3J_{\text{CH}}$) proton–carbon correlations, which are usually enough to trace out the carbon skeleton in structural studies of small- and medium-sized molecules. However, some expected cross-peaks can be missing sometimes, causing uncertainties in the structural analysis and data interpretation. For instance, $^2J_{\text{CH}}$ usually present small absolute values and they can present small intensities or be absent, and correlations separated by four or

more bonds are rarely observed. A classical strategy to observe such correlations lies in the reoptimization of Δ to longer values, corresponding to couplings up to 2–4 Hz provided that T_2 relaxation losses are not a problem.

The influence of the passive homonuclear proton–proton coupling constants (J_{HH}) plays an important role in HMBC/HSQMBC experiments. Recently, two detailed NMR studies conducted by Bigler and Furrer have determined the effects of J_{HH} in non-refocused⁵ and refocused⁶ versions of the HMBC and HSQMBC experiments. Thus, for a CHH' three-spin system (with $^nJ_{\text{CH}'} = 0$), the signal intensity dependence of a given cross-peak in a refocused HSQMBC experiment is defined by eq 1:

Received: January 15, 2020

Published: March 10, 2020



ACS Publications

© 2020 American Chemical Society and
American Society of Pharmacognosy

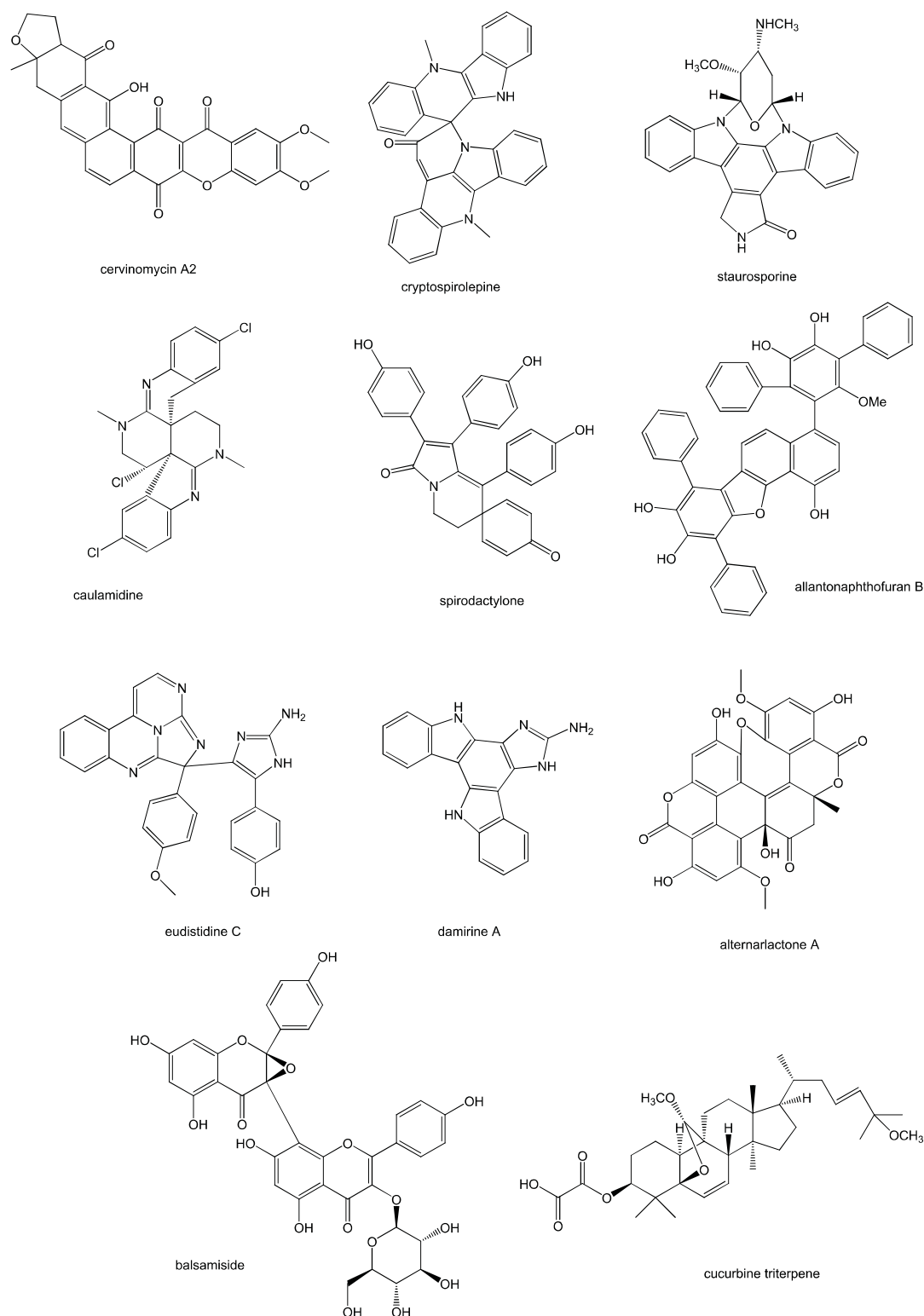


Figure 1. Some proton-deficient natural products characterized with the aid of the LR-HSQMBC experiment: the xanthone antibiotic cervinomycin A2,^{7,9} the spiroonacyclic indoloquinoline cryptospirolepine,¹⁰ the indolocarbazole derivative staurosporine,^{9,15} the chlorinated indole caulamidine A,¹³ the hexacyclic indolizidone spirodactylone,¹¹ the terphenyl allantonnaphthofuran B,¹² the bioactive marine alkaloid eudistidine C,¹⁴ the hexacyclic bisindole derivative damirine A,¹⁵ the dimeric antiparasitic alternarlactone A,¹⁶ the biflavonoid glycoside balsamside,¹⁷ and the cucurbitane triterpenoid derivative.¹⁸

$$I_{1x} \sin^2(\pi^n J_{CH} \Delta) \cos^2(\pi J_{HH'} \Delta) + I_{1x} I_{2z} \sin^2(\pi^n J_{CH} \Delta) \times \sin(2\pi J_{HH'} \Delta) \quad (1)$$

which means that HSQMBC cross-peaks arise from two independent contributions, one showing an in-phase (IP) nature and the other yielding an anti-phase (AP) character with respect to $J_{HH'}$. The superposition of these two terms generates cross-peaks with mixed absorptive and dispersive line shapes, which can make multiplet analysis highly complicated. These mixed phases are particularly relevant when the magnitudes of $J_{HH'}$ are of the same order as the line widths, a fact that can cause partial or full signal cancellation. Moreover, phase and intensity modulations due to $J_{HH'}$ become more pronounced in more demanding experimental conditions, such as when HSQMBC is optimized to smaller $^nJ_{CH}$ values, 2–3 Hz, as described in the LR-HSQMBC experiment.⁷ LR-HSQMBC has demonstrated its powerful practical utility in the structural verification and characterization of a number of highly challenging proton-deficient natural products, most of them having substructures with numerous contiguous nonprotonated carbons and heteroatoms (Figure 1),^{8–18} in addition to its perfect compatibility with DFT calculations¹⁹ and computer-assisted structural elucidation (CASE) programs.²⁰

In this study, a comparison of the performance of the selective version of the HSQMBC (selHSQMBC)^{21–26} with respect to its broadband counterpart has been made in order to evaluate the advantages of avoiding any signal phase or intensity modulation generated by $J_{HH'}$. Signal intensity in selHSQMBC presents a more predictable answer than HSQMBC, depending exclusively on

$$I_{1x} \sin^2(\pi^n J_{CH} \Delta) \quad (2)$$

which yields a pure IP character with respect both $^nJ_{CH}$ and $J_{HH'}$ and allows a much better qualitative and quantitative analysis. Due to the excellent impact demonstrated by LR-HSQMBC for the structural elucidation of natural products, we want to assess the potential of the long-range optimized selHSQMBC (LR-selHSQMBC) in the optimum detection of challenging weak signals that can be difficult to observe in LR-HSQMBC.

RESULTS AND DISCUSSION

The refocused HSQMBC and selHSQMBC pulse schemes used in this work are displayed in Figure 2. The major difference between them is the replacement of the hard 180° 1H pulse in both INEPT periods of the HSQMBC pulse train by the frequency-selective 180° pulses in selHSQMBC for selective 1H refocusing. Although a BIRD element could be included during the first INEPT to minimize direct responses in HSQMBC, it has been omitted for simplicity. On the other hand, a zero-quantum filter (ZQF) can be optionally included before 1H acquisition into selHSQMBC to remove antiphase contributions when mutually J -coupled protons are simultaneously excited by the selective 180° pulse.

Both HSQMBC and selHSQMBC schemes have been analyzed theoretically by simulating the signal modulation of several spin systems as a function of Δ delay (Figure 3). In the first example, a simple CHH' system has been chosen, defined by an active large coupling of $^nJ_{CH} = 8.0$ Hz and a passive large coupling of $J_{HH'} = 8.0$ Hz. The perfect $\sin^2(\pi^n J_{CH} \Delta)$ modulation of the doublet in selHSQMBC described in eq 2 is confirmed because the IP character of the signal is always retained, independent of the Δ setting (bottom Figure 3A). As predicted,

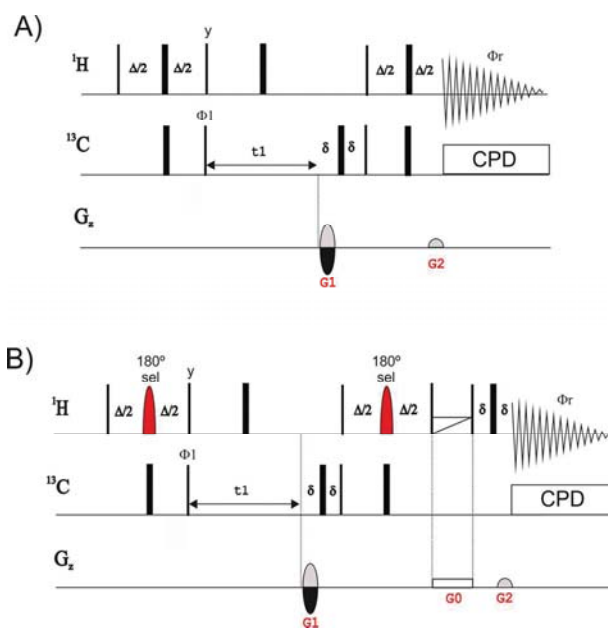


Figure 2. Pulse schemes of the (A) broadband HSQMBC and (B) frequency-selective HSQMBC (selHSQMBC) experiments used in this work. Thin and thick bars represent broadband 90° and 180° pulses, respectively, whereas shaped pulses are frequency-selective 180° pulses. The INEPT delays are set to $\Delta = 1/(2^n J_{CH})$. The basic phase cycling is $\Phi_1 = x, -x$ and $\Phi_{rec} = x, -x$; all other unlabeled pulses are from the x -axis. Coherence pathway selection is achieved using the echo/antiecho protocol, with a gradient G_1 : G_2 ratio set to ± 80 :20.1. A zero-quantum filter (ZQF) involving the simultaneous application of an adiabatic CHIRP pulse and a weak rectangular gradient can be optionally applied in (B) before acquisition to remove unwanted antiphase contributions due to $J_{HH'}$ evolution.

the null signal is found at Δ values of 125 and 250 ms, which correspond to experiment $^nJ_{CH}$ optimization of 4 and 2 Hz, respectively. On the other hand, the unwanted signal and phase modulation described in eq 1 are clearly visualized in HSQMBC (top in Figure 3A), obtaining phase distorted multiplets and a significant decrease in overall sensitivity. Note that null signal is also achieved at k/Δ values, but reduced signal intensity may also appear in other Δ settings due to the unexpected signal behavior. These unwanted modulations can be more pronounced in other situations, especially when small $^nJ_{CH}$ and $J_{HH'}$ magnitudes are present, as shown for a more complex five-spin $CHH'H''H'''$ spin system (Figure 3B). In this case, a predicted perfect IP maximum close to $\Delta = 165$ ms in selHSQMBC is obtained for an active $^nJ_{CH}$ coupling of 3.0 Hz, irrespective of the existence of different passive $J_{HH'}$ values (bottom in Figure 3B). On the other hand, the same HSQMBC cross-peak shows a more unpredictable behavior in both signal phase and intensity modulations, as well as a notorious decrease in overall sensitivity (top in Figure 3B). Under these conditions, the probability of suffering partial or full signal cancellation due to the presence of a mixture of multiple IP and AP contributions is strongly increased, as reflected with the minimum intensity obtained in the Δ interval between 100 and 150 ms, making it non-observable in practice. Although it is not detailed here, a similar behavior would also occur with the refocused version of the HMBC experiment.⁶ Other illustrative simulations with other spin systems can be found in the Supporting Information (Figures S1 and S2). In analogy, Figure S3 shows the theoretical

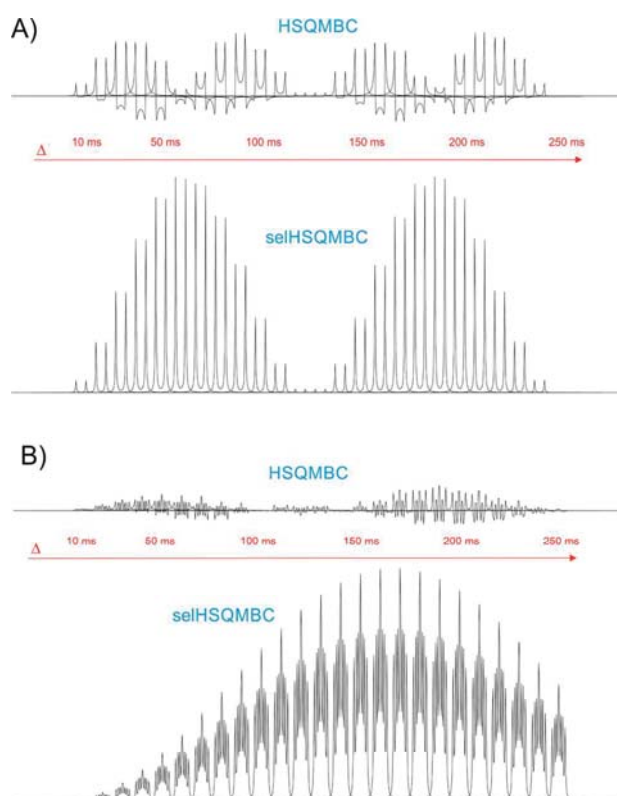
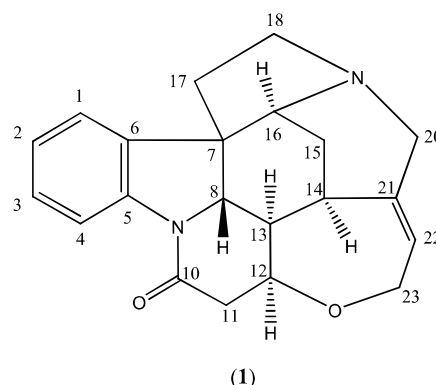


Figure 3. Signal modulation dependence in (A) CHH' three-spin and (B) CHH'H'' five-spin systems as a function of the interpulse Δ delay in (bottom) selHSQMBC and (top) HSQMBC experiments. Twenty-six NMR spectra were simulated using Δ increments of 10 ms, ranging from 0 to 250 ms. Parameters used in (A): $^1J_{CH} = 8.0$ Hz, $J_{HH'} = 8.0$ Hz, $^2J_{CH'} = 0$ Hz. Parameters used in (B): $^1J_{CH} = 3.0$ Hz, $J_{HH'} = 5.0$ Hz, $J_{HH''} = 3.5$ Hz, $J_{HH'''} = 2.0$ Hz, $^2J_{CH'} = ^2J_{CH''} = ^2J_{CH'''} = 0$ Hz. The spectra are displayed at the same signal-to-noise ratio and in phase-sensitive mode.

signal behavior for cross-peaks with an $^1J_{CH}$ of 2 and 8 Hz as a function of the passive $J_{HH'}$ in HSQMBC and selHSQMBC.

Both HSQMBC and selHSQMBC schemes have also been tested experimentally using the alkaloid strychnine (**1**) as a model natural product. Although selHSQMBC is a frequency-selective experiment, its practical application is not restricted to a single 1H signal. In this work, all selHSQMBC experiments were executed applying a 10 ms REBURP shaped 180° 1H pulse at 4.0 ppm for region-selective refocusing, which covers simultaneously six different 1H signals (H-12, H-23 β , H-23 α , H-16, H-8, and H-20 α) resonating in the range of 4.3–3.7 ppm. All these protons are not mutually coupled, except for the geminal H-23 β /H-23 α pair with a $^2J_{H23\alpha-H23\beta}$ of 13.7 Hz in magnitude. A ZQF was incorporated before acquisition in the selHSQMBC experiment to avoid the presence of AP contribution due to $^2J_{H23\alpha-H23\beta}$ modulation, keeping intact the full pure IP presentation for all cross-peaks. Two different data sets were collected for each HSQMBC and selHSQMBC pulse scheme, optimized to 8 Hz ($\Delta = 62.5$ ms) and 3 Hz ($\Delta = 166.6$ ms), respectively. Experiments at 3 Hz are referred to as LR-HSQMBC and LR-selHSQMBC, respectively. For a reliable comparison in terms of sensitivity, resolution, and experimental times, all data were acquired and processed exactly under the same conditions. Figure 4A and B display the 8 Hz optimized HSQMBC and 8 Hz optimized selHSQMBC spectra of **1**,

respectively. As expected, selHSQMBC shows a perfect IP multiplet character for all cross-peaks, confirming that signal intensity and phase are independent of the existence of passive $J_{HH'}$. On the other hand, all cross-peaks in HSQMBC show a mixture of IP and AP contributions, providing phase-distorted cross-peaks as well as reduced intensity. The superior performance of selHSQMBC versus HSQMBC can be easily evidenced by comparing the 1D slices extracted at different frequencies (Figure 4C vs D). The excellent IP properties obtained in selHSQMBC also allow obtaining useful information about the limits of signal detection with respect to the magnitude of $^1J_{CH}$. For instance, taking as a reference the column corresponding to the H-12 proton resonating at 4.23 ppm, seven well-differentiated cross-peaks can be observed and their intensities qualitatively correlated to the experimental $^1J_{CH}$ values measured by using IPAP-selHSQMBC:²¹ C-14 ($^3J_{H12-C14} = 1.3$ Hz), C-11 ($^2J_{H12-C11} = 2.1$ Hz), C-7 ($^4J_{H12-C7} = 1.7$ Hz), C-8 ($^3J_{H12-C8} = 5.9$ Hz), C-23 ($^3J_{H12-C23} = 2.6$ Hz), C-1 (this is the direct $^1J_{H12-C12}$ cross-peak), and C-10 ($^3J_{H12-C10} = 2.1$ Hz) carbon frequencies (Figure 5). Note that the expected two-bond correlation with C-13 is not observed (theoretical value of $^2J_{H12-C13} = 1.63$ Hz).²⁷ So, it can be affirmed that cross-peaks with $^1J_{CH}$ magnitudes in the range 10–1.5 Hz can be observed in an 8 Hz selHSQMBC experiment if the signal-to-noise ratio and the relaxation effects are not the limiting factors (see discussion below).



The benefits of selHSQMBC over HSQMBC are more evident in spectra optimized at 3 Hz (Figure 6). For instance, note that cross-peaks from H-20 α and H-12 are practically missing in LR-HSQMBC, whereas several of them are clearly visible in LR-selHSQMBC. On the other hand, several tiny but evident novel correlations become observable for the H-16 signal in LR-selHSQMBC: The three-bond H-16/C-17, the four-bond H-16/C-21, and the five-bond H-16/C-12 and H-16/C-10 connectivities (theoretical values of 0.62, -0.76 , 0.42, and 0.32 Hz were calculated in ref 27 using DFT). As an example, Figure 7 shows 1D slices taken at the nonprotonated C-10 and C-21 carbons for both LR-selHSQMBC and LR-HSQMBC experiments for a more realistic comparison. Note how LR-selHSQMBC affords an intense pure IP H-12/C-10 cross-peak (experimental $^1J_{CH}$ value of 2.1 Hz)²¹ when it appears strongly attenuated and distorted in the equivalent LR-HSQMBC. Much more relevant is the observation of the challenging $^5J_{C10-H6}$ cross-peak (predicted value of 0.32 Hz by DFT calculations)²⁷ in LR-selHSQMBC, which is not even intuited in LR-HSQMBC. Also evident is the slice for C-21, showing four well-defined cross-peaks with optimum sensitivity, of which it is important to emphasize the four-bond H-16/C-21 cross-peak

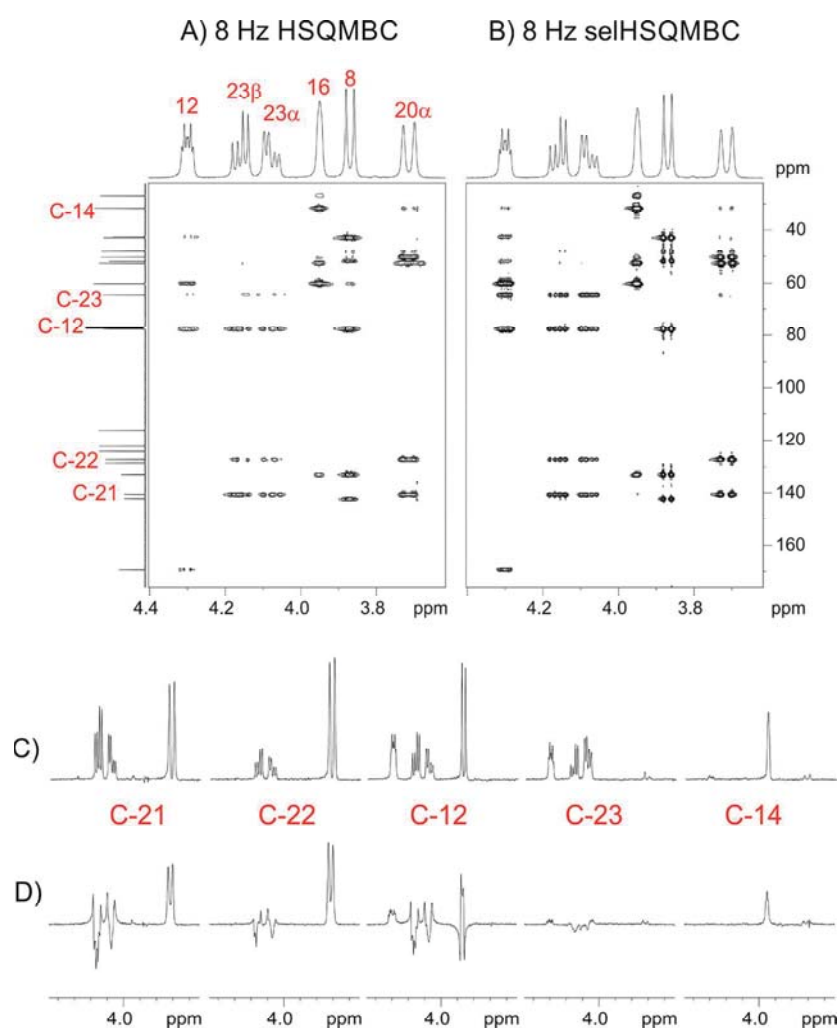


Figure 4. (Right) The 8 Hz optimized selHSQMBC and (left) 8 Hz optimized HSQMBC spectra of **1**, acquired with the pulse sequences shown in Figure 2B and A, respectively. The interpulse delay Δ was set to 62.5 ms. Data were acquired and processed under the same experimental conditions. Experimental times were 7 m 55 s and 8 m 6 s, respectively. 1D slices at several carbon frequencies have been extracted from the (C) selHSQMBC and (D) HSQMBC spectra for a better comparison of the spectral quality and relative sensitivities.

(corresponding to a predicted value of 0.76 Hz by DFT calculations).²⁷ Therefore, it can be affirmed that cross-peaks with $^nJ_{CH}$ magnitudes up to 0.3–0.5 Hz can be visualized in a 3 Hz selHSQMBC experiment if the signal-to-noise ratio and the relaxation effects are not the limiting factors (see discussion below).

A critical factor for the experimental success of LR-HSQMBC and LR-selHSQMBC experiment lies in having $T_2(^1H)$ relaxation times long enough to withstand the long Δ periods of evolution. $T_2(^1H)$ are very sensitive sample-dependent, pulse-sequence-dependent, and equipment-dependent parameters. Thus, eqs 1 and 2 should be multiplied by the same $\exp(-2\Delta/T_2(^1H))$ factor for better quantification of the amount of expected signal in both experiments. Aspects such as molecular size, temperature, magnetic field strength, solvent, and especially the concentration of the sample are relevant factors to influence $T_2(^1H)$. For example, it was described that the $T_2(^1H)$ times in strychnine can be reduced by 50% from a concentration of 60 to 478 mM.⁷ In our working conditions (500 MHz, 298 K, 100 mM) the $T_2(^1H)$ times range between 0.7 s for aromatic protons and 0.3 s for the most aliphatic protons. Figure S4 shows the

theoretical signal intensity dependence as a function of the $T_2(^1H)$ relaxation times in a 3 Hz optimized LR-selHSQMBC experiment. Thus, a cross-peak with an active coupling of $^nJ_{CH} = 3$ Hz would show a relative intensity of about 43% for $T_2 = 0.4$ s or 19% for $T_2 = 0.2$ s. Couplings around 2, 4, and 8 Hz would also yield good sensitivity (34% for $T_2 = 0.4$ s and 15% for $T_2 = 0.2$ s), but signals with $^nJ_{CH} = 5$ and 7 Hz would show tiny intensities (around 13% for $T_2 = 0.4$ s and only 5% for $T_2 = 0.2$ s), whereas cross-peaks around $^nJ_{CH} = 6$ Hz will be around the null point. On the other hand, Figure S5 shows the relative intensity of cross-peaks with $^nJ_{CH} = 3, 2,$ and 1 Hz as a function of the $T_2(^1H)$ relaxation times in a set of selHSQMBC optimized from 1 to 8 Hz. For instance, note that a cross-peak corresponding to $^nJ_{CH} = 2$ Hz should be better observed in a 3 Hz optimized experiment than in the 2 Hz experiment provided that $T_2(^1H) < 0.5$ s.

The utility of obtaining long-distance correlations above three bonds in structural characterization studies should be understood as a resource when the use of traditional experiments does not solve any unknown. Normally, the doubt in solving a structure lies in some specific parts of the molecule, not in its

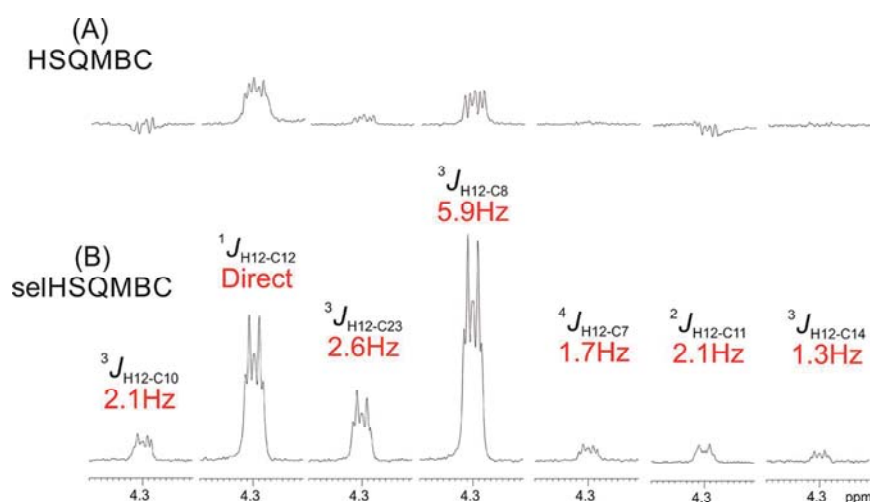


Figure 5. Cross-peaks corresponding to the H-12 proton with several carbons extracted from the (A) 8 Hz optimized HSQMBC and (B) 8 Hz optimized selHSQMBC spectra of Figure 4A and B, respectively. All signals are plotted using the same vertical scale. Note the direct correlation between signal intensity in selHSQMBC with respect to the quantitative $^1J_{CH}$ value measured from an IPAP-selHSQMBC experiment.²¹

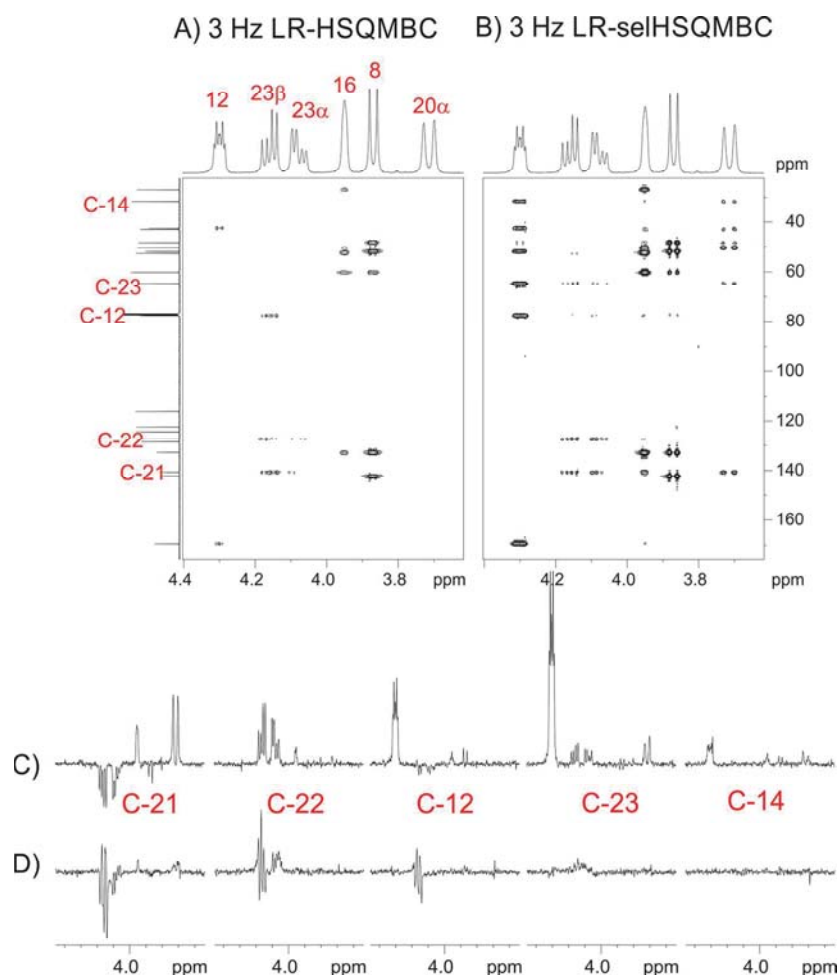


Figure 6. (Left) The 3 Hz optimized selHSQMBC and (right) 3 Hz optimized HSQMBC spectra of 1, acquired with the pulse sequences shown in Figure 2B and A, respectively. Data were acquired and processed under the same experimental conditions. Experimental times were 8 m 49 s and 9 m 0 s, respectively. 1D slices at several carbon frequencies have been extracted from the (C) selHSQMBC and (D) HSQMBC spectra for a better comparison of the spectral quality and relative sensitivities.

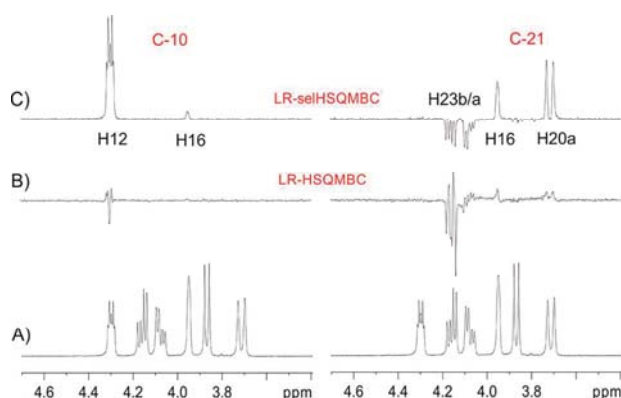


Figure 7. (A) Expansion of the ^1H NMR spectrum of **1**; 1D slices extracted at the carbonyl C-10 frequency resonating at 162.9 ppm (left) and aromatic C-21 resonating at 140.4 ppm (right) in (B) 3 Hz optimized LR-HSQMBC and (C) 3 Hz optimized LR-selHSQMBC spectra (see 2D spectra in Figure 6A and B, respectively). The negative signals for H-23 α and H-23 β are due to the J_{HH} evolution during the Δ periods.

entirety. Hence, the use of selective experiments has been very useful to specify the point to be resolved. Therefore, selHSQMBC is highly recommended to verify and reaffirm any ambiguities or to observe peaks that are not observed in traditional HMBC/HSQMBC spectra. Finally, selHSQMBC is also amenable for further enhancements that have not been detailed here. For instance, selHSQMBC allows accurate measurements of $^nJ_{\text{CH}}$ coupling values,^{21,26} even the relative positive/negative size,²⁸ and it is also fully compatible with pure-shift enhanced methods, which opens the doors to improve both signal resolution and sensitivity thanks to the simplification and collapse of the multiplet structure to a singlet (Figure S6).²⁴

CONCLUSIONS

It has been shown that the LR-selHSQMBC experiment is an attractive NMR tool to observe weak heteronuclear correlations that can be potentially missing in its broadband LR-HSQMBC counterpart or in standard HMBC/HSQMBC experiments. The technique avoids the accidental loss of expected signals due to the presence of AP contributions or signal modulation because of passive J_{HH} effects, allowing enhanced sensitivity, a more uniform response, and excellent pure IP multiplet character without phase distortions. Under optimum sensitivity and relaxation conditions, cross-peaks corresponding to coupling $^nJ_{\text{CH}}$ values up to 1.5 and 0.3 Hz can be seen relatively easily in 8 Hz selHSQMBC and 3 Hz LR-selHSQMBC spectra, respectively.

EXPERIMENTAL SECTION

General Experimental Procedures. NMR experiments were collected at 298 K on a Bruker AVANCE spectrometer operating at 500.13 MHz proton frequency, equipped with a 5 mm TCI cryoprobe including a z-axis pulsed-field gradient accessory (maximum strength of 53.5 G/cm). Experimental data were acquired with a sample of 20 mg of strychnine (**1**) dissolved in 600 μL of CDCl_3 .

All HSQMBC and selHSQMBC experiments were collected and processed under the same conditions. Two data sets for each pulse scheme displayed in Figure 1A and B were recorded with $\Delta = 62.5$ ms (optimized to $^nJ_{\text{CH}} = 8$ Hz) and $\Delta = 166.6$ ms (optimized to $^nJ_{\text{CH}} = 3$ Hz); ^1H and ^{13}C carrier frequencies were set at 4.5 and 90 ppm, respectively; spectral windows of 8 (^1H dimension) and 160 (^{13}C dimension) ppm; using a prescan delay of 1 and 2 scans per t_1

increment. Inversion ^{13}C 180° pulses are applied as adiabatic CHIRP of 500 μs duration. The region-selective 180° ^1H pulse in selHSQMBC was a REBURP shape of 10 ms duration. Data were acquired with 4096 complex points in the ^1H dimension and 128 complex points in the ^{13}C dimension using the echo/antiecho detection mode. The proportionality between gradients G1 and G2 was set to $\pm 80:20.1$, measured as the percentage of the absolute gradient strength of 53.5 G/cm. Sine-bell-shaped gradients of 1 ms duration were used, followed by a recovery delay of 20 μs . The total experimental time for each experiment was around 8–9 min, as described in captions of Figures 3 and 4. Zero filling up to 8K*1K was used prior to Fourier transformation using a 90° phase-shifted squared sine-bell apodization in both dimensions.

Spectral simulations were performed using the NMRSIM v6.2.1 module included in the TOPSPIN (Bruker-Biospin). One-dimensional pulse schemes equivalent to the first increment of the 2D pulse schemes shown in Figure 2 were used for simulations. The line width for all peaks used in the simulations is 0.4 Hz, and all 1D data were processed without any window function. Relaxation effects were neglected.

ASSOCIATED CONTENT

Supporting Information

The Supporting Information is available free of charge at <https://pubs.acs.org/doi/10.1021/acs.jnatprod.0c00058>.

Simulations on signal intensity behavior in HSQMBC and selHSQMBC experiments; signal intensity dependence as a function of experiment optimization and T_2 ^1H relaxation times; 2D selHSQMBC spectra of **1** under heteronuclear and homonuclear decoupling (PDF)

AUTHOR INFORMATION

Corresponding Author

Teodor Parella — Servei de Resonància Magnètica Nuclear, Universitat Autònoma de Barcelona, E-08193 Bellaterra, Barcelona, Spain; orcid.org/0000-0002-1914-2709; Phone: +34 935812291; Email: teodor.parella@uab.cat

Authors

Kumar Motiram-Corral — Servei de Resonància Magnètica Nuclear, Universitat Autònoma de Barcelona, E-08193 Bellaterra, Barcelona, Spain

Pau Nolis — Servei de Resonància Magnètica Nuclear, Universitat Autònoma de Barcelona, E-08193 Bellaterra, Barcelona, Spain; orcid.org/0000-0003-2360-1709

Josep Sauri — Structure Elucidation Group, Analytical Research & Development, Merck & Co., Inc., Boston, Massachusetts 02115, United States

Complete contact information is available at: <https://pubs.acs.org/doi/10.1021/acs.jnatprod.0c00058>

Notes

The authors declare no competing financial interest.

ACKNOWLEDGMENTS

Financial support for this research provided by Spanish MINECO (project PGC2018-095808-B-I00 and BES-2016-078903) is gratefully acknowledged. We also thank the Servei de Resonància Magnètica Nuclear, Universitat Autònoma de Barcelona, for allocating instrument time to this project.

REFERENCES

- (1) Furrer, J. *Concepts Magn. Reson., Part A* **2012**, 40A (3), 146–169.
- (2) Furrer, J. *Concepts Magn. Reson., Part A* **2014**, 43, 177.
- (3) Williamson, R. T.; Márquez, B. L.; Gerwick, W. H.; Kövér, K. E. *Magn. Reson. Chem.* **2000**, 38 (4), 265–273.

- (4) Castañar, L.; Parella, T. Recent Advances in Small Molecule NMR: Improved HSQC and HMQMBC Experiments. *Annu. Rep. NMR Spectrosc.* **2015**, *84*, 163.
- (5) Bigler, P.; Furrer, J. *Magn. Reson. Chem.* **2018**, *56* (11), 1101–1116.
- (6) Bigler, P.; Furrer, J. *Magn. Reson. Chem.* **2019**, *57* (2–3), 129–143.
- (7) Williamson, R. T.; Buevich, A. V.; Martin, G. E.; Parella, T. *J. Org. Chem.* **2014**, *79* (9), 3887–3894.
- (8) Williamson, R. T.; Buevich, A. V.; Martin, G. E. *Tetrahedron Lett.* **2014**, *55*, 3365–3366.
- (9) Blinov, K. A.; Buevich, A. V.; Williamson, R. T.; Martin, G. E. *Org. Biomol. Chem.* **2014**, *12* (47), 9505–9509.
- (10) Sauri, J.; Martin, G. E. Chapter 9. Nuclear Magnetic Resonance Experiments Applicable to the Elucidation and Characterization of Alkaloid Structures Part I: Direct ^1H – ^{13}C Heteronuclear Shift Correlation and Establishing Contiguous Protonated Carbon Spin Systems; *Modern NMR Approaches to the Structure Elucidation of Natural Products*; 2016; Vol. 2, pp 315–357.
- (11) Kang, U.; Caldwell, D. R.; Cartner, L. K.; Wang, D.; Kim, C. K.; Tian, X.; Bokesch, H. R.; Henrich, C. J.; Woldemichael, G. M.; Schnermann, M. J.; et al. *Org. Lett.* **2019**, *21* (12), 4750–4753.
- (12) Andernach, L.; Sandjo, L. P.; Liermann, J. C.; Schlämann, R.; Richter, C.; Ferner, J. P.; Schwalbe, H.; Schöffler, A.; Thines, E.; Opatz, T. *J. Nat. Prod.* **2016**, *79* (10), 2718–2725.
- (13) Milanowski, D. J.; Oku, N.; Cartner, L. K.; Bokesch, H. R.; Williamson, R. T.; Sauri, J.; Liu, Y.; Blinov, K. A.; Ding, Y.; Li, X. C.; et al. Unequivocal Determination of Caulamidines A and B: Application and Validation of New Tools in the Structure Elucidation Tool Box. *Chem. Sci.* **2018**, *9* (2), 307–314.
- (14) Chan, S. T. S.; Nani, R. R.; Schauer, E. A.; Martin, G. E.; Williamson, R. T.; Sauri, J.; Buevich, A. V.; Schafer, W. A.; Joyce, L. A.; Goey, A. K. L.; et al. *J. Org. Chem.* **2016**, *81* (22), 10631–10640.
- (15) Tran, T. D.; Cartner, L. K.; Bokesch, H. R.; Henrich, C. J.; Wang, X. W.; Mahidol, C.; Ruchirawat, S.; Kittakoop, P.; O’Keefe, B. R.; Gustafson, K. R. NMR Characterization of Rearranged Staurosporine Aglycone Analogues from the Marine Sponge *Damiria* Sp. *Magn. Reson. Chem.* **2019**, DOI: 10.1002/mrc.4932.
- (16) Shi, Y. N.; Pusch, S.; Shi, Y. M.; Richter, C.; Maciá-Vicente, J. G.; Schwalbe, H.; Kaiser, M.; Opatz, T.; Bode, H. B. *J. Org. Chem.* **2019**, *84* (17), 11203–11209.
- (17) Kim, C. S.; Bae, M.; Oh, J.; Subedi, L.; Suh, W. S.; Choi, S. Z.; Son, M. W.; Kim, S. Y.; Choi, S. U.; Oh, D. C.; et al. *J. Nat. Prod.* **2017**, *80* (2), 471–478.
- (18) Tuan, N. Q.; Lee, D. H.; Oh, J.; Kim, C. S.; Heo, K. S.; Myung, C. S.; Na, M. J. *Nat. Prod.* **2017**, *80* (7), 2018–2025.
- (19) Sauri, J.; Chan, S.; Buevich, A.; Gustafson, K.; Williamson, R.; Martin, G. Structure Elucidation of a Proton-Deficient Natural Product Using LR-HSQMBC Supported by DFT Calculations. *Planta Med.* **2015**, *81* (11), DOI: 10.1055/s-0035-1556366.
- (20) Guo, P.; Anderson, J.; Bozell, J.; Zivanovic, S. Investigation of Neighboring Heteroatoms and Coupling Pathway Effects on Long-Range Coupling Constants Using LR-HSQMBC. *Planta Med.* **2015**, *81* (11), DOI: 10.1055/s-0035-1556194.
- (21) Gil, S.; Félix, J.; Parella, T.; Espinosa, J. F.; Parella, T. *J. Magn. Reson.* **2011**, *213*, 145–150.
- (22) Sauri, J.; Sistaré, E.; Thomas Williamson, R.; Martin, G. E.; Parella, T. *J. Magn. Reson.* **2015**, *252*, 170–175.
- (23) Sauri, J.; Frédérich, M.; Tchinda, A. T.; Parella, T.; Williamson, R. T.; Martin, G. E. Carbon Multiplicity Editing in Long-Range Heteronuclear Correlation NMR Experiments: A Valuable Tool for the Structure Elucidation of Natural Products. *J. Nat. Prod.* **2015**, *78*, 2236.
- (24) Castañar, L.; Sauri, J.; Nolis, P.; Virgili, A.; Parella, T. *J. Magn. Reson.* **2014**, *238*, 63–69.
- (25) Sauri, J.; Parella, T.; Espinosa, J. F. *Org. Biomol. Chem.* **2013**, *11*, 4473–4478.
- (26) Sauri, J.; Liu, Y.; Parella, T.; Williamson, R. T.; Martin, G. E. *J. Nat. Prod.* **2016**, *79* (5), 1400–1406.
- (27) Buevich, A. V.; Elyashberg, M. E. Enhancing Computer Assisted Structure Elucidation with DFT Analysis of J -Couplings. *Magn. Reson. Chem.* **2020**, DOI: 10.1002/mrc.4996.
- (28) Sauri, J.; Espinosa, J. F.; Parella, T. *Angew. Chem., Int. Ed.* **2012**, *51* (16), 3919–3922.

Supporting Information

LR-HSQMBC *Versus* LR-selHSQMBC: Enhancing the Observation of Tiny Long-Range Heteronuclear NMR Correlations

Kumar Motiram-Corral,¹ Pau Nolis,¹ Josep Saurí,² and Teodor Parella^{1*}

¹ Servei de Ressonància Magnètica Nuclear, Universitat Autònoma de Barcelona, E-08193 Bellaterra, Barcelona, Catalonia, Spain

² Structure Elucidation Group, Analytical Research & Development, Merck & Co., Inc., 33 Av. Louis Pasteur, Boston, MA, 02215, USA

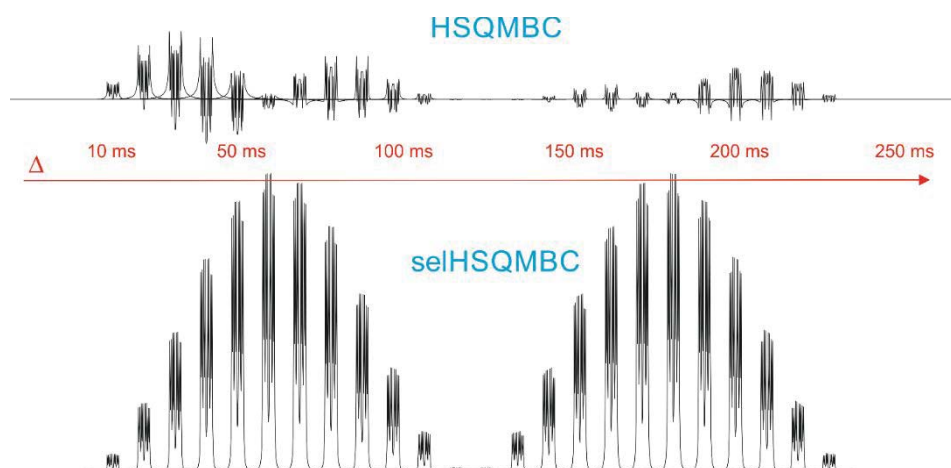


Figure S1: Signal modulation dependence in a CHH'H''H''' five-spin system as a function of the interpulse Δ delay in (bottom) selHSQMBC and (top) HSQMBC experiments. 26 NMR spectra were simulated using Δ increments of 10 ms, ranging from 0 to 250 ms. Parameters used: $^nJ_{CH} = 8.0$ Hz, $J_{HH'} = 8.0$ Hz, $J_{HH''} = 3.5$ Hz, $J_{HH'''} = 1.5$ Hz, $^nJ_{CH'} = ^nJ_{CH''} = ^nJ_{CH'''} = 0$ Hz. The spectra are displayed at the same signal-to-noise ratio and in phase-sensitive mode. Simulations have been performed with the BRUKER NMRSIM program v6.2.1.

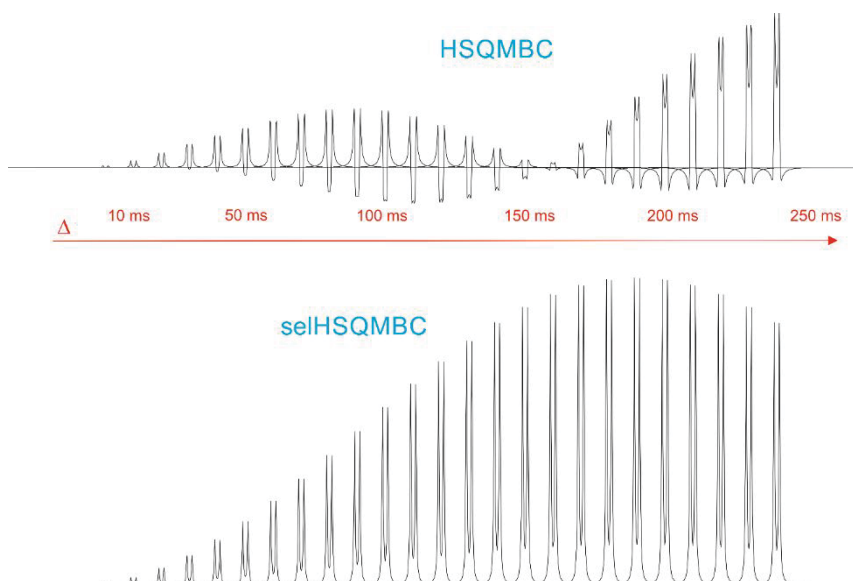


Figure S2: Signal modulation dependence in a CHH' three-spin system as a function of the interpulse Δ delay in (bottom) selHSQMBC and (top) HSQMBC experiments. 26 NMR spectra were simulated using Δ increments of 10 ms, ranging from 0 to 250 ms. Parameters used: $^nJ_{\text{CH}} = 2.5$ Hz, $J_{\text{HH}'} = 3.0$ Hz, $^nJ_{\text{CH}'} = 0$ Hz. The spectra are displayed at the same signal-to-noise ratio and in phase-sensitive mode. Simulations have been performed with the BRUKER NMRSIM program v6.2.1.

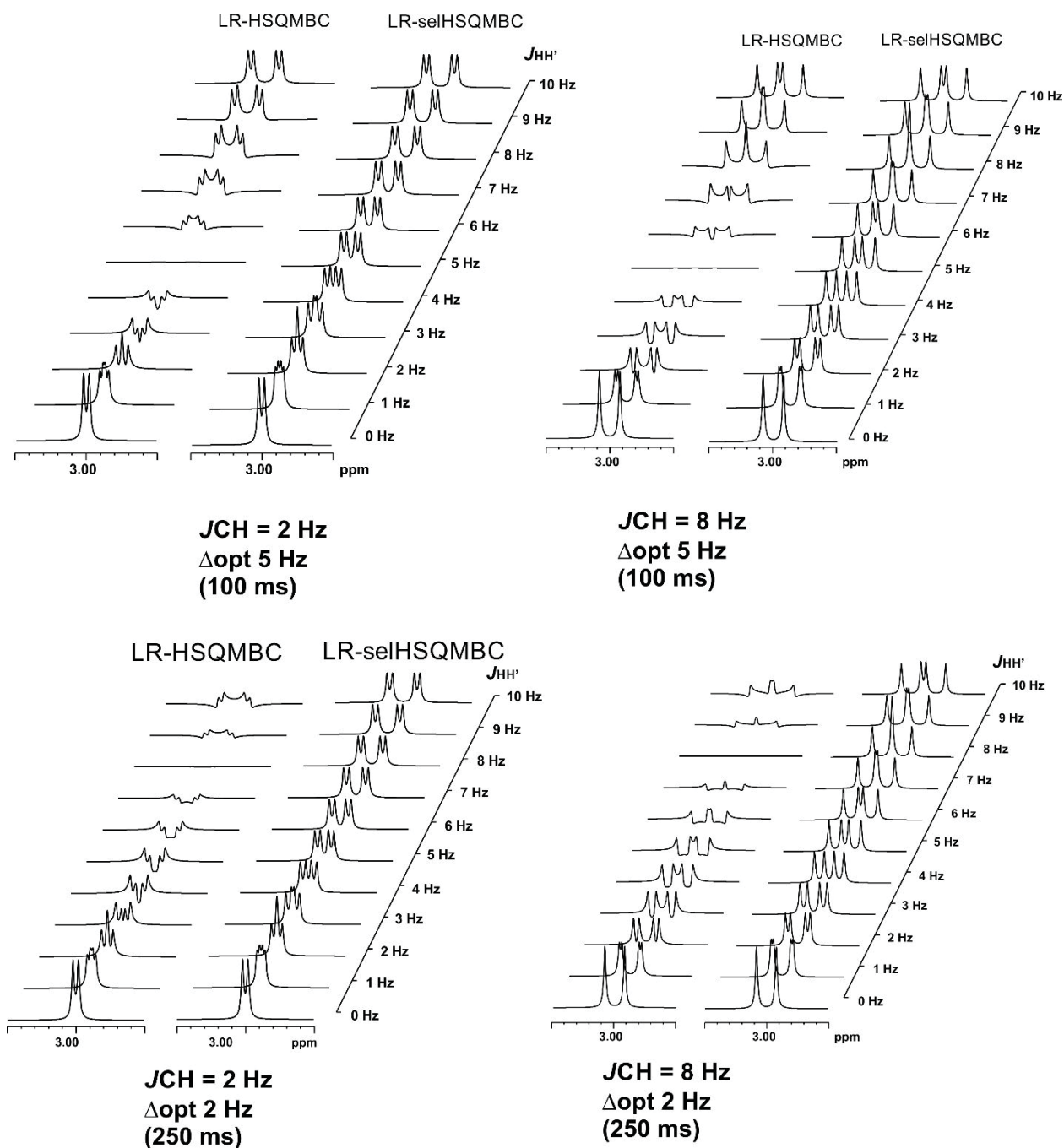


Figure S3: Simulation on the signal intensity dependence as a function of passive J_{HH} coupling constants in HSQMBC and selHSQMBC experiments optimized to (top) 5 Hz ($\Delta = 100$ ms) and (bottom) 2 Hz ($\Delta = 250$ ms). Two different simulations have been made using (right) ${}^nJ_{CH} = 8$ Hz and (left) ${}^nJ_{CH} = 2$ Hz. T_2 relaxation during Δ periods has been neglected.

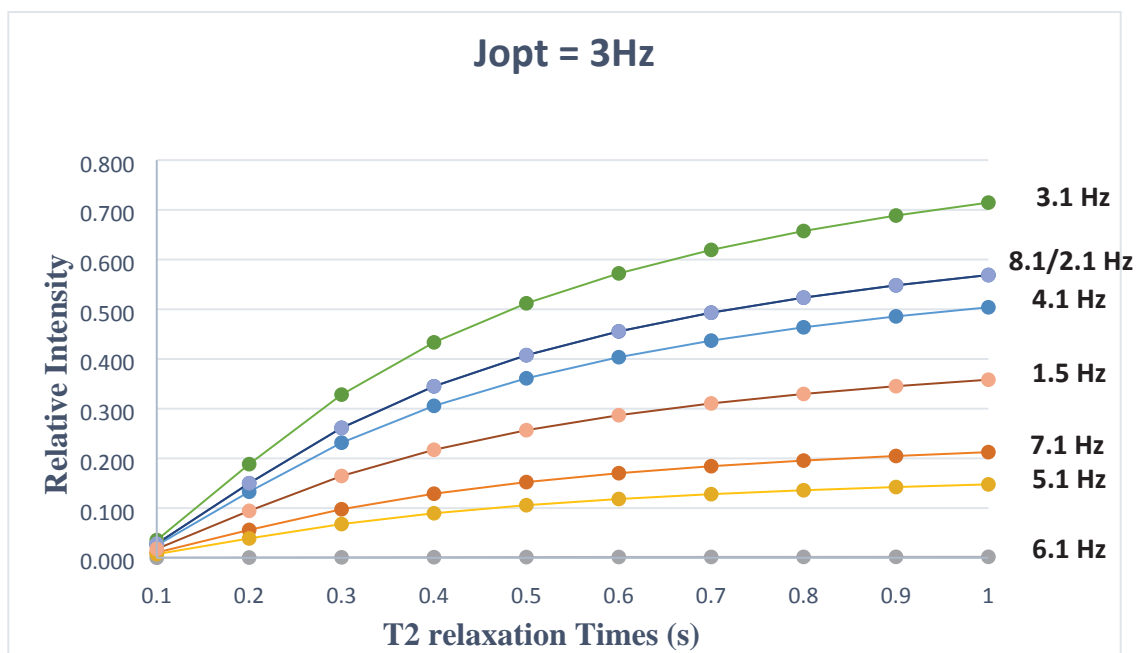
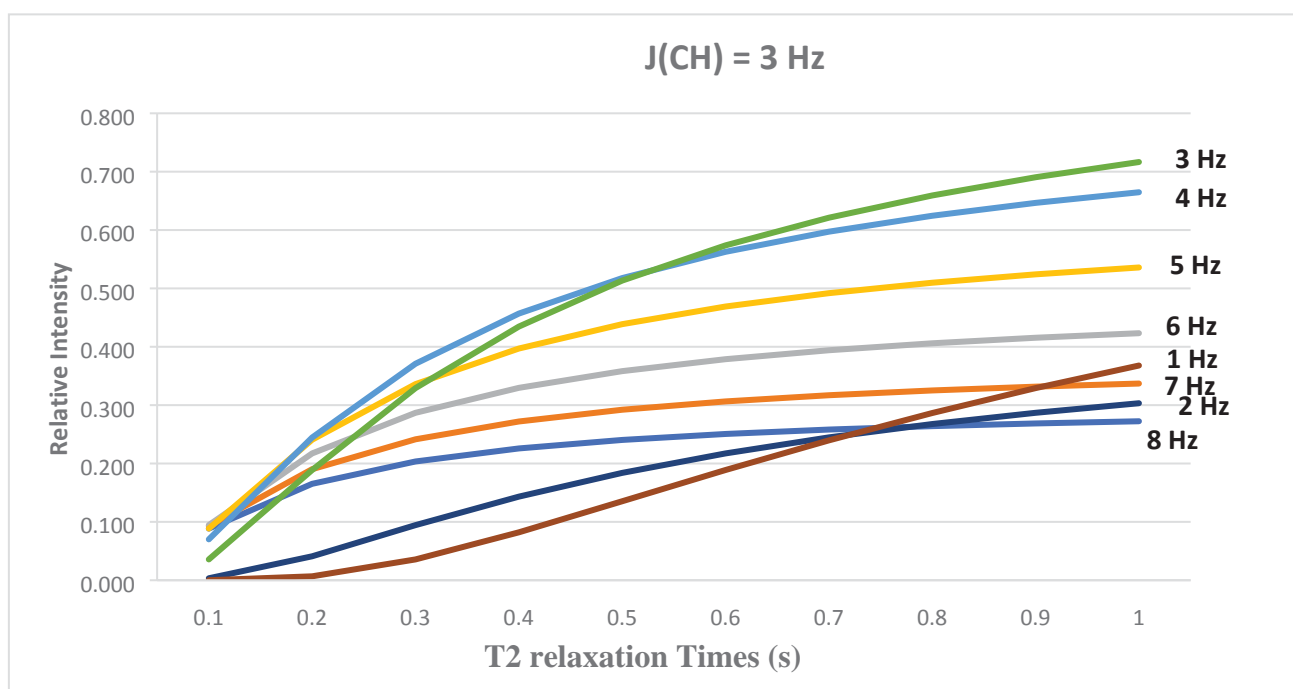
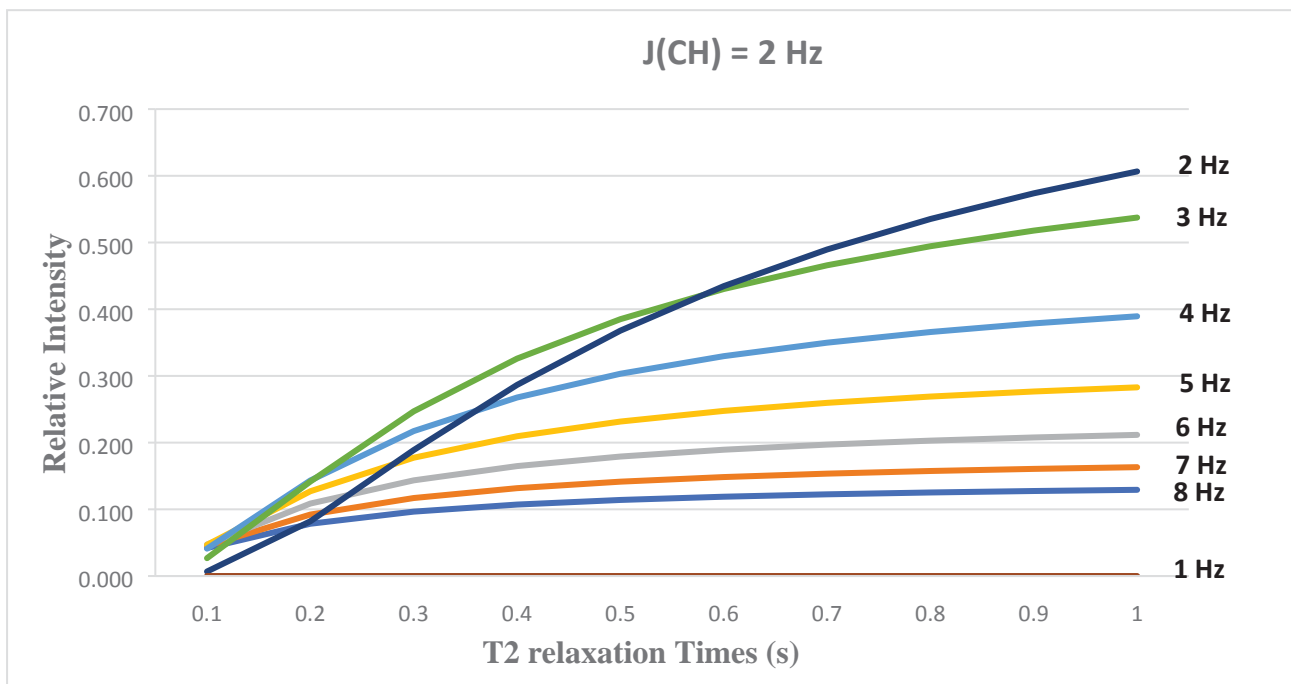


Figure S4: Theoretical prediction about the relative intensity of a cross-peak as a function of the T₂ relaxation times (in seconds) in a 3 Hz optimized selHSQMBC experiment.



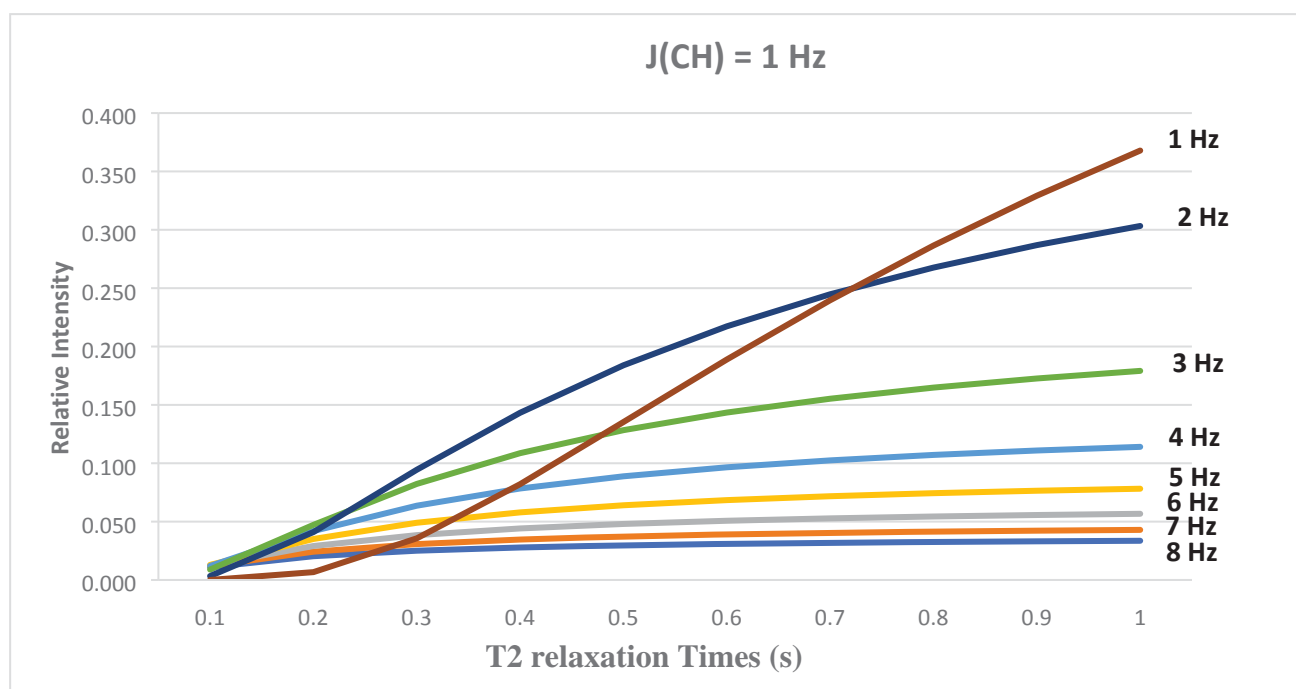


Figure S5: Theoretical prediction about the relative intensity of a cross-peak corresponding to a $^nJ_{\text{CH}}$ values of 3, 2 and 1 Hz as a function of the T₂ ¹H relaxation times (in seconds) in selHSQMBC experiments optimized from 8 Hz to 1 Hz.

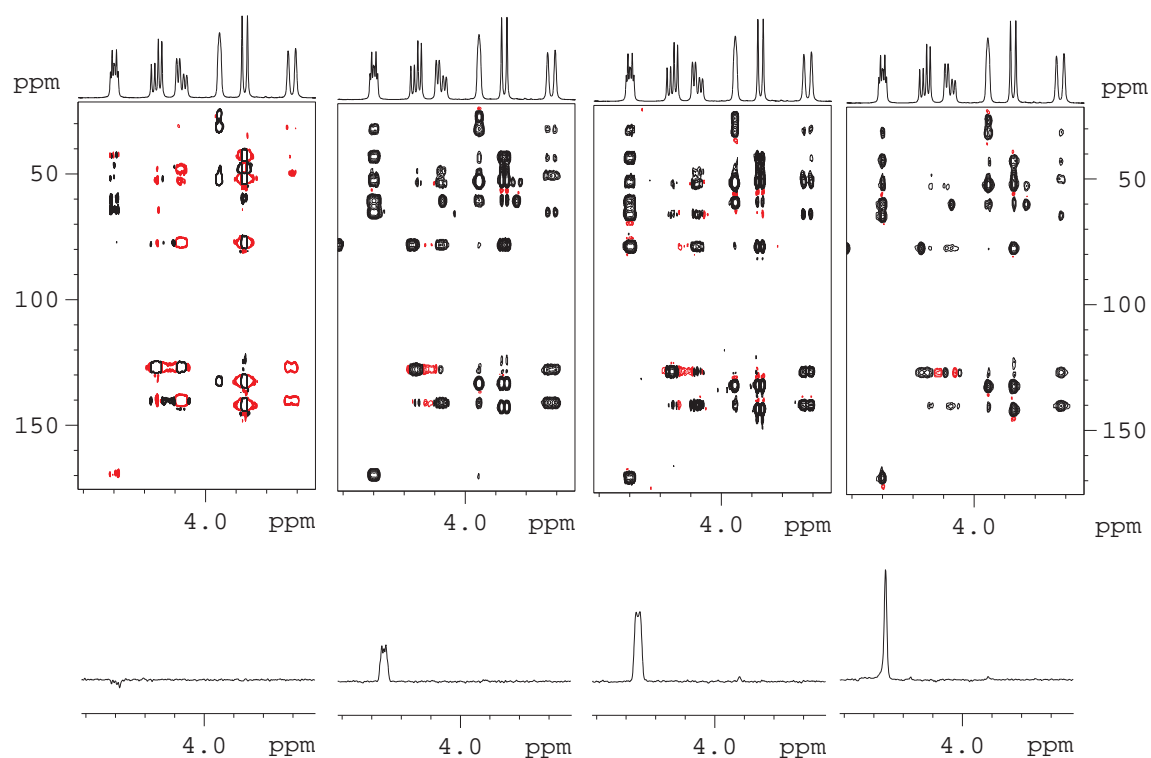


Figure S6. From left to right: 4 Hz optimized HSQMBBC spectrum of strychnine; 4 Hz optimized selHSQMBBC spectra acquired without ^{13}C -decoupling during ^1H acquisition; 4 Hz optimized selHSQMBBC spectra acquired with ^{13}C -decoupling during ^1H acquisition; 4 Hz optimized selHSQMBBC spectra acquired with ^{13}C -decoupling and homonuclear ^1H -HOBS decoupling during ^1H acquisition. ^1H 1D slices at the bottom of each 2D spectrum corresponds to the carbonyl C-10 frequency.

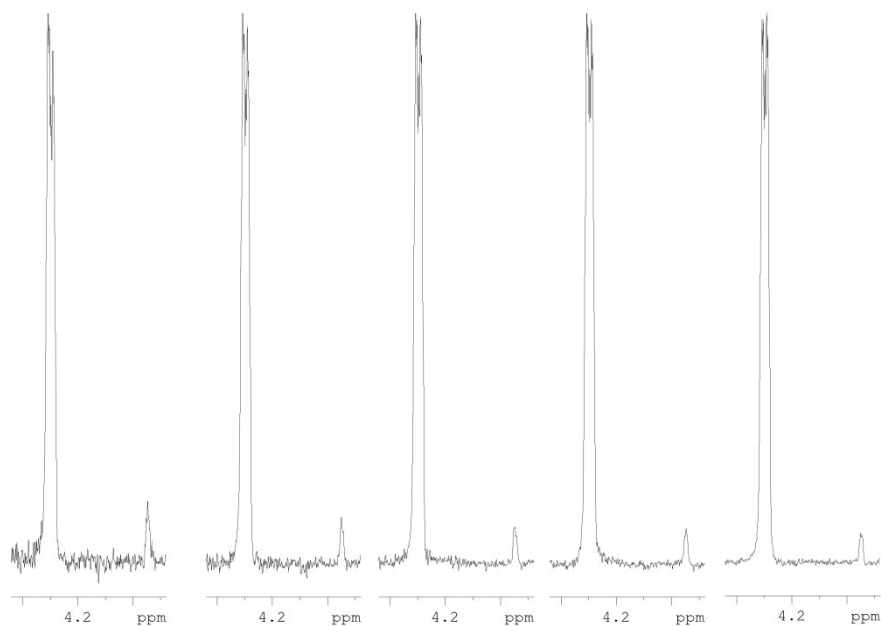


Figure S7: 1D slices taken at the carbonyl C-10 frequency of the 3 Hz optimized LR-selHSQMBC experiment. Several experiments were collected only changing the number of t_1 increments. From left to right: 64 increments (expt = 4 m 35 s); 128 increments (expt = 9 m 00 s); 256 increments (expt = 15 m 51 s); 512 increments (expt = 35 m 35 s); 768 increments (expt = 53 m 23 s). Signal-to-noise ratio (SNR) values for each expansion: 58.28, 90.50, 118.23, 176.93, and 182.42.

References:

- (1) Castañar, L.; Saurí, J.; Nolis, P.; Virgili, A.; Parella, T. Implementing Homo- and Heterodecoupling in Region-Selective HSQMBC Experiments. *J. Magn. Reson.* 2014, 238, 63–69. <https://doi.org/10.1016/j.jmr.2013.10.022>.

4.7. Publication 7: Simultaneous Enantiospecific Detection of Multiple Compounds in Mixtures using NMR Spectroscopy.

4.7.1. Introduction

Chirality plays a fundamental role in nature. Most biological molecules are chiral (e.g. metabolites, like amino acids, sugars, nucleotides, etc.) and many biological processes are stereospecific, i.e. specific to the stereochemistry (chirality) of metabolites. As well, chirality is of paramount importance to the pharmaceutical industry and synthetic chemistry.

Among chiral molecules, enantiomeric compounds (non-superimposable mirror-image molecules) are of particular interest. Despite their similar chemical structure and identical physical properties (except optical rotation), enantiomers are different molecules with different functionalities and biological activities; therefore, the importance of having accurate and efficient enantiospecific methods of analysis, which can detect differently each enantiomer and precisely identify them.

To date, the enantiospecific analysis of mixtures necessarily requires prior separation of the individual components. A current challenge, with substantial impact on fields like metabolism studies, metabolic phenotyping or chemical reaction monitoring among others, is the enantiospecific analysis of mixtures *in situ* and multicomponent. For instance, the simultaneous enantiospecific detection of multiple metabolites in a biological mixture represents a major challenge, which would lead to a significantly better understanding of the underlying biological processes, e.g. via enantiospecifically analysing metabolites in their native environment.

Enantiospecific Analysis
How to cite: *Angew. Chem. Int. Ed.* **2020**, 59, 23615–23619

International Edition: doi.org/10.1002/anie.202011727

German Edition: doi.org/10.1002/ange.202011727

Simultaneous Enantiospecific Detection of Multiple Compounds in Mixtures using NMR Spectroscopy

Lars T. Kuhn, Kumar Motiram-Corral, Toby J. Athersuch, Teodor Parella, and Míriam Pérez-Trujillo*

Abstract: Chirality plays a fundamental role in nature, but its detection and quantification still face many limitations. To date, the enantiospecific analysis of mixtures necessarily requires prior separation of the individual components. The simultaneous enantiospecific detection of multiple chiral molecules in a mixture represents a major challenge, which would lead to a significantly better understanding of the underlying biological processes; for example, via enantiospecifically analysing metabolites in their native environment. Here, we report on the first *in situ* enantiospecific detection of a thirty-nine-component mixture. As a proof of concept, eighteen essential amino acids at physiological concentrations were simultaneously enantiospecifically detected using NMR spectroscopy and a chiral solvating agent. This work represents a first step towards the simultaneous multicomponent enantiospecific analysis of complex mixtures, a capability that will have substantial impact on metabolism studies, metabolic phenotyping, chemical reaction monitoring, and many other fields where complex mixtures containing chiral molecules require efficient characterisation.

Chirality is a property fundamental to biological processes at a molecular level. Nevertheless, challenging questions regarding chiral analysis remain open and need to be addressed.^[1] Many mirror-image (enantiomeric) molecular pairs occur naturally, each of them having different functionalities, biological activities, and sometimes origin, such as in the case of amino acids (AAs). D-amino acids (AAs)—though in smaller quantities than L-AAs—are widely distributed in living organisms and their study has led to significant advances in the fields of microbiology and medicine, among others. For instance, D-serine and D-aspartic acid act as neurotransmitters in the human brain,^[2]

abnormal D-AA levels have been associated to various diseases including schizophrenia^[3] or ALS,^[4] and D-AAs play a relevant role in bacterial metabolism^[5] and in the host-microbe interface.^[6] Hence, the differentiation and identification of enantiomeric metabolites is of paramount importance to biological applications. Enantiospecific analyses are crucial in metabolism studies, as well as in metabolic profiling, and are mandatory in drug research.^[7] Despite of this fact, many of these investigations rely on non-enantiospecific analytical methods, which overlook the stereochemistry of the metabolites involved.

Enantiospecific detection can be achieved using appropriate spectroscopic techniques^[8–10] and via methods based on asymmetric separation platforms.^[11] However, these methods necessarily require the isolation of each enantiomeric pair or each individual enantiomer from its original matrix before detection (e.g. metabolites in a body fluid, in a cell or in a plant extract). Separation steps potentially introduce additional challenges and significant risks to the analysis, for example, sample degradation, stereochemical instability of analytes, sample contamination or analyte loss, and involve time- and cost-consuming procedures.

The direct and simultaneous enantiospecific detection of multiple compounds in a complex mixture would give access to a new level of complexity (i.e. enantiospecific data) from metabolites in their natural media and conditions, providing more precise information to explain better the biological processes under observation. Developing robust and efficient methods for such analyses represents a major analytical challenge, potentially explaining the limited number of studies demonstrating simultaneous multicomponent enantiospecific detection reported in the literature. In these examples, mixtures of two or three enantiomeric pairs were enantiodifferentiated using extremely non-physiological conditions utilizing methodologies whose applicability to more complex mixtures seems difficult.^[12–14] In a previous study, we enantiodifferentiated racemic RS-ibuprofen within a complex mixture (human urine) using NMR spectroscopy in combination with a chiral solvating agent (CSA) while introducing the concept of chiral metabolomics.^[15] The CSA-NMR method is based on the formation of diastereomeric complexes between analytes and the chiral agent, resulting in chemical shift differences between enantiomers (enantiodifferentiation, $\Delta\Delta\delta$) observed in the NMR spectra.^[16–18]


Here, we show for the first time the simultaneous enantiospecific detection of eighteen chiral metabolites within an aqueous mixture at physiological concentrations. A mixture corresponding to the twenty essential amino acids (AAs) in a low millimolar concentration range was analysed.

[*] Dr. L. T. Kuhn

 Institut für Physikalische Chemie
 Albert-Ludwigs-Universität Freiburg
 Albertstraße 21, 79104 Freiburg i. Br. (Germany)

 K. Motiram-Corral, Dr. T. Parella, Dr. M. Pérez-Trujillo
 Servei de Resonància Magnètica Nuclear, Facultat de Ciències
 i Biociències, Universitat Autònoma de Barcelona
 08193 Cerdanyola del Vallès, Catalonia (Spain)
 E-mail: miriam.perez@uab.cat

 Dr. T. J. Athersuch
 Division of Systems Medicine, Department of Metabolism, Digestion
 and Reproduction, Imperial College London
 South Kensington, London (UK)

 Supporting information and the ORCID identification number(s) for the author(s) of this article can be found under <https://doi.org/10.1002/anie.202011727>.

The sample contained the nineteen chiral essential AAs present as racemates plus glycine, giving a thirty-nine-component mixture, mixture **1** (Table S-1). Out of the twenty spectroscopically detected amino acids, fifteen were simultaneously enantiodifferentiated conducting a rapid ^1H NMR experiment only following the addition of a small amount of the CSA (–)-(18-crown-6)-2,3,11,12-tetracarboxylic acid, (–)-18C6H₄. In total, eighteen out of the nineteen chiral AAs were enantiospecifically detected using a combination of ^1H and ^{13}C NMR spectroscopy. (–)-18C6H₄ is a water soluble CSA, which has proven to enantiodiscriminate isolated enantiomeric pairs of a wide variety of molecules such as alpha- and beta-AAs, amino alcohols or alkyl amines, among others.^[19,20]

Initially, mixture **1** was titrated with (–)-18C6H₄ and monitored via the acquisition of a standard 1D ^1H NMR spectrum. After subsequent additions of the CSA, we observed that a relatively small amount (3.1 mg, corresponding to a final total concentration of 11.7 mM) induced enantiospecific changes in the spectrum that were sufficient to enantiodifferentiate most of the enantiomeric pairs of AAs in the mixture. Figure 1a–c shows the full 1D ^1H and 1D ^{13}C NMR spectra of mixture **1** as well as a few highlighted expanded regions of the spectra acquired before and after the addition of the chiral agent (Figure 1b and Figure 1c, respectively). The analysis of a similar AA mixture, enriched with L-enantiomers, mixture **2** (Table S-1), allowed the enantiodifferentiated spectral features to be matched unambiguously to their corresponding D- or L-enantiomer (Fig-

ure 1d). The method described above enabled the direct enantiospecific observation of the original mixture and provided access to stereochemical information about enantiomeric components via a simple spectral output, resulting in a ^1H and a ^{13}C NMR-based enantiospecific molecular profile of mixture **1** (Figure S-1 and Figure S-2).

In a second step, we conducted more advance NMR correlation experiments on mixture **1** after CSA addition (Figure 2). The ^1H pure shift^[21] J -resolved experiment, PS-JRES, allowed proton signals corresponding to resolved enantiomeric pairs to be clearly distinguished. These pairs were observed as identical, duplicated signals, displaced in the direct dimension by some ppb corresponding to $\Delta\Delta\delta(^1\text{H})$ (Figure 2a). A skyline projection in the direct dimension yielded a pure shift 1D ^1H NMR spectrum representing an enantiospecific molecular profile of the mixture (Figure S-1). Importantly, this profile exhibited significantly less signal overlap and higher spectral resolution than the standard 1D ^1H NMR spectrum due to the elimination of signal J_{HH} multiplicities obtained using the pure shift Scheme (Figure 2a, top, vs. Figure 2a, bottom). On the other hand, a spectrally aliased (SA) $^1\text{H},^{13}\text{C}$ -HSQC experiment enabled the simultaneous enantiospecific detection of ^1H and ^{13}C nuclei and the measurement of $\Delta\Delta\delta(^1\text{H})$ and $\Delta\Delta\delta(^{13}\text{C})$ of enantiodifferentiated signals, due to a significant increase in the resolution observed in the ^{13}C dimension compared to a conventional $^1\text{H},^{13}\text{C}$ -HSQC (Figure 2b).^[22,23] For the identification of the individual components of mixture **1** before the addition of the CSA, an NMR spectral data

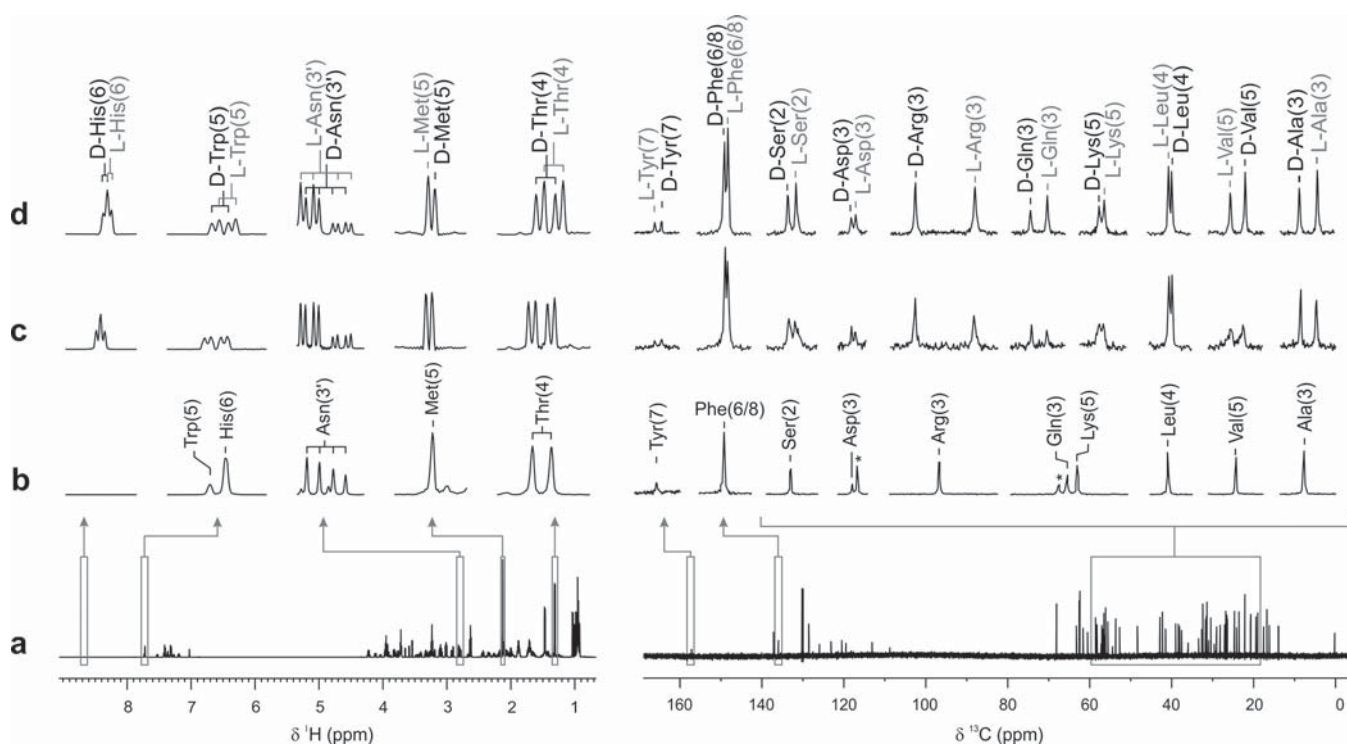


Figure 1. Simultaneous enantiospecific detection of a AA mixture by NMR spectroscopy. (a) 1D ^1H and ^{13}C NMR spectra of mixture **1**. (b) Highlighted ^1H and ^{13}C NMR signals of mixture **1**. (c) Same NMR signals after the addition of 3.1 mg (final concentration 11.7 mM) CSA (–)-18C6H₄. (d) Analogous to c but corresponding to mixture **2**, enriched with L-enantiomers. The enantiospecific assignment of spectral signals to the corresponding D/L-AA is indicated (number in brackets refers to the specific AA nucleus, see Table S-2).

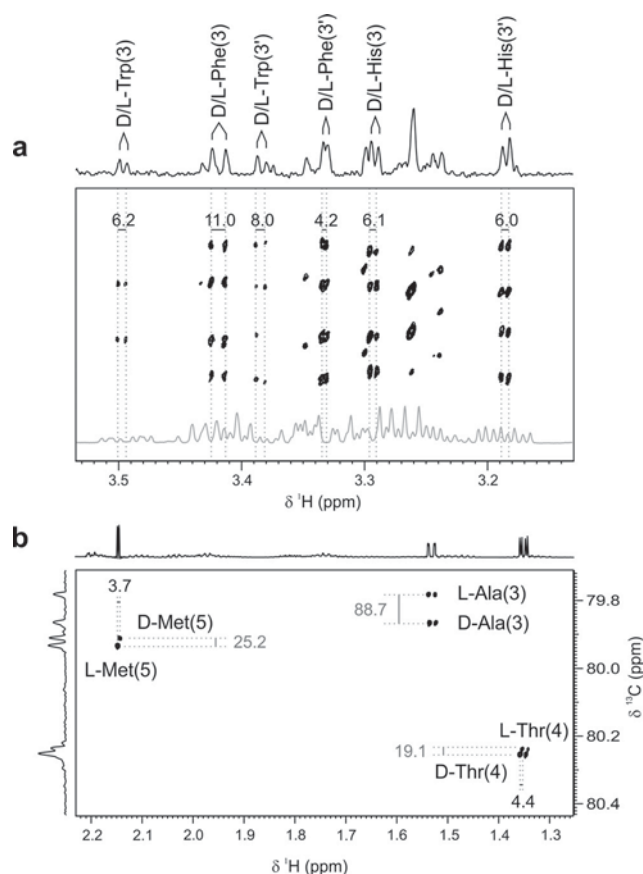


Figure 2. Example of state-of-the-art NMR experiments applied to mixture **1**. (a) Extension of PS-JRES spectrum, showing the internal projection (top) and a standard 1D ^1H NMR experiment (bottom). (b) Extension of SA-HSQC correlation, showing the ^{13}C NMR internal projection (left). Enantiodifferentiated AAs NMR signals and their values of $\Delta\Delta\delta$ (^1H) (black) and $\Delta\Delta\delta$ (^{13}C) (grey), in ppb, are indicated.

base commonly used in metabolomics research was utilized to assign ^1H and ^{13}C signals.^[24] After addition of the CSA, some signals of the original spectrum were split into two (enantioresolved) and most of the signals were slightly shifted with respect to the original spectrum. In this case, the spectral assignment workflow incorporated the NMR experiments described above with standard ^1H , ^1H -TOCSY and ^1H , ^{13}C -HSQC correlations (Figure S-3 and Figure S-4).

The enantiospecificity of the experiment was evaluated by the analysis of the enantiodifferentiated NMR signals and by the measurement of the parameters $\Delta\Delta\delta$ (enantiodifferentiation) and *E* (enantioresolution quotient, which provides information about the quality of the signal resolution)^[25] of each split signal. Further, the sign of $\Delta\Delta\delta$ (and *E*) was determined, which is related to the D/L identification; that is, the determination of the absolute configuration of the enantiodiscriminated AAs.^[16,25] The results of the enantio-specific detection of mixture **1** are summarized in Table S-2. In total, eighteen out of nineteen chiral AAs were enantiodiscriminated, all of which showed more than one enantiodifferentiated signal (except DL-Tyr). Fifteen AAs pairs were enantiodiscriminated via ^1H NMR spectroscopy and sixteen

via ^{13}C NMR spectroscopy, respectively. In thirteen AA pairs, enantiodifferentiation was observed by both nuclei. In the case of ^1H —from the PS-JRES internal projection (Figure S-1)—thirty-eight ^1H signals were enantiodifferentiated and identified, nineteen of them with $E \geq 1.0$ and only six of them with $E < 0.5$; $\Delta\Delta\delta$ and *E* values varied from 86.0 to 3.0 ppb and from 11.5 to 0.3, respectively. For ^{13}C —taken from the 1D ^{13}C NMR experiment (Figure S-2)—fifty NMR signals were enantiodifferentiated and identified, twenty-three of them with $E \geq 1.0$ and only six of them with $E < 0.5$; $\Delta\Delta\delta$ and *E* values varied from 307.2 to 10.0 ppb and from 6.8 to 0.3, respectively. In addition, all but two enantiodifferentiated AAs pairs were D/L identified, and in most cases more than one split signal was assigned to the corresponding enantiomer. In summary, excellent enantiodiscrimination results were observed by detection of both ^1H and ^{13}C nuclei.

To date, the CSA-NMR approach has been used to enantio-recognize just one enantiomeric pair at a time and, except in very few cases,^[15,26] with the sample being isolated from its original medium. Interestingly, when enantiospecifically detecting (complex) mixtures using NMR spectroscopy, the relatively low values of $\Delta\Delta\delta$ yielded by CSAs compared to other NMR auxiliaries (e.g. chiral derivatizing agents) turn out to be an advantage, as this facilitates the identification of resolved enantiomeric pairs in the complex spectra. Signals corresponding to an enantiomeric pair are normally close to one another. When applying the described method for the first time on a mixture, it is convenient to start titrating the sample with the CSA while monitoring it by ^1H NMR to determine the quantity of CSA needed for a proper enantiodifferentiation according to the specific objective (e.g. targeted or untargeted study). Further, following peak shifts during titration can help identifying signals corresponding to the same enantiomeric pair. Apart from adding more CSA, another way to increase $\Delta\Delta\delta$ and improve signal enantioresolution (*E*) consists in decreasing the temperature of the NMR experiment.^[25] This is helpful, for instance, when there is a good overall $\Delta\Delta\delta$ of signals but a specific target peak is not sufficiently enantioresolved (exemplified for the H-6 signal of DL-histidine in Figure 3). In addition, the absence of chemical reactions between the CSA and sample components avoids kinetic resolution, and, combined with the inherently quantitative nature of NMR spectroscopy, allows for quantitative enantiospecific methods to be considered, for example, by conducting a quantitative NMR experiment.^[27]

Finally, an issue that attracted our attention was the relatively small amount of CSA (–)-18C6H₄ (3.1 mg, 11.7 mM) needed to yield the described results, that is, to induce the enantiodifferentiation of eighteen AAs totalling a concentration of 42.3 mM. This means that only ca. 0.3 equivalents on average of CSA were required for each enantiodiscriminated AA. Typically, ≥ 1 equiv. is required for this type of experiments for an isolated enantiomeric pair.^[17–20] To explore this observation further, a similar experiment was performed separately to four enantiomeric pairs randomly selected from those in mixture **1** (DL-alanine, DL-asparagine, DL-methionine and DL-threonine); identical AA and CSA concentrations were used but, this time, dissolved in pure aqueous solutions. In this experiment, the

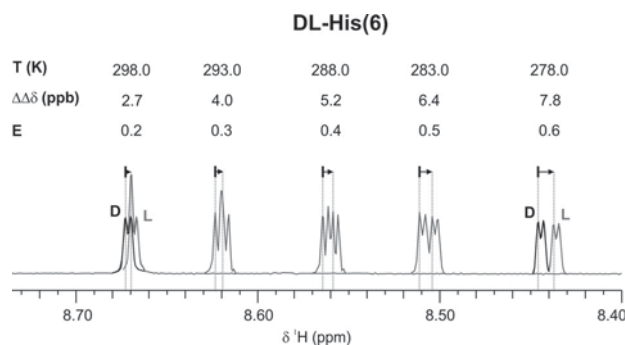


Figure 3. Increase of signal enantioresolution with temperature decrease. DL-His(6) signal region of ^1H NMR spectra of mixture **1** after the addition of 3.1 mg (11.7 mM) of CSA (–)-18C6H₄ at temperatures indicated.

relative proportions of CSA to AA (equivalents of CSA) were higher than in mixture **1**, ranging from 2.7 to 4.8 depending on the AA (the effective CSA/AA ratio would correspond to the experimental ratio shown in Table S-2). To reach these conditions, the individual titration of each AA with the CSA was carried out. Based on this, we initially hypothesized that the degree of enantiomeric differentiation (i.e. values of $\Delta\Delta\delta$) for the pure AAs would be much greater than in the presence of the other AAs on account of the reduced competition for interaction with the CSA. Remarkably, the results obtained for pure AAs were comparable to those obtained within the mixture and did not support this hypothesis (Table S-3). In general, slightly higher values were obtained for pure AAs, with some exceptions like C-4 of DL-threonine, C-2 and C-5 of DL-methionine or C-2 of DL-asparagine, among others. The $\Delta\Delta\delta$ values of pure AAs, corresponding to an addition of 0.3 equivalents of CSA (see titration curves in Figure S-5), and the $\Delta\Delta\delta$ values of same AAs in mixture **1** (Table S-2) were also compared. The results showed much greater $\Delta\Delta\delta$ values, that is, a better enantio-differentiation, when the AAs were present in the mixture. Thus, these results suggest that there is a synergistic effect that greatly favours enantiodifferentiation due to the presence of other (chiral) molecules in the solution, that is, a mixture effect.^[28] We also observed that the same signals were enantiodifferentiated (having the same $\Delta\Delta\delta$ sign) as compared to the mixture in practically all cases. This result suggests that similar AA-CSA diastereomeric complexes are formed in pure solution and in the mixture. Additional experiments are currently being carried out to explore this effect in greater detail.

In summary, we have demonstrated the simultaneous enantiospecific detection of multiple chiral metabolites within an aqueous mixture, at physiological concentrations and without a prior separation or derivatization of its components. This is, to the best of our knowledge, without precedent. Eighteen essential AAs were enantiospecifically detected within a thirty-nine-component mixture using NMR spectroscopy and a small quantity of a CSA. Furthermore, the method allowed the detection and identification of all components, yielding a ^1H and ^{13}C NMR-based enantiospecific molecular profile of the mixture in a straightforward way

with only minimal manipulation and a concomitant structural preservation of the sample. Compatible with untargeted and targeted quantitative studies, this work represents a first step towards the direct multicomponent enantiospecific analysis of complex mixtures, showing significant potential for application in metabolism studies, metabolic phenotyping, and in chemical reaction analysis, among others. Future research will include the study of other small-molecule metabolite mixtures and the evaluation of other compatible CSAs.

Acknowledgements

Financial support provided by the Spanish Ministry of Economy and Competitiveness (project PGC2018-095808-B-I00) is gratefully acknowledged. We also thank the “Servei de Ressonància Magnètica Nuclear (SeRMN)” of the Universitat Autònoma de Barcelona (UAB) for the generous allocation of spectrometer time.

Conflict of interest

The authors declare no conflict of interest.

Keywords: complex mixture · mixture effect · multicomponent · NMR spectroscopy · simultaneous enantiospecific analysis

- [1] D. Kondepudi in *Chiral Analysis. Advances in Spectroscopy, Chromatography and Emerging Methods* (Ed.: P. L. Polavarapu), Elsevier, Amsterdam, **2018**, pp. 3–28.
- [2] a) F. Hucho, *Angew. Chem. Int. Ed.* **2000**, *39*, 2849–2850; *Angew. Chem.* **2000**, *112*, 2969–2971; b) A. Hashimoto, T. Oka, *Prog. Neurobiol.* **1997**, *52*, 325–353.
- [3] I. Chumakov, M. Blumenfeld, O. Guerassimenko, L. Cavarec, M. Palicio, H. Abderrahim, et al., *Proc. Natl. Acad. Sci. USA* **2002**, *99*, 13675–13680.
- [4] J. Sasabe, T. Chiba, M. Yamada, K. Okamoto, I. Nishimoto, M. Matsuoka, S. Aiso, *Embo J.* **2007**, *26*, 4149–4159.
- [5] L. Hubert, O. Dong-Chan, F. Cava, C. N. Takacs, J. Clardy, M. A. de Pedro, M. K. Waldor, *Science* **2009**, *325*, 1552–1555.
- [6] J. Sasabe, M. Suzuki, *Front. Microbiol.* **2018**, *9*, 933.
- [7] K. Jozwiak, W. Lough, I. Wainer in *Drug Stereochemistry* (Eds.: K. Jozwiak, W. Lough, I. Wainer), CRC Press, Boca Raton, **2012**, pp. 1–332.
- [8] N. Berova, P. L. Polavarapu, K. Nakanishi, R. W. Woody in *Comprehensive Chiroptical Spectroscopy, Vol. 1 and 2* (Eds.: N. Berova, P. L. Polavarapu, K. Nakanishi, R. W. Woody), Wiley-VCH, Weinheim, **2012**, pp. 1–853.
- [9] D. Patterson, M. Schnell, J. Doyle, *Nature* **2013**, *497*, 475–477.
- [10] V. Schurig in *Differentiation of Enantiomers II*, (Ed.: V. Schurig), Springer International Publishing, Switzerland, **2013**, pp. 1–348.
- [11] “Enantiospecific bioanalysis: techniques and applications”: A. J. Hutt, B. K. Patel in *Drug Metabolism: Towards the Next Millennium* (Ed.: N. J. Gooderham), IOS Press, Amsterdam, **1998**, pp. 196–212.
- [12] M. M. R. Fanood, N. B. Ram, C. S. Lehmann, I. Powis, M. H. M. Janssen, *Nat. Commun.* **2015**, *6*, 7511.
- [13] C. Guo, R. D. Shah, R. K. Dukor, X. Cao, T. B. Freedman, L. A. Nafie, *Anal. Chem.* **2004**, *76*, 6956–6966.
- [14] Y. Li, L. Wen, H. Meng, J. Lv, G. Luo, Y. Zhao, *Cell Rep. Phys. Sci.* **2020**, <https://doi.org/10.1016/j.xcrp.2020.100100>.

- [15] M. Pérez-Trujillo, J. C. Lindon, T. Parella, H. C. Keun, J. K. Nicholson, T. J. Athersuch, *Anal. Chem.* **2012**, *84*, 2868–2874.
- [16] F. Balzano, G. Uccello-Barretta, F. Aiello in *Chiral Analysis. Advances in Spectroscopy, Chromatography and Emerging Methods* (Ed.: P. L. Polavarapu), Elsevier, **2018**, pp. 367–427.
- [17] M. Pérez-Trujillo, E. Monteagudo, T. Parella, *Anal. Chem.* **2013**, *85*, 10887–10894.
- [18] M. Pérez-Trujillo, A. Virgili, *Tetrahedron: Asymmetry* **2006**, *17*, 2842–2846.
- [19] T. J. Wenzel, J. E. Thurston, *J. Org. Chem.* **2000**, *65*, 1243–1248.
- [20] Y. Machida, M. Kagawa, H. Nishi, *J. Pharm. Biomed. Anal.* **2003**, *30*, 1929–1942.
- [21] a) M. Foroozandeh, R. W. Adams, P. Kiraly, M. Nilsson, G. A. Morris, *Chem. Commun.* **2015**, *51*, 15410–15413; b) J. Aguilar, S. Faulkner, M. Nilsson, G. Morris, *Angew. Chem. Int. Ed.* **2010**, *49*, 3901–3903; *Angew. Chem.* **2010**, *122*, 3993–3995.
- [22] D. Jeannerat, *Magn. Reson. Chem.* **2003**, *41*, 3–17.
- [23] M. Pérez-Trujillo, L. Castañar, E. Monteagudo, L. T. Kuhn, P. Nolis, A. Virgili, R. T. Williamson, T. Parella, *Chem. Commun.* **2014**, *50*, 10214–10217.
- [24] E. L. Ulrich, A. Hideo, J. F. Doreleijers, Y. Harano, Y. E. Ioannidis, J. Lin, M. Livny, S. Mading, D. Maziuk, Z. Miller, E. Nakatani, C. F. Schulte, D. E. Tolmie, R. K. Wenger, H. Yao, J. L. Markley, *Nucleic Acids Res.* **2008**, *36*, D402–D408.
- [25] M. Pérez-Trujillo, T. Parella, L. T. Kuhn, *Anal. Chim. Acta* **2015**, *876*, 63–70.
- [26] T. Wang, Q. Liu, M. Wang, J. Zhou, M. Yang, G. Chen, F. Tang, E. Hatzakis, L. Zhang, *Anal. Chem.* **2020**, *92*, 3636–3642.
- [27] S. K. Bharti, R. Roy, *Trends Anal. Chem.* **2012**, *35*, 5–26.
- [28] R. Altenburger, M. Scholze, W. Busch, B. I. Escher, G. Jakobs, M. Krauss, J. Krüger, P. A. Neale, S. Ait-Aissa, A. C. Almeida, T.-B. Seiler, F. Brion, K. Hilscherová, H. Hollert, J. Novák, R. Schlichting, H. Serra, Y. Shao, A. Tindall, K. E. Tollefsen, G. Umbuzeiro, T. D. Williams, A. Kortenkamp, *Environ. Int.* **2018**, *114*, 95–106.

Manuscript received: August 27, 2020

Accepted manuscript online: September 22, 2020

Version of record online: October 23, 2020

Supporting Information

Simultaneous Enantiospecific Detection of Multiple Compounds in Mixtures using NMR Spectroscopy

*Lars T. Kuhn, Kumar Motiram-Corral, Toby J. Athersuch, Teodor Parella, and Míriam Pérez-Trujillo**

anie_202011727_sm_miscellaneous_information.pdf

Table of Contents

Material and Methods.....	1
Material.....	1
Sample preparation.....	1
NMR experiments.....	3
Enantiomer identification.....	4
Results and Discussion.....	5
¹ H and ¹³ C NMR-based enantiospecific molecular profile of AAs mixtures.....	5
Identification of ¹ H and ¹³ C NMR signals in AAs mixtures.....	7
Results of the enantiodifferentiation experiment of AAs mixtures.....	9
Results of the enantiodifferentiation experiments of pure AAs.....	11

Material and Methods

Material

DL- and L-alanine, D- and L-arginine, DL- and L-asparagine, DL- and L-aspartic acid, DL- and L-cysteine, DL- and L-glutamic acid, D- and L-glutamine, glycine, DL- and L-histidine, DL- and L-isoleucine, D- and L-leucine, DL- and L-lysine HCl, DL- and L-methionine, D- and L-phenylalanine, DL- and L-proline, DL- and L-serine, DL- and L-threonine, DL- and L-tryptophan, D- and L-tyrosine, DL- and D-valine, (-)-(18-crown-6)-2,3,11,12-tetracarboxylic acid (18C6H₄) and 3-(trimethylsilyl)-[2,2,3,3-²H₄]-propionic acid sodium salt (TSP) were purchased from Sigma-Aldrich S.A. (Tres Cantos, Madrid, Spain). Deuterium oxide (99.96 % D) was obtained from Cortecnet (Voisins-le-Bretonneux, France).

Sample preparation

Individual racemic and enantiopure AA stock solutions in D₂O (1 mL of ca. 200 mM each) were prepared (see Table S-1 for exact concentrations). 1.7 mL of stock solution 1 (129.83 mM) was prepared by the addition of individual AA stock solutions (volumes indicated in Extended Data Table 1). Mixture **1** was prepared directly in the NMR tube mixing 200 μL of stock solution 1 and 400 μL of D₂O. Likewise, 288 μL of stock solution 2 (16.78 mM) was prepared by the addition of enantiopure AA stock solutions (volumes indicated in Extended Data Table 1). Mixture **2** was prepared in the NMR tube mixing 200 μL of stock solution 1, 200 μL of stock solution 2 and 200 μL of D₂O.

For the enantiospecific analysis, 3.1 mg (11.7 mM) of (-)-18C6H₄ was added to mixture **1** and mixture **2** respectively before NMR analysis. Initially, a titration experiment (0-0.28 equivalents of (-)-18C6H₄) was carried out in mixture 1 by the sequential addition of 1.0, 1.0 and 1.1 mg of (-)-18C6H₄ into the NMR tube.

Enantiospecific analyses of pure AAs solutions were conducted similarly to that of the mixtures. 0.6 mL of a pure DL-alanine solution in D₂O (2.42 mM) was titrated with (-)-18C6H₄ until reaching a total amount of 3.1 mg (4.8 eq. of CSA). Analogous

procedures were followed for DL-asparagine (2.42 mM and 4.7 eq. of CSA), DL-methionine (3.31 mM and 3.5 eq. of CSA) and DL-threonine (4.03 mM and 2.7 eq. of CSA).

Table S-1. Composition of mixture 1 and mixture 2 and stock solutions utilized to prepare them.

AA (symbol)		AA Individual stock sol. ^(a)	Stock solution 1 (1,700mL; 129,83mM) ^(b)		Mixture 1 (0,6mL; 43,28mM) ^(c)	Stock solution 2 (288 μL; 16,78 mM) ^(d)		Mixture 2 (0,6mL; 48,87mM) ^(e)
		Concentration (mM)	Volume of stock sol. (μL)	Concentr. (mM)	Concentr. (mM)	Volume of stock sol. (mL)	Concentr. (mM)	Concentr. (mM)
Alanine-DL	Ala	198,8	60	7,27	2,42	0,00	0,00	2,42
Alanine-L	Ala	198,8	0	0,00	0,00	12,00	1,33	0,44
Arginine_L	Arg	197,6	40	4,82	1,61	12,00	1,32	2,05
Arginine-D	Arg	195,3	40	4,76	1,59	0,00	0,00	1,59
Asparagine-DL	Asn	200,6	60	7,34	2,45	0,00	0,00	2,45
Asparagine-L	Asn	182,5	0	0,00	0,00	12,00	1,22	0,41
Aspartic acid-DL	Asp	27,1	120	1,98	0,66	0,00	0,00	0,66
Aspartic acid-L	Asp	25,6	0	0,00	0,00	22,00	0,31	0,10
Cysteine-DL	Cys	27,0	120	1,98	0,66	0,00	0,00	0,66
Cysteine-L	Cys	26,2	0	0,00	0,00	22,00	0,32	0,11
Glutamic Acid-DL	Glu	27,2	120	1,99	0,66	0,00	0,00	0,66
Glutamic Acid-L	Glu	27,9	0	0,00	0,00	15,00	0,23	0,08
Glutamine,L	Gln	202,0	20	2,46	0,82	8,00	0,90	1,12
Glutamine-D	Gln	204,0	20	2,49	0,83	0,00	0,00	0,83
Glycine	Gly	12,0	120	0,88	0,29	0,00	0,00	0,29
Histidine-DL	His	202,5	120	14,82	4,94	0,00	0,00	4,94
Histidine-L	His	203,1	0	0,00	0,00	15,00	1,69	0,56
Isoleucine-DL	Ile	198,3	80	9,67	3,22	0,00	0,00	3,22
Isoleucine-L	Ile	192,2	0	0,00	0,00	10,00	1,07	0,36
Leucine-L	Leu	194,5	30	3,56	1,19	8,00	0,86	1,47
Leucine-D	Leu	197,6	30	3,61	1,20	0,00	0,00	1,20
Lysine-DL, HCl	Lys	201,9	60	7,39	2,46	0,00	0,00	2,46
Lysine-L, HCl	Lys	206,0	0	0,00	0,00	8,00	0,92	0,31
Methionine-DL	Met	204,0	80	9,95	3,32	0,00	0,00	3,32
Methionine-L	Met	207,3	0	0,00	0,00	10,00	1,15	0,38
Phenylalanine-L	Phe	202,9	30	3,71	1,24	8,00	0,90	1,54
Phenylalanine-D	Phe	204,8	30	3,75	1,25	0,00	0,00	1,25
Proline-DL	Pro	199,0	60	7,28	2,43	0,00	0,00	2,43
Proline-L	Pro	204,2	0	0,00	0,00	8,00	0,91	0,30
Serine-DL	Ser	199,9	60	7,31	2,44	0,00	0,00	2,44
Serine-L	Ser	201,8	0	0,00	0,00	8,00	0,90	0,30
Threonine-DL	Thr	199,1	100	12,14	4,05	0,00	0,00	4,05
Threonine-L	Thr	192,3	0	0,00	0,00	10,00	1,07	0,36
Tryptophan-DL	Trp	26,9	180	2,96	0,99	0,00	0,00	0,99
Tryptophan-L	Trp	26,0	0	0,00	0,00	30,00	0,43	0,14
Tyrosine-L	Tyr	6,6	30	0,12	0,04	60,00	0,22	0,11
Tyrosine-D	Tyr	6,6	30	0,12	0,04	0,00	0,00	0,04
Valine-DL	Val	204,1	60	7,47	2,49	0,00	0,00	2,49
Valine-D	Val	187,1	0	0,00	0,00	10,00	1,04	0,35
TOTAL	-	-	1700	129,83	43,28	288,00	16,78	48,87

(a) A 200 mM (1 mL) stock solution of each AA was prepared, except in cases of low AA solubility, where saturated solutions were prepared. (b) Stock solution 1 (1,700 mL; 129,83 mM): indicated amounts of AA stock solutions were mixed to get stock solution 1. (c) Mixture 1 (0,6 mL; 43,28 mM): 200 μ L of stock solution 1 were mixed with 400 μ L of D₂O in an NMR tube. (d) Stock solution 2 (288 mL; 16,78 mM): indicated amounts of AA stock solutions were mixed to get stock solution 2. (e) Mixture 2 (0,6 mL; 48,87 mM): 200 μ L of stock solution 1 were mixed with 200 μ L of stock solution 2 and 200 μ L of D₂O in an NMR tube.

NMR experiments

All NMR experiments, except 1D ¹³C NMR, were conducted on a Bruker AVANCE 600 spectrometer (600.13 MHz frequency for ¹H) equipped with a 5 mm TBI probehead (Bruker BioSpin, Rheinstetten, Germany). 1D ¹³C NMR experiments were carried out on a Bruker AVANCE 500 spectrometer (500.13 MHz frequency for ¹H) equipped with a high-sensitivity (helium-)cooled triple-resonance TCI probehead (Bruker BioSpin, Rheinstetten, Germany). The probe temperature was maintained at 298.0 K for all experiments.

Standard 1D ^1H NMR experiments were carried out using the pulse sequence 1D NOESY-presat in order to suppress the residual water signal. Data were collected into 64k data points during an acquisition time of 4.1 s using a recycle delay of 2 s. Spectra were recorded in the time domain as interferograms (FID) across a spectral width of 8012 Hz and as the sum of 128 transients. The resulting experimental time was 13 min. FIDs were automatically Fourier transformed (FT) and the spectra were phased, and baseline corrected.

1D ^{13}C NMR experiments were recorded using the standard power gated proton-decoupled pulse sequence. Data were collected into 64k data points during an acquisition time of 1.2 s using a recycle delay of 2 s. Spectra were collected in the time domain as FIDs across a spectral width of 27778 Hz and as the sum of 16384 transients. The experimental time was 12 h and 54 min. After FT, spectra were phased, and baseline corrected.

Pure shift 2D ^1H *J*-resolved experiments, PS-JRES, were performed with the PSYCHE scheme for broadband homonuclear decoupling, using 180° chirp and saltire pulses of 40 and 30 ms, respectively, described in reference 21 of the main text. Spectra were acquired into 8k data points in the F2 dimension with 8 transients per each of 128 increments, during an acquisition time of 0.68 s using a recycle delay of 2 s. Spectral widths in F2 and F1 dimensions were 6002 and 100 Hz, respectively and the total experimental time was 53 min. FIDs resolution in the F2 dimension corresponded to 1.46 Hz. Prior to FT, the FIDs were weighted in both dimensions using a sine-bell function and zero-filled in the F2 and F1 dimensions to 16k and 1k data points, respectively, giving a final resolution in F2 of 0.37 Hz/pt. The spectra were tilted by 45° before extracting the F2 internal projection that was used as a 1D PS ^1H NMR spectrum.

Conventional ^1H , ^{13}C - HSQC experiment with spectral aliasing, SA-HSQC described in reference 22 of the main text, were recorded with ^{13}C decoupling during acquisition. Spectra were acquired into 4k data points in the F2 dimension, using 16 transients per each of 128 increments during an acquisition time of 0.34 s. The recycle delay was set to 1 s and the interpulse delay in the INEPT module was optimized for 140 Hz ($\Delta=3.57$ ms). The spectral widths in the F2 and F1 dimensions were 6009 Hz and 151 Hz (1.0 ppm), respectively, giving an FID resolution of 2.93 and 2.36 Hz, respectively. The resulting experimental time was 53 min. Data were acquired and processed using the echo/anti-echo protocol. Prior to FT, the FIDs were weighted using a sine-bell-squared function in both dimensions and were zero-filled in the F2 and F1 dimensions to 8k and 1k data points, respectively, giving a final resolution of 0.73 and 0.15 Hz/pt in F2 and F1, respectively.

Conventional ^1H - ^1H TOCSY (Total Correlation Spectroscopy), using a mixing time of 60 ms, and ^1H - ^{13}C HSQC (Heteronuclear Single Quantum Coherence) correlations were acquired using standard Bruker pulse sequences and routine conditions.

TSP (10 mM in D_2O) in a glass capillary, placed as an insert in the NMR tube, was used as external reference ($\delta(^1\text{H})$ and $\delta(^{13}\text{C})$ at 0.00 ppm).

Enantiomer identification

The analysis of the L-enantiomerically enriched sample, mixture **2**, allowed the D/L-assignment of almost all ^{13}C enantiodifferentiated signals and of many ^1H split signals. At least one enantiodifferentiated signal of most AAs was D/L-assigned, allowing the identification of each enantiomer.

The D/L-assignment of ^1H signals was carried out via the comparison of the 1D ^1H NMR spectra (1D NOESY-presat) of mixture **1** and mixture **2** performed under identical conditions (see previous section).

The D/L-assignment of ^{13}C signals was carried out via the comparison of the 1D ^{13}C NMR spectra of mixture **1** and mixture **2** performed under identical conditions (see previous section). In this case, similar relaxation behaviour of the D- and the L-enantiomer of a same enantiomeric pair at identical experimental conditions was assumed based on the results described in reference 17 of the main text.

The D/L-assignment of an enantiodifferentiated NMR signal was represented with the sign of the $\Delta\Delta\delta$ and E parameters. The convention $\Delta\delta(\text{R})-\Delta\delta(\text{S})$ was adopted, which coincides with $\Delta\delta(\text{D})-\Delta\delta(\text{L})$ for all AAs studied. In the case of threonine and isoleucine, AAs with two chiral centres, $\Delta\delta(\text{R})-\Delta\delta(\text{S})$ refers to the stereochemistry of the α -carbon, C-2.

Enantiomer identification could also be done through the standard addition of enantiopure AAs into the sample.

Results and Discussion

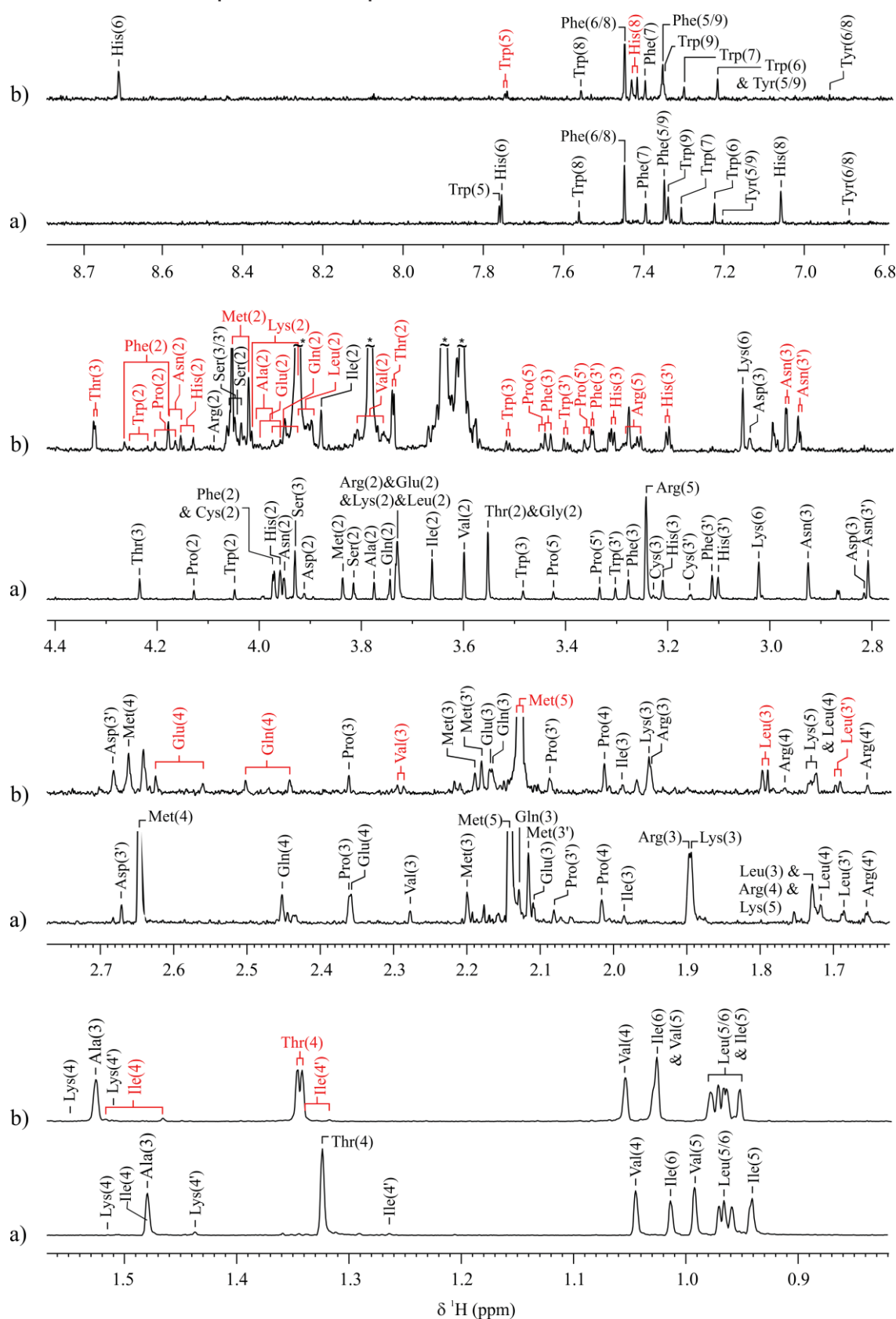
 ^1H and ^{13}C NMR-based enantiospecific molecular profile of AAs mixtures

Figure S-1. ^1H PS-JRES projection of mixture 1 before and after the addition of the CSA. (a) Before the addition of the CSA. (b) After the addition of 3.1 mg (11.7 mM) of CSA (–)- $^{18}\text{C}_6\text{H}_4$. Asterisks denote peaks of CSA.

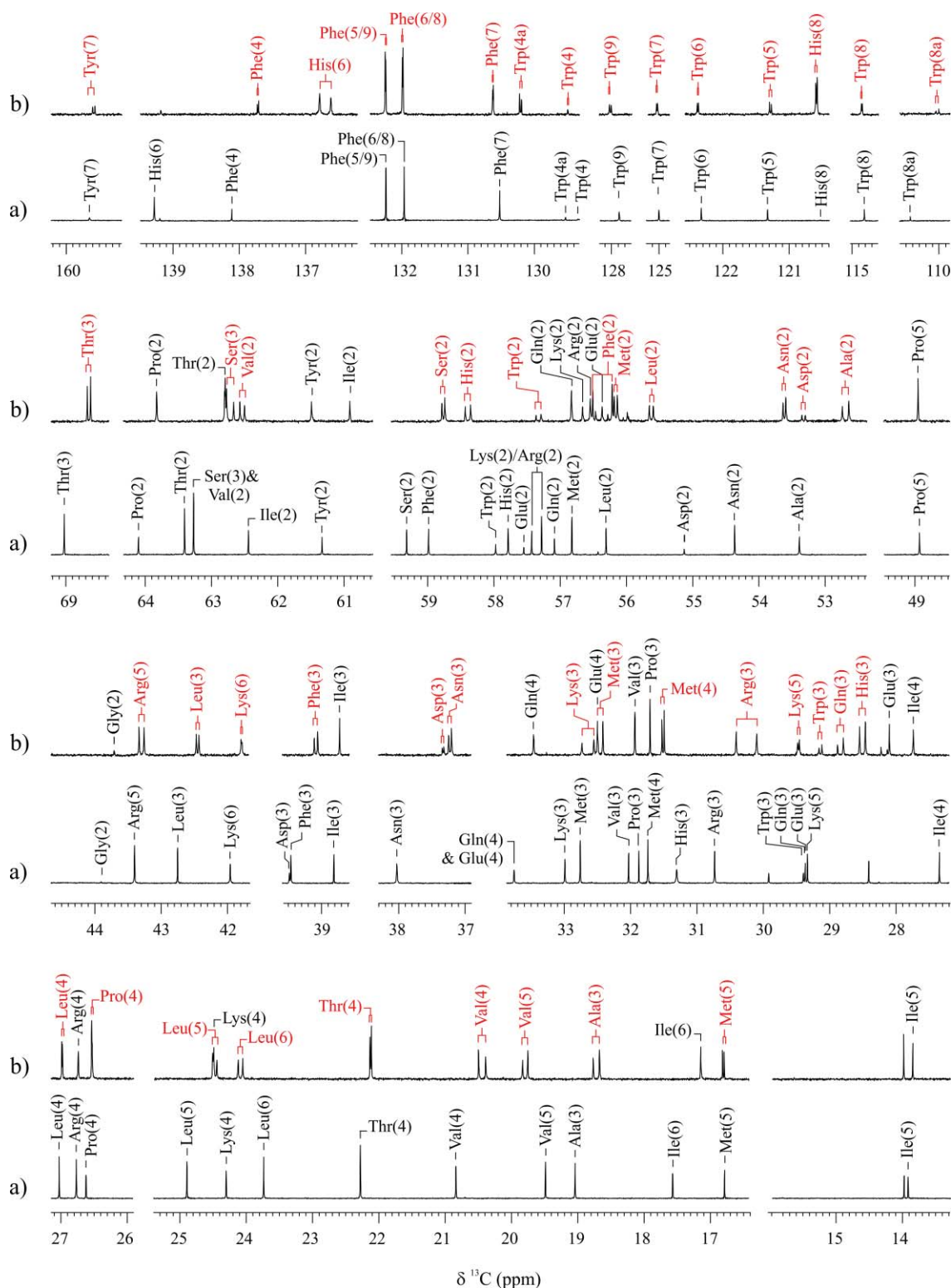


Figure S-2. ^{13}C NMR spectrum of mixture **2** before and after the addition of the CSA. (a) Before the addition of the CSA. (b) After the addition of 3.1 mg (11.7 mM) of CSA ($(-)\text{-}^{18}\text{C}_6\text{H}_4$).

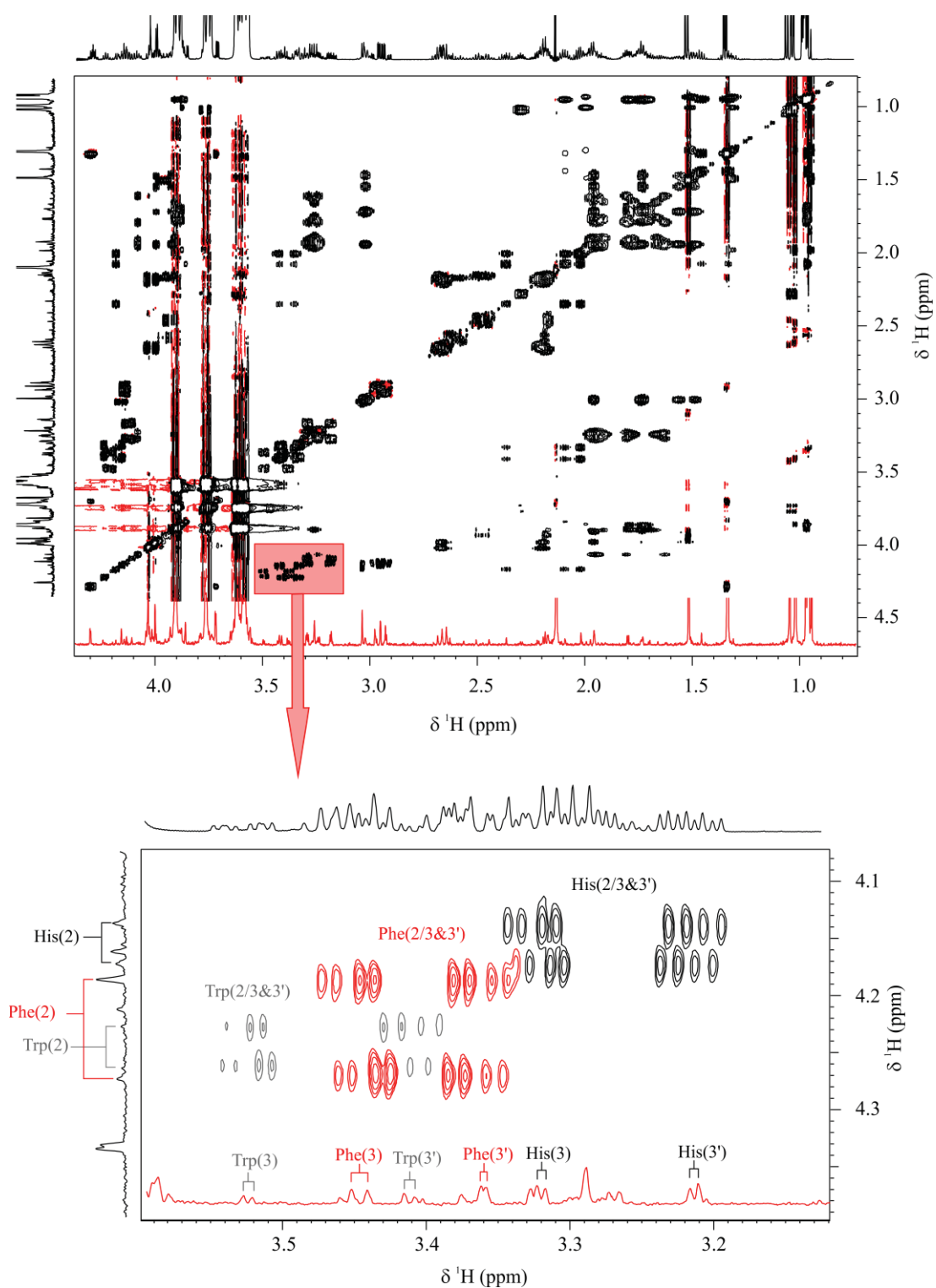
Identification of ^1H and ^{13}C NMR signals in AAs mixtures

Figure S-3. ^1H , ^1H -TOCSY of mixture **1** after the addition of the CSA. Expanded regions of ^1H , ^1H -TOCSY after the addition of 3.1 mg (11.7 mM) of CSA (-)- $^{18}\text{C}_6\text{H}_4$. Projections in the direct dimension correspond to the 1D ^1H spectrum (at the top, black) and to the internal projection of PS-JRES (at the bottom, red).

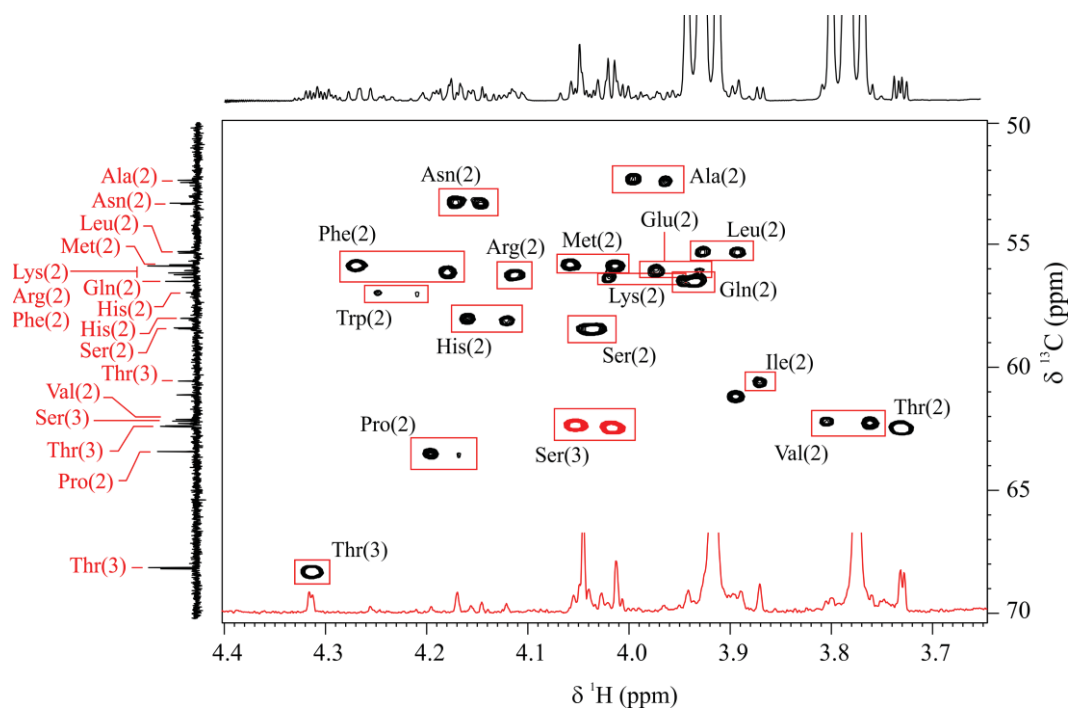
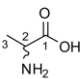
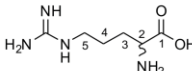
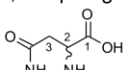
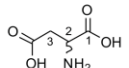
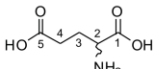
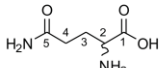
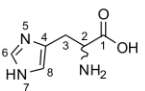
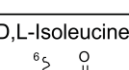
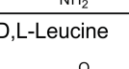
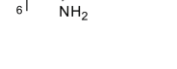
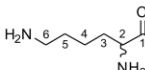
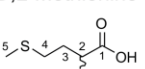
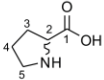
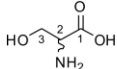
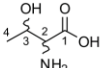
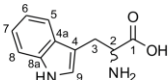
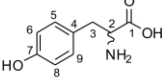
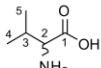


Figure S-4. Expanded region of ^1H , ^{13}C -HSQC of mixture **1** after the addition of the CSA. Expanded region of ^1H , ^{13}C -HSQC for the identification of C-2 signals of AAs in mixture **1** after the addition of 3.1 mg (11.7 mM) of CSA ($-\text{18C6H}_4$). Projections in the direct dimension correspond to the 1D ^1H spectrum (at the top, black) and to the internal projection of PS-JRES (at the bottom, red).

Results of the enantiodifferentiation experiment of AAs mixtures

Table S-2. NMR Enantiodifferentiation results of AAs in mixture 1 and mixture 2 with the addition of 3.1 mg (11.7 mM) of CSA (-)-18C6H₄.

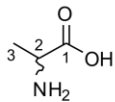
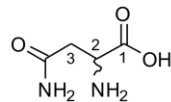
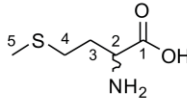
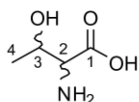
AA	Conc. (mM)	[AA] / [CSA]	¹ H					¹³ C				
			Nuc.	ΔΔδ (ppb)	W ^a (ppb)	IEI ^a	Sign ^b	Nuc.	ΔΔδ (ppb)	W (ppb)	IEI	Sign
D,L-Alanine 	2,42	1:4,8	H-2 H-3	24,7 2,0 ^d	4,0 14,2	2,1 0,1	n.d. ^c -	C-2 C-3	96,0 88,7	15,2 13,9	2,1 2,1	+ +
D,L-Arginine 	2,05	1:5,7	H-5	41,4	3,0	4,6	n.d.	C-3 C-5	307,2 42,3	15,0 14,0	6,8 1,0	- +
D,L-Asparagine 	2,45	1:4,8	H-2 H-3 H-3'	23,4 3,0 4,5	4,2 3,1 3,1	1,9 0,3 0,5	n.d. + -	C-2 C-3	40,2 42,3	14,0 14,0	1,0 1,0	+ +
D,L-Aspartic acid 	0,66	1:17,7						C-2 C-3	49,0 22,8	14,0 14,2	1,2 0,5	n.d. +
D,L-Glutamic acid 	0,66	1:17,7	H-2 H-4	35,7 64,2	ov. 2,6	- 8,2	n.d. n.d.					
D,L-Glutamine 	1,12	1:10,4	H-2 H-4	37,0 60,3	ov. 2,9	- 6,9	n.d. n.d.	C-3	85,0	14,0	2,0	+
D,L-Histidine 	4,94	1:2,4	H-2 H-3 H-3' H-6 H-8	33,6 6,1 6,0 2,7 ^d 14,0	3,5 3,1 3,0 4,7 3,2	3,2 0,7 0,7 0,2 1,4	n.d. n.d. - + -	C-2 C-3 C-6 C-8	80,6 84,0 165,3 20,2	13,0 13,0 14,3 13,0	2,1 2,2 3,9 0,5	+ + - +
D,L-Isoleucine 	3,22	1:3,6	H-4 H-4'	51,2 22,0	2,8 2,8	6,1 2,6	n.d. n.d.					
D,L-Leucine 	1,47	1:8,0	H-2 H-3 H-3'	34,2 7,8 6,8	ov. 3,0 3,0	- 0,9 0,8	n.d. n.d. n.d.	C-2 C-3 C-4 C-5 C-6	60,7 37,4 12,7 67,3 67,8	12,0 14,0 14,0 14,0 14,0	1,7 0,9 0,3 1,6 1,6	- - n.d. - -
D,L-Lysine 	2,46	1:4,8	H-2	68,0	2,6	8,7	n.d.	C-3 C-5 C-6	175,0 25,8 13,1	14,0 16,5 14,0	4,2 0,5 0,3	n.d. - n.d.
D,L-Methionine 	3,32	1:3,5	H-2 H-5	32,3 3,7	2,5 2,6	4,3 0,5	n.d. -	C-2 C-3 C-4 C-5	49,8 81,0 34,4 25,2	14,0 14,0 12,3 13,1	1,2 1,9 0,9 0,6	n.d. n.d. + -
D,L-Phenylalanine 	1,54	1:7,6	H-2 H-3 H-3'	86,0 18,4 13,2	2,5 3,2 4,1	11,5 1,9 1,1	n.d. n.d. n.d.	C-2 C-3 C-4 C-5/9 C-6/8 C-7	157,0 51,8 20,8 10,1 10,8 10,1	14,0 14,0 7,1 7,0 8,2 9,0	3,7 1,2 1,0 0,5 0,4 0,4	n.d. + + - + +

D,L-Proline	2,43	1:4,8	H-2	39,4	2,4	5,5	n.d.	C-4	18,2	14,0	0,4	+
			H-5	11,0	3,8	1,0	n.d.					
			H-5'	4,2	3,7	0,4	n.d.					
D,L-Serine	2,44	1:4,8						C-2	42,6	13,1	1,1	+
								C-3	107,1	13,0	2,7	n.d.
D,L-Threonine	4,05	1:2,9	H-2	ov.	-	-	n.d.	C-3	50,1	8,0	2,1	+
			H-3	3,5	2,7	0,4	+	C-4	19,1	11,2	0,6	+
			H-4	4,4	3,3	0,4	+					
D,L-Tryptophan	0,99	1:11,8	H-2	36,1	2,5	4,8	n.d.	C-2	176,0	14,0	4,2	+
			H-3	6,2	2,6	0,8	+	C-3	41,8	15,2	4,3	+
			H-3'	8,0	2,6	1,0	n.d.	C-4	10,0	10,1	0,3	n.d.
			H-5	5,4	3,0	0,6	+	C-4a	29,2	7,2	1,4	-
								C-5	29,3	7,0	1,4	-
								C-6	18,7	7,3	0,9	+
								C-7	17,1	8,0	0,7	+
								C-8	14,5	8,1	0,6	+
								C-8a	42,3	9,8	1,4	+
								C-9	27,0	8,2	1,1	+
D,L-Tyrosine	0,24	1:48,8						C-7	35,9	9,5	1,3	+
												
D,L-Valine	2,49	1:4,7	H-2	39,8	2,6	5,1	n.d.	C-2	67,1	14,0	1,6	+
			H-3	9,2	3,0	1,0	n.d.	C-4	105,1	13,2	2,7	+
								C-5	76,3	13,8	1,8	-

(a) E (and W) of ^1H signals measured from internal projection of PS-JRES spectrum. (b) For the sign of $\Delta\Delta$ and E, the convention $\Delta\delta(\text{R})-\Delta\delta(\text{S})$ was adopted, which coincides with $\Delta\delta(\text{D})-\Delta\delta(\text{L})$ for all AAs studied. (c) Not determined. (d) Measured from the 1D ^1H NMR experiment.

Results of the enantiodifferentiation experiments of pure AAs

Table S-3. NMR Enantiodifferentiation results of pure AAs with CSA (-)-18C6H₄.

AA	Conc. (mM)	[AA] / [CSA]	Nuclei	$ \Delta\Delta\delta $ (ppb)	Sign ^a
D,L-Alanine 	2,42	1:4,8	H-2	27,9	-
			H-3	2,5	-
			C-2	96,0	+
			C-3	108,8	+
D,L-Asparagine 	2,42	1:4,8	H-2	27,2	-
			C-2	38,1	+
			C-3	45,6	+
D,L-Methionine 	3,31	1:3,5	H-2	35,5	-
			H-5	3,0	-
			C-2	45,8	n.d. ^b
			C-3	136,0	+
			C-4	48,3	+
			C-5	23,1	-
D,L-Threonine 	4,03	1:2,7	H-2	4,6	-
			H-3	3,3	+
			H-4	4,5	+
			C-2	33,6	+
			C-3	55,4	+
			C-4	13,6	+

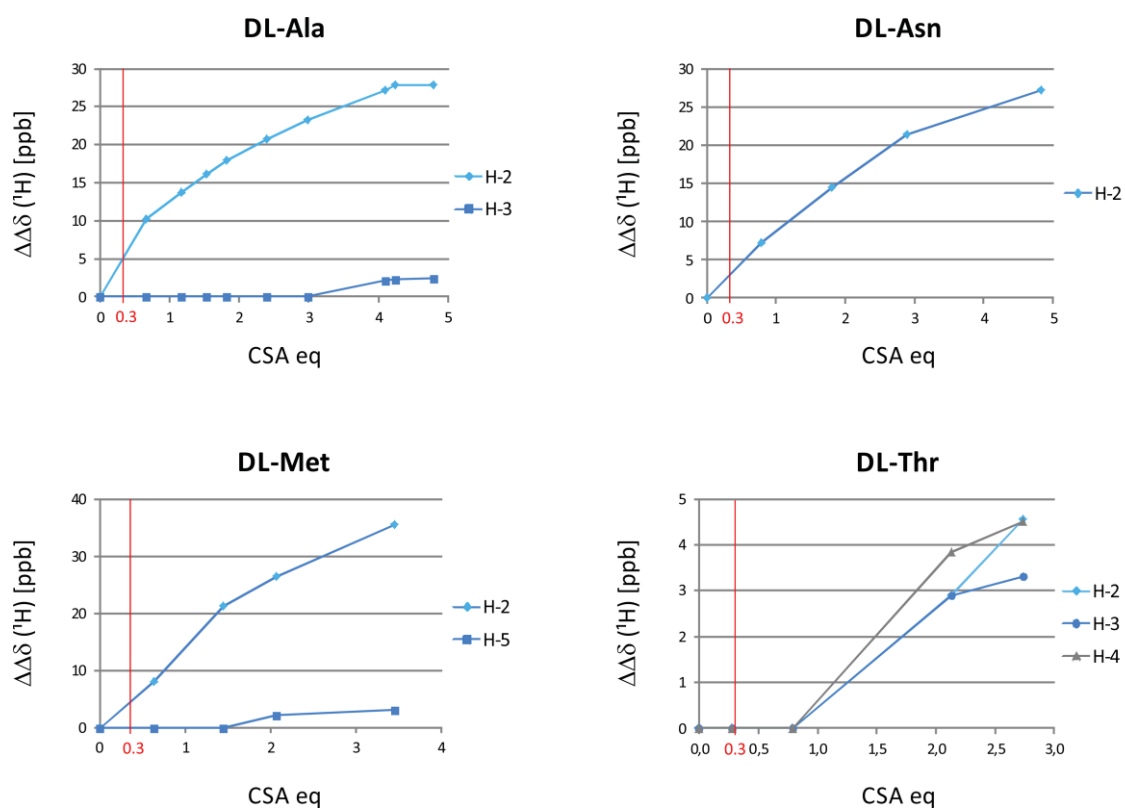


Figure S-5. Titration curves of pure AAs in D₂O with CSA (-)-18C₆H₄ monitored by standard 1D ¹H NMR experiments.

Author Contributions

M.P.-T. designed the experiments and the research. L.T.K., K. M.-C., T.J.A. and M.P.-T. performed the experiments. L.T.K., K. M.-C., and M. P.-T. analysed the data. L.T.K., T.P. and M.P.-T. wrote the paper. All authors discussed the results and commented on the manuscript.

5. Conclusions

A. Publication 1: Implementing one-shot multiple-FID acquisition into homonuclear and heteronuclear NMR experiments.

- ❖ The MFA-COSY/RELAY3 experiment affords complementary COSY and RELAY spectra in a single-shot acquisition and facilitates the sequential ^1H NMR assignment of a whole spin system without ambiguities.
- ❖ An isotropic TOCSY mixing period can be incorporated after the acquisition of HMQC-like and HMBC-like experiments, allowing the propagation of magnetization into an entire spin system. For instance, MFA pulse schemes providing simultaneously HMBC and HMBC-TOCSY spectra can be collected at the same time.
- ❖ MFA-MBOB-COSY experiment solves the main drawback found in HMBC experiments which is the distinction between two- and three-bond correlation peaks. HMQC-COSY affords two-bond correlation peaks via $^1J(\text{CH}) + J(\text{HH})$ and HMBC-COSY spectra can distinguish up to four-bond peaks correlation via $^nJ(\text{CH}) + J(\text{HH})$.
- ❖ NMR experiments based on MFA has shown their effectivity in terms of decreasing experimental time, collecting up to four experiments in a single acquisition.
- ❖ The main drawback in the MFA approach is the decreasing of sensitivity on the consecutive experiments. This sensitivity is compromised by T_2 which must be long enough.

B. Publication 2. Simultaneous acquisition of two 2D HSQC spectra with different ^{13}C spectral widths.

- ❖ Spectral aliasing has demonstrated its efficiency in terms of spectral resolution, especially for HSQC-type experiments.
- ❖ SADA-HSQC experiment collects two HSQC 2D spectra in one acquisition. The first spectrum is an HSQC with a scaled SA factor and the second FID corresponds to a conventional HSQC.
- ❖ This experiment avoids the main limitation of a single SA-HSQC which is the impossibility to assign chemical shift values in F1.
- ❖ The losing of sensitivity by using MFA in FID2 is compensated with the high spectral resolution and signal dispersion achieved in FID1.

C. Publication 3. Interleaved Dual NMR Acquisition of Equivalent Transfer Pathways in TOCSY and HSQC Experiments.

- ❖ The combination of two different isotropic mixing periods separately stored provides a powerful experiment called MFA-TOCSY/TOCSY.
- ❖ Despite the loss of sensitivity on the second FID, the sum of the positive projections shows only a decrease of around 20% of sensitivity.
- ❖ The same scheme can be applied to the HSQC-type experiment. PEP components can be managed separately to obtain two different HSQC spectra into the same scan.
- ❖ Separate 2D HSQC and HSQC-TOCSY spectra can be simultaneously obtained using the MFA-HSQC/HSQC-TOCSY experiment.

D. Publication 4. Broadband homodecoupled time-shared ^1H - ^{13}C and ^1H - ^{15}N HSQC experiments.

- ❖ Novel NMR methods combining time-sharing and pure-shift NMR have been developed.

- ❖ A properly combination between time-shared methods and BIRD building blocks has shown its efficiency in terms of spectrometer time and spectral resolution.
- ❖ ^{13}C and ^{15}N pure-shift HSQC spectra are simultaneously obtained in a single-shot acquisition.
- ❖ CN- J -psHSQC experiment allows measuring $^1J_{\text{CH}}$ and $^1J_{\text{NH}}$ simultaneously along both dimensions.

E. Publication 5. LR-selHSQMBC: Simultaneous Detection and Quantification of Very Weak Long-Range Heteronuclear NMR Correlations.

- ❖ The combination of the selHSQMBC experiment with the time-sharing method has demonstrated its efficacy for the simultaneous measurement of the long-range coupling constant (up to 6J) for protonated and non-protonated ^{13}C and ^{15}N .
- ❖ IPAP methodology has shown its powerfulness for the accurate measurement of small coupling constants.
- ❖ $^{13}\text{C}/^{15}\text{N}$ -selHSQMBC experiment with IPAP methodology allows us the measurements of J even smaller than the linewidth and is also adequate to determine the positive/negative sign in related LR-selHSQMBC-TOCSY experiments.

F. Publication 6. LR-HSQMBC versus LR-selHSQMBC: Enhancing the Observation of Tiny Long-Range Heteronuclear NMR Correlations.

- ❖ LR-selHSQMBC achieves more intense IP cross-peaks in comparison with the LR-HSQMBC experiment.
- ❖ LR-selHSQMBC shows cross-peaks that are missed on LR-HSQMBC spectra.
- ❖ LR-selHSQMBC combined with the IPAP methodology has demonstrated its robustness to measure very small coupling constants.

- ❖ The LR-selHSQMBC experiment avoids the presence of AP contributions providing a considerably enhanced sensitivity concerning HMBC/HSQMBC-type experiments.

G. Publication 7. Simultaneous Enantiospecific Detection of Multiple Compounds in Mixtures using NMR Spectroscopy.

- ❖ As a proof of concept, thirty-six chiral amino acids at physiological concentrations were simultaneously enantiospecifically detected using NMR spectroscopy and a chiral solvating agent. The analysis did not require the prior separation or derivatization of its components from the original mixture.
- ❖ A minimal quantity of CSA was required to get an excellent enantiodifferentiation.
- ❖ The analyses yielded a ^1H NMR-based enantiospecific metabolic profile of the original mixture, based on the projection in the direct dimension of a pure-shift J -resolved spectrum, and a ^{13}C NMR-based enantiospecific metabolic profile based on a 1D conventional ^{13}C NMR spectrum.
- ❖ The method allowed, as well, the detection and identification of all components of the mixture.
- ❖ The SA ^1H - ^{13}C -HSQC experiment demonstrated its efficiency for the simultaneous enantiospecific detection of both ^1H and ^{13}C nuclei and allowed the direct measurements of chemical shift separation (enantiodifferentiation) between enantiomers.
- ❖ Compatible with untargeted and targeted quantitative studies, this work represents a first step towards the *in situ* multicomponent enantiospecific analysis of complex mixtures, showing significant potential for application in metabolism studies, metabolic phenotyping, and chemical reaction analysis, among others.